Metal and tyrocidine nano-assemblies to create broad-spectrum metal-peptide formulations

by

Carmen de Villiers

BScHons (Biochemistry)

March 2023

Thesis presented for the degree

Masters of Science (Biochemistry)

in the
Faculty of Science
at the
University of Stellenbosch

Supervisor: Prof. Marina Rautenbach

Department of Biochemistry

University of Stellenbosch

Declaration

By submitting this thesis electronically, I ***Carmen de Villiers*** declare that the entirety of the work contained therein is my own, original work, that I am the sole author thereof (save to the content explicitly stated otherwise), that reproduction and publication thereof by Stellenbosch University will not infringe any third-party rights and that I have not previously in its entirety or in part submitted it for obtaining any qualification.

Carmen de Villiers
Name

March 2023
Date

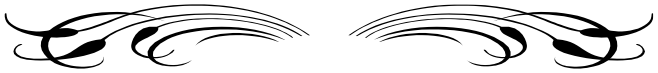

“Incuriosity is the oddest and most foolish failing there is”

- Stephen Fry, 13 September 2010

Summary

Without the discovery or development of novel drugs, the phenomena of antimicrobial resistance (AMR) will continue to threaten the effective treatment of pathogenic microbes and diseases across the globe. Combinational therapies of antimicrobial peptides (AMPs) with metal nanoparticles (MNPs) have shown promise for the creation of potent nano-drugs with broad spectrum antimicrobial activity, alternative applications, and lowered risk of resistance development. In this study the combinational formulation of biologically relevant metals (magnesium, calcium, iron, copper, silver, gold, and zinc) with a group of natural antimicrobial cyclodecapeptides (CDPs) was investigated for the fabrication of potent AMP-MNP nanodrugs. The CDPs selected for this study include an aromatic residue rich peptide complex (tyrocidine mixture, Trc mix) and tryptophan rich purified analogues (tyrocidine C, TrcC and tryptocidine C, TpcC). Mass spectrophotometric studies revealed that these peptides form peptide-metal complexes with certain metals, and that the absence or presence of such complexes in formulations altered the peptides oligomerisation behaviour. Although formulations with group 11 metals lacked peptide-metal complexes, changes in peptide oligomerisation and analogue-specific prevalence was observed. Since the aromatic rich structure of these CDPs holds potential for synthesis of MNPs, it was hypothesised that the absence of peptide-metal complexes in group 11 formulations is likely due to the reduction of metal ions and formation of MNPs. This hypothesis was confirmed by spectrophotometric and spectrofluorometric studies which reported the formation of silver nanoparticles (AgNPs) in Trc mix, TpcC and TrcC formulations with silver. These studies also indicated alterations in peptide conformation when in formulation and highlighted the critical role of tryptophan for successful CDP-AgNP fabrication. Scanning transmission microscopy revealed that the peptide-synthesised spherical AgNPs were encapsulated by CDP nanostructures, a promising conjugate structure for drug delivery. Solid surface antimicrobial assays and reported additive and synergistic antimicrobial actions between CDPs and MNPs against model organisms, Gram positive *Staphylococcus aureus* and Gram-negative *Escherichia coli*, respectively. The innate self-assembly of these aromatic amino acid rich CDPs therefore holds potential to streamline the synthesis of potent yet versatile CDP-MNP nanoformulations for topical or antimicrobial surface treatments against Gram-positive and Gram-negative bacteria. Moreover, unprecedented antibacterial activity was also reported for TpcC, which could have applications in future therapies.

Opsomming

Sonder die ontdekking of ontwikkeling van nuwe geneesmiddels, sal die verskynsel van antimikrobiese weerstand (AMW) die effektiewe behandeling van patogene en infeksies wêreldwyd bedreig. Kombinasie-terapie met antimikrobiese peptiede (AMPs) en metaalnanopartikels (MNPs) toon belofte vir die skepping van kragtige nano-geneesmiddels met breëspektrum antimikrobiese aktiwiteit en alternatiewe toepassings met ‘n verlaagde risiko van weerstandsontwikkeling. In hierdie studie, was die kombinasie-formulering van biologies relevante metale (magnesium, kalsium, yster, koper, silwer, goud en sink) met 'n groep natuurlike antimikrobiese siklodekapeptiede (SDP'e) ondersoek vir die vervaardiging van kragtige AMP-MNP-nanogeneesmiddels. Die SDP'e wat vir hierdie studie gekies is, sluit 'n aromatiese residu-ryk peptied kompleks (tirosidien mensel, Trc mix) en triptofaan-ryk gesuiwerde analoë (tirosidien C, TrcC en triptosidien C, TpcC) in. Massaspektrofotometriese studies het onthul dat hierdie peptiede peptied-metaalkomplekse met sekere metale vorm, en dat die afwesigheid of teenwoordigheid van sulke komplekse in formulerings die peptiede-oligomeriseringsgedrag verander. Alhoewel peptied-metaalkomplekse in formulerings met groep 11-metale komplekse afwesig was, was veranderinge in peptied-oligomerisasie en analoog-spesifieke voorkoms waargeneem. Aangesien die aromaties-ryk struktuur van hierdie SDP's potensiaal skep vir sintese van MNP's, is ‘n voorgestelde hipotese dat die afwesigheid van peptied-metaal komplekse in groep 11 formulerings waarskynlik te wyte is aan die vermindering van metaalione en vorming van MNPs. Hierdie hipotese was bevestig deur spektrofotometriese en spektrofluorometriese studies wat die vorming van silwer nanopartikels (AgNPs) in Trc mix, TpcC en TrcC formulerings met silwer gerapporteer het. Hierdie studies het ook peptiedkonformasie veranderinge in formulering getoon, sowel as die kritieke rol van triptofaan in suksesvolle SDP-AgNP vervaardiging. Skandeertransmissie-mikroskopie het gewys dat die peptied-gesintetiseerde AgNP's deur SDP-nanostrukture ingekapsuleer was, 'n belowende gekonjugeerde struktuur vir geneesmiddelaflewering. Soliede-oppervlak antimikrobiese toetse het additiewe en sinergistiese antimikrobiese aksies tussen SDP's en MNP's teen model organismes, Gram-positiewe *Staphylococcus aureus* en Gram-negatiewe *Escherichia coli*, onderskeidelik gerapporteer. Die inhirente selfassosieëring van hierdie aromatiese aminosuurryke SDP's hou dus die potensiaal om die sintese van kragtige dog veelsydige SDP-MNP nanoformulerings te stroomlyn vir aktuele of antimikrobiese oppervlakbehandelings teen Gram-positiewe en Gram-negatiewe bakterieë. Boonop is ongekende antibakteriese aktiwiteit ook aangemeld vir TpcC wat dus toepassings in toekomstige terapieë kan hê.

Acknowledgements

I would like to express my thanks and gratitude to the following persons and institution:

- My Supervisor, Prof Marina Rautenbach:
  Thank you for everything you have done to aid me with my postgraduate studies and my growth as a scientist. I appreciate it all.

- Dr Marietjie Stander & colleagues (Central Analytical Facilities, Stellenbosch University):
  Thank you for your expertise and technical assistance during mass spectrometry analysis.

- The Department of Biochemistry (Stellenbosch University) and BIOPEP Peptide Fund:
  Thank for financially aiding the completion of my MSc degree.

- My loving family; Lourens, Isabella and Liam:
  For allowing me the freedom to chase my own dreams and suppling me with the love and support I needed to conquer them. As I write this, I cannot believe that the young girl dissecting her dinner at the dining room table, asking endless questions about everything, is the same woman writing out the acknowledgements of her own MSc thesis. Thank You.

- My lovely Godmother, Annamé:
  Thank you for your adventurous spirit, limitless curiosity, unconditional love and support.
  I've kept my brittle star in my pocket – it's still burning.

- My dear Hugh.
  Thank you for your loving support, compassion and patience.

- My beloved friends:
  Thank you for respecting my journey, understanding my absence, and reminding me to live a little every now and then. I am grateful for you all.

- The BIOPEP Peptide Group and Rautenstrauss Team:
  A group of brilliant scientists. Thank you for supplying me with continuous guidance and support. Especially on those days when experiments didn't run smoothly, data seemed incomprehensible, and science seemed just a little too hard.

- Everyone I have lost throughout the duration of my MSc and everyone I have gained. Thank you for playing your special role in my life. It has been a beautiful adventure.

- And finally, my past self. Thank you for never giving up. You did it!

Table of Contents

Abbreviations and Acronyms

$[2M+2H]^{2+}$	doubly charged dimer ion
$[4M+3H]^{3+}$	triply charged tetramers
$[6M+4H]^{4+}$	quadruply charged hexamers
$[M+2H]^{2+}$	doubly charged monomeric molecular ion
$[M+H]^{+}$	singly charged monomer ion
$[M+Metal±nH]^{3+}$	triply charged peptide:metal complexes
a.u.	arbitrary units
aa	amino acid
ACN	acetonitrile
ADP	antimicrobial peptide database
Ag^{+}	silver (I) ion
$AgNO_3$	silver nitrate
AgNPs	silver nanoparticles
AMP(s)	antimicrobial peptide(s)
AMP-MNP	antimcrobial peptide - metal nanoparticle conjugate
AMR	antimicrobial resistance
Au^{3+}	gold (III) ion
AuNPs	gold nanoparticles
Br. parabrevis	*Brevibacillus parabrevis*
BSI	bloodstream infections
C. albicans	*Candida albicans*
Ca^{2+}	calcium (ii) ion
$CaCl_2$	calcium chloride
CAUTIs	catheter-associated urinary tract infections
CCS	collision cross sections
CD	circular dichroism spectroscopy
Cu^{2+}	copper (ii) ion
$CuCl_2$	copper chloride
CuNPs	copper nanoparticles
CVADs	central vascular access devices
DBSAAP	database of antimicrobial activity and structure of peptides
DEE	diethyl ether
DMSO	dimethyl sulfoxide
DNA	deoxyribonucleic acid
E. coli	*Escherichia coli*
E. faecium	*Enterococcus faecium*
EHT	electron high tension (SEM Imaging)
ESI	electrospray ionisation
ESI-MS	electrospray ionisation mass spectrometry
EtOH	ethanol
EtOH-water	ethanol in water
Fe^{2+}	iron (II) ion
$FeCl_2$	iron (II) chloride
FIC	fractional inhibitory concentration
FICI	fractional inhibitory concentration index
FTIR	fourier-transform infrared spectroscopy
Grms	gramicidin
GS	gramacidin S
$HAuCl_4$	gold (III) chloride
HIV	human immunodeficiency virus

HPLC ..... high performance liquid chromatography
HR ..... high resolution
HR-ESMS ..... high-resolution electrospray mass spectrometry
IC_{50} ..... peptide concentration leading to 50 % microbial growth inhibition
IM-MS ..... ion mobility mass spectrometry
KCl ..... potassium chloride
K. pneumoniae ..... *Klebsiella pneumoniae*
L. monocytogenes ..... *Listeria monocytogenes*
Lys ..... lysine
m/m ..... *mass/mass*
m/v ..... *mass/volume*
m/z ..... mass over charge ratio
MDR ..... multi-drug resistant
MeOH ..... methanol
$Mg(NO_3)_2$ ..... magnesium nitrate
Mg^{2+} ..... magnesium (II) Ion
$MgCl_2$ ..... magnesium chloride
MIC ..... minimum inhibitory concentration
MilliQ ..... analytical grade water
MNPs ..... metal nanoparticles
M_r ..... relative molar mass
MRSA ..... methicillin-resistant *Staphylococcus aureus*
N_2 ..... nitrogen
NaCl ..... sodium chloride
$NaNO_3$ ..... sodium nitrate
NMR ..... nuclear magnetic resonance spectroscopy
NPs ..... nanoparticles
O ..... ornithine
OD ..... optical density
Orn ..... ornithine
P. aeruginosa ..... *Pseudomonas aeruginosa*
PBS ..... phosphate buffered saline
PDR ..... pan drug-resistant
Phcs ..... phenycidines
Phe ..... phenylalanine
Poly-Ala ..... poly-DL-alanine
ppm ..... parts per million
Q-TOF ..... quadrupole time-of-flight
RNA ..... ribonucleic acid
RP-HPLC ..... reverse phase high performance liquid chromatography
R_t ..... retention time of analyte in column chromatography
S. aureus ..... *Staphylococcus aureus*
SD ..... standard deviation
SEM ..... standard error of the mean
SFP ..... *Staphylococcus* food poisonings
STEM ..... scanning transmission electron microscopy
TFA ..... trifluoroacetic acid
TGS ..... tryptone glucose and salts culture medium
T-I ..... amphiphatic dimer of tryptocidine C
T-II ..... non-amphiphatic dimer of tryptocidine C
TOF ..... time of flight
Tpc(s) ..... tryptocidines(s)

TpcA .....tryptocidine A
TpcB .....tryptocidine B
$TpcB_1$.....tryptocidine B_1
TpcC .....tryptocidine C
$TpcC_1$.....tryptocidine C_1
Trc mix.....tyrocidine mixture (purified from commercial tyrothricin)
Trc(s) .....tyrocidine(s)
TrcA .....tyrocidine A
$TrcA_1$.....tyrocidine A_1
TrcB/B'.....tyrocidine B/B'
$TrcB_1$.....tyrocidine B_1
TrcC.....tyrocidine C
$TrcC_1$ .....tyrocidine C_1
Trp .....tryptophan
TSB..... tryptone soy broth
TWIM-MS .....travelling wave Ion mobility mass spectrometry
Tyr .....tyrosine
UPLC-MS .....ultra-performance liquid chromatography linked to mass spectroscopy
UV-Vis .....UV-Visible light spectrophotometry
v/v.....volume/volume
VGA.....linear gramicidins
VGA^{UF}.....linear gramicidins (without formyl group)
WD .....working distance (SEM Imaging)
WHO.....world health organisation
XDR.....extensively drug-resistant
Zn^{2+}.....Zinc (II) ion
$ZnCl_2$.....Zinc chloride
λ_{em} .....emission maxima
λ_{max} .....absorbance maxima

For the natural amino acids found in proteins standard 1- and 3-letter abbreviations were used, with capital 1-letter abbreviations for L-amino acid residues and lower case 1-letter abbreviations for D-amino acid residues in peptides

Preface

Advances in combination drug therapies and nanotechnology has created a new field for the design and development of novel antimicrobial treatments to address the rise in drug resistant microbes. Combination of antimicrobial peptides (AMPs) and metal nanoparticles (MNPs) have shown applications as potent antimicrobial treatments in biomedical, agricultural, and industrial applications. The peptide-assisted synthesis of MNPs is a greener alternative to more conventional MNP synthesis techniques and has been shown to fabricate versatile AMP-MNP conjugate structures with multifaceted antimicrobial actions and applications. Interactions between metal ions and the aromatic residues of peptides allow the reduction and subsequent nucleation of metal ions to form MNPs. The tyrocidines and analogues are a group of antimicrobial cyclodipeptides (CDPs) naturally produced by the soil bacterium *Brevibacillus parabrevis* (*Br. parabrevis*) rich in aromatic residues. These peptides display a broad spectrum of antibacterial, antifungal and even antimalarial activity. Formulations of these CDPs with a variety of commercial materials has already shown great potential for the incorporation of these CDPs in surface treatments to prevent the colonisation and spread microbial pathogens or biofilms. For this study, the potential of an aromatic residue rich tyrocidine peptide mixture (Trc mix) and purified tryptophan rich analogues (TpcC and TrcC) for the fabrication of antimicrobial CDP-MNP conjugates was investigated for future applications in surface treatments. To achieve this the following aims and objective needed to be met:

Aim 1: Production and purification of tryptophan-rich antimicrobial cyclodecapeptides and analogues

To achieve this aim the following objectives were met and summarised in Chapter 2 of this study:

- Manipulation of peptide production profile of producer organism *Brevibacillus parabrevis* (*ACCT 8185* and *ACCT 10068*) via amino acid supplementation of producer cultures to promote production of tryptophan-rich tyrocidines and analogues.
- Confirming production profile shifts by analysing peptide composition of crude production extracts via electrospray mass spectrometry and ultra-performance liquid chromatography.
- Organic solvent extraction of tyrocidines and tyrocidine analogues from the tyrothricin complex and commercial tyrocidine peptide mixture.

- Purification of single tyrocidines and analogues via RP-HPLC to obtain pure tryptophan-rich C analogues.
- Confirming peptide identity and purity of purified analogues via electrospray mass spectrometry and ultra-performance liquid chromatography

Aim 2: Mass spectrometry studies on the interaction of the tyrocidines and analogues with metal salts

To achieve this aim the following objectives were met and summarised in Chapter 3 of this study:

- Titration and formulation of purified tyrocidine mixture (Trc mix) with magnesium, calcium, iron, copper, silver, gold and zinc metal salts.
- IM-MS analysis of formulations to characterise and track peptide-metal interactions and changes in peptide oligomerisation behaviour

Aim 3: Biophysical and bioactive characterisation of tryptophan-rich cyclodecapeptide nanoformulations

To achieve this aim the following objectives were met and summarised in Chapter 4 of this study:

- Confirm photo-induced peptide-assisted nanoparticle formation via colloid colour changes.
- Optimisation of peptide:metal formulations for nanoparticle fabrication by assessing different solvent conditions, precursor concentrations and peptide:metal ratios.
- Characterise peptide:metal nanoformulations and peptide-metal interactions via UV-Visible light and fluorescence spectrophotometry.
- Characterise peptide:metal nanoformulations via STEM analysis to determine formulation and nanoparticle shape and structure.
- Asses antimicrobial activity of select peptide:metal nanoformulations against target organisms *S. aureus* and *E. coli*.

Chapter 1 serves as an introduction and background to the study while Chapter 5 includes the concluding remarks, final discussion, and future studies. Each experimental chapter (2-4) was written as independent units in article format. Although this may have led to some repetition, it was attempted to keep repetition to a minimum.

Outputs of MSc study

Oral Presentations

Oral presentation on “The Nano-formulation of Natural Cyclodecapeptides for Antimicrobial Applications” (Nov 2020) Thesis progress, Biochemistry Forum, University of Stellenbosch.

Oral presentation on “Metal and tyrocidine nano-assemblies to create broad-spectrum metal-peptide formulations” (Feb 2023) Thesis defence, Biochemistry Forum, University of Stellenbosch.

Oral presentation on “Modulation of oligomerization and antimicrobial activity in cyclic decapeptide-metal nanoformulations” (Nov 2022) World Health Organisation World Antimicrobial Awareness Week (WAAW) symposium, University of Stellenbosch.

Awarded “Best Oral Presentation in Biological Sciences” for oral presentation on “Metal-Modulated Cyclic Deca-Peptide Oligomerization and Bioactivity” (Nov 2022) Stellenbosch University Faculty of Science Postgraduate Conference, University of Stellenbosch.

Poster presentation

Presented Scientific Poster on “Introducing Metals: Formulations for Directing Peptide Nano-Assembly” (May 2022) AC21 Workshop for Antimicrobial Peptides, University of Strasbourg, Strasbourg, France.

Peer-reviewed articles

V. Kumar, W. van Rensburg, J.L. Snoep, H.H. Paradies, C. Borrageiro, C. de Villiers, R. Singh, K.B. Joshi, M. Rautenbach, Antimicrobial nano-assemblies of tryptocidine C, a tryptophan-rich cyclic decapeptide, from ethanolic solutions, Biochimie. (2023) 204, 22-32, DOI: 10.1016/j.biochi.2022.08.017 (co-author and experimental contribution of materials and data from chapters 2, 3 and 4)

Expected outputs

De Villiers, C, Rautenbach, M. Paradies, H.H, Kumar V. Tryptocidine C encapsulated nano-silver assemblies with modulated antibacterial activity, a draft article from Chapter 4 prepared for submission to Antibiotics in February 2023

De Villiers, C, Stander, M, Rautenbach, M. Ion mobility mass spectrometry: a tool for characterising cyclodecapeptide-metal interactions, a draft article from Chapter 3 prepared for submission to Rapid Communications in Mass Spectrometry in March 2023

Chapter 1
Literature Review

1.1 Introduction

The demand for novel antimicrobial agents has increased in recent years with the rise in drug-resistant pathogens [1,2]. Although there has been a great need for the discovery of novel antimicrobial drugs, the discovery of new agents has stagnated in recent years with no new classes of antibiotics discovered since the late 1980's (Fig. 1.1) [3,4]. Moreover, with the rise in drug resistance pathogens, the promise of discovering novel classes of antimicrobial drugs, unlikely to have resistance developed against it in future, grows slim [1,3,4].

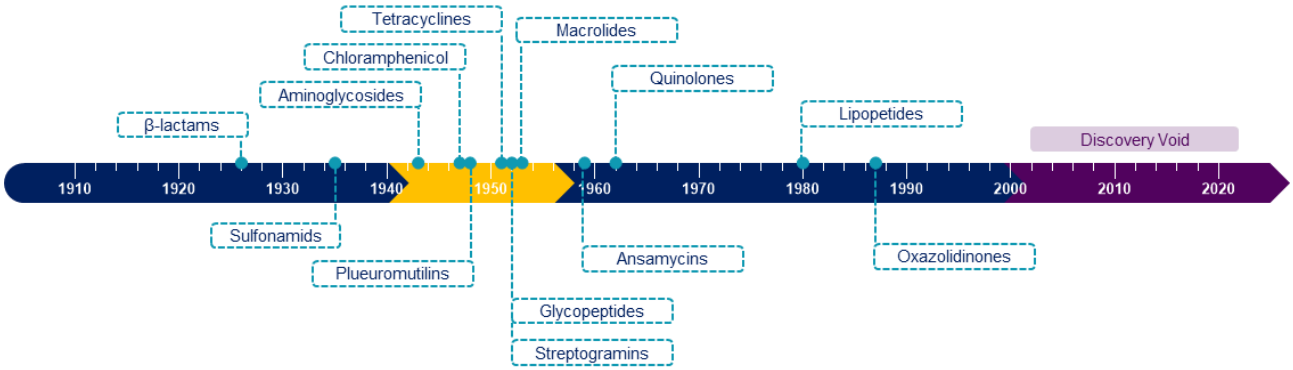

Figure 1.1 Timeline of antibiotic discovery and the stagnation of novel classes. Figure adapted from timeline shown in Lewis *et al.* [4].

However, addressing antimicrobial resistance (AMR) remains to be a complex task. Modern medicine and agriculture rely on the availability of effective antimicrobial drugs [3,5]. Since the use of antimicrobial agents has become seemingly synonymous with modern biomedical and agricultural practises, simply eradicating antimicrobial use to prevent AMR is an unlikely option [1,3]. In 2001, the World Health Organisation (WHO) released the "Global Strategy for Containment of Antimicrobial Resistance" which provided a framework to manage and prevent the rise and spread of resistant microbes [6]. This framework was revised in 2015 with a "Global Action Plan" which outlined a 'One Health' strategy for optimal antimicrobial use, surveillance, and research [2]. These global strategies highlight two major steps towards fighting the rise in AMR, first the management antimicrobial stock and second the making of new antimicrobial stock. The making of new drug stocks attempts to address the stagnation of novel antimicrobial drug discovery and development [2,6,7]. However, these novel drugs need to be either active against currently resistant pathogens and/or unlikely to

have AMR developed against them in future [3,8]. Since the discovery of novel classes of drugs with no risk of resistance development is unlikely, researchers have opted to relook and refocus drug developments towards improving the antimicrobial actions of and preventing resistance development against currently available antimicrobials [3,7]. Although some of these drugs may already have resistance reported against them, scientific advances such as the development of nanotechnologies are promising for the development of a new-era of nano-drugs and drug delivery systems [3,9]. This, in turn, has created new opportunities for revitalising and/or improving the drug therapies of older drugs.

1.2 The dilemma of antimicrobial resistance

1.2.1 Antimicrobial resistant pathogens and mechanisms of resistance

The development of AMR is a natural phenomenon rooted in Darwin's theory of evolution "the survival of the fittest". In the natural environment, microbes instinctively evolve advantageous characteristics through evolutionary mechanisms to withstand harsh environmental conditions or settle into a particular environmental niche. It is these same mechanisms which enable microbes to develop AMR [1,10]. Microbes simply evolve mechanisms of resistance, through genetic changes over time, against the antimicrobial agents they are exposed to. These changes consequently decrease the efficacy of the drugs used to treat infections caused by these microorganisms [11]. Unfortunately, the mismanagement of antimicrobial drugs has accelerated the rate of resistance development in recent years by exposing microbes to antimicrobials frequently and often unnecessarily [1,2,5].

By reducing their sensitivity to approved drug treatments, drug-resistant microbes such as the ESKAPE pathogens threaten our ability to treat infectious diseases effectively. The term "ESKAPE" is an acronym used to describe a priority group of drug-resistant pathogens which include: *Enterococcus faecium* (*E. faecium*), *Staphylococcus aureus* (*S. aureus*), *Klebsiella pneumoniae* (*K. pneumoniae*), *Acinetobacter baumannii* (*A. baumannii*), *Pseudomonas aeruginosa* (*P. aeruginosa*), and *Enterobacter spp* [11]. These microbes have evolved several mechanisms by which they can "escape" the biocidal effects of many known antibacterial agents leading to persistent, chronic, or even lethal infections [10–12]. The WHO has listed these ESKAPE pathogens as priority pathogens for which novel antibiotics need to be developed [13]. The ESKAPE pathogens, like many other drug-resistant microbes, exhibit multiple mechanisms of resistance [10–12]. However, like any pathogen,

the tendency of these microbes to form biofilms makes them especially challenging to treat [14]. A biofilm is defined as a structured polymicrobial population which adheres to either abiotic and biotic surfaces through specific (i.e., ligand–receptor interactions) or non-specific (i.e. ionic or electrostatic) interactions [10]. Biofilms can grow rapidly and produce characteristic extracellular matrices consisting of polysaccharides, lipids, proteins, and extracellular DNA. The polymicrobial nature and matrix composition makes the effective clearance of established biofilms more challenging than the eradication of planktonic pathogens [14–16]. Biofilms therefore act as a physical barrier preventing effective antimicrobial action whilst protecting resistant drug-tolerant persister cells [16]. Biofilms also allow for genetic transfer between resistant and non-resistant pathogens therefore increasing the risk of resistance development [16,17]. Although microbial biofilms are naturally found in the soil and can be beneficial for plant growth [18,19], the proliferation of pathogenic biofilms leads to the microbial contamination of water systems [20], hospital surfaces [21] medical devices [22,23], public transport surfaces [24], food packing [25] and processing environments [26,27] resulting in disease spread.

1.2.2 The global and national impact of AMR

The impact of AMR is difficult to quantify as many factors need to be considered. Statistical models in a study by Murray *et al.* [5] estimated that in 2019 approximately 4.95 million deaths were associated with, and 1.27 million deaths were directly caused by bacterial AMR, with Sub-Saharan Africa showing the highest death rate of 27.3 deaths per 100 000 cases. More than 1.5 million of the deaths associated with AMR were due to lower respiratory infections. The leading pathogens associated with the recorded AMR deaths include the six ESKAPE pathogens. These pathogens alone were responsible for 929 000 deaths attributable to AMR and 3.57 million associated to AMR with Methicillin-resistant *Staphylococcus aureus* (MRSA) causing >100 000 deaths and drug resistant *Escherichia coli* causing 50 000–100 000 deaths [5].

One of the largest threats in the medical industry is the aggressive nature of opportunistic infections and formation of biofilms in immuno-compromised individuals. According to the WHO, South Africa is one of the 30 high burden countries for both multi-drug resistant tuberculosis (MDR-TB) and HIV [28]. This high number of immuno-compromised individuals along with inadequate infrastructure and care may feed the development of resistant pathogens. Hospitalised patients often rely on the use of indwelling urinary catheters [22] and central vascular access devices (CVADs) [29] during treatment. However, catheter-

associated urinary tract infections (CAUTIs) and CVADs related bloodstream infections (BSI) are commonly associated with increased hospital-related infections and morbidities [29]. A study performed at the Red Cross War Memorial Children's Hospital in Cape Town (South Africa) found a high prevalence of bloodstream infections (BSI) in children undergoing chemotherapy. A total of 150 BSI episodes were recorded amongst 89 patients. Gram-positive bacteria, mainly *Streptococcus* and *Staphylococcus* species, was responsible for BSIs in 49 (44%) patients whereas a Gram-negative bacterium, *E. coli*, contributed to BSIs in 41 (37%) patients [29]. Together these microorganisms were responsible for 90% of the BSIs recorded [29].

S. aureus and *E. coli* can be commonly found both on and in humans or animals and the surfaces they interact with. Although the presence of these bacteria can be harmless, the pathogenesis and rapid multiplication of these organisms at room temperature make them an overwhelming threat for microbial contamination [12,27]. Moreover, the transmission and the subsequent production of bacterial toxins is a risk for contamination and disease spread [15,27]. Another major contributor to the dilemma of AMR is the prevalence of drug-resistant microbes in agriculture, spread of foodborne diseases and resistance [30]. Some of the bacteria associated with foodborne illnesses include *Listeria monocytogenes* [30], *E. coli* [27,31] and *S. aureus* [27,32]. Although sanitary measures are taken in such practices, the bacterial matrix of biofilms often resists the penetration of disinfectants and other biocides commonly used making effective disinfection of contact surfaces challenging [14]. *L. monocytogenes* has been shown to form biofilms on both hydrophobic and hydrophilic surfaces frequently used in food processing environments including plastic, stainless steel and even Teflon® [25,30]. While *S. aureus* and *E. coli* are frequently detected in dairy and meat processing environments [26,27,31].

In South Africa farmers are legally allowed to purchase veterinary drugs without a prescription under the Stock Remedies Act (Act 36 of 1947) [33] this unmediated use of antimicrobials is a risk factor for resistance development [6,27]. Although South Africa is responsible for the production and supply of livestock and meat products across the African continent [1, 3], a study conducted by Jaja *et al.* [27] found multiple antibiotic resistance phenotypes in *S. aureus* and *E. coli* isolates in meat from both formal and informal meat processing sectors in South Africa. While a similar study reported biofilm forming MDR *L. monocytogenes* isolates in water (boreholes and rivers) and food (meat, vegetables and milk off-the shelf) samples randomly collected in the North West province of South Africa

[34]. Unfortunately, as aforementioned, a major draw-back in the fight against drug-resistant pathogens and biofilms is the lack of novel antimicrobial classes (Fig. 1.1) [2–4,6,7]. Meanwhile. the increased prevalence of resistant microbes and the seemingly inescapable need for antimicrobial use continues to raise concern on the potentially life-changing impact of AMR [1,5,13]. The development of novel antimicrobials and antimicrobial treatments is therefore imperative, not only in the context of South Africa, but globally as well [3,7].

1.3 Alternative antimicrobials

1.3.1 Antimicrobial peptides

Antimicrobial peptides (AMPs) are a group of antimicrobials naturally produced by organisms across the prokaryotic and eukaryotic kingdoms as part of their primary defence mechanisms [35,36]. A major benefit of AMPs is their widespread production, versatile biological function, and structural diversity. AMPs mostly differ from more traditional antibiotics by their alternate and broad range of inhibitory mechanisms towards a variety of cellular targets [37–39]. These characteristics, in turn, lower the likelihood of de novo resistance development against AMPs [3,39].These agents have therefore been noted as ideal alternatives to more conventional antimicrobial treatments against microbial infection, drug-resistant pathogens and biofilms [3,39,40]. A plethora of AMPs have already been discovered and synthesised across the globe and have been widely classified according to a variety of factors including: their biosynthetic machinery (i.e. ribosomal or non-ribosomal), biological sources (i.e. bacteria, fungi, plants, or animals), biological functions (i.e. antimicrobial, antifungal or anti-parasitic), peptide properties (i.e. charge, hydrophobicity, amino acid composition, or size), covalent bonding patterns (Class I to IV i.e. linear, cyclic, loop, knotted), secondary structures (i.e. α structures, β-structures, α- and β-structures, or undefined secondary structures) and molecular targets (i.e. cell surface or Intracellular targeting etc.) [36,41–43]. Fig. 1.3 shows the total number of AMPs recorded in the database of antimicrobial activity and structure of peptides (DBAASP) according to their biosynthetic machinery, reported synergy and antimicrobial activity against *S. aureus* and *E. coli* [1,2]. Table 1.1 summarises some of the common biological functions of AMPS currently recorded on antimicrobial peptide database (ADP) hosted by the University of Nevada [36,43].

Table 1.1 Summary of structural classes and select biological functions of AMPs currently recorded and adapted from APD (University of Nevada) [36,43].

Structural Class	**Number of AMPs***	**Percentage (%) ***
Unknown 3D structure	2166	60.8
α-helical	513	14.4
α-helical and β-sheet	121	3.4
unusual amino acid rich	114	3.2
β-sheet	89	2.5
Neither α-helical and β-sheet	24	0.7
Biological Function	**Number of AMPs***	**Percentage (%) ***
Antibacterial	3021	84.8
Antifungal	1277	35.8
Anticancer	271	7.6
Antiviral	201	5.6
Antiparasitic	140	3.9
Antibiofilm	81	2.3
Insecticidal	42	1.2
Anti-inflammatory	39	1.1
Enzyme/protease inhibitory	33	0.9
Antioxidant	31	0.9

*numbers and percentages based on total of 3563 AMPs recorded in the APD [36,43].

AMPs are often described by their biological functions (i.e., antibacterial) as shown in Table 1.1. However, to simplify scientific discussions, AMPs are more commonly divided into categories according to their secondary structures (α-helical, β-sheet, α-helical and β-sheet, non α- β, or unusual amino acid rich peptides) [36,44] and covalent bonding classes (linear, cyclic, looped, or knotted) [36,44]. Examples of AMPs categorised according to their secondary structures are shown in Fig. 1.2 and include: magainin 2 and human cathelicidin (LL-37) (Linear α-helical structures), bovine lactoferricin and human defensin 5 (β-sheet structures), *Pisum sativum* defensin 1 and human β-defensin 1 (α-helical and β-sheet structures), and indolicidin (no α or β structures). The diversity in structure and biological function of AMPs is complimented by their variety in modes of action (Table 1.1). β-sheet AMPs often contain hydrophobic and cationic amino acid residues allowing the formation of characteristic amphipathic secondary β-sheet structures. These amphipathic structures have been shown to associate with the hydrophobic bi-lipid membrane layer of microorganisms resulting in the disruption of the microbial membrane structure [35,37,45].

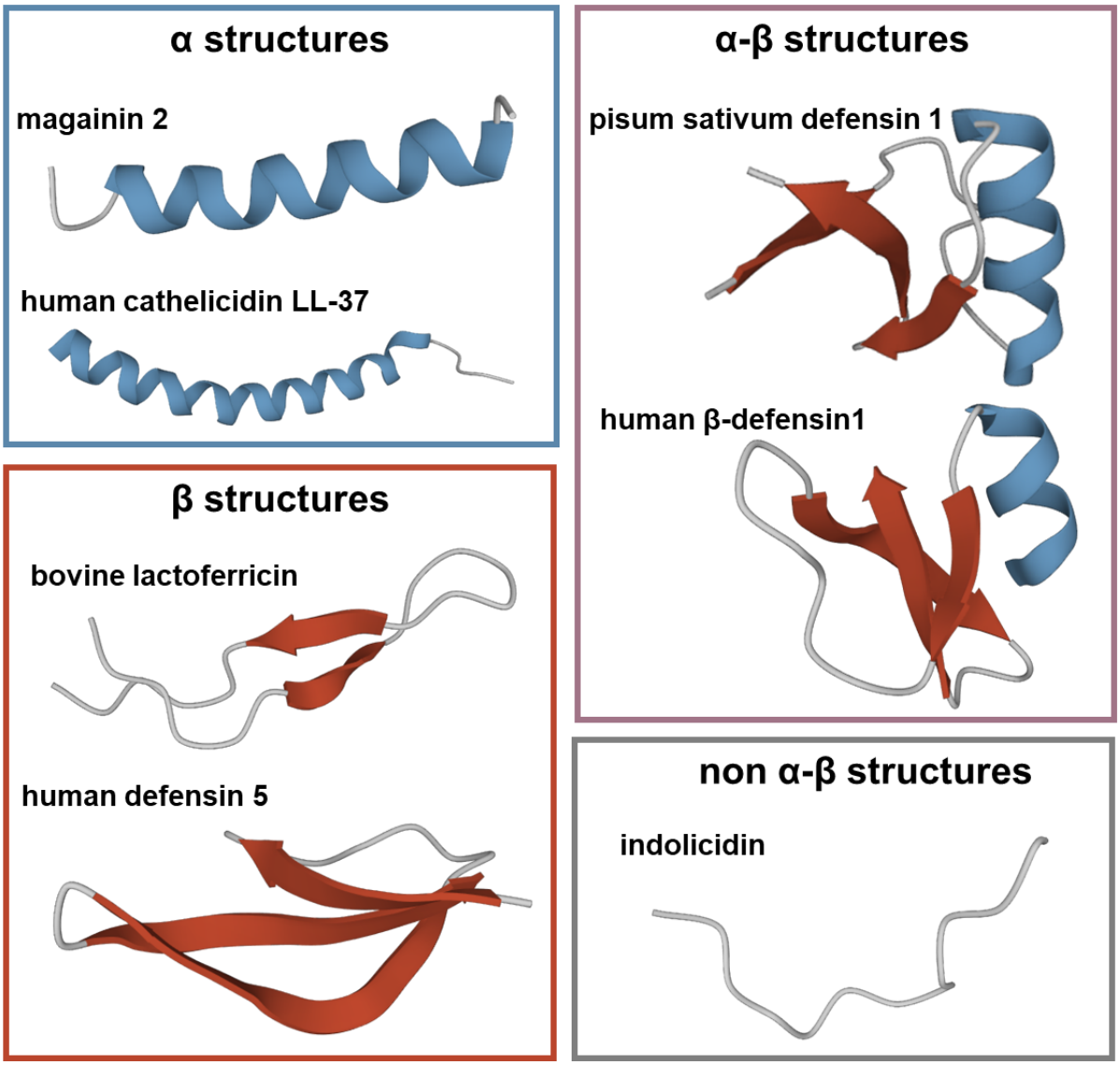

Figure 1.2 Examples of AMPs according to their 3-D secondary structure classifications. Images of AMPs were created using Protein Data Bank: magainin 2 (PBD ID: 2MAG, DOI: 10.2210/pdb2MAG/pdb), human cathelicidin LL-37 (PDB ID 2K6O; DOI:10.2210/pdb1LFC/pdb), bovine lactoferricin (PBD ID: 1LFC, DOI: 10.2210/pdb1LFC/pdb) human defensin 5 (PBD ID: 1ZMP DOI: 10.2210/pdb1ZMP/pdb), pisum sativum defensin (PBD ID: 11JKZ DOI: 10.2210/pdb1JKZ/pdb), human β-defensin1 (PBD ID: 1IJU, DOI: 10.2210/pdb1IJU/pdb), indolicidin (PBD ID: 1G89 DOI: 10.2210/pdb1G89/pdb).

Meanwhile, the cationic residues and net positive charge of some AMPs, allow for selective interactions with negatively charged bacterial cell membranes [35,37,45]. However, many other modes of actions have been reported. The multifaceted modes of action of AMPs (Fig. 1.5) have been extensively reviewed [3,44,46] and proposed to include (1) membrane alterations, (2) translation/transcription inhibition, (3) cell membrane formation inhibition, and (4) metabolic pathway inhibition [3,46]. A major benefit of membrane active antimicrobial agents is that target microbes would need to alter their membrane structures to achieve

resistance which is a much more complicated mechanism compared to more conventional mutations such as modifications in enzyme binding sites [47,48].

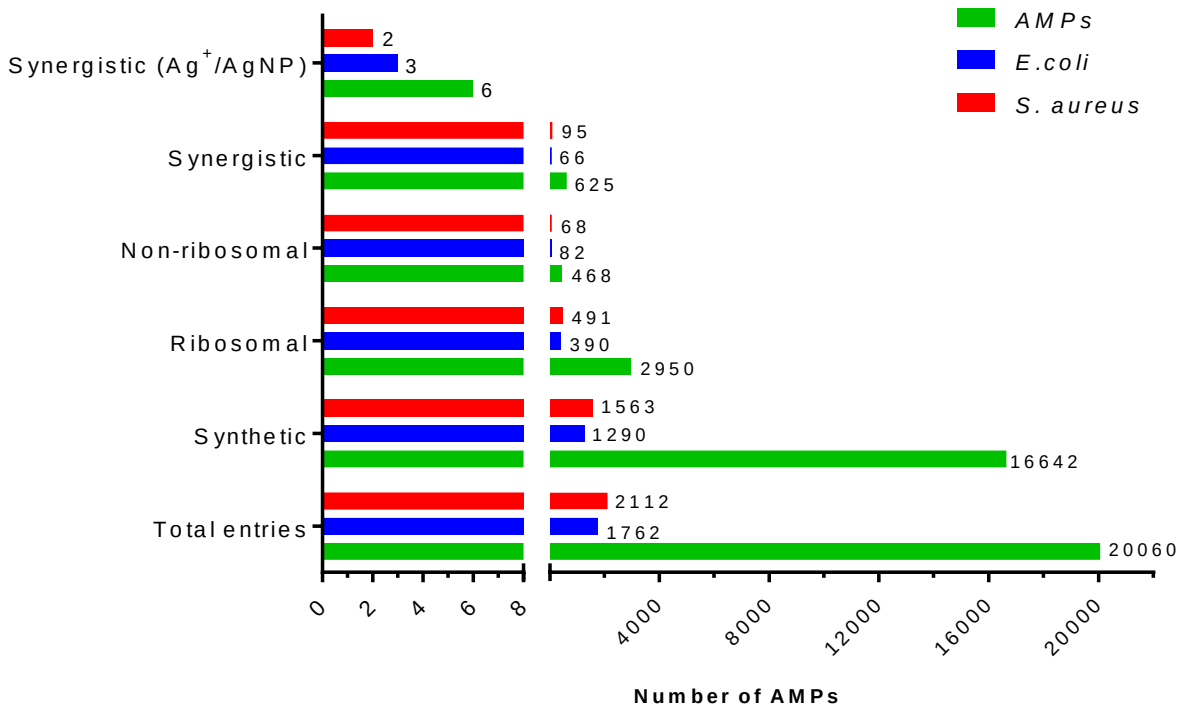

Figure 1.3 Total number of antimicrobial peptides (AMPs) recorded in DBAASP v 3.0 [41,42]. Total number of AMP entries for each criterion are indicated in green. AMPs that have antimicrobial activity recorded against Gram-negative *E. coli* are indicated in blue and Gram-positive *S. aureus* in red. Entry numbers are indicated at the end of each respective bar. Criteria include: synthesis type (synthetic, non-ribosomal or ribosomal), recorded antimicrobial synergy (synergistic) and recorded antimicrobial synergy against silver or silver nanoparticles (Synergistic (Ag^+/AgNP)). Entries are in accordance to date accessed [42].

Table 1.2 summarises four AMPs that have successfully registered for stage III clinical trials for applications in intravenous [49], oral [50,51], and topical applications [52]. Unfortunately, despite making it to phase 3 trails, most of these treatments have reported no improvement in activity compared to currently available alternatives [53]. Due to the nature of AMP structures and their closely related microbial action, chemical or conformational peptide modifications (specifically the introduction or substitution of charged amino acids or moieties), has been shown to have a major impact on the AMPs specificity and activity [54]. The manipulation of AMP characteristics via combinational therapies capable of modifying peptide structure has therefore become of increasing interest to improve the antimicrobial actions of AMPs and their drug delivery [3].

Table 1.2 Summary of AMPs in stage III clinical trials

Administration	Peptide name	Description	Treatment	Mechanism	Clinical Trial
Intravenous	Daptomycin	cyclic lipopeptide	bacteraemia	Membrane disruption/	NCT01922011
Oral	Nisin	lantibiotic	Gram-positive infections	Depolarization of cell membrane	NCT02928042
	Surotomycin	cyclic lipopeptide	Diaherria	Membrane disruption	NCT01597505
Topical	Gramicidin	Polycyclic peptide	Wounds	Membrane disruption	NCT00534391

Adapted from Martinez-Vazquez *et al.* [53].

1.3.2 Antimicrobial metal-derived nanomaterials

Another emerging field in antimicrobial treatment is metal-derived nanomaterials with inherent antimicrobial activity. Antimicrobial nanomaterials are distinctive in their physiochemical properties which allows application prospects in a variety of therapies including biomedical and agricultural fields [55–57]. A nanoparticle is defined as any particle of matter smaller than 100 nm in diameter. Metal nanoparticles (MNPs) have gained scientific interest due to their high surface-to-volume ratios and unique optical, electronic, and catalytic properties [3,58,59]. Silver, gold, copper, iron, magnesium, and zinc nanoparticles have all been investigated for nano fertilisers to promote crop growth and nano-pesticides to prevent crop disease [59]. Whilst in the medical field silver and gold nanoparticles have already been used for biosensing and biomedical treatments [60–62] and the development of new treatments continues to show promise for new applications against drug resistant pathogens. A study by Yang *et al.* has indicated potential use of pharmaceutical-capped gold nanoparticles for the treatment of drug resistant bacteria [60]. While another study [63] has shown potential for the treatment of drug resistant biofilms with silver nanoparticles (AgNPs). The use of silver in every-day practices is already popular, AgNPs have shown applications in medicine, agriculture, and industry as antimicrobial nanomaterials. Table 1.3 shortly summaries a selection of patented AgNP products and their applications in dental treatments [64], wound healing [64], food packing [65] and even water purification [66] within recent years [62].

Table 1.3 Patented AgNP products and applications.

Treatment	Product	Patent	Year
Dental	silver aqueous gel	US9192626B	2015
Wounds	AgNPs-polysaccharide gel matrix	WO2013050794A1	2013
Food packaging	AgNP treated polymer	US20080185311A1	2008
Water Purification	immobilised AgNPs in filters	WO2012140520A	2013

Adapted from Sim *et al.* [62].

Like AMPS an advantage of MNPs is their broad spectrum of activity and multiple modes of action which makes them unlikely to have resistance developed against them [3]. However, the antimicrobial mechanisms of MNPs are complex and depend strongly on the physiochemical properties of the nanoparticles [3,58]. Currently proposed modes of action [3], of MNPs are summarised in Fig. 1.5 and include (1) disruption of membrane permeability [67], (2) DNA and RNA interactions [68], (3) metal ion release and reactive oxygen species (ROS) [69]. MNPs have also been shown to inhibit the formation of biofilms [63]. Besides their multiple modes of action, MNPS also have many other characteristics that make them great alternatives to more traditional antimicrobials. One of the most promising characteristics is the synergistic effect MNPs tend to have when combined with other antimicrobials [70,71].

Fig. 1.3 shows the total number of AMPs submitted to the ADP that have shown synergistic activity with AgNPs. It's important to note here that the number of AMPs is not representative of mutually inclusive entries. The synergy of AMPs with silver therefore does not necessarily account for their antibacterial activity against *S. aureus* or *E. coli*. It should therefore be stated that of the six AMPs that have reported synergistic activity with silver, three have also shown activity against *E. coli,* and two have shown activity against *S. aureus*. However, upon investigation only two of these AMPs reported activity against *E. coli* when synergistically interacting with Ag^{+}/AgNPs. One of these peptides includes the β-sheet cyclic decapeptide gramicidin S [37,71]. Gramicidin S is an analogous peptide to cyclic decapeptides found in tyrothricin [72–74] which is discussed in further detail later in this chapter. The synergistic activity between AMPs and MNPs is an indicator of peptide-metal interactions capable of enhancing the antimicrobial action of these agents. The combination of AMPs with MNPs is therefore a promising avenue of investigation for the development of novel antimicrobial drugs and antimicrobial materials.

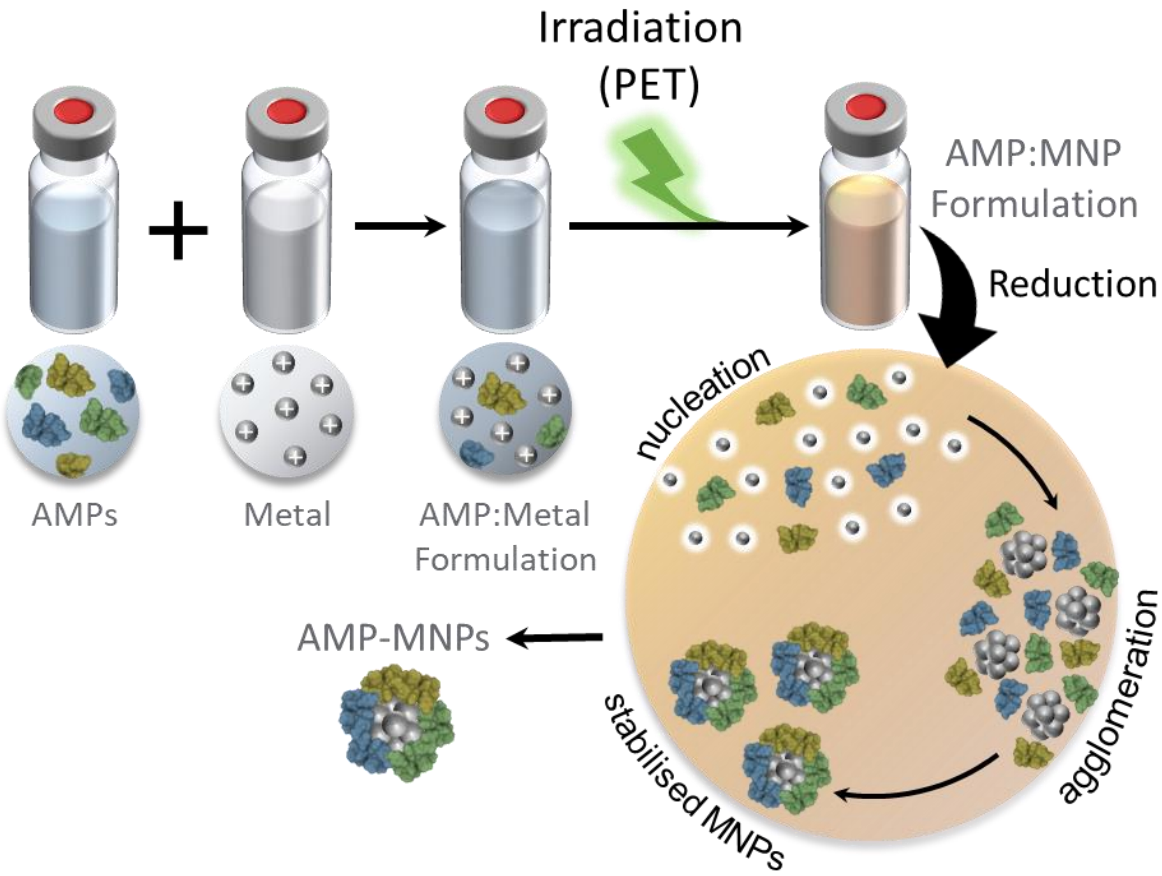

Figure 1.4 Schematic illustrating the proposed mechanism of photo-induced peptide-assisted MNP formation and subsequent green synthesis of AMP-MNP conjugates. Light irradiation of AMP:MNP formulations allows photo-induced electron transfer (PET) between AMP and metal ions accelerating the reduction reaction. Figure adapted from illustrations by Shah *et al.* [75] and the proposed role of AMPs in MNP fabrication by other studies [76,77].

Detailed accounts on MNP properties, synthesis methodologies and applications have been made. MNPs can be fabricated using one of two methods: top-down or bottom-up [78,79]. The top-down approach includes mechanical or physical breakdown of bulk metals into smaller nanostructures [78,79]. Whilst the bottom-up approach includes a variety of chemical methods [78,79]. Including two popular methodologies: photo-induced [80,81] and chemical-induced reduction [82–84]. More recently, the principles of photo-induced/chemical reduction methodologies have been reapplied using biological methods as a more cost effective and greener alternative to chemical synthesis of MNPs [3,75,80]. One of these biological methods of MNPs synthesis is the use of certain amino acids and peptides including AMPs [76,78,85,86]. Traditionally chemical synthesis requires three main components: metal precursors, reducing agents, and stabilising/capping agents to allow the reduction of metal salts and subsequent nucleation and growth of metal nanoparticles (see

Fig. 1.4) [84,87]. Studies have shown that peptides can, like traditional chemical capping and stabilisation agents, aid the reduction and stabilisation of metal particles [88,89] to allow the biosynthesis and growth of MNPs [76,77]. Moreover, the irradiation of peptide:metal mixtures, with a laser [80] or even sunlight [90], can be used as a tool to induce photo-electron transfer (PET) [88] to accelerate this biological reduction.

1.3.3 Combinational drug therapies

In more recent years, there has been an increased interest in combinational drug therapies because of the low probability of a pathogen developing resistance against the combined inhibitory mechanisms of antimicrobial agents. Moreover, synergism between antimicrobial agents in combination allows for the creation of drugs with an enhanced therapeutic index. Combinational therapies have already been shown to broaden the spectrum of activity and subsequently improve drug efficacy against multi-pathogen infections including ESKAPE pathogens [3,71,91–93]. Fig. 1.3 shows the number of AMPs that have reported synergistic activity when formulated with other antimicrobial agent, drugs, or materials. Similarly, MNPs have also shown to be synergistic when formulated with other agents [70] including AMPs [70,71,94]. The combinational therapy of these two antimicrobial agents therefore shows promise for improved activity due to combined antimicrobial action, and lowered risk of resistance development due to the combined modes of action (Fig. 1.5) [3].

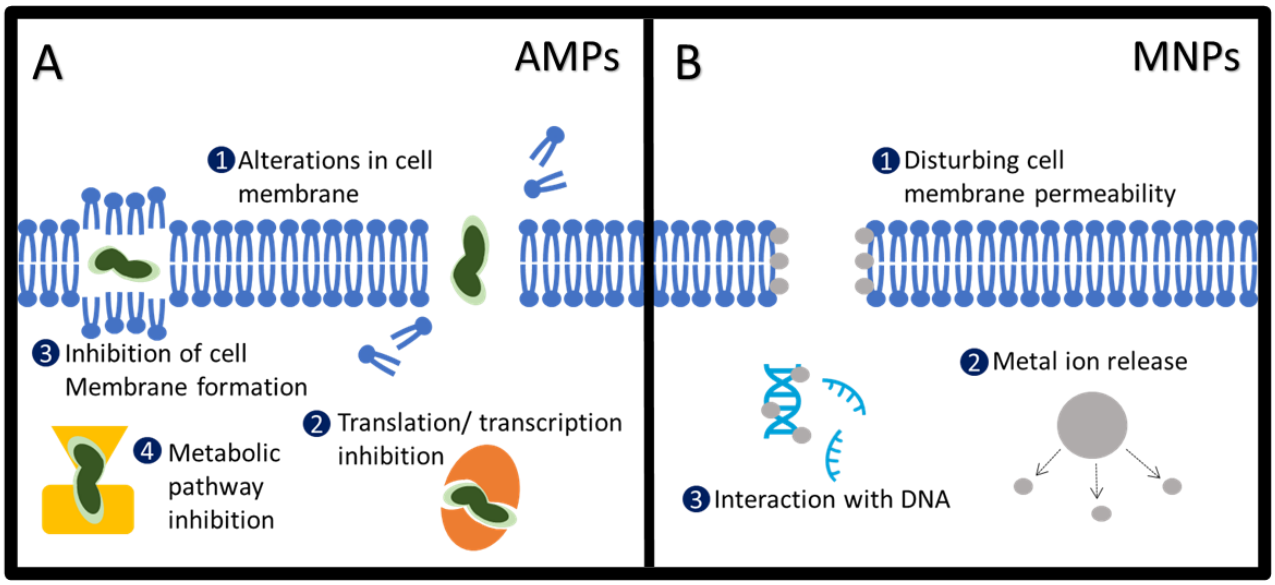

Figure 1.5 Schematic illustrating the common antimicrobial modes of action for (**A**) AMPs and (**B**) MNPs adapted from Leo-Buitimea *et al.* [3]

A major benefit of using AMPs for MNP synthesis is their variability in amino acids, amino acid sequences and thereby peptide structure. This versatility allows the synthesis of MNPs of different sizes, shapes, and compositions [78]. A study by Ramakrishan *et al.* [95] reported that peptides predictably formed specified configurations when interacting with platinum (Pt) nanoparticle structures, and that these configurations were dictated by peptide structure and peptide-Pt interactions. Meanwhile, a study by Gupta *et al.* [80] showed changes in the size and shape of AgNPs due to peptide concentration, structure and self-assembly. Moreover, this study showed that larger peptide structures engulf MNPs showing potential for the modulation of MNP drug delivery. The variability in peptide-metal interactions therefore allows the modulation of AMP-MNP drug structure and delivery [78,96].

1.3.4 AMP-MNP hybrids and the role of tryptophan in green synthesis

Several studies have already reported the formation of MNPs, aa-MNPs and peptide-MNP conjugates by formulations metals with aromatic amino acids and aromatic-amino acid containing peptides [76,77,97,98]. The intrinsic fluorescence of tryptophan and tryptophan-based peptides has become a popular tool to aid the characterisation and track the peptide-assisted fabrication of AMP-MNP hybrid nanostructures [76,99–106]. Multiple studies have reported interactions between aromatic residues and metal ions including co-ordination based complex formation and the reduction of certain ions [78,84,86,98,107–110]. Selvakannan *et al.* [85] reported the reduction of silver and gold ions, and subsequent AgNP and AUNP formation, is prompted by the ionization of tyrosine phenolic group. While Polavarapu *et al* [111] illustrated that histidine can be used as a stabiliser for AuNP synthesis. A study by Nasrolahi Shirazi *et al.* [77] further reported that aromatic-rich cyclic peptides can act as both a reducing and stabilising agent for the formation of AuNPs. While Ray *et al.* [112] proved that the absence of aromatic residues in oligopeptides fails to synthesise MNPs. Moreover, all these studies note the critical impact of peptide and residue structure/integrity and/or concentration on the formation of MNPs. The role of aromatic amino acids is thereby not only crucial for the synthesis of peptide-MNP conjugates but requires careful consideration when selecting aromatic-rich peptides.

1.4 The AMP complex of Tyrothricin

1.4.1 The tyrothricin complex and the tyrocidines

A potent antimicrobial, previously limited to topical applications, has gained a rejuvenated interest due to potent antimicrobial nature of the tyrothricin [48,113]. Tyrothricin is produced during the *Brevibacillus parabrevis's* sporulation phase via non-ribosomal pathways [114–116] making the tyrothricin peptides part of the 468 documented non-ribosomally produced peptides (Fig. 1.3) [41,42]. Interestingly, tyrothricin was the first antibiotic in clinical use in the 1940's [73,74,116] for topical applications due to its haemolytic characteristics [117]. Despite being widely used for topical treatments for years, comparisons between current and past MICs show little change in the tyrothricin's susceptibility to its broad spectrum of target microbes [113] which includes Gram-positive [37,47,118–121] bacteria, some Gram-negative bacteria [47,120,121], yeasts [93,122–124], filamentous fungi [125,126] and even malarial parasites [117,127].

The two peptide families found in the tyrothricin peptide complex include the basic cyclic tyrocidines (Trcs) and the neutral linear gramicidins (Grms) [114,128]. The Trcs and Grms are believed to be, like many AMPs, predominantly membrane lytic [37]. A major benefit of membrane active antimicrobial agents such as found in the tyrothricin complex is that target microbes would need to alter their membrane structures to achieve resistance which is a much more complicated mechanism compared to more conventional mutations such as modifications in enzyme binding sites [39,47,48,113]. However, Trcs have also shown other mechanisms of action including intracellular targets such as RNA transcription inhibition by interacting with DNA and resulting in hyperchromicity [129,130]. Both Trcs and Grms are rich in D-amino acids making them part of a small percentage (3.2 %) of AMPs (see Table 1.1) that have unusual amino acids [36,43]. The Trcs are also rich in hydrophobic amino acid side chains. The cyclic nature and presence of unusual amino and hydrophobic residues improve peptide stability in the presence of most proteolytic enzymes and could allow the peptide to bypass mechanisms of resistance such as enzymatic degradation [48].

1.4.2 Tryptophan-rich cyclodecapeptides

The Trcs are antimicrobial decapeptides with a highly conserved amino acid sequence, *cyclo*-(f^{1}P^{2}X^{3}x^{4}N^{5}Q^{6}X^{7}V^{8}O^{9}L^{10}) with variance in residues at positions 3, 4, 5, 7 and 9 giving rise to a large natural library of tyrocidines and tyrocidine analogues. Fig. 1.6 is an example of how individual amino acid substitutions gives rise to different Trcs. Amino acid variance

at position 7 (X^7) designates tyrocidines (Tyr^7), phenycidines (Phe^7) and tryptocidines (Trp^7) whilst variance in the dipeptide unit at position 3 and 4 (X^3x^4) allows for peptide analogues A (Phe^3Phe^4), B (Phe^3Trp^4 or Trp^3Phe^4) or C (Trp^3Trp^4). Substitution of ornithine at position 9 (O^9) with lysine (Lys^9) gives rise to the respective A_1, B_1 and C_1 analogues as shown in Fig. 1.6 with the case of Trc A and Trc A_1 [131–133]. The conserved amino acid sequence of Trcs and analogues make them structurally similar (refer Fig. 1.6). Moreover, these peptides have shown a high tendency to oligomerise and aggregate in different aqueous solutions [119,124,134–137]. This, in turn, makes the purification of single analogues from natural tyrothricin extracts challenging as reported by previous studies [105,115,126,128] and discussed in detail in Chapter 2 of this study. Although challenging to purify, the different tyrocidine analogues have shown promising broad-spectrum activity with proposed multiple modes of action [37,39,44,45,47,118,119,138–141].

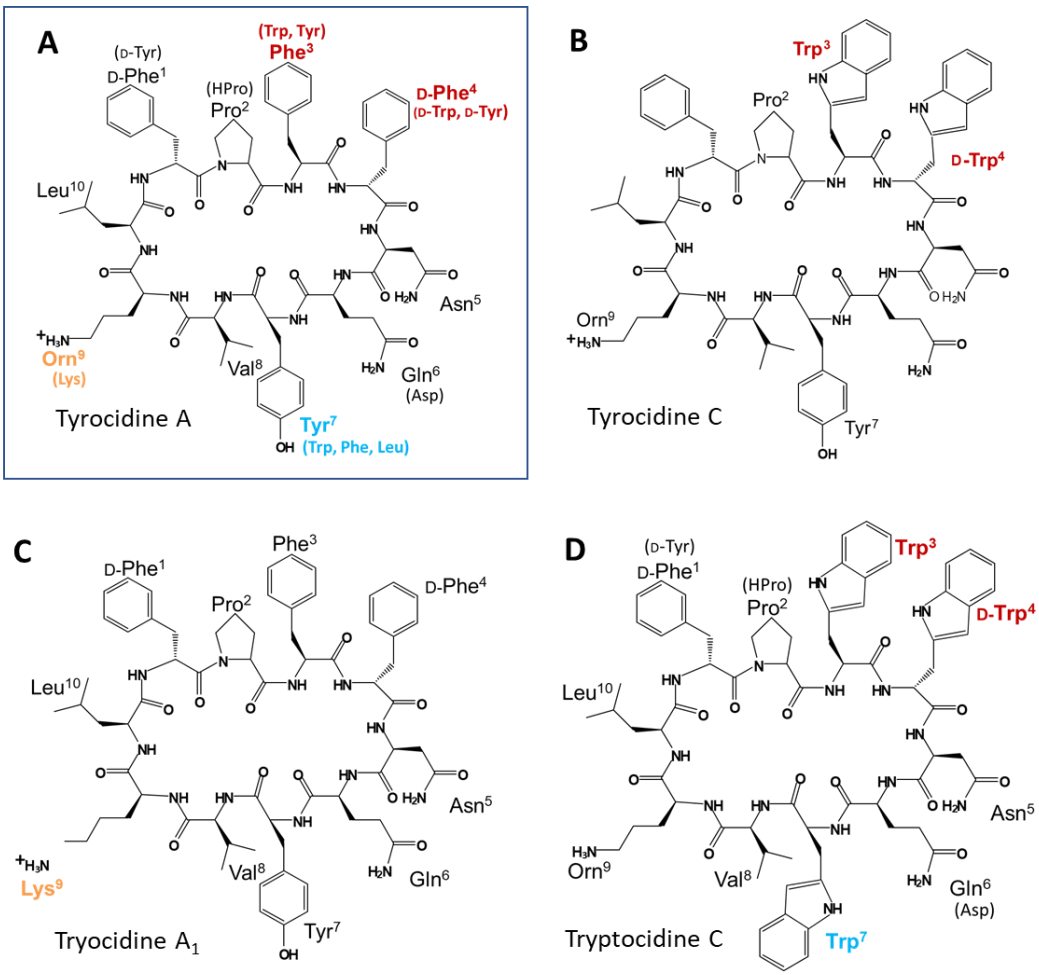

Figure 1.6 Cyclic decapeptide structures of Tyrocidines. The tyrocidine A (Trc A) structure (**A**) indicates the ammino acid residue variances in brackets at each respective residue position numbered 1 to 10. Variances at position 3 (red), 4 (red) and 7 (blue) and 9 (orange) give rise to tyrocidine C (**B**) tyrocidine A_1 (**C**) and tryptocidine C (**D**) analogues. Figure adapted from Wenzel *et al.* [37].

Since tyrothricin is naturally produced by *Br. parabrevis* [74], culturing conditions can be manipulated to favour the large-scale production of different peptide analogues as shown by Vosloo *et al.* [128]. Amino acid supplementation of producer cultures alters the peptide production profile of the producer by promoting amino acid substitutions within the tyrothricin complex resulting in a production preference of certain peptide analogues [115,128,131,142]. Not only does this production profile alteration ease purification, it is also a cost-effective tool to improve the yields and extract previously under-produced analogues like the tryptocidines (Tpcs) [115,128]. The isolation of single analogues is of interest due to favourable, yet analogue-specific, characteristics of the different peptides. Modification of tyrocidine A (TrcA) via single amino acid substitutions by Marques *et al.* [47] revealed that the antimicrobial activity of the peptide is dictated by the type, position, and abundance of amino acid residues likely due to the changes in the peptides' amphipathic nature. This is further supported by multiple findings which report differences in structure [45,133,142,143], oligomerisation [45,124,135,143], target specificity and activity [37,120,144] between peptide analogues. This variability in peptide analogues, although complex to characterise, allows the broad-spectrum activity of tyrothricin and its minimal risk of resistance development [73,113,116]. Moreover, the diversity in analogue character and behaviour is advantageous for the development and modification of novel drugs with distinct properties and/or versatile applications.

1.4.3 Tyrocidine's active structures, oligomerisation and self-assembly

Tyrocidines fall into the 2.50 % of β-sheet structured AMPs discovered (see Table 1.1). The β-sheet structure of Trcs allows the formation of a curved amphipathic dimer [45,124,143]. A study by Loll *et al.* [143] modelled how the stabilisation of the amphipathic dimer, through H-bonding and hydrophobic interactions, allows the peptide to integrate itself into the cell membrane of its target organism. The hydrophilic dimer region was shown to be facing the external environment whilst its hydrophobic counterpart interacts with the cell membrane. This dimeric structure disrupts the microbial bilipid membrane layer resulting in cell leakage and ultimately cell death [143]. A study by Munyuki *et al.* [45] proposed that these dimeric moieties also act as seeding units for the formation of pore-like structures within the cell membrane of target organisms. Tyrocidines have been shown to self-assemble into a variety of nanostructures [119,124,135–137,145]. Moreover, multiple studies have indicated that the structure and oligomerisation behaviour of tyrocidines dictate the antimicrobial efficacy of these agents and are largely influenced by the peptide concentration, analogue and

environment [37,47,118–120]. A study by Ruttenberg *et al.* [100] highlighted that although modification of TrcB aromatic ring structures prevents peptide aggregation, the lack of oligomerisation adversely impacted the bioactivity of the peptide. Rautenbach *et al.* [124] showed that although structurally similar peptide analogues TrcA, TrcC and TpcC (Fig. 1.6) all formed amphipathic type-U anti-parallel β-sheet dimeric structures, each analogue showed different oligomerisation preferences. TrcA preferred to form larger oligomeric structures while TpcC had the strongest propensity to form dimers. Wenzel *et al.* [37] noted that TrcC is more active than TrcA and suggested that the substitution of Phe with a Trp residue at position 3 and 4 (Fig. 1.6) improves the pore-forming capacity of TrcC. Yet, other studies have shown that structurally analogous TpcC, which has an additional Trp residue at position 7 (Fig. 1.6) is less active than TrcC [93,125,138].

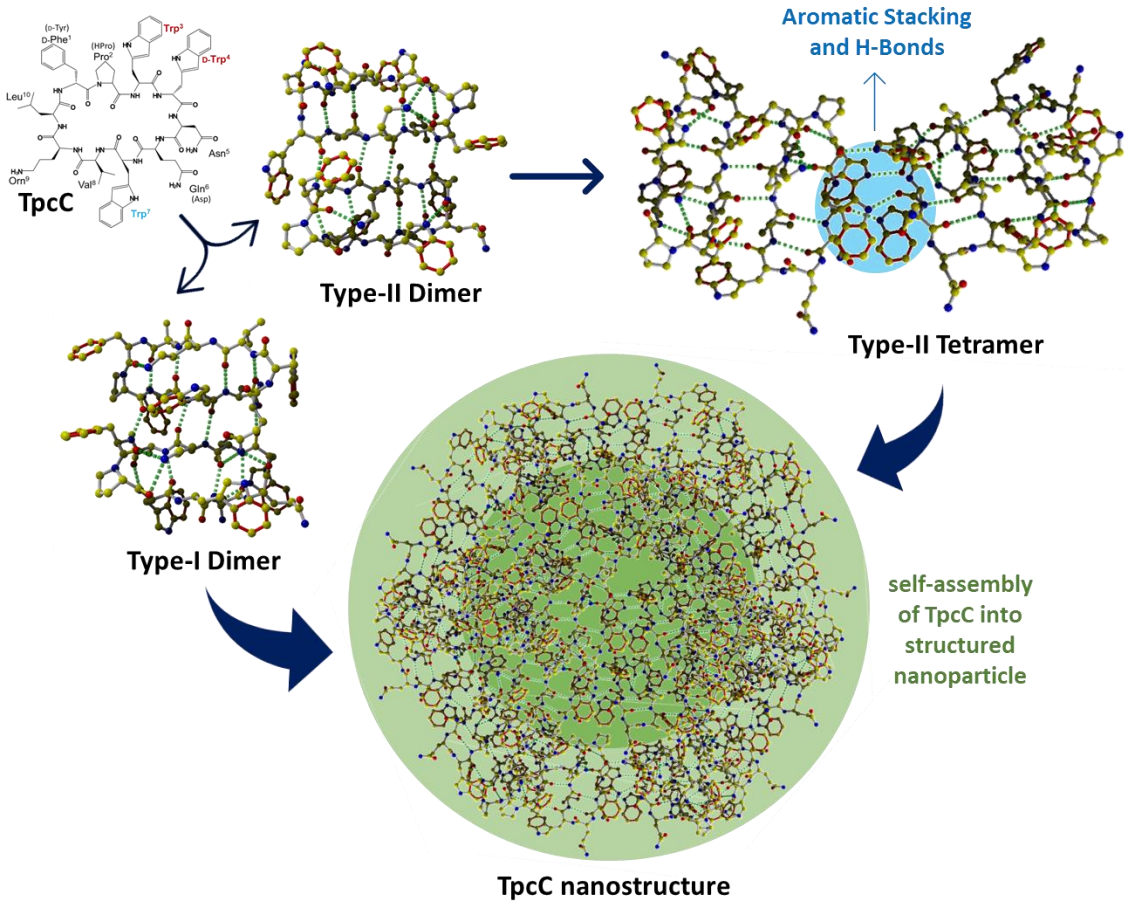

Figure 1.7 A schematic adapted from Rautenbach *et al.* [124] and Kumar *et al.* [119] representing the TpcC molecular modelling and docking (YASARA2) results of non-amphipathic Type-II (T-II) tryptocidine C dimer 3-D structure and its respective Type-II non-amphipathic β-sheet tetramer. Inter-molecular interactions (H-Bonds and aromatic stacking) are indicated by the blue circle. Type-II TpcC monomers, dimers, and oligomers form core (darker green) of the TpcC nanostructure, while non-amphipathic Type-I (T-I) TpcC structures (tetramer structure not shown) form the outer shell (light green) of the TpcC nanostructure. TpcC cyclic peptide structure (TpcC) is also shown.

As indicated by Ruttenberg *et al.*[100] peptide-assembly has been closely associated to the presence and interactions by/with aromatic amino acids [47,134]. Studies by Kumar *et al.*[119] illustrated the critical role of aromatic stacking and hydrophobic interactions between peptide monomers and dimers in the formation of larger antimicrobial TpcC nanostructures. The schematic in Fig. 1.7 illustrates the proposed intrinsic self-assembly dynamic of TpcC as described by Rautenbach *et al.* [124] and Kumar *et al.* [119]. These studies showed that TpcC forms two prominent dimeric structures, one amphipathic (T-I) and the other a non-amphipathic (T-II), which undergo ordered self-assembly to form larger TpcC nanostructures in ethanol-water solutions. It was proposed that the non-amphipathic moieties construct the core of these nano-assemblies while the amphipathic moieties assemble on the outer shell of the TpcC nanostructure and interact with the solution environment and/or target membranes. The intrinsic self-assembly and ordered oligomerisation of tyrocidines and analogues into different oligomeric structures likely play a role in the peptide's membrane interactions and therefore membranolytic activity.

1.5 Potential of tyrocidine formulations with metals

The tyrocidines have already shown promising applications as potent antimicrobial agents on their own and in formulation with different materials and drugs. Troskie *et al.* [93] reported the synergistic activity of different tyrocidines and tryptocidines against C. albicans biofilms when formulated with antifungal drugs caspofungin and amphotericin. While other studies have showed promise for maintained antimicrobial activity when formulated with celluloses [146–148]. The tyrocidines and analogues have shown potent activity against a variety of organisms including drug resistant Gram-positive bacteria such as *S. aureus* [37,47,118,119] and *L. monocytogenes* [120]. However, poor activity is shown against *E. coli* [47,120] The formulation of these cyclodecapeptides with metals, for example silver which has shown activity against Gram-negative bacteria such as *E. coli* [63,149,150], could improve the antibacterial activity of these peptides.

Previous work by Troskie *et al.* [120] also reported changes in the anti-fungal activity of different tyrocidine analogues when formulated with different metal chloride salts: magnesium (Mg^{2+}), calcium (Ca^{2+}), sodium (Na^{+}) and potassium (K^{+}). It was noted that the changes observed were both analogue and cation specific. In this study, the activity of a purified commercial tyrocidine mixture (Trc mix) and its A (TrcA), B (TrcB) and C (TrcC) analogues against fungal pathogens, *Fusarium solani* and *Botrytis cinerea*, was shown to be insensitive to the pre-incubation of peptides with metal chloride salts. All three peptides

maintained activity for 48 hours after exposure to doubly charged (Mg^{2+}) and singly charged (Na^{+} and K^{+}) metal cations while dose-dependent and analogue specific sensitivity was observed towards Ca^{2+} ions. The lack of sensitivity towards the di-valent Mg^{2+} ions indicated that the loss in activity after Ca^{2+} exposure was not due to ion-interference with peptide membranolytic interactions, but more likely the formation of peptide-Ca^{2+} complexes and subsequent alterations of peptide structure or oligomerisation/aggregation behaviour [45,117,131,143]. Although a loss in activity was observed in the case of these tyrocidines against Fungi, the results confirmed interactions between tyrocidines and metals and hinted towards the formation of peptide-metal complexes. Since green synthesis of MNPs requires the effective reduction and subsequent stabilisation of metal cations, the peptide-metal interactions proposed by Troskie *et al.* [120] therefore suggests that the tyrocidines may behave as both reducing and capping agents for the formation of MNPs (Fig. 1.7).

1.5.1 Trp-rich cyclodecapeptide-metal nanoparticle hybrids

As aforementioned, the role of aromatic amino acids is critical for the peptide-assisted green-synthesis of nanoparticles and that the choice of peptide dictates MNP fabrication. Interestingly, a study by Roy *et al.* [99] confirmed interactions between all three non-polar aromatic amino acids phenylalanine (Phe), tyrosine (Tyr) and tryptophan (Trp) with AgNPs. This work suggested that the aromatic residue not only partake in metal ion reduction but continue to interact with already synthesised MNPs. Meanwhile, research by Shoeib *et al.* [86] and Tan *et al.* [78] showed that tryptophan residues have a higher affinity for silver ions and therefore stronger binding and reduction ability than its other aromatic amino acid counterparts. Peptide structure stability and self-assembly has been strongly associated with the interactions between aromatic amino acids, particularly tryptophan, and their environment [96,106,119,124,151,152]. The Trp-driven self-assembly of peptides into nanostructures, and the interactions of these aromatic residues with MNPs, is therefore promising for the encapsulation of MNPs and formation of AMP-MNP hybrids with unique applications in drug-delivery [96]. A study by Mishra *et al.* [153] successfully reported that the self-assembly nature of a biotin-di-tryptophan peptide forms larger peptide nano-assemblies via aromatic stacking and that such structures are capable of encapsulating metal nanoparticles [154]. Since the tyrocidines are known to readily self-assemble into stable oligomeric structures, the application of such peptides in formulations with metals therefore holds the potential for encapsulation of MNPs. Moreover, the high-Trp amino acid composition of the Trcs makes them promising candidates for the fabrication of potent

cyclodecapeptide-metal nanoparticle (CDP-MNP) hybrids [47,103,119]. Formulation of these antimicrobial peptides with metals could therefore bridge the gap where peptides have previously shown poorer activity against certain target organisms. In turn, creating a novel nanodrug with broad spectrum activity and even lower risk of resistance development [3]. Moreover, the manipulation of *Br. parabrevis* producer cultures and subsequent isolation potent tryptophan-rich C analogues [128], for the use of such Trp-rich peptides for CDP-MNP hybrid fabrication could yield conjugates with improved and/or novel antimicrobial activity. Furthermore, the large-scale natural production of the tyrocidines and analogues may be a useful tool for upscaling the green synthesis of MNPs.

1.5.2 AMP-MNP surface applications and the potential for CDP-MNPs

The contamination of human and food contact surfaces and environments is a continual daily threat for the spread of disease. The incorporation of antimicrobials active agents into nanomaterials has become an avenue of investigation for the development of self-sterilising surfaces to prevent and/or treat surface contamination. Such surface treatments either prevent the adhesion of microbes to surfaces or eradicate microbes via slow-release or contact killing [155]. Thereby mitigating surface contamination, biofilm formation and disease spread. Two major requirements for the successful fabrication of surface treatment materials includes: (1) the incorporation of the active agent into the material and (2) the adhesion of such nanomaterials to the target surface [156]. Moreover, the stability of these surface nanomaterials is essential for effective treatment. The stable incorporation of active agents is commonly achieved via non-covalent interactions in formulation or polymer entanglement [156].Metal nanoparticles have already gained popularity for the incorporation into nanomaterials and nanoformulations for surface treatments (as shown in Table 1.3) with AgNPs being one of the more popular commercially available treatments due to their well-established bactericidal properties and topical biocompatibility [62]. Meanwhile cationic membranolytic antimicrobials have also gained interest for surface applications due to their mode of action and likelihood to bind with materials via non-covalent interactions [156,157]. Investigations of combinatorial therapies of antimicrobial peptides with AgNPs have therefore become particularly popular [3,158,159]. The preparation of AMP and AgNPs hybrids thereby presents an exciting new era of antimicrobial treatment [3]. Nonetheless, AMP-MNP combinations with gold, copper and zinc have also shown improved antimicrobial action against drug-resistant pathogens and have shown potential surface applications

[160–164] in fields such as agricultural practices [165], packaging [166] and industrial treatments [167].

Although combined therapies are of particular interest, the biochemical conjugation of organic materials to metals is an interesting nontechnological drug development technique itself [103]. The characteristic changes in metal colloids could be used as a convenient tool for the fabrication of antimicrobial peptide-incorporated nanomaterials [58]. These colour changes can thereby provide important information on the characteristics of MNPs in nanoformulations, in turn, minimising the time and money spent on further material characterisation. The streamlined, large-scale, and eco-friendly fabrication combined antimicrobial action rapid characterisation of AMP-MNP conjugate makes the application of these hybrid formulations a promising and economical alternative in topical or surface treatments. The creation of CDP-MNP hybrids therefore presents an exciting new era of antimicrobial surface treatment.

Van Rensburg *et al.* [146,168] noticed that the tyrocidines and analogues tend to adhere to certain celluloses and polystyrene surfaces. Further investigation and formulation of peptide with a variety of commercial materials (plastic, cling film and tissue paper) led to the development of a robust antimicrobial materials with strong antimicrobial action against *L monocytogenes*. These Trc-containing materials are now patented for applications to prevent microbial growth on surfaces [169]. The potential of Trcs for the fabrication of active nanomaterials and the applications of such materials in antimicrobial surface treatments has therefore already been established [146,168,169]. The broad-spectrum antimicrobial activity of tyrocidines, the role of tryptophan in the fabrication of metal nanoparticles, and the likelihood of MNP encapsulation via peptide self-assembly possesses exciting potential for the development of a novel CDP-MNP nanoformulations. Moreover, the fabrication and development of antimicrobial CDP-MNP surface treatments and/or nanomaterials holds great potential for biomedical, agricultural, and other commercial applications. Furthermore, the development of CDP-MNP materials and/or treatments could lead to patenting. The successful creation, biophysical analysis, and antimicrobial characterisation of CDP-MNP nanoformulations is therefore an essential first step towards developing this novel antimicrobial nanodrug.

An integral part in developing such nanoformulations would be the procurement of pure peptides. Although an aromatic residue-rich peptide mixture (Trc mix) can easily be isolated from a commercial tyrothricin via organic extractions, the production and isolation of

tryptophan rich C analogues will require the manipulation of *Br. parabrevis* producer cultures [74,93,123,128]. These naturally produced amphipathic peptides would need separated from their linear gramicidin counter parts in tyrothricin complex via organic solvent extraction purified using high performance liquid chromatography techniques to isolate single analogues of high purity (>90%) as confirmed by mass spectrometry analysis (see Chapter 2). Analysis of formulation of these peptides with different metals may give valuable insight on the peptide-metal interactions and could serve as an indicator of favourable peptide:metal combinations for the fabrication of CDP-MNP conjugates [170]. Moreover, this dynamic biophysical analysis could also highlight favourable or unfavourable changes in peptide structure or oligomerisation behaviour [124,171]. This, in turn, would serve as useful tool to indicate changes in antimicrobial action and peptide nano-assemblies (see Chapter 3). Nonetheless, the formation of CDP-MNP conjugates would still need to be confirmed, optimised, and characterised to define hybrid structures. Most importantly, these CDP-MNPs would need to be tested against model target organisms to determine interaction between agents and the viability of these conjugates for the incorporation and development of nanodrugs and nanomaterials for topical or surface applications (see Chapter 4).

1.6 References

[1] F. Prestinaci, P. Pezzotti, A. Pantosti, Antimicrobial resistance: a global multifaceted phenomenon, Pathog Glob Health. 109 (2015). https://doi.org/10.1179/2047773215Y.0000000030.

[2] World Health Organisation, Global Action Plan on Antimicrobial Resistance, Microbe Magazine. 10 (2015) 354–355. https://doi.org/10.1128/microbe.10.354.1.

[3] A. León-Buitimea, C.R. Garza-Cárdenas, J.A. Garza-Cervantes, J.A. Lerma-Escalera, J.R. Morones-Ramírez, The Demand for New Antibiotics: Antimicrobial Peptides, Nanoparticles, and Combinatorial Therapies as Future Strategies in Antibacterial Agent Design, Front Microbiol. 11 (2020). https://doi.org/10.3389/fmicb.2020.01669.

[4] K. Lewis, The Science of Antibiotic Discovery, Cell. 181 (2020) 29–45. https://doi.org/10.1016/J.CELL.2020.02.056.

[5] C.J. Murray, K.S. Ikuta, F. Sharara, L. Swetschinski, G. Robles Aguilar, A. Gray, C. Han, C. Bisignano, P. Rao, E. Wool, S.C., Global burden of bacterial antimicrobial resistance in 2019: a systematic analysis, The Lancet. 399 (2022) 629–655. https://doi.org/10.1016/S0140-6736(21)02724-0.

[6] World Health Organization, WHO Global Strategy for Containment of Antimicrobial Resistance, (2001) 1–50. https://doi.org/WHO/CDS/CSR/DRS/2001.2.

[7] World Health Organization, 2020 Antibacterial Agents in Clinical and Preclinical Development, 2021. https://www.who.int/publications/i/item/9789240021303.

[8] E. Tacconelli, E. Carrara, A. Savoldi, S. Harbarth, M. Mendelson, D.L. Monnet, C. Pulcini, G. Kahlmeter, J. Kluytmans, Y. Carmeli, M. Ouellette, K. Outterson, J. Patel, M. Cavaleri, E, Discovery, research, and development of new antibiotics: the WHO priority list of antibiotic-resistant bacteria and tuberculosis, Lancet Infect Dis. 18 (2018) 318–327. https://doi.org/10.1016/S1473-3099(17)30753-3.

[9] Y. Liu, J. Tan, A. Thomas, D. Ou-Yang, V.R. Muzykantov, The shape of things to come: Importance of design in nanotechnology for drug delivery, Ther Deliv. 3 (2012) 181–194. https://doi.org/10.4155/tde.11.156.

[10] H.-C. Flemming, J. Wingender, U. Szewzyk, P. Steinberg, S.A. Rice, S. Kjelleberg, Biofilms: an emergent form of bacterial life, Nature Publishing Group. (2016). https://doi.org/10.1038/nrmicro.2016.94.

[11] S. Santajit, N. Indrawattana, Mechanisms of Antimicrobial Resistance in ESKAPE Pathogens, Biomed Res Int. 2016 (2016). https://doi.org/10.1155/2016/2475067.

[12] G.M. Abebe, The Role of Bacterial Biofilm in Antibiotic Resistance and Food Contamination, Int J Microbiol. 2020 (2020) 1–10. https://doi.org/10.1155/2020/1705814.

[13] World Health Organization, Prioritization of pathogens to guide discovery, research, and development of new antibiotics for drug-resistant bacterial infections, including tuberculosis. World Health Organization, Geneva, 2017. https://apps.who.int/iris/handle/10665/311820.

[14] Y. Pan, F. Breidt, S. Kathariou, Resistance of Listeria monocytogenes biofilms to sanitizing agents in a simulated food processing environment, Appl Environ Microbiol. 72 (2006) 7711–7717. https://doi.org/10.1128/AEM.01065-06/FORMAT/EPUB.

[15] C. Hung, Y. Zhou, J.S. Pinkner, K.W. Dodson, J.R. Crowley, J. Heuser, M.R. Chapman, M. Hadjifrangiskou, J.P. Henderson, S.J. Hultgren, *Escherichia coli* biofilms have an organized and complex extracellular matrix structure, MBio. 4 (2013) 1–10. https://doi.org/10.1128/mBio.00645-13.

[16] K. Lewis, Persister cells, dormancy and infectious disease, Nat Rev Microbiol. 5 (2007) 48–56. https://doi.org/10.1038/nrmicro1557.

[17] W. DeFlorio, S. Liu, A.R. White, T.M. Taylor, L. Cisneros-Zevallos, Y. Min, E.M.A. Scholar, Recent developments in antimicrobial and antifouling coatings to reduce or prevent contamination and cross-contamination of food contact surfaces by bacteria, Compr Rev Food Sci Food Saf. 20 (2021) 3093–3134. https://doi.org/10.1111/1541-4337.12750.

[18] W.A. Kasim, R.M. Gaafar, R.M. Abou-Ali, M.N. Omar, H.M. Hewait, Effect of biofilm forming plant growth promoting rhizobacteria on salinity tolerance in barley, Annals of Agricultural Sciences. 61 (2016) 217–227. https://doi.org/10.1016/J.AOAS.2016.07.003.

[19] S. Gouda, R.G. Kerry, G. Das, S. Paramithiotis, H.S. Shin, J.K. Patra, Revitalization of plant growth promoting rhizobacteria for sustainable development in agriculture, Microbiol Res. 206 (2018) 131–140. https://doi.org/10.1016/J.MICRES.2017.08.016.

[20] J. Wingender, H.C. Flemming, Biofilms in drinking water and their role as reservoir for pathogens, Int J Hyg Environ Health. 214 (2011) 417–423. https://doi.org/10.1016/j.ijheh.2011.05.009.

[21] J.T. Freeman, J. Nimmo, E. Gregory, A. Tiong, M. de Almeida, G.N. McAuliffe, S.A. Roberts, Predictors of hospital surface contamination with Extended-spectrum β-lactamase-producing *Escherichia coli* and *Klebsiella pneumoniae*: Patient and organism factors, Antimicrob Resist Infect Control. 3 (2014) 1–7. https://doi.org/10.1186/2047-2994-3-5.

[22] J.M. Schierholz, J. Beuth, Implant infections: A haven for opportunistic bacteria, Journal of Hospital Infection. (2001). https://doi.org/10.1053/jhin.2001.1052.

[23] B. Gottenbos, H.C. van der Mei, H.J. Busscher, Initial adhesion and surface growth of Staphylococcus epidermidis and Pseudomonas aeruginosa on biomedical polymers, J Biomed Mater Res. 50 (2000) 208–214. https://doi.org/10.1002/(SICI)1097-4636(200005)50:2<208:AID-JBM16>3.0.CO;2-D.

[24] J.A. Otter, G.L. French, Bacterial contamination on touch surfaces in the public transport system and in public areas of a hospital in London, Lett Appl Microbiol. 49 (2009) 803–805. https://doi.org/10.1111/J.1472-765X.2009.02728.X.

[25] S. Stepanović, I. Ćirković, L. Ranin, M. Švabić-Vlahović, Biofilm formation by *Salmonella spp*. and *Listeria monocytogenes* on plastic surface, Lett Appl Microbiol. 38 (2004) 428–432. https://doi.org/10.1111/J.1472-765X.2004.01513.X.

[26] P. Pacha, M. Munoz, G. González-Rocha, I. San Martín, M. Quezada-Aguiluz, A. Aguayo-Reyes, H. Bello-Toledo, A. Latorre, Molecular diversity of *Staphylococcus aureus* and the role of milking

equipment adherences or biofilm as a source for bulk tank milk contamination, J Dairy Sci. 104 (2021) 3522–3531. https://doi.org/10.3168/jds.2020-19121.

[27] I.F. Jaja, C.-J.I. Jaja, N.V. Chigor, M.U. Anyanwu, E.K. Maduabuchi, J.W. Oguttu, E. Green, Antimicrobial Resistance Phenotype of *Staphylococcus aureus* and Escherichia coli Isolates Obtained from Meat in the Formal and Informal Sectors in South Africa, Biomed Res Int. 2020 (2020) 1–11. https://doi.org/10.1155/2020/3979482.

[28] World Health Organization, Global tuberculosis report 2015, World Health Organization. 14 (2015) 1–192. https://apps.who.int/iris/handle/10665/191102 (accessed January 10, 2023).

[29] T. Mvalo, B. Eley, C. Bamford, C. Stanley, M. Chagomerana, M. Hendricks, A. van Eyssen, A. Davidson, Bloodstream infections in oncology patients at Red Cross War Memorial Children's Hospital, Cape Town, from 2012 to 2014, International Journal of Infectious Diseases. 77 (2018) 40–47. https://doi.org/10.1016/j.ijid.2018.09.012.

[30] I.C. Blackman, J.F. Frank, Growth of Listeria monocytogenes as a Biofilm on Various Food-Processing Surfaces, J Food Prot. 59 (1996) 827–831. http://meridian.allenpress.com/jfp/article-pdf/59/8/827/1666294/0362-028x-59_8_827.pdf (accessed December 22, 2022).

[31] A.P. Williams, L.M. Avery, K. Killham, D.L. Jones, Persistence of *Escherichia coli* O157 on farm surfaces under different environmental conditions, J Appl Microbiol. 98 (2005) 1075–1083. https://doi.org/10.1111/j.1365-2672.2004.02530.x.

[32] D. Gutiérrez, S. Delgado, D. Vázquez-Sánchez, B. Martínez, M.L. Cabo, A. Rodríguez, J.J. Herrera, P. García, Incidence *of Staphylococcus aureus* and Analysis of Associated Bacterial Communities on Food Industry Surfaces, Appl Environ Microbiol. 78 (2012) 8547–8554. https://doi.org/10.1128/AEM.02045-12.

[33] G. Gazette, G. Notice, Fertilizers, Farm Feeds, Agricultural Remedies and Stock Remedies Act: South African Policy on Animal Feeds, (2008).

[34] C.-D. Kaptchouang Tchatchouang, J. Fri, M. de Santi, G. Brandi, G.F. Schiavano, G. Amagliani, C.N. Ateba, microorganisms Listeriosis Outbreak in South Africa: A Comparative Analysis with Previously Reported Cases Worldwide, (n.d.). https://doi.org/10.3390/microorganisms8010135.

[35] H. Jenssen, P. Hamill, R.E.W. Hancock, Peptide Antimicrobial Agents, Clin Microbiol Rev. 19 (2006) 491–511. https://doi.org/10.1128/CMR.00056-05.

[36] G. Wang, X. Li, Z. Wang, Antimicrobial Peptide Database, University of Nebraska, Medical Center. (2021). https://aps.unmc.edu/ (accessed January 7, 2023).

[37] M. Wenzel, M. Rautenbach, J.A. Vosloo, T. Siersma, C.H.M. Aisenbrey, E. Zaitseva, W.E. Laubscher, W. van Rensburg, J.C. Behrends, B. Bechinger, L.W. Hamoen, The Multifaceted Antibacterial Mechanisms of the Pioneering Peptide Antibiotics Tyrocidine and Gramicidin S, MBio. 9 (2018). https://doi.org/10.1128/mBio.00802-18.

[38] K. Hilpert, B. McLeod, J. Yu, M.R. Elliott, M. Rautenbach, S. Ruden, J. Bürck, C. Muhle-Goll, A.S. Ulrich, S. Keller, R.E.W. Hancock, Short Cationic Antimicrobial Peptides Interact with ATP, Antimicrob Agents Chemother. 54 (2010) 4480–4483. https://doi.org/10.1128/AAC.01664-09.

[39] M. Rautenbach, J.W. Hastings, Cationic peptides with antimicrobial activity - The new generation of antibiotics ?, Chim Oggi. 17 (1999) 81–89.

[40] N. Delattin, K. de Brucker, K. de Cremer, B. P.A. Cammue, K. Thevissen, Antimicrobial Peptides as a Strategy to Combat Fungal Biofilms, Curr Top Med Chem. 17 (2017) 604–612. https://doi.org/10.2174/1568026616666160713142228.

[41] Antimicrobial Peptide Database - DBAASP, (n.d.). https://dbaasp.org/home (accessed January 7, 2023).

[42] M. Pirtskhalava, A.A. Amstrong, M. Grigolava, M. Chubinidze, E. Alimbarashvili, B. Vishnepolsky, A. Gabrielian, A. Rosenthal, D.E. Hurt, M. Tartakovsky, DBAASP v3: Database of antimicrobial/cytotoxic activity and structure of peptides as a resource for development of new therapeutics, Nucleic Acids Res. 49 (2021) D288–D297. https://doi.org/10.1093/nar/gkaa991.

[43] G. Wang, X. Li, Z. Wang, APD3: The antimicrobial peptide database as a tool for research and education, Nucleic Acids Res. 44 (2016) D1087–D1093. https://doi.org/10.1093/nar/gkv1278.

[44] M. Rautenbach, A.M. Troskie, J.A. Vosloo, Antifungal peptides: To be or not to be membrane active, Biochimie. 130 (2016) 132–145. https://doi.org/10.1016/j.biochi.2016.05.013.

[45] G. Munyuki, G.E. Jackson, G.A. Venter, K.E. Kövér, L. Szilágyi, M. Rautenbach, B.M. Spathelf, B. Bhattacharya, D. van der Spoel, β-sheet structures and dimer models of the two major tyrocidines, antimicrobial peptides from *Bacillus aneurinolyticus*, Biochemistry. 52 (2013) 7798–7806. https://doi.org/10.1021/bi401363m.

[46] L.T. Nguyen, E.F. Haney, H.J. Vogel, The expanding scope of antimicrobial peptide structures and their modes of action, Trends Biotechnol. 29 (2011) 464–472. https://doi.org/10.1016/j.tibtech.2011.05.001.

[47] M.A. Marques, D.M. Citron, C.C. Wang, Development of Tyrocidine A analogues with improved antibacterial activity, Bioorg Med Chem. 15 (2007) 6667–6677. https://doi.org/10.1016/j.bmc.2007.08.007.

[48] C. Lang, C. Staiger, Tyrothricin - An underrated agent for the treatment of bacterial skin infections and superficial wounds?, Pharmazie. 71 (2016) 299–305. https://doi.org/10.1691/ph.2016.6038.

[49] J.S. Bradley, A.C. Arrieta, V.A. Digtyar, M.W. Popejoy, A. Grandhi, P. Bokesch, E. Hershberger, M.B. Dorr, C.M. Tan, Y. Murata, D.J. Wolf, M. Bensaci, Daptomycin for Pediatric Gram-Positive Acute Hematogenous Osteomyelitis, Pediatric Infectious Disease Journal. 39 (2020) 814–823. https://doi.org/10.1097/INF.0000000000002790.

[50] Y. Alexandre, R. le Berre, G. Barbier, G. le Blay, Screening of Lactobacillus spp. for the prevention of Pseudomonas aeruginosa pulmonary infections, BMC Microbiol. 14 (2014) 107. https://doi.org/10.1186/1471-2180-14-107.

[51] V. Boix, R.N. Fedorak, K.M. Mullane, Y. Pesant, U. Stoutenburgh, M. Jin, A. Adedoyin, L. Chesnel, D. Guris, K.B. Larson, Y. Murata, Primary Outcomes From a Phase 3, Randomized, Double-Blind, Active-Controlled Trial of Surotomycin in Subjects With Clostridium difficile Infection, Open Forum Infect Dis. 4 (2017). https://doi.org/10.1093/ofid/ofw275.

[52] P. Hirunwiwatkul, K. Wachirasereechai, Effectiveness of combined antibiotic ophthalmic solution in the treatment of hordeolum after incision and curettage: a randomized, placebo-controlled trial: a pilot study., J Med Assoc Thai. 88 (2005) 647–650.

[53] M. Martinez-Vazquez, S. Gonçalves, P. Bergman, K. Institutet, K.I. Sweden, B.K.H.L. Boekema, G.S. Dijksteel, M.M.W. Ulrich, E. Middelkoop, Review: Lessons Learned From Clinical Trials Using Antimicrobial Peptides (AMPs), (2021). https://doi.org/10.3389/fmicb.2021.616979.

[54] K. Scheinpflug, H. Nikolenko, I. v. Komarov, M. Rautenbach, M. Dathe, What goes around comes around-A comparative study of the influence of chemical modifications on the antimicrobial properties of small cyclic peptides, Pharmaceuticals. 6 (2013) 1130–1144. https://doi.org/10.3390/ph6091130.

[55] R. Bhatia, D. Gulati, G. Sethi, Biofilms and nanoparticles: applications in agriculture, Folia Microbiol (Praha). 66 (2021) 159–170. https://doi.org/10.1007/s12223-021-00851-7.

[56] M. Guzman, J. Dille, S. Godet, Synthesis and antibacterial activity of silver nanoparticles against gram-positive and gram-negative bacteria, Nanomedicine. 8 (2012) 37–45. https://doi.org/10.1016/j.nano.2011.05.007.

[57] M. Carbone, D.T. Donia, G. Sabbatella, R. Antiochia, Silver nanoparticles in polymeric matrices for fresh food packaging, J King Saud Univ Sci. 28 (2016) 273–279. https://doi.org/10.1016/J.JKSUS.2016.05.004.

[58] K.L. Kelly, E. Coronado, L.L. Zhao, G.C. Schatz, The optical properties of metal nanoparticles: The influence of size, shape, and dielectric environment, Journal of Physical Chemistry B. 107 (2003) 668–677. https://doi.org/10.1021/jp026731y.

[59] H. Chhipa, Nanofertilizers and nanopesticides for agriculture, Environ Chem Lett. 15 (2017) 15–22. https://doi.org/10.1007/s10311-016-0600-4.

[60] X. Yang, J. Yang, L. Wang, B. Ran, Y. Jia, L. Zhang, G. Yang, H. Shao, X. Jiang, Pharmaceutical Intermediate-Modified Gold Nanoparticles: Against Multidrug-Resistant Bacteria and Wound-Healing Application via an Electrospun Scaffold, ACS Nano. 11 (2017) 5737–5745. https://doi.org/10.1021/acsnano.7b01240.

[61] L. Wang, C. Hu, L. Shao, The antimicrobial activity of nanoparticles: Present situation and prospects for the future, Int J Nanomedicine. 12 (2017) 1227–1249. https://doi.org/10.2147/IJN.S121956.

[62] W. Sim, R. Barnard, M.A.T. Blaskovich, Z. Ziora, Antimicrobial Silver in Medicinal and Consumer Applications: A Patent Review of the Past Decade (2007–2017), Antibiotics. 7 (2018) 93. https://doi.org/10.3390/antibiotics7040093.

[63] K. Kalishwaralal, S. BarathManiKanth, S.R.K. Pandian, V. Deepak, S. Gurunathan, Silver nanoparticles impede the biofilm formation by Pseudomonas aeruginosa and Staphylococcus epidermidis, Colloids Surf B Biointerfaces. 79 (2010) 340–344. https://doi.org/10.1016/j.colsurfb.2010.04.014.

[64] M. Miraftab, Polysaccharide Fibres for Wound Dressings., WO2013050794A1, 2013.

[65] R.A. Maggio, R.C. Pearson, Rotationally Molded Plastic Refuse Container with Microbial Inhibiting Inner Surface and Method, US20080185311A1, 2008.

[66] T. Pradeep, A. Chaudhary, M.U. Sankar, G. Rajarajan, Sustained Silver Release Composition for Water Purification, WO2012140520A, 2013.

[67] K.J. Woo, C.K. Hye, W.K. Ki, S. Shin, H.K. So, H.P. Yong, Antibacterial activity and mechanism of action of the silver ion in *Staphylococcus aureus* and *Escherichia coli*, Appl Environ Microbiol. 74 (2008) 2171–2178. https://doi.org/10.1128/AEM.02001-07.

[68] R.M. Izatt, J.J. Christensen, J.H. Rytting, Sites and thermodynamic quantities associated with proton and metal ion interaction with ribonucleic acid, deoxyribonucleic acid, and their constituent bases, nucleosides, and nucleotides, Chem Rev. 71 (1971) 439–481. https://doi.org/10.1021/cr60273a002.

[69] M. Pratap Reddy, A. Venugopal, M. Subrahmanyam, Hydroxyapatite-supported Ag–TiO2 as Escherichia coli disinfection photocatalyst, Water Res. 41 (2007) 379–386. https://doi.org/10.1016/j.watres.2006.09.018.

[70] C. Bankier, R.K. Matharu, Y.K. Cheong, G.G. Ren, E. Cloutman-Green, L. Ciric, Synergistic Antibacterial Effects of Metallic Nanoparticle Combinations, Sci Rep. 9 (2019) 16074. https://doi.org/10.1038/s41598-019-52473-2.

[71] S. Ruden, K. Hilpert, M. Berditsch, P. Wadhwani, A.S. Ulrich, Synergistic interaction between silver nanoparticles and membrane-permeabilizing antimicrobial peptides, Antimicrob Agents Chemother. 53 (2009) 3538–3540. https://doi.org/10.1128/AAC.01106-08.

[72] A.L. Llamas-Saiz, G.M. Grotenbreg, M. Overhand, M.J. Van Raaij, Double-stranded helical twisted β-sheet channels in crystals of gramicidin S grown in the presence of trifluoroacetic and hydrochloric acids, Acta Crystallogr D Biol Crystallogr. 63 (2007) 401–407. https://doi.org/10.1107/S0907444906056435.

[73] R.J. Dubos, R.D. Hotchkiss, A.F. Coburn, the Effect of Gramicidin and Tyrocidine on Bacterial Metabolism, Journal of Biological Chemistry. 146 (1942) 421–426. https://doi.org/10.1016/s0021-9258(18)44961-7.

[74] R.D. Hotchkiss, R.J. Dubos, The isolation of bactericidal substances from cultures of Bacillus Brevis, Journal of Biological Chemistry. 141 (1941) 155–162. https://doi.org/10.1016/s0021-9258(18)72830-5.

[75] M. Shah, D. Fawcett, S. Sharma, S.K. Tripathy, G.E.J. Poinern, M. Elbahri, Green Synthesis of Metallic Nanoparticles via Biological Entities, (2015). https://doi.org/10.3390/ma8115377.

[76] M. Iosin, P. Baldeck, S. Astilean, Study of tryptophan assisted synthesis of gold nanoparticles by combining UV–Vis, fluorescence, and SERS spectroscopy, Journal of Nanoparticle Research. 12 (2010) 2843–2849. https://doi.org/10.1007/s11051-010-9869-6.

[77] A. Nasrolahi Shirazi, D. Mandal, R.K. Tiwari, L. Guo, W. Lu, K. Parang, Cyclic Peptide-Capped Gold Nanoparticles as Drug Delivery Systems, Mol Pharm. 10 (2013) 500–511. https://doi.org/10.1021/mp300448k.

[78] Y.N. Tan, J.Y. Lee, D.I.C. Wang, Uncovering the Design Rules for Peptide Synthesis of Metal Nanoparticles, J Am Chem Soc. 132 (2010) 5677–5686. https://doi.org/10.1021/ja907454f.

[79] S. Iravani, H. Korbekandi, S. v. Mirmohammadi, B. Zolfaghari, Synthesis of silver nanoparticles: Chemical, physical and biological methods, Res Pharm Sci. 9 (2014) 385–406.

[80] S. Gupta, V. Kumar, K.B. Joshi, Solvent mediated photo-induced morphological transformation of AgNPs-peptide hybrids in water-EtOH binary solvent mixture, J Mol Liq. 236 (2017) 266–277. https://doi.org/10.1016/j.molliq.2017.03.114.

[81] R. Jin, Y. Cao, C.A. Mirkin, K.L. Kelly, G.C. Schatz, J.G. Zheng, Photoinduced Conversion of Silver Nanospheres to Nanoprisms, Science (1979). 294 (2001) 1901–1903. https://doi.org/10.1126/science.1066541.

[82] R. Brause, H. Möltgen, K. Kleinermanns, Characterization of laser-ablated and chemically reduced silver colloids in aqueous solution by UV/VIS spectroscopy and STM/SEM microscopy, Appl Phys B. 75 (2002) 711–716. https://doi.org/10.1007/s00340-002-1024-3.

[83] A. Khan, A. Rashid, R. Younas, R. Chong, A chemical reduction approach to the synthesis of copper nanoparticles, Int Nano Lett. 6 (2016) 21–26. https://doi.org/10.1007/s40089-015-0163-6.

[84] N.R. Jana, L. Gearheart, C.J. Murphy, Evidence for Seed-Mediated Nucleation in the Chemical Reduction of Gold Salts to Gold Nanoparticles, Chemistry of Materials. 13 (2001) 2313–2322. https://doi.org/10.1021/cm000662n.

[85] P.R. Selvakannan, A. Swami, D. Srisathiyanarayanan, P.S. Shirude, R. Pasricha, A.B. Mandale, M. Sastry, Synthesis of aqueous Au core-Ag shell nanoparticles using tyrosine as a pH-dependent reducing agent and assembling phase-transferred silver nanoparticles at the air-water interface, Langmuir. 20 (2004) 7825–7836. https://doi.org/10.1021/la049258j.

[86] T. Shoeib, K.W.M. Siu, A.C. Hopkinson, Silver ion binding energies of amino acids: Use of theory to assess the validity of experimental silver ion basicities obtained from the kinetic method, Journal of Physical Chemistry A. 106 (2002) 6121–6128. https://doi.org/10.1021/jp013662z.

[87] N.T.K. Thanh, N. Maclean, S. Mahiddine, Mechanisms of nucleation and growth of nanoparticles in solution, Chem Rev. 114 (2014) 7610–7630. https://doi.org/10.1021/cr400544s.

[88] S. Dadashi-Silab, S. Doran, Y. Yagci, Photoinduced Electron Transfer Reactions for Macromolecular Syntheses, Chem Rev. 116 (2016) 10212–10275. https://doi.org/10.1021/acs.chemrev.5b00586.

[89] M.L. Marin, K.L. McGilvray, J.C. Scaiano, Photochemical strategies for the synthesis of gold nanoparticles from Au(III) and Au(I) using photoinduced free radical generation, J Am Chem Soc. 130 (2008) 16572–16584. https://doi.org/10.1021/ja803490n.

[90] G.A. Bhaduri, R. Little, R.B. Khomane, S.U. Lokhande, B.D. Kulkarni, B.G. Mendis, L. Šiller, Green synthesis of silver nanoparticles using sunlight, J Photochem Photobiol A Chem. 258 (2013) 1–9. https://doi.org/10.1016/j.jphotochem.2013.02.015.

[91] H. Kaysadu, Y. Duman, Y. Yakupogulları, Investigation of synergistic, additive and antagonist effect of antimicrobial combinations used for *Brucella* spp, with E-test combination method, Eastern Journal of Medicine. 24 (2019) 96–101. https://doi.org/10.5505/ejm.2019.66588.

[92] E. Kamble, P. Sanghvi, K. Pardesi, Synergistic effect of antibiotic combinations on *Staphylococcus aureus* biofilms and their persister cell populations, Biofilm. 4 (2022) 100068. https://doi.org/10.1016/j.bioflm.2022.100068.

[93] A.M. Troskie, M. Rautenbach, N. Delattin, J.A. Vosloo, M. Dathe, B.P.A. Cammue, K. Thevissen, Synergistic activity of the tyrocidines, antimicrobial cyclodecapeptides from *Bacillus aneurinolyticus*, with amphotericin B and caspofungin against Candida albicans biofilms, Antimicrob Agents Chemother. 58 (2014) 3697–3707. https://doi.org/10.1128/AAC.02381-14.

[94] S.H. Haji, F.A. Ali, S.T.H. Aka, Synergistic antibacterial activity of silver nanoparticles biosynthesized by carbapenem-resistant Gram-negative *bacilli*, Sci Rep. 12 (2022). https://doi.org/10.1038/s41598-022-19698-0.

[95] S.K. Ramakrishnan, M. Martin, T. Cloitre, L. Firlej, F.J.G. Cuisinier, C. Gergely, Insights on the Facet Specific Adsorption of Amino Acids and Peptides toward Platinum, J Chem Inf Model. 53 (2013) 3273–3279. https://doi.org/10.1021/ci400630d.

[96] G. Pandit, K. Roy, U. Agarwal, S. Chatterjee, Self-Assembly Mechanism of a Peptide-Based Drug Delivery Vehicle, ACS Omega. 3 (2018) 3143–3155. https://doi.org/10.1021/acsomega.7b01871.

[97] V. Kumar, S. Gupta, N.K. Mishra, R. Singh, S.K.S. Yadav, K.B. Joshi, Laser-induced fabrication of gold nanoparticles on shellac-driven peptide nanostructures, Mater Res Express. 4 (2017) 035036. https://doi.org/10.1088/2053-1591/aa63e0.

[98] S. Si, T.K. Mandal, Tryptophan-based peptides to synthesize gold and silver nanoparticles: A mechanistic and kinetic study, Chemistry - A European Journal. 13 (2007) 3160–3168. https://doi.org/10.1002/chem.200601492.

[99] S. Roy, T.K. Das, Study of Interaction Between Tryptophan, Tyrosine, and Phenylalanine Separately with Silver Nanoparticles by Fluorescence Quenching Method, J Appl Spectrosc. 82 (2015) 598–606. https://doi.org/10.1007/s10812-015-0151-7.

[100] M.A. Ruttenberg, T.P. King, L.C. Craig, J. SvU, R. Breslow, D. Chipman, The Use of the Tyrocidines for the Study of Conformation and Aggregation Behavior, J Am Chem Soc. 87 (1965) 4196–4198. https://doi.org/10.1021/ja01096a040.

[101] A.B.T. Ghisaidoobe, S.J. Chung, Intrinsic Tryptophan Fluorescence in the Detection and Analysis of Proteins: A Focus on Förster Resonance Energy Transfer Techniques, Int. J. Mol. Sci. 15 (2014) 22518–22538. https://doi.org/10.3390/ijms151222518.

[102] J.R. Akowicz, Protein Fluorescence, in: Principles of Fluorescence Spectroscopy, Springer, Boston, MA, 2006: pp. 529–530. https://doi.org/10.1007/978-0-387-46312-4_16.

[103] I. Pal, V.P. Brahmkhatri, S. Bera, D. Bhattacharyya, Y. Quirishi, A. Bhunia, H.S. Atreya, Enhanced stability and activity of an antimicrobial peptide in conjugation with silver nanoparticle, J Colloid Interface Sci. 483 (2016) 385–393. https://doi.org/10.1016/j.jcis.2016.08.043.

[104] F.W.J. Teale, G. Weber, Ultraviolet fluorescence of the aromatic amino acids, Biochemical Journal. 65 (1957) 476–482. https://doi.org/10.1042/bj0650476.

[105] M.F. Pignataro, M.G. Herrera, V.I. Dodero, Evaluation of peptide/protein self-assembly and aggregation by spectroscopic methods, Molecules. 25 (2020). https://doi.org/10.3390/molecules25204854.

[106] C. Duy, J. Fitter, How aggregation and conformational scrambling of unfolded states govern fluorescence emission spectra, Biophys J. 90 (2006) 3704–3711. https://doi.org/10.1529/BIOPHYSJ.105.078980.

[107] P.M. Liskova, R. Fiser, P. Macek, J. Chmelik, J. Sykora, L. Bednarova, I. Konopasek, L. Bumba, Probing the Ca 2+-assisted p-p interaction during Ca 2+-dependent protein folding †, Cite This: Soft Matter. 12 (2016) 531. https://doi.org/10.1039/c5sm01796c.

[108] N.T.T. Nga, H.V. Tran, C.H. Dang, An Investigation on the Synthesis, Structure and Specific Properties of Zn(II) and Cu(II) Complexes with Tryptophan, Biointerface Res Appl Chem. 13 (2023). https://doi.org/10.33263/BRIAC131.002.

[109] P.R. Selvakannan, S. Mandal, S. Phadtare, A. Gole, R. Pasricha, S.D. Adyanthaya, M. Sastry, Water-dispersible tryptophan-protected gold nanoparticles prepared by the spontaneous reduction of aqueous chloroaurate ions by the amino acid, J Colloid Interface Sci. 269 (2004) 97–102. https://doi.org/10.1016/S0021-9797(03)00616-7.

[110] S. Kéki, J. Török, G. Deák, L. Daróczi, M. Zsuga, Silver nanoparticles by PAMAM-assisted photochemical reduction of Ag+, J Colloid Interface Sci. 229 (2000) 550–553. https://doi.org/10.1006/jcis.2000.7011.

[111] L. Polavarapu, Q.H. Xu, A single-step synthesis of gold nanochains using an amino acid as a capping agent and characterization of their optical properties, Nanotechnology. 19 (2008). https://doi.org/10.1088/0957-4484/19/7/075601.

[112] M.N. Nadagouda, R.S. Varma, Synthesis of thermally stable carboxymethyl cellulose/metal biodegradable nanocomposites for potential biological applications, Biomacromolecules. 8 (2007) 2762–2767. https://doi.org/10.1021/bm700446p.

[113] M. Stauss-Grabo, S. Atiye, T. Le, M. Kretschmar, N. Manuela Stauss-Grabo, Decade-long use of the antimicrobial peptide combination tyrothricin does not pose a major risk of acquired resistance with gram-positive bacteria and *Candida* spp, Pharmazie. 69 (2014) 838–841. https://doi.org/10.1691/ph.2014.4686.

[114] R.J.R.J. Dubos, R.D. Hotchkiss, R.J.R.J. Dubos, The production of bactericidal substances by aerobic sporulating *bacilli*, Journal of Biological Chemistry. 141 (1941) 155–162. https://doi.org/10.1016/S0021-9258(18)72830-5.

[115] J.A. Vosloo, M. Rautenbach, Following tyrothricin peptide production by Brevibacillus parabrevis with electrospray mass spectrometry, Biochimie. 179 (2020) 101–112. https://doi.org/10.1016/j.biochi.2020.09.004.

[116] R.J. Dubos, C. Cattaneo, Studies on a bactericidal agent extracted from a soil bacillus iii. Preearation and activity of a protein-free fraction, Journal of Experimental Medicine. 70 (1939) 249–256. https://doi.org/10.1084/jem.70.3.249.

[117] M. Rautenbach, N.M. Vlok, M. Stander, H.C. Hoppe, Inhibition of malaria parasite blood stages by tyrocidines, membrane-active cyclic peptide antibiotics from Bacillus brevis, Biochim Biophys Acta. 1768 (2007) 1488–1497. https://doi.org/10.1016/j.bbamem.2007.01.015.

[118] A.N. yango N. Leussa, M. Rautenbach, Detailed SAR and PCA of the tyrocidines and analogues towards leucocin A-sensitive and leucocin A-resistant *Listeria monocytogenes*, Chem Biol Drug Des. 84 (2014) 543–557. https://doi.org/10.1111/cbdd.12344.

[119] V. Kumar, W. van Rensburg, J.L. Snoep, H.H. Paradies, C. Borrageiro, C. de Villiers, R. Singh, K.B. Joshi, M. Rautenbach, Antimicrobial nano-assemblies of tryptocidine C, a tryptophan-rich cyclic decapeptide, from ethanolic solutions, Biochimie. (2022). https://doi.org/10.1016/j.biochi.2022.08.017.

[120] B.M. Spathelf, M. Rautenbach, Anti-listerial activity and structure-activity relationships of the six major tyrocidines, cyclic decapeptides from *Bacillus aneurinolyticus*, Bioorg Med Chem. 17 (2009) 5541–5548. https://doi.org/10.1016/j.bmc.2009.06.029.

[121] J.A. Vosloo, Optimised bacterial production and characterisation of natural antimicrobial peptides with potential application in agriculture, Stellenbosch University,Stelllenbosch, South Africa., 2016.

[122] Y. Masoudi, W. van Rensburg, B. Barnard-Jenkins, M. Rautenbach, The influence of cellulose-type formulants on anti-candida activity of the tyrocidines, Antibiotics. 10 (2021). https://doi.org/10.3390/antibiotics10050597.

[123] Y. Masoudi, Characterisation and formulation of natural cyclodecapeptides with anti-Candida activity, Stellenbosch University,Stellenbosch, South Africa, 2021.

[124] M. Rautenbach, V. Kumar, J.A. Vosloo, Y. Masoudi, R.J. van Wyk, M.A. Stander, Oligomerisation of tryptocidine C, a Trp-rich cyclodecapeptide from the antimicrobial tyrothricin complex, Biochimie. (2021). https://doi.org/10.1016/j.biochi.2020.12.006.

[125] M. Rautenbach, A.M. Troskie, J.A. Vosloo, M.E. Dathe, Antifungal membranolytic activity of the tyrocidines against filamentous plant fungi, Biochimie. 130 (2016) 122–131. https://doi.org/10.1016/j.biochi.2016.06.008.

[126] A.Mari. Troskie, Tyrocidines , cyclic decapeptides produced by soil *bacilli* , as potent inhibitors of fungal pathogens, Stellenbosch University, Stellenbosch, South Africa, 2014.

[127] N.-N.A. Leussa, Characterisation of small cyclic peptides with antilisterial and antimalarial activity, Stellenbosch University, Stellenbosch, South Africa, 2014.

[128] J.A. Vosloo, M.A. Stander, A.N.N. Leussa, B.M. Spathelf, M. Rautenbach, Manipulation of the tyrothricin production profile of *Bacillus aneurinolyticus*, Microbiology (N Y). 159 (2013) 2200–2211. https://doi.org/10.1099/mic.0.068734-0.

[129] H. Ristow, B. Schazschneider, H. Kleinkauf, Effects of the peptide antibiotics tyrocidine and the linear gramicidin on RNA synthesis and sporulation of Bacillus brevis, Biochem Biophys Res Commun. 63 (1975) 1085–1092. https://doi.org/10.1016/0006-291X(75)90680-4.

[130] B. Schazschneider, H. Ristow, H. Kleinkauf, Interaction between the antibiotic tyrocidine and DNA in vitro, Nature. 249 (1974) 757–759. https://doi.org/10.1038/249757a0.

[131] M.A. Ruttenberg, B. Mach, Studies on Amino Acid Substitution in the Biosynthesis of the Antibiotic Polypeptide Tyrocidine, Biochemistry. 5 (1966) 2864–2869. https://doi.org/10.1021/bi00873a013.

[132] X.J. Tang, P. Thibault, R.K. Boyd, Characterisation of the tyrocidine and gramicidin fractions of the tyrothricin complex from *Bacillus brevis* using liquid chromatography and mass spectrometry, Int J Mass Spectrom Ion Process. 122 (1992) 153–179. https://doi.org/10.1016/0168-1176(92)87015-7.

[133] A. Paladini, L.C. Craig, V. 76, A. Paladini1, The Chemistry of Tyrocidine. III. The Structure of Tyrocidine A, J Am Chem Soc. 76 (1954) 688–692. https://doi.org/10.1021/ja01632a015.

[134] R.C. Williams, D.A. Yphantis, L.C. Craig, Noncovalent association of tyrocidine B, Biochemistry. 11 (1972) 70–77. https://doi.org/10.1021/bi00751a013.

[135] H. Henrich Paradies, H.H. Paradies, Structure of tyrocidine micelles in isotropic aqueous solution, J Pharm Sci. 78 (1989) 230–234. https://doi.org/10.1002/jps.2600780312.

[136] H.H. Paradies, Aggregation of tyrocidine in aqueous solutions, Biochem Biophys Res Commun. 88 (1979) 810–817. https://doi.org/10.1016/0006-291X(79)91480-3.

[137] H.H. Paradies, H. Reichelt, Formation and structures of tyrocidine B in solution in the presence of water, AIP Adv. 10 (2020) 75007. https://doi.org/10.1063/1.5144852.

[138] A.M. Troskie, A. de Beer, J.A. Vosloo, K. Jacobs, M. Rautenbach, Inhibition of agronomically relevant fungal phytopathogens by tyrocidines, cyclic antimicrobial peptides isolated from *Bacillus aneurinolyticus,* Microbiology (N Y). 160 (2014) 2089–2101. https://doi.org/10.1099/mic.0.078840-0.

[139] V. Vadyvaloo, S. Arous, A. Gravesen, Y. Héchard, R. Chauhan-Haubrock, J.W. Hastings, M. Rautenbach, Cell-surface alterations in class IIa bacteriocin-resistant *Listeria monocytogenes* strains, Microbiology (N Y). 150 (2004) 3025–3033. https://doi.org/10.1099/mic.0.27059-0.

[140] M. Rautenbach, G.D. Gerstner, N.M. Vlok, J. Kulenkampff, H. V. Westerhoff, Analyses of dose-response curves to compare the antimicrobial activity of model cationic α-helical peptides highlights the necessity for a minimum of two activity parameters, Anal Biochem. 350 (2006) 81–90. https://doi.org/10.1016/j.ab.2005.11.027.

[141] C. Qin, X. Zhong, X. Bu, N. Lee, J. Ng, Z. Guo, Dissociation of Antibacterial and Hemolytic Activities of an Amphipathic Peptide Antibiotic, (2003). https://doi.org/10.1021/jm0341352.

[142] J.A. Vosloo, J.L. Snoep, M. Rautenbach, Modelling the variable incorporation of aromatic amino acids in the tyrocidines and analogous cyclodecapeptides, J Appl Microbiol. 127 (2019) 1665–1676. https://doi.org/10.1111/jam.14430.

[143] P.J. Loll, E.C. Upton, V. Nahoum, N.J. Economou, S. Cocklin, The high resolution structure of tyrocidine A reveals an amphipathic dimer, Biochim Biophys Acta Biomembr. 1838 (2014) 1199–1207. https://doi.org/10.1016/j.bbamem.2014.01.033.

[144] A. Rothen, The behavior of the tyrocidines at interfaces, Biochimica et Biophysica Acta (BBA) - Specialized Section on Biophysical Subjects. 88 (1964) 606–619. https://doi.org/10.1016/0926-6577(64)90103-2.

[145] M. Thies, H.H. Paradies, Self-assembly of tyrocidines in nanotubular structures, MRS Online Proceedings Library. 489 (1998) 145–151. https://doi.org/10.1557/proc-489-145.

[146] W. Van Rensburg, M. Rautenbach, The tyrocidines in the creation of antimicrobial cellulose and sterilising materials, Stellenbosch University, Stellenbosch, South Africa, 2020.

[147] W. van Rensburg, M. Rautenbach, Creating Robust Antimicrobial Materials with Sticky Tyrocidines, Antibiotics. 11 (2022). https://doi.org/10.3390/antibiotics11020174.

[148] D.W. Juhl, W. van Rensburg, X. Bossis, J.A. Vosloo, M. Rautenbach, B. Bechinger, Tyrocidine A interactions with saccharides investigated by CD and NMR spectroscopies, Journal of Peptide Science. 25 (2019) 3163. https://doi.org/10.1002/psc.3163.

[149] M.C. Crisan, M. Teodora, M. Lucian, Copper Nanoparticles: Synthesis and Characterization, Physiology, Toxicity and Antimicrobial Applications, Applied Sciences. 12 (2021) 141. https://doi.org/10.3390/app12010141.

[150] D. Chudobova, S. Dostalova, B. Ruttkay-Nedecky, R. Guran, M.A.M. Rodrigo, K. Tmejova, S. Krizkova, O. Zitka, V. Adam, R. Kizek, The effect of metal ions on *Staphylococcus aureus* revealed by biochemical and mass spectrometric analyses, Microbiol Res. 170 (2015) 147–156. https://doi.org/10.1016/j.micres.2014.08.003.

[151] M.L. Waters, Aromatic interactions in peptides: Impact on structure and function, Peptide Science. 76 (2004) 435–445. https://doi.org/10.1002/BIP.20144.

[152] D.P. Malenov, S.D. Zarić, Stacking interactions of aromatic ligands in transition metal complexes, Coord Chem Rev. 419 (2020) 213338. https://doi.org/10.1016/j.ccr.2020.213338.

[153] N.K. Mishra, V. Kumar, K.B. Joshi, Fabrication of gold nanoparticles on biotin-di-tryptophan scaffold for plausible biomedical applications, RSC Adv. 5 (2015) 64387–64394. https://doi.org/10.1039/C5RA11121H.

[154] V. Kumar, N.K. Mishra, S. Gupta, K.B. Joshi, Short Peptide Amphiphile Cage Facilitate Engineering of Gold Nanoparticles Under the Laser Field, ChemistrySelect. 2 (2017) 211–218. https://doi.org/10.1002/slct.201601548.

[155] Z. Li, D. Lee, X. Sheng, R.E. Cohen, M.F. Rubner, Two-Level Antibacterial Coating with Both Release-Killing and Contact-Killing Capabilities, Langmuir. 22 (2006) 9820–9823. https://doi.org/10.1021/la0622166.

[156] J.-B.D. Green, T. Fulghum, M.A. Nordhaus, A review of immobilized antimicrobial agents and methods for testing, Biointerphases. 6 (2011) MR13–MR28. https://doi.org/10.1116/1.3645195.

[157] M. Bagheri, M. Beyermann, M. Dathe, Mode of Action of Cationic Antimicrobial Peptides Defines the Tethering Position and the Efficacy of Biocidal Surfaces, Bioconjug Chem. 23 (2012) 66–74. https://doi.org/10.1021/bc200367f.

[158] X.-F. Zhang, Z.-G. Liu, W. Shen, S. Gurunathan, Silver Nanoparticles: Synthesis, Characterization, Properties, Applications, and Therapeutic Approaches, Int J Mol Sci. 17 (2016) 1534. https://doi.org/10.3390/ijms17091534.

[159] Z.E. Nazari, M. Banoee, A.A. Sepahi, F. Rafii, A.R. Shahverdi, The combination effects of trivalent gold ions and gold nanoparticles with different antibiotics against resistant Pseudomonas aeruginosa, Gold Bull. 45 (2012) 53–59. https://doi.org/10.1007/s13404-012-0048-7.

[160] S. Mangala Praveena, • Ahmad, Z. Aris, Application of Low-Cost Materials Coated with Silver Nanoparticle as Water Filter in *Escherichia coli* Removal, Water Qual Expo Health. (n.d.). https://doi.org/10.1007/s12403-015-0167-5.

[161] G. Grass, C. Rensing, M. Solioz, Metallic copper as an antimicrobial surface, Appl Environ Microbiol. 77 (2011) 1541–1547. https://doi.org/10.1128/AEM.02766-10/FORMAT/EPUB.

[162] S. Jadhav, S. Gaikwad, M. Nimse, A. Rajbhoj, Copper Oxide Nanoparticles: Synthesis, Characterization and Their Antibacterial Activity, J Clust Sci. 22 (2011) 121–129. https://doi.org/10.1007/s10876-011-0349-7.

[163] N. Cioffi, L. Torsi, N. Ditaranto, L. Sabbatini, P.G. Zambonin, G. Tantillo, L. Ghibelli, M. D'Alessio, T. Bleve-Zacheo, E. Traversa, Antifungal activity of polymer-based copper nanocomposite coatings, Appl Phys Lett. 85 (2004) 2417–2419. https://doi.org/10.1063/1.1794381.

[164] H. Chandra, D. Patel, P. Kumari, J.S. Jangwan, S. Yadav, Phyto-mediated synthesis of zinc oxide nanoparticles of *Berberis aristata*: Characterization, antioxidant activity and antibacterial activity with special reference to urinary tract pathogens, Materials Science and Engineering: C. 102 (2019) 212–220. https://doi.org/10.1016/j.msec.2019.04.035.

[165] A. Reyes-Jara, N. Cordero, J. Aguirre, M. Troncoso, G. Figueroa, Antibacterial Effect of Copper on Microorganisms Isolated from Bovine Mastitis, Front Microbiol. 7 (2016). https://doi.org/10.3389/fmicb.2016.00626.

[166] A.A. Gvozdenko, S.A. Siddiqui, A. v Blinov, A.B. Golik, A.A. Nagdalian, D.G. Maglakelidze, E.N. Statsenko, M.A. Pirogov, A.A. Blinova, M.N. Sizonenko, A.N. Simonov, R.B. Zhukov, R.O. Kolesnikov, S.A. Ibrahim, Synthesis of CuO nanoparticles stabilized with gelatin for potential use in food packaging applications, Scientific Reports |. 12 (123AD) 12843. https://doi.org/10.1038/s41598-022-16878-w.

[167] S. Pal, M. Das, K. Naskar, Exploring Copper-Amino Acid Complexes in Cross-Linking of Maleated Ethylene Propylene Rubber, Ind Eng Chem Res. 58 (2019) 17802–17813. https://doi.org/10.1021/acs.iecr.9b03254.

[168] W. Van Rensburg, Characterization of natural antimicrobial peptides adsorbed to different matrices, 2015.

[169] M. Rautenbach, W. van Rensburg, Method for preventing or treating microbial growth on a manufactured product, (PCT patent application published as WO2015186058A1). National validations in South Africa (ZA2016/08601, Granted); China (CN106793774, Granted), 2017.

[170] S. Trimpin, D.E. Clemmer, Ion mobility spectrometry/mass spectrometry snapshots for assessing the molecular compositions of complex polymeric systems, Anal Chem. 80 (2008) 9073–9083. https://doi.org/10.1021/ac801573n.

[171] B.T. Ruotolo, C.C. Tate, D.H. Russell, Ion mobility-mass spectrometry applied to cyclic peptide analysis: Conformational preferences of gramicidin S and linear analogs in the gas phase, J Am Soc Mass Spectrom. 15 (2004) 870–878. https://doi.org/10.1016/j.jasms.2004.02.006.

Chapter 2
Production and purification of tryptophan-containing antimicrobial cyclodecapeptides and their analogues

2.1 Introduction

To investigate the biophysical characteristics and antimicrobial properties of the peptide-metal formulations in this study, both a mixture of tryptophan containing peptides and pure peptide (>90% purity) was required. Tyrothricin is a bactericidal complex naturally produced by the soil bacterium *Brevibacillus parabrevis (B. parabrevis)* consisting of two peptide groups: the cyclic tyrocidines (Trcs) and the linear gramicidin (Grms) [1,2]. The Trcs are decapeptides with a highly conserved amino acid sequence, cyclo-($f^1P^2X^3x^4N^5Q^6X^7V^8O^9L^{10}$) with variance in residues at positions 3, 4, 5, 7 and 9. The tyrocidine analogues that are commonly found in culture extracts are summarized in Table 2.1. The variance in positions 3 and 4 ($Phe^{3,4}$, $Trp^{3,4}$), defines the A, B and C analogues and the variance at position 7 (Tyr^7/Phe^7/Trp^7) indicates the tyrocidines, tryptocidines and phenycidines. Whereas the variance at position 9 (Orn^9/Lys^9) indicates the A, A_1, B, B_1, C and C_1 analogues [1–5]. The production of tyrothricin from *Br. parabrevis* cultures is a complex process with a multitude of factors influencing the peptide production rate, yield, and profile [6–8]. However, it is the structural similarity between the different Trcs and their propensity to self-assemble, oligomerise and aggregate [9–12] which makes the purification of single analogues from peptide mixtures an arduous challenge. To aid in this process, the BIOPEP^{TM} Peptide Group developed a large-scale method to produce and extract Trcs [7,13]. This method shifts the peptide production profile of *Br. parabrevis* by supplementing the cultures with select amino acids, subsequently promoting the production of specific peptide analogues and allowing larger yields of these peptides during the purification process [5–7,13]. For this study this method of supplementation was utilised to shift the *Br. parabrevis* peptide production profile towards the tryptophan-rich Trc's (the C analogues), allowing successful extraction and purification of these analogues with higher yields. Peptides were isolated using a series of organic solvent extractions followed by reverse-phase high-performance liquid chromatography (RP-HPLC). The composition of peptide extracts, identity of peptides and purity of isolated analogues were analysed using ultra-performance liquid chromatography linked to high-resolution electrospray ionisation mass spectrometry (UPLC-MS). Peptide analogues of the highest purity (>90%) were used for the fabrication, biophysical and antimicrobial characterisation of peptide-metal nanoformulations in Chapters 3 and 4.

Table 2.1 Summary of the possible cyclodecapeptides and linear gramicidins, their sequences, theoretical monoisotopic masses (M_r) and protonated ion *m/z* values in *Br. parabrevis* tyrothricin extracts adapted from Vosloo *et al.* [7].

Peptide in tyrothricin	Abbr.	Short Abbr [a]	Sequence [b]	Monomer Theoretical M_r [c]	Singly charged ion *m/z* [d]	Doubly charged ion *m/z* [e]
A analogues (Ff)						
Phenycidine A*	PhcA	FA	Cyclo-(fPFfNQFVOL)	1253.6597	1254.6675	627.8377
Phenycidine A_1**	$PhcA_1$	FA_1	Cyclo-(fPFfNQFVKL)	1267.6753	1268.6832	634.8455
Tyrocidine A	TrcA	YA	Cyclo-(fPFfNQYVOL)	1269.6546	1270.6624	635.8351
Tyrocidine A_1	$TrcA_1$	YA_1	Cyclo-(fPFfNQYVKL)	1283.6703	1284.6781	642.8430
Tryptocidine A	TpcA	WA	Cyclo-(fPFfNQWVOL)	1292.6706	1293.6784	647.3431
Tryptocidine A_1**	$TpcA_1$	WA_1	Cyclo-(fPFfNQWVKL)	1306.6862	1307.6941	654.3509
B analogues (Wf)						
Tyrocidine B	TrcB	YB	Cyclo-(fPWfNQYVOL)	1308.6655	1309.6733	655.3406
Tyrocidine B'	TrcB'	YB'	Cyclo-(fPFwNQYVOL)	1308.6655	1309.6733	655.3406
Tyrocidine B_1	$TrcB_1$	YB_1	Cyclo-(fPWfNQYVKL)	1322.6812	1323.6890	662.3484
Tyrocidine B_1'	$TrcB_1$'	YB_1'	Cyclo-(fPFwNQYVKL)	1322.6812	1323.6890	662.3484
Tryptocidine B	TpcB	WB	Cyclo-(fPWfNQWVOL)	1331.6815	1332.6893	666.8486
Tryptocidine B'**	TpcB'	WB'	Cyclo-(fPFwNQWVOL)	1331.6815	1332.6893	666.8486
Tryptocidine B_1	$TpcB_1$	WB_1	Cyclo-(fPWfNQWVKL)	1345.6971	1346.7050	673.8564
Tryptocidine B_1'**	$TpcB_1$'	WB_1'	Cyclo-(fPFwNQWVKL)	1345.6971	1346.7050	673.8564
C analogues (Ww)						
Tyrocidine C	TrcC	YC	Cyclo-(fPWwNQYVOL)	1347.6764	1348.6842	674.8460
Tyrocidine C_1	$TrcC_1$	YC_1	Cyclo-(fPWwNQYVKL)	1361.6921	1362.6999	681.8539
Tryptocidine C	TpcC	WC	Cyclo-(fPWwNQWVOL)	1370.6924	1371.7002	686.3540
Tryptocidine C_1	$TpcC_1$	WC_1	Cyclo-(fPWwNQWVKL)	1384.7080	1385.7159	693.3618
Linear gramicidins						
Val-Gramicidin A	VGA	CHO-VGAlAvVvWlWlWlW-NH$(CH_2)_2$OH		1881.0783	1882.0862	941.5470
VGA minus formyl	VGA^{UF}	VGAlAvVvWlWlWlW-NH$(CH_2)_2$OH		1853.0834	1854.0913	927.5495
Val-Gramicidin B*	VGB	CHO-VGAlAvVvWlFlWlW-NH$(CH_2)_2$OH		1842.0674	1843.0753	922.0415
VGB minus formyl**	VGB^{UF}	VGAlAvVvWlFlWlW-NH$(CH_2)_2$OH		1814.0725	1815.0804	908.0441
Val-Gramicidin C*	VGC	CHO-VGAlAvVvWlYlWlW-NH$(CH_2)_2$OH		1858.0624	1859.0702	930.0390
VGC minus formyl**	VGC^{UF}	VGAlAvVvWlYlWlW-NH$(CH_2)_2$OH		1830.0675	1831.0753	916.0416
Ile-Gramicidin A	IGA	CHO-IGAlAvVvWlWlWlW-NH$(CH_2)_2$OH		1895.0940	1896.1018	948.5548
IGA minus formyl**	IGA^{UF}	IGAlAvVvWlWlWlW-NH$(CH_2)_2$OH		1867.0991	1868.1069	934.5574
Ile-Gramicidin B*	IGB	CHO-IGAlAvVvWlFlWlW-NH$(CH_2)_2$OH		1856.0831	1857.0909	929.0494
IGA minus formyl**	IGB^{UF}	IGAlAvVvWlFlWlW-NH$(CH_2)_2$OH		1828.0882	1829.0960	915.0519
Ile-Gramicidin C*	IGC	CHO-IGAlAvVvWlYlWlW-NH$(CH_2)_2$OH		1872.0780	1873.0858	937.0468
IGA minus formyl**	IGC^{UF}	IGAlAvVvWlYlWlW-NH$(CH_2)_2$OH		1844.0831	1845.0909	923.0494

[a] Abbreviations referring to the amino acid residues phenylalanine (Phc/F), tyrosine (Trc/Y) and tryptophan (Tpc/W) at position seven.
[b] Amino acid sequences using conventional one-letter abbreviations as obtained from Tang *et al.* [1] with lower case letters representing D-amino acids and O representing ornithine.
[c] Sum of the monoisotopic residual molecular masses of constituent amino acids within the peptide. [d] *m/z* of $[M_r+H]^+$ and [e] *m/z* of $[M_r+2H]^{2+}$.
*Low to extremely low levels in tyrothricin.
** Rarely detected.

2.2 Materials

2.2.1 Production and supplementation

The American Type Culture Collection (Manassas, VA, USA) supplied the *Brevibacillus parabrevis* ATCC8185 and ATCC10068 strains used to produce the tyrothricin complex from which the single tyrocidine peptides and their analogues were purified. The tryptone soy broth (TSB) and agar used to prepare TSB agar plates for the culturing of *Br. parabrevis* strains, were supplied by Merck (Darmstadt, Germany). The D-glucose, tryptone, monopotassium phosphate (KH_2PO_4), magnesium sulphate ($MgSO_4$), calcium chloride ($CaCl_2$), ferric sulphate ($FeSO_4$), manganese sulphate ($MnSO_4$) and sodium chloride (NaCl) used in the preparation of TGS (tryptone, glucose and salts culturing medium) were supplied by Merck (Darmstadt, Germany) and the potassium chloride (KCl) by Sigma-Aldrich (St Louis, USA).

2.2.2 Extraction and purification of tyrocidines from the tyrothricin complex

The analytical grade ethanol (EtOH, >99.8 %), diethyl ether (DEE) and acetone were supplied by Merck (Darmstadt, Germany). Methanol (MeOH) and trifluoroacetic acid (TFA, >98 %) were supplied by Sigma-Aldrich (St Louis, USA) and acetonitrile (ACN, HPLC-grade, far UV cut-off) by Romil Ltd (Cambridge, United Kingdom). Analytical grade water (MilliQ H_2O) was prepared by filtering water using a reverse osmosis plant through a Millipore-Q® water purification system (Milford, USA). MilliQ water was used in all solvents and media preparations. Lurgi (Frankfurt, Germany) supplied activated carbon and Sigma-Aldrich (St Louis, USA) commercial tyrothricin extract and phosphorous pentoxide. Merck-Millipore (Massachusetts, USA) supplied mixed cellulose syringe filters (0.22 µm). Falcon® tubes and Petri dishes were purchased from Becton Dickson Labware (Lincoln Park, USA) and Lasec (Cape Town, South Africa), respectively. The Nova-Pak HR C_{18} RP-HPLC semi-preparative column (6 µm particle size, 300 mm x 7.8 mm), C_{18} Nova-Pak® analytical RP-HPLC column (5 µm particle size, 150 mm x 3.9 mm) and Acquity HSS T3 (2.1×150 mm; 1.8 µm particle size) ultra-performance liquid chromatography (UPLC) column was purchased from Waters (Milford, USA).

2.3 Methods

2.3.1 Production of tyrothricin complex from Br. parabrevis

The producer strains *Br. parabrevis* ATCC8185 and ATCC10068 were plated from freezer stocks onto TSB agar plates (30 g/L TSB and 1.5 % *m/v* agar) using standard sterile techniques and incubated at 37°C for 48 hours. Fast-growing brown colonies from the *Br. parabrevis* pre-culture plates were selected, re-plated onto fresh TSB plates, and incubated at 37°C for 48 hours. Overnight cultures were prepared by inoculating 20 mL TSB media with a single well-defined colony from each *Br. parabrevis* culture agar plates and incubated at 37°C on a shaker (150 rpm) for 24 hours. Overnight cultures were sub-cultured into 200 mL of either supplemented or unsupplemented TGS culture media (Table 2.2) and incubated at 37 °C for 24 hours for 10 days.

Table 2.2 Summary of amino acid supplemented *Br. parabrevis* cultures and respective productions

Culture Organism	Prod.[a]	Amino Acid Supplemention	Culture Number	Supplementation concentration (mM)	Abbrev.[b]
Br. parabrevis ATCC10068	1	Unsupplemented	1	-	P1U
		Tryptophan	1	20	P1W
Br. parabrevis ATCC10068	2	Unsupplemented	1	-	P2U-1,
			2	-	P2U-2
		Tryptophan	1	10	P2W-1
			2	10	P2W-2
		Phenylalanine	1	10	P2F-1,
			2	10	P2F-2
Br. parabrevis ATCC8185	3	Unsupplemented	1	-	P3U
		Tryptophan	1	10	P3W
		Phenylalanine	1	10	P3F

[a] Production set of *Br. parabrevis* cultures are grown from different colonies of the same culture plate (cultured under the same conditions).
[b] Abbreviations of production (P) number (1,2 or 3) and culture number (-1 or -2).

Peptide production by *Br. parabrevis* proceeded as described by Vosloo *et al.* [7,13]. The optimized culture method is currently protected under a non-disclosure agreement (NDA) with BIOPEP™ and Stellenbosch University. For the first production series, a *Br. parabrevis* ATCC10068 medium was supplemented with 20 mM Trp (P1W). For the second production series, *a Br. parabrevis* ATCC10068 medium was supplemented with 10 mM Trp (P2W).

For the third production series, *a Br. parabrevis* ATCC8185 medium was supplemented with either 10 mM Phe (P3F) or 10 mM Trp (P3W). All three supplementations were performed in duplicate for the second and third production series. After the 10-day incubation period, the supplemented cultures for all productions were subjected to a series of extraction and precipitation steps as described below to obtain a production crude extract containing a complex mixture of tyrocidines and analogues.

2.3.2 Extraction of cyclodecapeptides from the tyrothricin complex

The details of the optimized extraction and purification method were developed by BIOPEP™ (Stellenbosch, South Africa) and are currently protected under a non-disclosure agreement (NDA). Briefly, peptides were extracted from supplemented *Br. parabrevis* cultures via acidification and centrifuged for 10 minutes at 10 621 ×*g* to obtain the culture biomass. The culture pellets were subsequently subjected to a series of organic solvent extraction and precipitation steps followed by carbon treatments. The resulting crude peptide extract was subjected to a series of ether: acetone (3:2 *v/v*) washing and centrifugation (5-10 minutes at 3030 ×*g*) steps to remove linear gramicidins. Thereafter, the crude production extracts were dried under N_2 gas flow. Dried crude production extract pellets were resuspended in ACN: water (1:1 *v/v*), transferred to a pyrolyzed and analytically weighed 20 mL vial and subsequently lyophilisation for further purification and analysis. Commercial tyrothricin was also subjected to a series of ether: acetone (3:2 *v/v*) washing and centrifugation (5-10 minutes at 3030×*g*) steps to remove linear gramicidins in the supernatant and purify a tyrocidine mixture (Trc mix). The Trc mix extract in the pellet was dried under N_2 gas flow. Thereafter the dried Trc Mix pellet was resuspended in ACN:water (1:1 *v/v*), transferred to a pyrolyzed and analytically weighed 20 mL vial and subsequently lyophilised for further purification and analysis. The dried mass (mg) and peptide composition of the crude production and Trc mix extracts are summarised in Table 2.6.

2.3.3 Semi-preparative HPLC purification of the cyclodecapeptides from crude peptide extracts

The crude production extracts were prepared to a concentration of 10 mg/mL in 50% ACN:water (*v/v*) and purified using an established semi-preparative reverse-phase high-performance liquid chromatography (RP-HPLC) method previously described by Rautenbach *et al.* [14] and Eyéghé-Bickong [15]. The 10 mg/mL crude peptide preparation was injected onto a Nova-Pak HR C_{18} semi-preparative HPLC column with injection volumes

of 100 µL. The chromatography system was controlled by Millenium 32 software (Waters, Milford, USA) and consisted of a Waters 6000A pump, Waters 510 pump and a Waters 440 absorbance detector (set at 254 nm). The column temperature was set at 35ºC and a set gradient programme (Table 2.3) was used at a flow rate of 3 mL/min. Eluent A consisted of 0.1 % (*v/v*) TFA in analytical quality water and eluent B of 10 % (*v/v*) eluent A in ACN. HPLC fractions were collected as shown in Fig. 2.3 then transferred into weighed and pyrolyzed 20 mL vials, lyophilised and stored at room temperature.

Table 2.3 Semi-preparative HPLC purification non-linear gradient program.

Minutes	% Eluent A	% Eluent B	Curve*
0.0	50	50	-
0.5	50	50	linear (6)
23.0	20	80	non-linear (5)
24.0	0	100	-
26.0	0	100	-
30.0	50	50	linear (6)
35.0	50	50	-

*Curves from Waters™ gradient programmes.

2.3.4 Characterisation of crude peptide extracts and purified cyclodecapeptides with ESI-MS and UPLC-MS analysis

Electrospray ionisation mass spectrometry (ESI-MS) and UPLC linked MS (UPLC-MS) were used to identify the peptides present within the HPLC-purified peptide fractions and the crude production extracts. The samples were resuspended in 50% ACN in water (*v/v*) and subsequently centrifuged at 10 621×*g* for 10 minutes to remove any particulate material. Crude production extracts were prepared to a concentration of 500 µg/mL and HPLC purified fractions to a concentration of 250 µg/mL. For direct injection ESI-MS analysis, 2 or 3 µL of the sample was injected and analysed using Waters Synapt G2 quadrupole TOF mass spectrometer (Milford, MA, USA) with an electrospray source at a capillary voltage of 2.5-3 kV and cone voltage of 15 V. The desolvation temperature was 275 ºC and nitrogen was used as a desolvation gas at 650 L/hour. Data acquisition was performed in the continuum positive mode (ES+) scanning over an *m/z* range of 300-2000. For UPLC-MS analysis 2 µL of the sample was injected into a Waters Synapt G2 quadrupole time-of-flight (TOF) mass spectrometer connected to a Waters Acquity UPLC® and Acquity photodiode array detector. The Waters Acquity UPLC® HSS T3 column (2.1 × 150 mm; 1.8 µm particle size) had a minimum and maximum column temperature of 45°C and 60°C, respectively. Peptides were eluted using a linear gradient program (Table 2.4) with solvent A (1 % formic acid (*v/v*) in

water) and solvent B (1 % formic acid (*v/v*) in ACN) at a flow rate of 0.3 mL/min. The eluted peptide was then analysed using Waters Synapt G2 quadrupole TOF mass spectrometer (Milford, MA, USA) with an electrospray source at a capillary voltage of 2.5-3 kV and cone voltage of 15 V. The desolvation temperature was 275 ºC and nitrogen was used as a desolvation gas at 650 L/hour. Data acquisition was performed in the positive mode (ES+) scanning over an *m/z* range of 300-2000 (same as direct injection ESI-MS analysis).

Table 2.4 UPLC-MS linear gradient program

Minutes	% Eluent A	% Eluent B	Curve*
0.0	100	0	-
0.5	100	0	-
1.0	70	30	linear (6)
10.0	40	60	linear (6)
15.0	20	80	linear (6)
15.1	0	100	linear (6)
18.0	100	0	linear (6)

*Curves are from Waters™ gradient programmes.

All samples were analysed and characterised further using Waters MassLynx V4.1 software (Milford, USA). The integrity and identity of peptides in each crude production extract and HPLC purified fraction was determined using the *m/z* values of the high-resolution ESI-MS in combination with the calculated monoisotopic M_r (using MaxEnt 3 algorithm of Waters MassLynx V4.1 software) and assessed using parts per million (ppm) mass error:

$$\text{ppm} = \frac{M\text{r (theoretical)} - M\text{r(experimental)}}{M\text{r (theoretical)}} \text{x} 10^6 \qquad \textbf{Equation 2.1}$$

The estimated contribution (%) of each peptide peak signal to the total % signal intensity of the sample was analysed using ESI-MS mass spectrum derived via MassLynx 4.01 MaxEnt 3 algorithm and calculated as follows:

$$\text{Contribution (\%)} = \frac{\text{Signal Intensity of Peak}}{\sum \text{ Peak Signal Intensities}} \times 100 \qquad \textbf{Equation 2.2}$$

The relative percentage purity (%) of each peptide in selected samples was calculated from the peak area obtained from UPLC-MS:

$$\text{Purity (\%)} = \frac{\text{Area Under Curve for Single Peak}}{\sum \text{Area Under Curves}} \times 100 \qquad \textbf{Equation 2.3}$$

2.3.5 Cleaning of Nova-Pak HR C_{18} semi-preparative HPLC column

The Nova-Pak HR C_{18} semi-preparative HPLC column was cleaned after the purification of crude peptide extracts. The solvents used in each cleaning step are summarised in Table 2.5, Eluent A and B are always used to prime the pumps before cleaning the column. For the first cleaning step (1) the column was washed for 10 minutes at a gradient of 50 % (*v/v*) eluent A in eluent B. Thereafter, the column was treated with three DMSO or DMF injections, each with an injection volume of 100 µL and a minimum of 10 minutes (step 2). For the third cleaning step (3) the column was washed with 100 % Eluent B with a flow rate of 3 mL/min for 15 minutes. The column was subsequently washed with 100 % MeOH (step 4) with a flow rate of 3 mL/min for 30 minutes. Thereafter, the column was washed at a gradient of 50 % (*v/v*) MeOH in IPA with a flow rate of 1.5 mL/min for 15 minutes (step 5). The column was washed again with 100 % MeOH at a flow rate of 3 mL/min for 15 minutes (step 6) followed by a final wash step with 100 % eluent B for 15 minutes at 3 mL/min (step 7).

Table 2.5 Summary of solvents and steps for regeneration of Nova-Pak HR C_{18} semi-preparative HPLC columns.

Acronym	Solvent Name	Molecular Formula	% Composition	Cleaning Step
Eluent A	HPLC Eluent A	-	0.1 % (*v/v*) TFA in Milli-Q water*	1
Eluent B	HPLC Eluent B	-	10 % (*v/v*) Eluent A in ACN*	1, 3 & 7
DMSO	Dimethyl sulfoxide	$(CH_3)_2SO$	100% Analytical Grade	2
DMF	Dimethylformamide	$(CH_3)_2NC(O)H$	100% Analytical Grade	2
MeOH	Methanol	CH_3OH	100% Analytical Grade	2, 4 ,5 & 6
IPA	Isopropyl alcohol	C_3H_8O	100% Analytical Grade	5

* Filtered using 0.45µm cellulose filter then degassed and sonicated for 10 minutes.

2.4 Results and Discussion

2.4.1 Production and characterisation of tyrothricin complex from supplemented Br. parabrevis cultures

For this study, the culture media of *Br. parabrevis* ATCC8185 and ATCC10068 was either unsupplemented or supplemented with tryptophan and phenylalanine to encourage the

production of Trp-rich and Phe-rich cyclodecapeptides, respectively. Trp and Phe were used for the amino acid supplemented cultures at a final concentration of either 20 mM or 10 mM as summarised in Table 2.2. All cultures were incubated at 37°C as stationary cultures for 10 days. Thereafter, the cultures were subjected to a series of organic solvent extractions, precipitation steps, carbon treatments and ether-acetone washing steps to yield a crude production extract. Production crude extracts are abbreviated as denoted in Table 2.2 and will be referred to as such for the remainder of this study. To determine the peptide composition and to confirm the successful production of the peptides of interest in the culture extracts samples were analysed with direct injection ESI-MS. Examples of the mass spectra derived via MassLynx 4.01 MaxEnt 3 algorithm for six of the crude production extract samples are shown in Fig. 2.1. The peptide profiles of phenylalanine supplemented extracts are not shown but are summarised in Table 2.6 (see discussion below) and illustrated in Fig. S2.1 (supplementary data).

The ESI-MS spectra show that the productions yielded both cyclodecapeptides and linear gramicidins. Both P2W and P2U crude extracts are nearly void of linear gramicidins, yet P1W and P1U extracts had a higher prevalence of linear gramicidins. The peptide identity and percentage contribution of the most predominant peptides in each production extract were determined via UPLC-MS and summarised in Table 2.6. A putative identification of the compound with *m/z* = 1854.08 was proposed as a Val-Gramicidin A analogue without a formyl capping group on the N-terminal (VGA^{UF}). This compound contributes 4.8 % and 1.2 % to the total signal intensity of P1U and P1W, respectively. Interestingly, VGA as denoted in Table 2.1, occurs in relatively low levels of tyrothricin produced by the *Br. parabrevis* strains used in this study, as seen in Table 2. Although higher prevalence of the tryptophan-rich VGA is expected with tryptophan media supplementation [7]. The higher contribution of the putative modified gramicidin to the MS signal in production one is indicative of aberrated tyrothricin production by the *Br. parabrevis* ATCC10068 cultures. Both production one and two used the same strain (*Br. parabrevis* ATCC10068), grown under the same conditions and extracted using the same extraction methods. The modified VGA^{UF} was present in both the supplemented and unsupplemented extracts of production one but near absent (≤ 0.3 % contribution) in production two. Moreover, production three with *Br. parabrevis* ATCC8185 culture extracts was near void of VGA^{UF} (≤ 0.3 % contribution). Since the colonies used in each production series were collected from the same specified starter culture (see Table 2.2), the production of VGA^{UF} could potentially be attributed to the selection of the modified colonies in production one. This is further

supported by the lowered biomass of the crude extracts from production one compared to that of production two (refer to the discussion below), suggesting the non-classical production of tyrothricin from cultures of *Br. parabrevis* ATCC8185 colonies in the first production series.

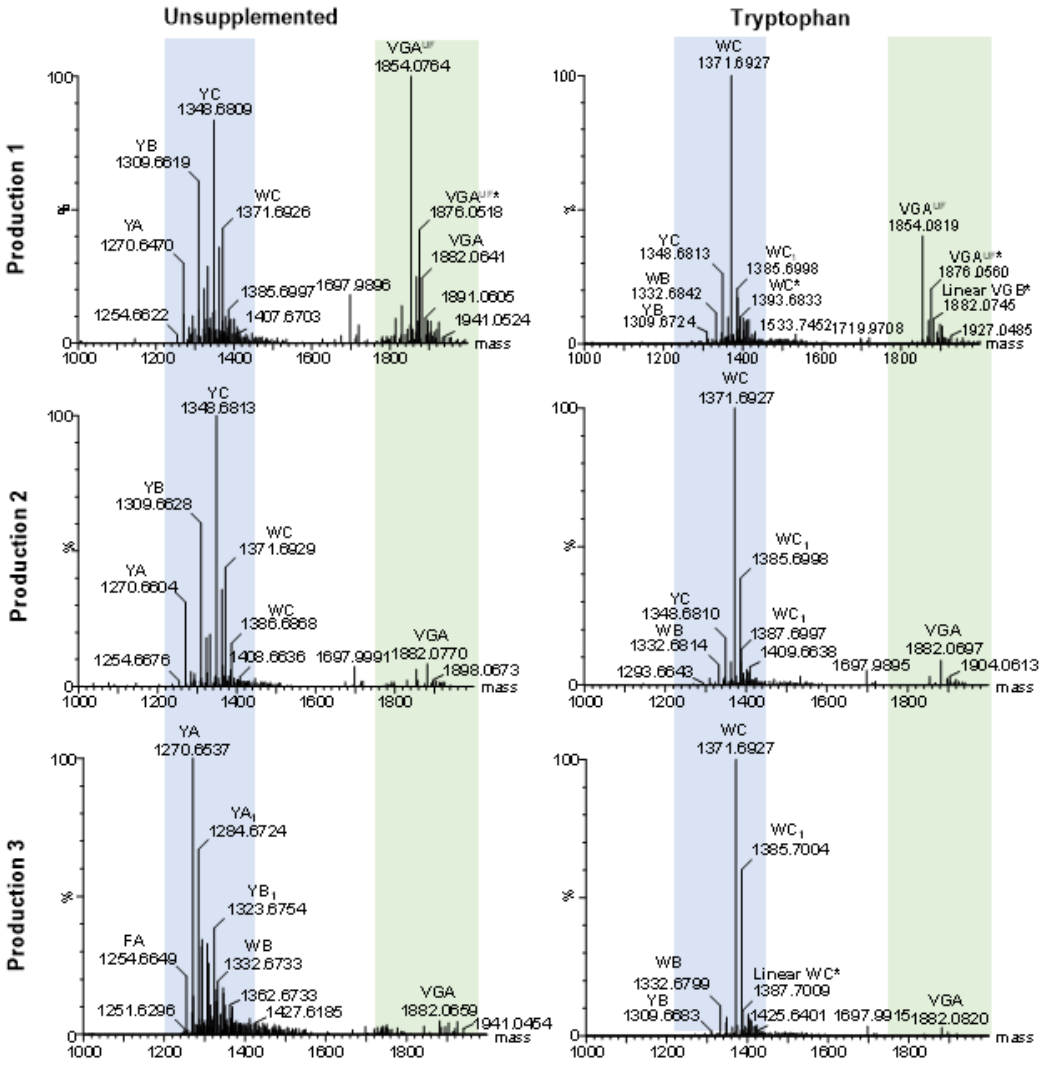

Figure 2.1 ESI-MS mass spectra derived via MassLynx 4.01 MaxEnt 3 algorithm of crude production extracts with mass in Da on the x-axis (mass) and percentage signal intensity on the y-axis (%). The cyclodecapeptides are highlighted in blue and the linear gramicidins in green. The singly charged peptide masses are annotated on the spectra with the peptide identity of the most predominant peptide analogues indicated. A putative identification of a modified linear gramicidin (*m/z* = 1854.08) was annotated as VGA^{UF}. Peptides with sodium adducts are annotated denoted with an Asterix (peptide*).

The milligram crude peptide extract yield per 200 mL culture varied across the three productions. For the first production, the 20 mM Trp supplemented *Br. parabrevis* ATCC10068 (P1W) culture extract yielded only 29.9 mg of lyophilised crude extract per 200 mL culture and the unsupplemented culture (P1U) yielded 20.2 mg. However, the

second production unsupplemented *Br. parabrevis* ATCC10068 cultures had a higher yield of 301.7 mg and 276.9 mg crude extract for P2U-1 and P2U-2, respectively. Moreover, the first (P2W-1) and second (P2W-2) 10 mM Trp supplemented cultures also had a higher yield of 137.6 mg and 168.3 mg, respectively. Interestingly, for the third production series with *Br. parabrevis* ATCC8185, the yield per 200 mL culture for unsupplemented (P3U) and Trp supplemented (P3W) cultures dropped to 38.3 mg and 109.8 mg, respectively. Conversely the Phe supplemented media cultures yielded less crude than the tryptophan and unsupplemented cultures with 111.5 mg and 123.0 mg for production two (P2F-2 and P2F-2), and production three (P3F) yielded a higher crude extract mass than both P3U and P3W with 175.9 mg and 152.7 mg, respectively.

The variation in crude extract mass across productions and media supplementations emphasises the complexity and importance of maintaining optimal culturing conditions for peptide production. As mentioned above, a multitude of factors influence the production rate, yield, and peptide profile. It was observed in this study that higher Trp supplementation concentration and greater production yield were not directly corelated. Trp can be toxic at high concentrations and could therefore lead to a decrease in production biomass [7,16]. Nonetheless, the production profile successfully shifted the % contribution of TpcC and TrcC indicating the more Trp-rich analogues were produced compared to the unsupplemented cultures. Work by Vosloo *et al.* [6,7,13] and Borragerio, C [unpublished] reported differences in peptide profiles even between producer strains alone. This indicated that variances in Trcs and Grms production, observed between producer strains in the absence of amino acid supplementation, are strongly influenced by the regulation of Phe and/or Trp availability, among other factors [5,6,16,17]. The increased crude extract mass in this study could therefore be influenced by the producer strain, colony selection and culture conditions: not only the amino acid supplementation and its concentration. However, the influence of amino acid supplementation on the production profile of the *Br. parabrevis* cultures is not to be dismissed. Prompted by the clear differences in peptide composition and yields between the different productions, the culture extracts were characterized in more detail using UPLC-MS (see Fig. 2.2). Fig. 2.2 illustrates the UPLC-MS chromatograms for the unsupplemented and tryptophan supplemented crude extracts of the three productions. The phenylalanine supplemented productions are summarised in Fig. S2.2. The UPLC-MS solvent gradient (Table 2.4) programs used in this study allow for the elution of the hydrophilic analogues first followed by the more hydrophobic peptides. The hydrophobicity of each peptide analogue depends on the position and identity of its aromatic amino acid residues (position

3, 4, and 7) as shown in Table 2.1 and Fig. 1.6 in Chapter 1. The amphipathic nature of the aromatic amino acids Trp and Tyr allows the tyrocidines and tryptocidines to elute earlier than the phenycidines (Phcs) with hydrophobic Phe residues in positions 3, 4 and 7. According to the amino acid sequences summarised in Table 2.1 and previous results from the BIOPEP Peptide Group [7,14,15,18–20] the elution sequence of the major peptides in this study was found to be as expected: C analogues > B analogues > A analogues > linear gramicidins.

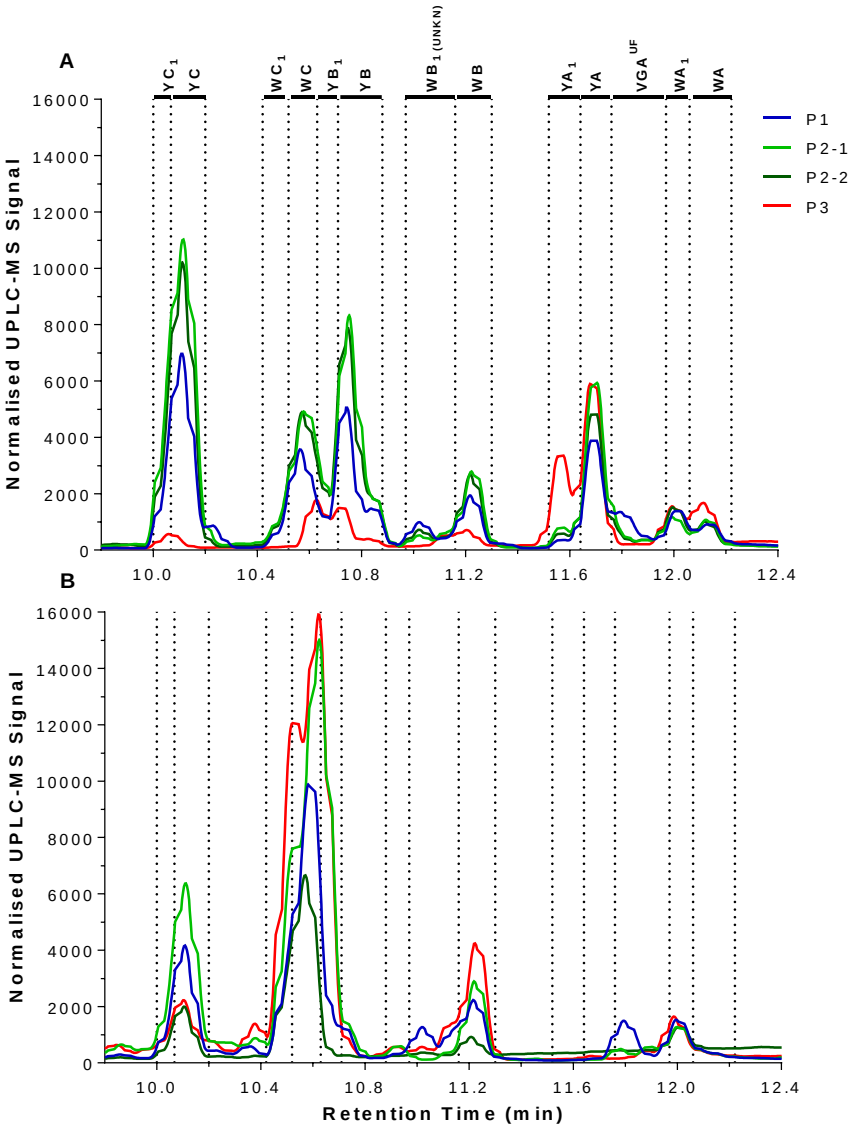

Figure 2.2 Shifts in UPLC elution profiles of crude production extracts after amino acid supplementation of *Br. parabrevis* culture mediums. Unsupplemented (**A**) and tryptophan supplemented (**B**) productions were plotted separately with production one (P1) in blue, two (P2) in green and three (P3) in red. The approximate retention time range of each respective peptide analogue (A/A_1, B/B_1 and C/C_1) as denoted in Table 2.1 is indicated with dotted lines. Unknown peptide elution is indicated at $WB_{1(UNKWN)}$ as shown in Table 2.6 (WB_1+uknwn).

The UPLC chromatograms of the crude extracts in Fig. 2.2 follow the expected elution profile across each production and supplementation. Moreover, the peptide elution profile remains conserved for each supplementation across the three productions. The culture supplementation with Trp shifts the production profile to favour the tryptocidine C/C_1 analogues which elute at a retention time range of 10.30 minutes to 10.56 minutes. Although the characteristic cyclodecapeptide elution sequence is mostly maintained in the experimental results of this study, it is important to note that the co-elution of peptides analogues (even in the case of high-resolution UPLC) is common and can be expected due to the structural similarities between peptides and their tendency to aggregate into higher-order structures [1,5,9,10,21]. For this reason, the percentage contribution (Equation 2.2) was calculated, using the signal contribution of each peptide's extracted doubly charged monomer ion $[M+2H]^{2+}$ profile, and used to deduce the peptide composition of all extracts. The identity of the predominant peptides was confirmed by *m/z* extraction at 20 ppm error and comparison of the extracted peptide ion peak retention time with that of the known analogue in Trc mix. The ESI-MS spectrum within each chromatographic peak was also used to confirm the identity of the peptide in terms of accurate mass (results not shown). From Table 2.6 it can also be noted that the solvent extraction of commercial tyrothricin yielded 20.5 mg of purified tyrocidine peptide mixture (Trc mix) of 96% purity as determined by Equation 2.3. Example UPLC-MS profiles with the extracted peptide peaks are summarised in Figs. S2.3 and S2.4 (supplementary data). A summary of the normalised UPLC-MS signal contributions is also summarised in Table S2.1 in supplementary data.

As shown in the heat map data presented in Table 2.6 the lower Trp supplementation concentration does not adversely influence the peptide production profile. Both Trp-supplemented cultures from production one and two successfully shifted the production profile to favour the production of Trp-rich C analogues, particularly tryptocidine WC/C_1. However, the UPLC-MS chromatogram in Fig. 2.2 showed an overall increase in the normalised UPLC-MS signal for P2W-1 and P3W indicating a higher abundance of Trp-rich peptides in these crude extracts compared to that of the first production. This is complemented by the signal contribution of the tryptocidine C analogues for these productions (refer to Table S2.1). The increased UPLC-MS signal for the second major peak (Rt ≈ 10.55) is of particular interest as this is where the tryptophan-rich tryptocidine C analogues (WC and WC_1) are expected to elute [7,18,22].

Table 2.6. Heat map summary of peptide contributions in the crude production extracts to the ESI-MS signal utilising UPLC-MS. The mg yield is that of the crude extract. Peptide identity (ID) was derived from correlating the doubly charged monomer $[M+2H]^{2+}$ ions in tyrothricin complex (20 ppm error) in extracted chromatograms with that of peptide ions in the standard commercial tyrocidine mixture. The absolute peptide signal of the doubly changed ion was used to calculate the % signal contribution in each extract and depicted as a heat map with blue the lowest contribution and red the highest contribution in each extract. Refer to supplementary data (Table S2.1) for the absolute signal intensities of each peptide in the extracts.

Peptide ID	Rt (minutes)	Trc mix	P1U	P2U-1	P2U-2	P3U	P2F-1	P2F-2	P3F-1	P3F-2	P1W	P2W-1	P2W-2	P3W
WA_1	12.04	0.7	0.4	0.3	0.3	4.8	1.3	1.2	2.5	2.6	0.1	0.0	0.1	0.1
WA	12.12	1.0	1.9	1.7	1.8	7.2	6.3	5.4	5.5	5.1	0.3	0.3	0.3	0.3
YA_1	11.59	9.2	1.8	1.4	1.3	15.4	11.9	10.0	7.8	8.9	0.1	0.0	0.0	0.0
YA	11.69	9.3	7.2	7.8	7.4	27.1	43.0	47.2	18.9	13.9	0.2	0.1	0.1	0.2
FA_1	11.98	0.1	0.1	0.0	0.0	2.0	4.0	3.9	0.3	0.4	0.0	0.0	0.0	0.0
FA	12.09	0.2	0.4	0.3	0.3	4.7	21.0	21.6	0.9	1.1	0.0	0.0	0.0	0.0
WB_1+ unkwn	11.12	1.3	1.0	1.2	1.1	2.6	0.2	0.1	3.0	3.6	1.1	1.4	0.7	1.8
WB	11.20	4.0	7.4	7.8	8.5	5.7	1.5	1.4	9.5	10.7	8.6	8.5	5.5	10.3
YB_1	10.62	14.2	4.5	4.5	5.1	8.9	0.8	0.7	11.3	11.5	0.3	0.1	0.2	0.1
YB	10.71	13.2	11.2	12.9	14.2	9.6	4.4	3.9	13.9	13.5	1.4	1.0	0.9	0.6
WC_1	10.49	2.7	4.1	4.3	4.2	1.1	0.3	0.3	4.1	5.1	17.6	23.7	19.1	33.4
WC	10.55	4.3	12.5	13.4	14.0	1.2	0.8	0.7	5.8	6.3	42.9	39.5	43.8	43.6
YC_1	10.05	11.5	5.8	6.8	5.9	1.1	0.1	0.1	3.7	4.3	3.1	3.3	2.1	1.1
YC	10.10	24.4	24.9	29.7	29.7	3.3	1.4	1.3	7.8	9.1	15.3	12.3	11.6	5.5
IGC	14.37	0.1	0.2	0.1	0.1	0.1	0.0	0.0	0.0	0.0	0.1	0.0	0.0	0.0
IGB	11.74	0.2	2.6	0.8	0.2	0.1	0.1	0.1	0.1	0.0	0.7	0.1	0.1	0.0
IGA	14.67	0.5	1.5	0.8	0.8	0.9	0.4	0.3	1.0	0.6	1.4	1.5	2.7	0.6
VGC	13.25	0.6	0.5	0.4	0.4	0.2	0.1	0.1	0.1	0.1	0.1	0.0	0.0	0.0
VGB	15.31	0.1	0.3	0.1	0.2	0.7	0.3	0.3	0.3	0.3	0.1	0.0	0.0	0.0
VGA^{uf}	11.75	0.3	4.8	1.3	0.3	0.3	0.1	0.2	0.3	0.1	1.2	0.2	0.4	0.1
VGA	14.22	1.9	6.7	4.5	4.4	3.0	1.9	1.2	3.1	2.6	5.3	7.9	12.3	2.2
Yield (mg)		20.5	20.2	301.7	276.9	38.3	111.5	123.0	175.9	152.7	29.9	137.6	168.3	109.8

The combined contribution of WC and WC_1 is 60.5 % to the total signal intensity of P1W. For the first and second cultures of tryptophan supplemented production two, P2W-1 and P2W-2, the combined contribution of tryptocidine C analogues was 63.2 % and 62.9 % to the total signal intensity, respectively. While P3W had a combined contribution of 77% for WC and WC_1. This increase in abundance of tryptocidines in the second and third production is supported by the increase in signal observed for the P3W and P2W UPLC chromatograms. Unsupplemented productions showed a much lower abundance of WC compared to that of the tryptophan supplemented productions as can be seen in the heatmap summary (Table 2.6). The major cyclodecapeptides in the unsupplemented productions were YC and YB, as denoted in Table 2.6. After confirming the successful shifts in production profiles and determining the peptide composition of the crude extracts via ESI-MS and UPLC-MS, the extracts were purified using HPLC.

2.4.2 Semi-preparative RP-HPLC purification of the cyclodecapeptides from crude peptide extracts

RP-HPLC is a powerful tool for the isolation of hydrophobic Trcs from the production of crude extracts [23]. However, the co-elution of and low resolution between Trc analogues makes the HPLC purification of single analogues challenging [1,5,9,10,21]. The absorbance of UV-light above 250 nm by the aromatic amino acids and the prevalence of these aromatic residues in the tyrothricin complex allows for the quantitative analysis and purification of the crude peptide extracts via HPLC [6,15,24]. The semi-preparative HPLC chromatograms in Fig. 2.3 show the shift in both the retention time and absorbance at 254 nm for the different crude production extracts. These shifts in elution profiles correlate to the UPLC-MS chromatograms in Fig. 2.2 and indicate a shift in the peptide production profile between the different *Br. parabrevis* cultures and different supplemented media. A decrease in absorbance indicates a decreased abundance of peptides and a shift in retention time indicates the presence of different peptide analogues and probably oligomers. Fig. 2.3 shows the fraction collection profiles of each production and their respective retention time ranges for the purification of the different peptide analogues. All samples were subject to the gradient program described in Table 2.3 over 20 minutes with 15 minutes washing and re-equilibration and absorbance was measured at 254 nm.

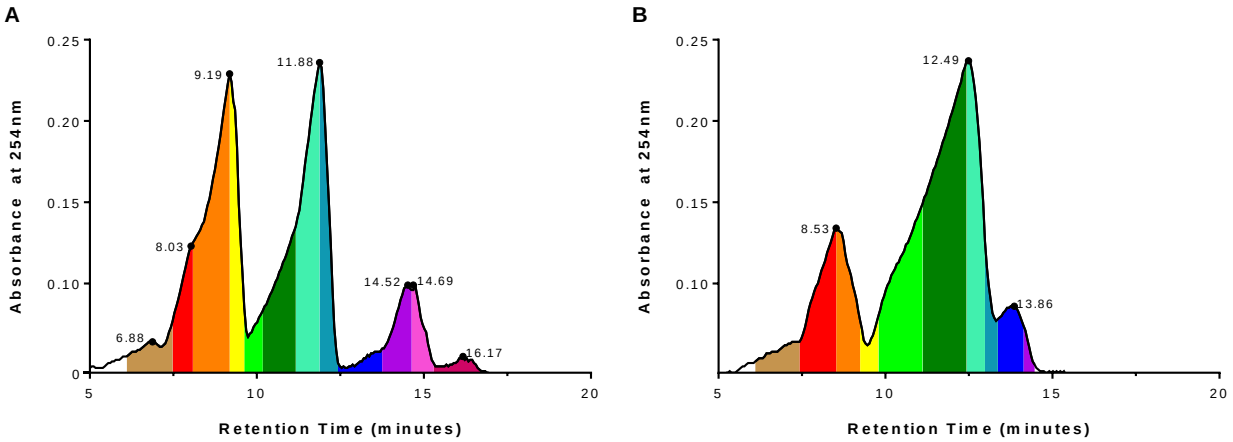

C

		Supplementation			
		Unsupplemented		Tryptophan	
Fraction[a]	colour	Rt_s	Rt_f	Rt_s	Rt_f
1		6.11	7.48	6.11	7.48
2		7.54	8.09	7.54	8.53
3		8.14	9.19	8.58	9.24
4		9.24	9.63	9.30	9.79
5		9.68	10.18	9.85	11.11
6		10.23	11.17	11.17	12.43
7		11.22	11.88	12.49	12.98
8		11.94	12.43	13.04	13.37
9		12.49	13.75	13.42	14.14
10		13.81	14.58	14.47	14.25
11		14.63	15.40	-	-
12		15.35	16.94	-	-

Figure 2.3. HPLC fraction collection profiles of respective supplementations from production two.(**A**) Unsupplemented productions HPLC fraction collection profile (**B**) Tryptophan supplemented productions HPLC fraction collection profile. (**C**) Table summarising each HPLC fraction and their respective retention time ranges at which collection starts (Rt_s) and finished (Rt_f). Each fraction collection is highlighted by a different colour and numbered consecutively, starting from the first fraction (F1) collected highlighted in beige, F2 in red, F3 in orange, F4 in yellow, F5 in light green, F6 in dark green, F7 in cyan, F8 in light blue, F9 in dark blue, F10 in purple, F11 in pink and F12 in magenta. Absorbance was measured at 254 nm over 35 minutes with a gradient program described in Table 2.3. [a] HPLC fraction collection.

The general elution sequence of the major peptides across each production was in accordance with what was predicted previously and by the BIOPEP group [7,14,15,18–20] by UPLC-MS analyses and peptide amino acid structures and is as follows: YC_1/C > WC_1/C > YB_1/B > WB_1/B> YA_1/A > linear gramicidins. The collection Rt ranges for each fraction were therefore selected in agreement with the expected peptide elution profiles for each production as determined via UPLC-MS (Fig. S2.2). Tables 2.7-2.9 summarises the

proposed peptide identity (ID) and signal contribution, as determined by ESI-MS analysis, of each of the HPLC fractions purified from the production crude extracts.

Table 2.7 Summary of the proposed peptide identity (ID) and signal contribution as determined by ESI-MS analysis of each of the HPLC fractions purified from the unsupplemented production one crude extract.

	Medium Suppl.[a]	Frac.[b]	Mass (mg)[c]	Experimental M_r $[M+H]^+$	Theoretical M_r $[M+H]^+$	Mass Error[d] (ppm)	Signal Contrib.[e] (%)	Peptide ID[f]
Production 1	Unsupplemented	1	0.608	1362.6882	1362.6999	8.6	15.8	YC_1
		2	1.259	1362.6924	1362.6999	5.5	33.6	YC_1
				1348.6813	1348.6842	2.2	30.5	YC
		3	1.938	1348.6813	1348.6842	2.2	59.9	YC
				1349.6818	1349.6683	10.0	10.4	YC^D
		4	1.33	1348.6813	1348.6842	2.2	19.5	YC
				1323.6850	1323.6890	3.0	15.8	YB_1
		5	0.7	1309.6650	1309.6733	6.3	44.9	YB
				1323.6812	1323.6890	5.9	23.0	YB_1
		6	2.257	1309.6680	1309.6733	4.0	48.4	YB
		7	1.924	1309.6656	1309.6733	5.9	33.0	YB
				1338.6831	1338.6761	5.2	11.6	YB_1^O
				1371.6927	1371.7002	5.5	17.0	WC
		8	0.909	1371.6927	1371.7002	5.5	28.0	WC
				1400.7073	1400.7030	3.1	10.5	WC_1^O
		9	0.803	1270.6534	1270.6624	7.1	36.6	YA
				1271.6620	1271.6465	12.2	13.3	YA^D
		10	0.792	1270.6525	1270.6624	7.8	43.3	YA
				1332.6838	1332.6893	4.1	19.8	YB
		11	0.914	1270.6549	1270.6624	5.9	28.0	YA
				1299.6716	1299.6652	4.9	18.1	YA_1^O
				1332.6798	1332.6893	7.1	10.3	WB
		12	1.101	1270.6735	1270.6624	8.7	14.5	YA
				1309.6843	1309.6733	8.4	10.6	YB

[a] Amino acid supplementation of *Br. parabrevis* cultures as described in Table 2.2.
[b] HPLC fraction numbers as outlined in Fig. 2.3.
[c] lyophilised fraction sample mass.
[d] Parts per million error or ppm errors calculated as per Equation 2.1.
[e] Percentage contribution calculated using Equation 2.2. Only percentages >5 % are reported in Table 2.7.
[f] Peptide modifications indicated as follows: Deamination ($peptide^D$), oxidised ($peptide^O$), linear sodium adduct, ($peptide^\$$) and single amino acid substitution ($peptide^?$).

Looking at the HPLC collection profile in Fig. 2.3 it can be expected that fractions 2,3,4,6,7,8,9,10 and 11 would yield more peptide for all productions as they are collected across the Rt ranges for the two major elution peaks (Table 2.7). For the unsupplemented production, the total mass (mg) of peptide collected in fractions 2,3,4,6,7,8,10 and 11 is higher than that of fractions 1,5,9 and 12 (Table 2.7). The highest yield of peptide in P1U was in fraction 6 (2.257 mg) consisting predominantly of YB (48.4 %). The fraction with the

highest percentage of WC for P1U is fraction 8 (28.0 %). Meanwhile fraction 3 had the highest prevalence of YC (59.9 %) with its major contaminant probably being a deaminated YC (10.4 %).

Table 2.8 Summary of the proposed peptide identity (ID) and signal contribution as determined by ESI-MS analysis of each of the HPLC fractions purified from the tryptophan supplemented production one crude extract.

	Medium Suppl.[a]	Frac.[b]	Mass (mg)[c]	Experimental M_r $[M+H]^+$	Theoretical M_r $[M+H]^+$	Mass Error[d] (ppm)	Signal Contrib.[e] (%)	Peptide ID[f]
Production 1	20mM Tryptophan	1	0.518	1362.6882	1362.6999	8.6	12.0	YC_1
		2	2.017	1349.6816	1349.6683	9.9	31.4	YC^D
				1362.6882	1362.6999	8.6	15.5	YC_1
				1348.7242	1348.7478	17.5	12.9	YC
		3	1.154	1348.6813	1348.6842	2.2	21.2	YC
				1377.6957	1377.6870	6.3	11.6	YC_1^O
		4	0.705	1309.6667	1309.6733	5.1	25.2	YB
				1385.7008	1385.7159	10.9	12.4	WC_1
		5	1.050	1371.6927	1371.7002	5.5	40.9	WC
				1385.7020	1385.7159	10.0	23.5	WC_1
		6	5.784	1371.6927	1371.7002	5.5	54.4	WC
		7	2.083	1371.6927	1371.7002	5.5	29.1	WC
				1400.7073	1400.7030	3.1	20.3	WC_1^O
				1332.6823	1332.6893	5.3	16.0	WB
		8	0.782	1332.6755	1332.6893	10.4	36.5	WB
				1270.6602	1270.6624	1.8	15.2	YA
		9	0.982	1293.6785	1293.6784	0.1	19.7	WA
		10	0.350	1332.6794	1332.6893	7.4	28.0	WB
		11	0.950	1371.6927	1371.7002	5.5	27.5	WC

[a] Amino acid supplementation of *Br. parabrevis* cultures as described in Table 2.2.
[b] HPLC fraction numbers as outlined in Fig.2.3.
[c] lyophilised fraction sample mass.
[d] Parts per million error or ppm errors calculated as per Equation 2.1.
[e] Percentage contribution calculated using Equation 2.2. Only percentages >5 % are reported in Table 2.8.
[f] Peptide modifications indicated as follows: Deamination ($peptide^D$), oxidised ($peptide^O$), linear sodium adduct, ($peptide^\$$) and single amino acid substitution ($peptide^?$)

For the tryptophan supplemented productions, the expected fractions with the highest amount of peptide eluted are fractions 6 and 7 (Tables 2.8 and 2.9). For P1W (Table 2.8) fraction 6 and 7 yielded 5.784 mg and 2.083 mg, respectively. For P2W (Table 2.9) fraction 6 and 7 yielded 2.31 mg and 6.36 mg, respectively. The highest yield of WC for P1W was fraction 6 with 54.4 % contribution with no contaminants above >5 % contribution. Fraction

5 also had a high tryptocidine contribution of 40.9 % WC and 23.5 % WC_1 contribution. Fractions two and three had the highest contribution of tyrocidine C's. Unfortunately, both fractions were contaminated with modified YC analogues, that were putatively identified as deaminated YC (31.4%) and oxidised YC_1 (11.6%). Meanwhile, the combined contribution of tyrocidine C analogues remains high with 59.9% for fraction 2 and 32.9% for fraction 3.

Table 2.9 Summary of the proposed peptide identity (ID) and signal contribution as determined by ESI-MS analysis of each of the HPLC fractions purified from the tryptophan supplemented production two crude extracts.

	Medium Suppl.[a]	Frac.[b]	Mass (mg)[c]	Experimental M_r $[M+H]^+$	Theoretical M_r $[M+H]^+$	Mass Error[d] (ppm)	Signal Contrib.[e] (%)	Peptide ID[f]
Production 2	10mM Tryptophan	1	0.521	1362.6886	1362.6999	8.3	12.0	YC_1
		2	0.91	1348.6813	1348.6842	2.2	39.6	YC
				1362.6884	1362.6999	8.4	23.9	YC_1
		3	1.187	1348.6812	1348.6842	2.3	47.0	YC
		4	0.776	1348.6813	1348.6842	2.2	11.0	YC
		5	2.12	1371.6927	1371.7002	5.5	31.3	WC
				1385.7013	1385.7159	10.5	27.2	WC_1
				1309.6638	1309.6733	7.3	14.0	YB
		6	2.231	1371.6927	1371.7002	5.5	45.1	WC
				1385.6998	1385.7159	11.6	28.3	YC
		7	6.356	1371.6927	1371.7002	5.5	69.9	WC
				1385.7062	1385.7159	7.0	13.9	WC_1
		8	1.419	1371.6927	1371.7002	5.5	37.6	WC
				1332.6820	1332.6893	5.5	14.4	WB
				1378.6963	1378.6836	9.2	11.2	$YA^{?}$
		9	0.504	1332.6761	1332.6893	9.9	58.0	YB
		10	0.709	1332.6874	1332.6893	1.4	25.9	YB
				1387.6908	1387.6689	15.8	16.0	$YC^{\$}$
		11	1.851	1371.6927	1371.7002	5.5	35.1	YC

[a] Amino acid supplementation of *Br. parabrevis* cultures as described in Table 2.2.
[b] HPLC fraction numbers as outlined in Fig. 2.3.
[c] lyophilised fraction sample mass.
[d] Parts per million error or ppm errors calculated as per Equation 2.1.
[e] Percentage contribution calculated using Equation 2.2. Only percentages >5 % are reported in Table 2.9.
[f] Peptide modifications indicated as follows: Deamination ($peptide^{D}$), oxidised ($peptide^{O}$), linear sodium adduct, ($peptide^{\$}$) and single amino acid substitution ($peptide^{?}$).

P2W had the highest yield across all productions with fraction 7 (6.36 mg) consisting of 69.9 % WC and 13.9% WC_1. Fraction 8 is contaminated with an unknown peptide that has been putatively identified as a modified single amino acid substitution of YA ($YA^{?}$). Both fractions 2 and 9 had no contaminants above >5 % contribution, therefore, making them the fractions with the highest YC and YB purity, respectively. The structural similarity between

the peptide analogues and their tendency to aggregate and/or form hetero- and homo-oligomers causes them to co-elute making the isolation of single analogues [9,10] from HPLC purified fractions particularly challenging and laborious. Although the direct injection ESI-MS analysis gives a good indication of the peptide composition, UPLC-MS analysis is required to accurately determine the peptide purity. Fractions predominantly containing C analogues (YC/C_1 and WC/C_1) with a percentage contribution larger than 30 % were therefore selected for further analysis using UPLC-MS to determine their percentage purity. Fraction 3 yielded 1.19 mg of 47.0 % YC and fraction 9 yielded 0.50 mg of 58.0 % YB.

2.4.3 Characterisation and peptide purity determination of selected C analogues using UPLC-MS.

The purification of the tryptophan-rich C-analogues (YC/C_1 and WC/C_1) is of particular interest for this study due to the intrinsic fluorescence of tryptophan and its role in the photo-induced fabrication of biologically active cyclo-decapeptide metal nanoparticle (CDP-MNP) hybrid nanostructures (See Chapter 3 and 4) [25–30]. Fractions with the highest abundance of C analogues were selected for UPLC-MS analyses to determine their percentage peptide purity. From this selection, the fractions with the purest (percentage purity >90 %) C analogues are summarised in Table 2.10 and illustrated in Figs. 2.4-2.7. Only peptide analogues with >90 % purity were identified using ESI-MS mass spectra derived via the MassLynx 4.01 MaxEnt 3 algorithm. The calculated mass error for each analogue present in the pure fractions was smaller than 10 ppm, confirming the accurate peptide identification. The ESI-MS analysis of the selected fractions, summarised in Table 2.10, revealed that each fraction contained a high purity (>90 %) of either WC or YC with the main contaminants being their C_1 analogues or deaminated counterparts. The fraction with the highest purity and yield is fraction 7 (Fig. 2.7) from P2W with a combined purity of 99.2% WC/C_1 and a yield of 6.356 mg. P1U fraction 3 yielded 1.938 mg tyrocidine C (94.2% purity). While the fraction with the least contaminants (percentage of contaminants <4 %) is fraction 3 (Fig. 2.6) from P2W with a yield of 1.187 mg. This fraction has a high purity of YC (92.6%) but is contaminant by the sodium adducts of YA (YA$^{\$}$). Sodium adducts often result due to the exposure of peptides to sodium ions in in-culture production and extraction [7,8,20,22]. Even though this fraction has a very low percentage of contaminants; it does not have the highest combined purity. Contaminants lower than <2% were not summarised in Table 2.10. Therefore, despite contributing less than two percent each, the combined contribution of the remainder of the contaminants contributes 3.5%.

Table 2.10 Summary of purified C analogues from selected HPLC fractions for this study.

Suppl.[a]	Frac.[b]	Mass (mg)[c]	Experimental M_r $[M+H]^+$	Theoretical M_r $[M+H]^+$	Mass Error[d] (PPM)	% Purity[e]	Peptide ID[f]	% Comb.[g]
P1U	3	1.938	1348.6814	1348.6842	2.1	82.7	YC	94.2
			1349.6706	1349.6683	1.7	11.5	YC^D	
P1W	6	5.784	1371.6927	1371.7002	5.5	78.2	WC	97.5
			1385.7067	1385.7159	6.6	11.4	WC_1	
			1372.6904	1372.6842	4.5	7.9	WC^D	
P2W	3	1.187	1348.6813	1348.6842	2.2	92.6	YC	96.5
			1387.6960	1387.6689	19.5	3.9	$YC^\$$	
	7	6.356	1371.6927	1371.7002	5.5	85.6	WC	99.2
			1385.7075	1385.7159	6.0	13.6	WC_1	

[a] Amino acid supplementation of *Br. parabrevis* cultures as described in Table 2.2
[b] HPLC Fraction numbers as outlined in Fig.2.3
[c] lyophilised fraction sample mass
[d] Parts per million error or ppm errors calculated as per Equation 2.1.
[e] Percentage purity was calculated by expressing the peak area of the UPLC-MS chromatogram for each peptide as a percentage of the sum of the peak areas of all the peptides present. It was assumed that the response factors of all peptides are similar due to their analogue structures. Only fractions with a combined purity >90 % are summarised in this Table. For each fraction, the peptide with >5 %purity was summarised and identified via UPLC-MS.
[f] Peptide modifications indicated as follows: Deamination ($peptide^D$), oxidised ($peptide^O$), linear sodium adduct ($peptide^\$$) and single amino acid substitution ($peptide^?$)
[g] Combined percentage purity of C analogues for tryptocidine ($WC/C_1/C^D$) or tyrocidine ($WC/C_1/C^D$)

As shown in the UPLC chromatograms and associated MaxEnt 3 ESI-MS mass spectra (Figs. 2.4-2.7), the retention times of these analogues and modified peptides are close to one another. The general elution sequence for these analogues is WC_1 > WC > WC^D for the tryptocidines and YC_1 > YC > YC^D for the tyrocidines as shown in Figs. 2.4-2.7. The relationship between these peptide analogues is illustrated well in Fig. 2.5 with the elution of WC (M_r =1371.6927) at Rt= 9.18, WC_1 (M_r = 1385.7067) at Rt = 9.06 and WC's deaminated counterpart (M_r = 1372.6904) at Rt=9.32. The co-elution of these peptides and their C_1-analogue or modified counterparts can be expected in lower resolution semi-preparative RP-HPLC. Moreover, Rautenbach *et al.* [10] have shown that the Trp-rich peptide C analogues (WC/C_1 and YC/C_1) have a high propensity to oligomerise or self-assemble. All the above-mentioned factors complicate further purification of these already HPLC purified fractions. The samples were therefore not purified further and the percentage purity of the C, C_1, deaminated and modified analogues was combined to give a percentage purity of $YC/C_1/C^D$ and $WC/C_1/C^D$. All fractions summarised in Table 2.10 had a combined purity larger than 90 % and yields ≥ 1 mg. The purity and yield were therefore sufficient for further use in this study (Chapters 3 and 4).

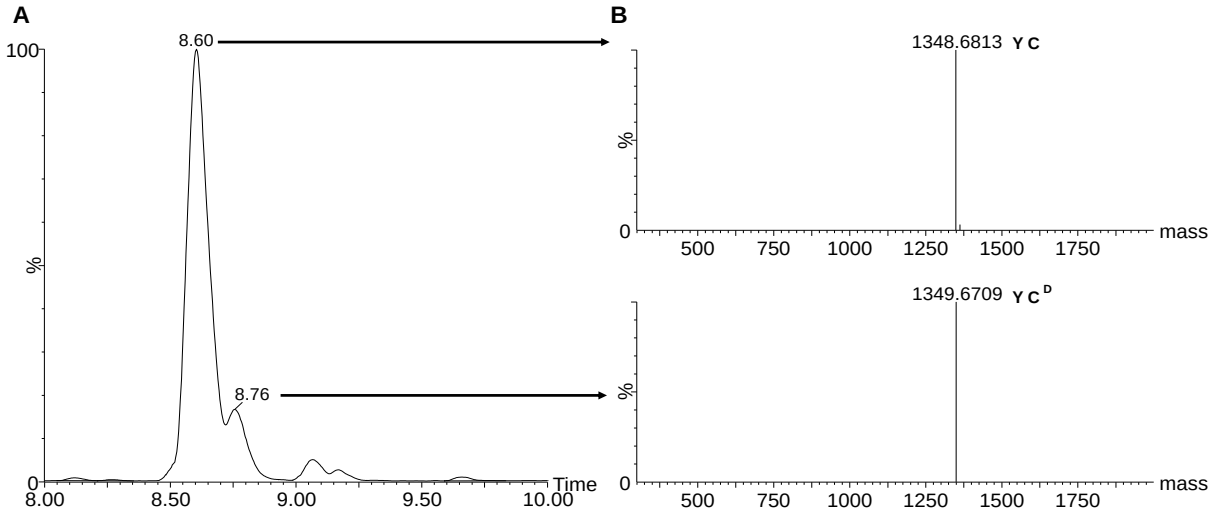

Figure 2.4 UPLC-MS and ESI-MS analysis of HPLC purified fraction three from unsupplemented production one (P1U). (**A**) UPLC-MS chromatogram of HPLC purified P1U fraction 3 with the retention time annotated at the top of each predominant peak (percentage purity >2%).(**B**) ESI-MS mass spectrum derived via MassLynx 4.01 MaxEnt 3 algorithm for each peak (as indicated by arrows) with the experimental M_r $[M+H]^+$ of each peptide peak annotated on the spectra.

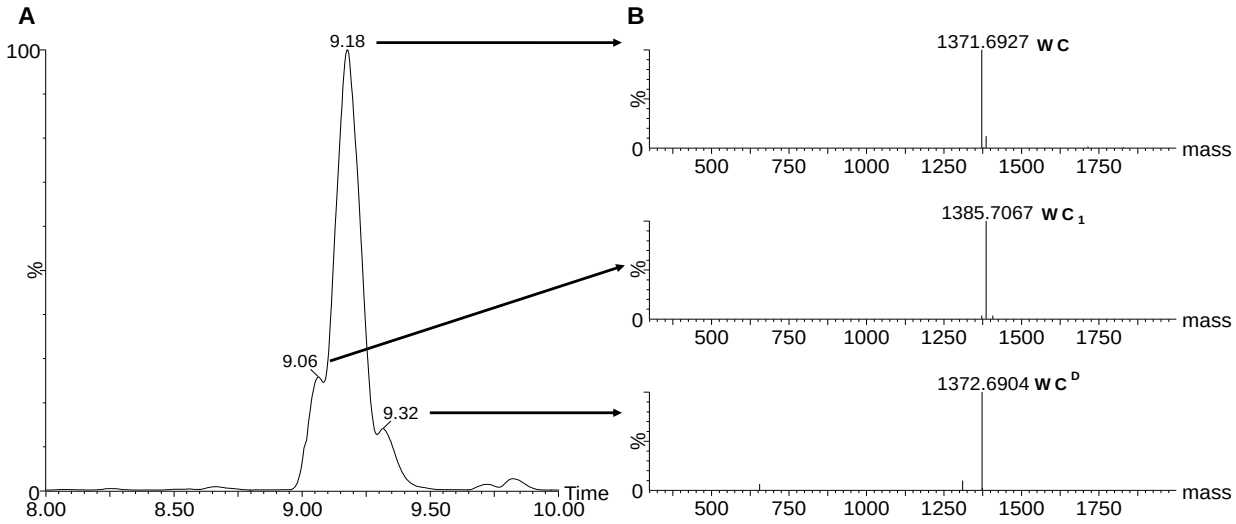

Figure 2.5 UPLC-MS and ESI-MS analysis of HPLC purified fraction six from tryptophan supplemented production one (P1W). (**A**) UPLC-MS chromatogram of HPLC purified P1W fraction 6 with the retention time annotated at the top of each predominant peak (percentage purity >2 %). (**B**) ESI-MS mass spectrum derived via MassLynx 4.01 MaxEnt 3 algorithm for each peak (as indicated by arrows) with the experimental M_r $[M+H]^+$ of each peptide peak annotated on the spectra.

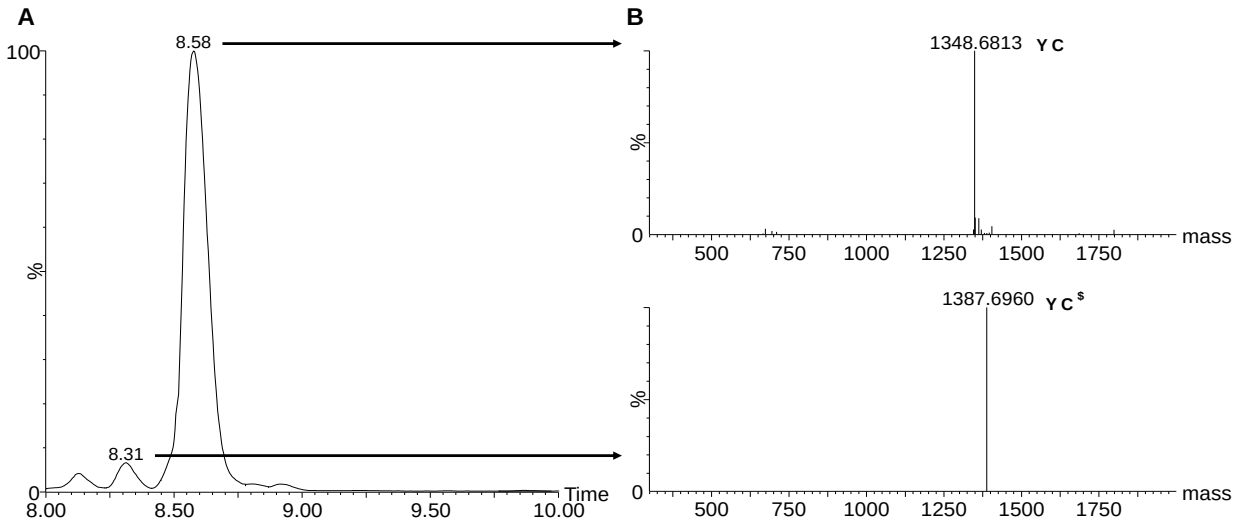

Figure 2.6 UPLC-MS and ESI-MS analysis of HPLC purified fraction three from tryptophan supplemented production two (P2W). (**A**) UPLC-MS chromatogram of HPLC purified P2W fraction 3 with the retention time annotated at the top of each predominant peak (percentage purity >2 %). (**B**) ESI-MS mass spectrum derived via MassLynx 4.01 MaxEnt 3 algorithm for each peak (as indicated by arrows) with the experimental M_r $[M+H]^+$ of each peptide peak annotated on the spectra.

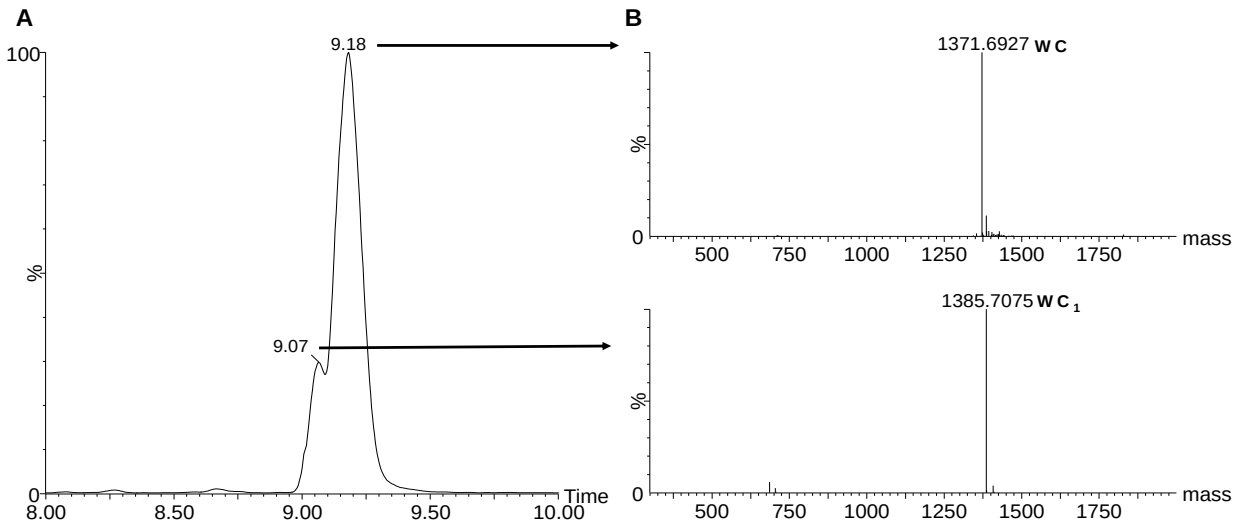

Figure 2.7 UPLC-MS and ESI-MS analysis of HPLC purified fraction seven from tyrptophan supplemented production two (P2W). (**A**) UPLC-MS chromatogram of HPLC purified P2W fraction 7 with the retention time annotated at the top of each predominant peak (percentage purity >2 %). (**B**) ESI-MS mass spectrum derived via MassLynx 4.01 MaxEnt 3 algorithm for each peak (as indicated by arrows) with the experimental M_r $[M+H]^+$ of each peptide peak annotated on the spectra.

2.5 Conclusions

Production profiles of *Br. parabrevis* cultures were successfully shifted to produce Trcs using the methodologies developed by BIOPEP peptide group at Stellenbosch University [7]. Supplementation of *Br. parabrevis* cultures with tryptophan promoted the production of Trp-rich C analogues, particularly the tryptocidines. This aided in the purification process for the isolation of C analogues for future applications in Chapters 3 and 4. Unfortunately, the first production series indicated aberrated production with lower yields and a high prevalence of modified linear gramicidins (VGA^{UF}). Peptide production is a complex process influenced by a multitude of factors. It is therefore challenging to pinpoint the cause of this non-ribosomal production of peptides. However, production two and three had a reduced amino acid supplementation concentration, higher mg yields and were void of VGA^{UF}. Production two had an amino acid supplementation concentration of 10 mM and production one had a 20 mM for both Trp and Phe. Although the work in this study cannot determine the influence of amino acid supplementation concentration on the production yield and aberrated production of modified peptides, future work could investigate this relationship for applications in optimised peptide production and purification. The sequence similarity and tendency of the tyrocidines to self-assemble, oligomerise and co-elute, made purification of single peptide analogues challenging. Yet, the self-assembling nature of the tyrocidines is promising for future formulations and peptide-assisted nanoformulation fabrication. Tyrocidine C and tryptocidine C analogues of sufficient yield (≥ 1 mg) and purity (>90 %), as determined by UPLC-MS, were successfully purified from production crude extracts using established RP-HPLC methodologies. While a tyrocidine peptide mixture (Trc mix) was successfully purified (>90% purity) via organic solvent extractions for the removal of linear gramicidins. These peptides required no further purification for the purpose of this study, therefore, conserving the time, resources and money needed for further RP-HPLC or higher resolution purification. Only peptides with high purity (>90 %) were selected for use for the remainder of this study.

2.6 References

[1] X.J. Tang, P. Thibault, R.K. Boyd, Characterisation of the tyrocidine and gramicidin fractions of the tyrothricin complex from *Bacillus brevis* using liquid chromatography and mass spectrometry, Int. J. Mass Spectrom. Ion Process. 122 (1992) 153–179. https://doi.org/10.1016/0168-1176(92)87015-7.

[2] R.D. Hotchkiss, R.J. Dubos, The isolation of bactericidal substances from cultures of *Bacillus Brevis,* J. Biol. Chem. 141 (1941) 155–162. https://doi.org/10.1016/s0021-9258(18)72830-5.

[3] R.J. Dubos, C. Cattaneo, Studies on a bactericidal agent extracted from a soil bacillus III. Pre-earation and activity of a protein-free fraction, J. Exp. Med. 70 (1939) 249–256.

https://doi.org/10.1084/jem.70.3.249.

[4] A. Paladini, L.C. Craig, V. 76, A. Paladini1, The chemistry of tyrocidine. III. The structure of tyrocidine A, J. Am. Chem. Soc. 76 (1954) 688–692. https://doi.org/10.1021/ja01632a015.

[5] J.A. Vosloo, J.L. Snoep, M. Rautenbach, Modelling the variable incorporation of aromatic amino acids in the tyrocidines and analogous cyclodecapeptides, J. Appl. Microbiol. 127 (2019) 1665–1676. https://doi.org/10.1111/jam.14430.

[6] J.A. Vosloo, M. Rautenbach, Following tyrothricin peptide production by *Brevibacillus parabrevis* with electrospray mass spectrometry, Biochimie. 179 (2020) 101–112. https://doi.org/10.1016/j.biochi.2020.09.004.

[7] J.A. Vosloo, M.A. Stander, A.N.N. Leussa, B.M. Spathelf, M. Rautenbach, Manipulation of the tyrothricin production profile of *Bacillus aneurinolyticus*, Microbiology. 159 (2013) 2200–2211. https://doi.org/10.1099/mic.0.068734-0.

[8] S.N. Berge, Production and characterisation of analogues of the antimicrobial tyrocidine peptides with modified aromatic amino acid residues, Stellenbosch University, Stellenbosch, South Africa, 2018. http://hdl.handle.net/10019.1/103710.

[9] H.H. Paradies, Aggregation of tyrocidine in aqueous solutions, Biochem. Biophys. Res. Commun. 88 (1979) 810–817. https://doi.org/10.1016/0006-291X(79)91480-3.

[10] M. Rautenbach, V. Kumar, J.A. Vosloo, Y. Masoudi, R.J. van Wyk, M.A. Stander, Oligomerisation of tryptocidine C, a Trp-rich cyclodecapeptide from the antimicrobial tyrothricin complex, Biochimie. (2021). https://doi.org/10.1016/j.biochi.2020.12.006.

[11] M. Thies, H.H. Paradies, Self-assembly of tyrocidines in nanotubular structures, MRS Online Proc. Libr. 489 (1998) 145–151. https://doi.org/10.1557/proc-489-145.

[12] M.A. Ruttenberg, T.P. King, L.C. Craig, J. SvU, R. Breslow, D. Chipman, The use of the tyrocidines for the study of conformation and aggregation behavior, J. Am. Chem. Soc. 87 (1965) 4196–4198. https://doi.org/10.1021/ja01096a040.

[13] J.A. Vosloo, Optimised bacterial production and characterisation of natural antimicrobial peptides with potential application in agriculture, Stellenbosch University,Stelllenbosch, South Africa., 2016. https://hdl.handle.net/10019.1/98411.

[14] M. Rautenbach, N.M. Vlok, M. Stander, H.C. Hoppe, Inhibition of malaria parasite blood stages by tyrocidines, membrane-active cyclic peptide antibiotics from *Bacillus brevis*, Biochim Biophys Acta. 1768 (2007) 1488–1497. https://doi.org/10.1016/j.bbamem.2007.01.015.

[15] H.A. Eyéghé-bickong, Role of surfactin from *Bacillus subtilis* in protection against antimicrobial peptides produced by Bacillus species., Stellenbosch University,Stelllenbosch, South Africa., 2011. https://hdl.handle.net/10019.1/6773.

[16] J.L. Stokes, C.R. Woodward, Formation of tyrothricin in submerged cultures of *Bacillus Brevis*, J. Bacteriol. 46 (1943) 83–88. https://doi.org/10.1128/jb.46.1.83-88.1943.

[17] M.A. Ruttenberg, B. Mach, Studies on amino acid substitution in the biosynthesis of the antibiotic polypeptide tyrocidine, Biochemistry. 5 (1966) 2864–2869. https://doi.org/10.1021/bi00873a013.

[18] M. Rautenbach, N.M. Vlok, H.A. Eyéghé-Bickong, M.J. van der Merwe, M.A. Stander, An electrospray ionization mass spectrometry study on the "*in vacuo*" hetero-oligomers formed by the antimicrobial peptides, surfactin and gramicidin S, J. Am. Soc. Mass Spectrom. 28 (2017) 1623–1637. https://doi.org/10.1007/s13361-017-1685-0.

[19] Y. Masoudi, Characterisation and formulation of natural cyclodecapeptides with anti-*Candida* activity, Stellenbosch University,Stellenbosch, South Africa, 2021. http://hdl.handle.net/10019.1/109933.

[20] R.J. Van Wyk, Development of cyclodecapeptides from the tyrothricin complex as anticancer peptides, Stellenbosch University, Stellenbosch, South Africa, 2019. http://hdl.handle.net/10019.1/105712.

[21] G. Munyuki, G.E. Jackson, G.A. Venter, K.E. Kövér, L. Szilágyi, M. Rautenbach, B.M. Spathelf, B. Bhattacharya, D. Van Der Spoel, β-sheet structures and dimer models of the two major tyrocidines, antimicrobial peptides from *Bacillus aneurinolyticus*, Biochemistry. 52 (2013) 7798–7806. https://doi.org/10.1021/bi401363m.

[22] B. Spathelf, Qualitative structure-activity relationships of the major tyrocidines, cyclic decapeptides from *Bacillus aneurinolyticus*, Stellenbosch University,Stellenbosch, South Africa., 2013.

http://hdl.handle.net/10019.1/4001.

[23] J.X. Huang, G. Guiochon, Applications of preparative high-performance liquid chromatography to the separation and purification of peptides and proteins, J. Chromatogr. 492 (1989) 431–467. https://doi.org/10.1016/S0378-4347(00)84477-1.

[24] C. Eaborn, Tables of spectral data for structure determination of organic compounds, 2nd ed., Springer, Berlin, 1984. https://doi.org/10.1016/0022-328x(84)80083-2.

[25] A.B.T. Ghisaidoobe, S.J. Chung, Intrinsic tryptophan fluorescence in the detection and analysis of proteins: A focus on Förster resonance energy transfer Techniques, Int. J. Mol. Sci. 15 (2014) 22518–22538. https://doi.org/10.3390/ijms151222518.

[26] S. Roy, T.K. Das, Study of Interaction Between tryptophan, tyrosine, and phenylalanine separately with silver nanoparticles by fluorescence quenching method, J. Appl. Spectrosc. 82 (2015) 598–606. https://doi.org/10.1007/s10812-015-0151-7.

[27] S. Si, T.K. Mandal, Tryptophan-based peptides to synthesize gold and silver nanoparticles: A mechanistic and kinetic study, Chem. - A Eur. J. 13 (2007) 3160–3168. https://doi.org/10.1002/chem.200601492.

[28] V. Kumar, N.K. Mishra, S. Gupta, K.B. Joshi, Short peptide amphiphile cage facilitate engineering of gold nanoparticles under the laser field, ChemistrySelect. 2 (2017) 211–218. https://doi.org/10.1002/slct.201601548.

[29] A. Nasrolahi Shirazi, D. Mandal, R.K. Tiwari, L. Guo, W. Lu, K. Parang, Cyclic peptide-capped gold nanoparticles as drug delivery systems, Mol. Pharm. 10 (2013) 500–511. https://doi.org/10.1021/mp300448k.

[30] N.T.T. Nga, H.V. Tran, C.H. Dang, An Investigation on the synthesis, structure and specific properties of Zn(II) and Cu(II) complexes with tryptophan, Biointerface Res. Appl. Chem. 13 (2023). https://doi.org/10.33263/BRIAC131.002.

2.7 Supplementary data

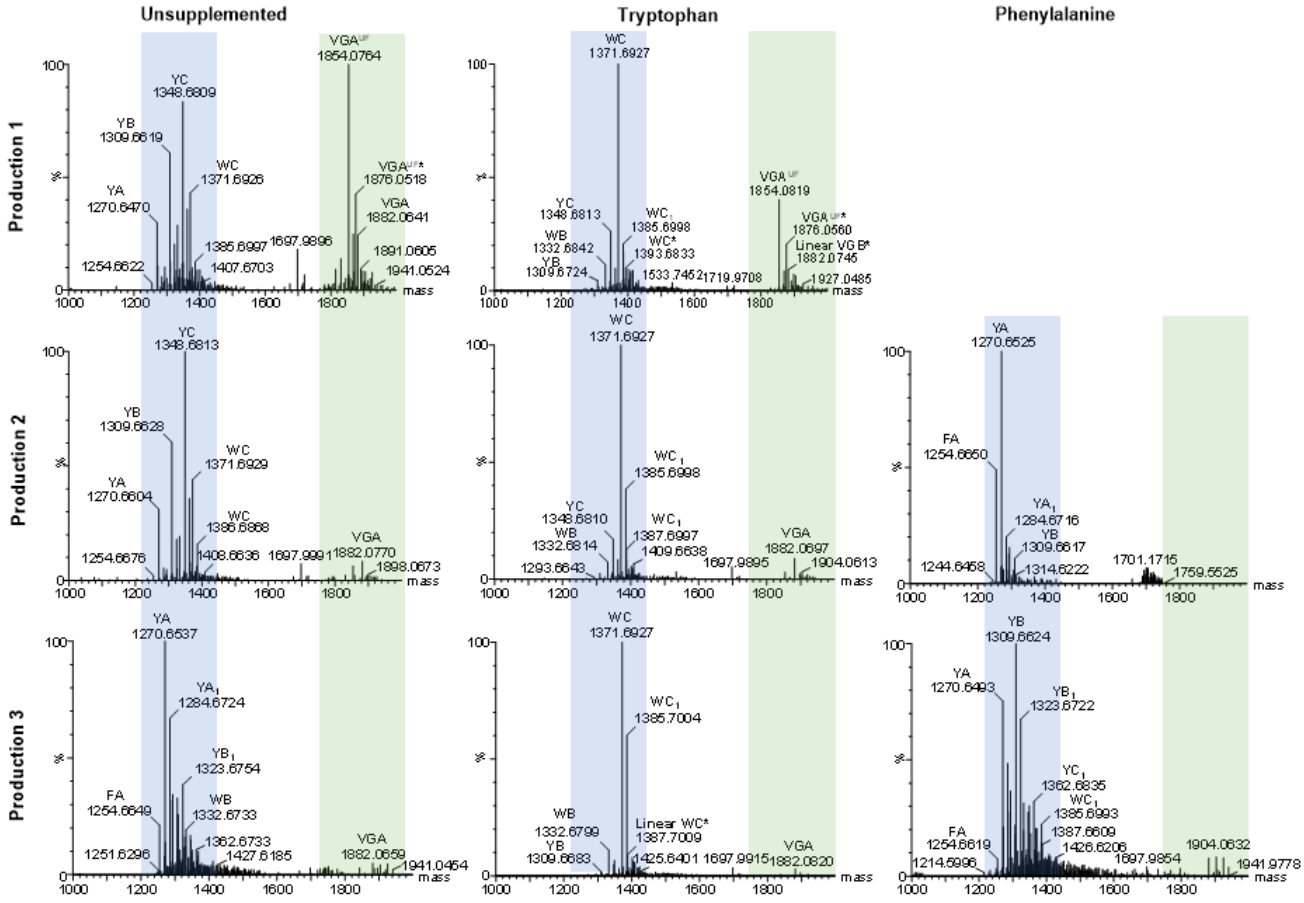

Figure S2.1 ESI-MS mass spectra derived via MassLynx 4.01 MaxEnt 3 algorithm of crude production extracts with mass in Da on the x-axis (mass) and percentage signal intensity on the y-axis (%). The cyclodecapeptides are highlighted in blue and the linear gramicidins in green. The singly charged peptide masses are annotated on the spectra with the peptide identity of the most predominant peptide analogues indicated. A modified linear gramicidin was identified and annotated as VGA^{UF}. All peptides' ions observed as sodium adducts are indicated with a *.

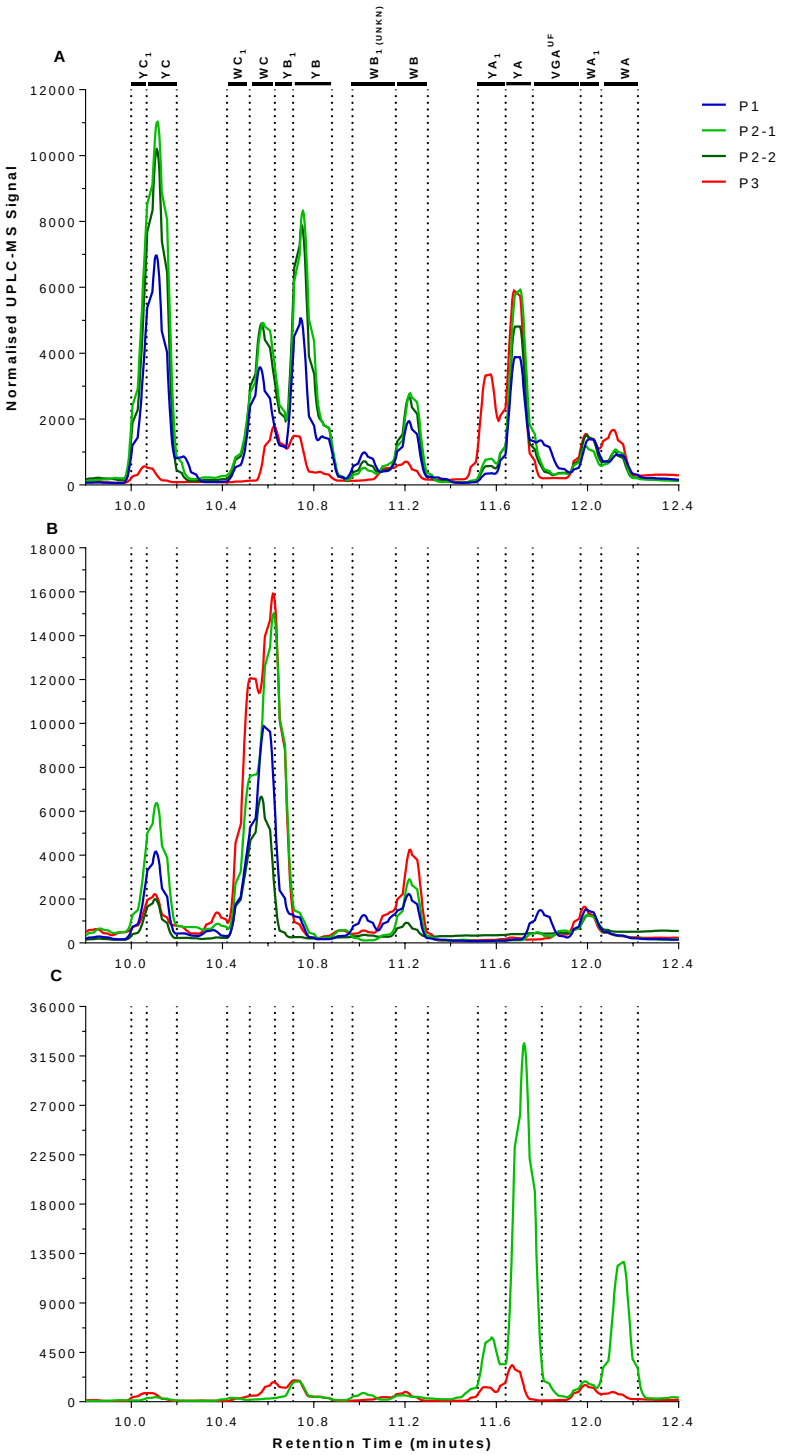

Figure S2.2 Shift in UPLC elution profiles of crude production extracts after amino acid supplementation of *Br. parabrevis* culture mediums. Unsupplemented (**A**), tryptophan supplemented (**B**) and phenylalanine supplemented (**C**) productions were plotted separately with production one (P1) in blue, two (P2) in green and three (P3) in red. The retention time range of each respective peptide analogue (A, B and C) and linear gramicidin (Grms) is indicated with dotted lines.

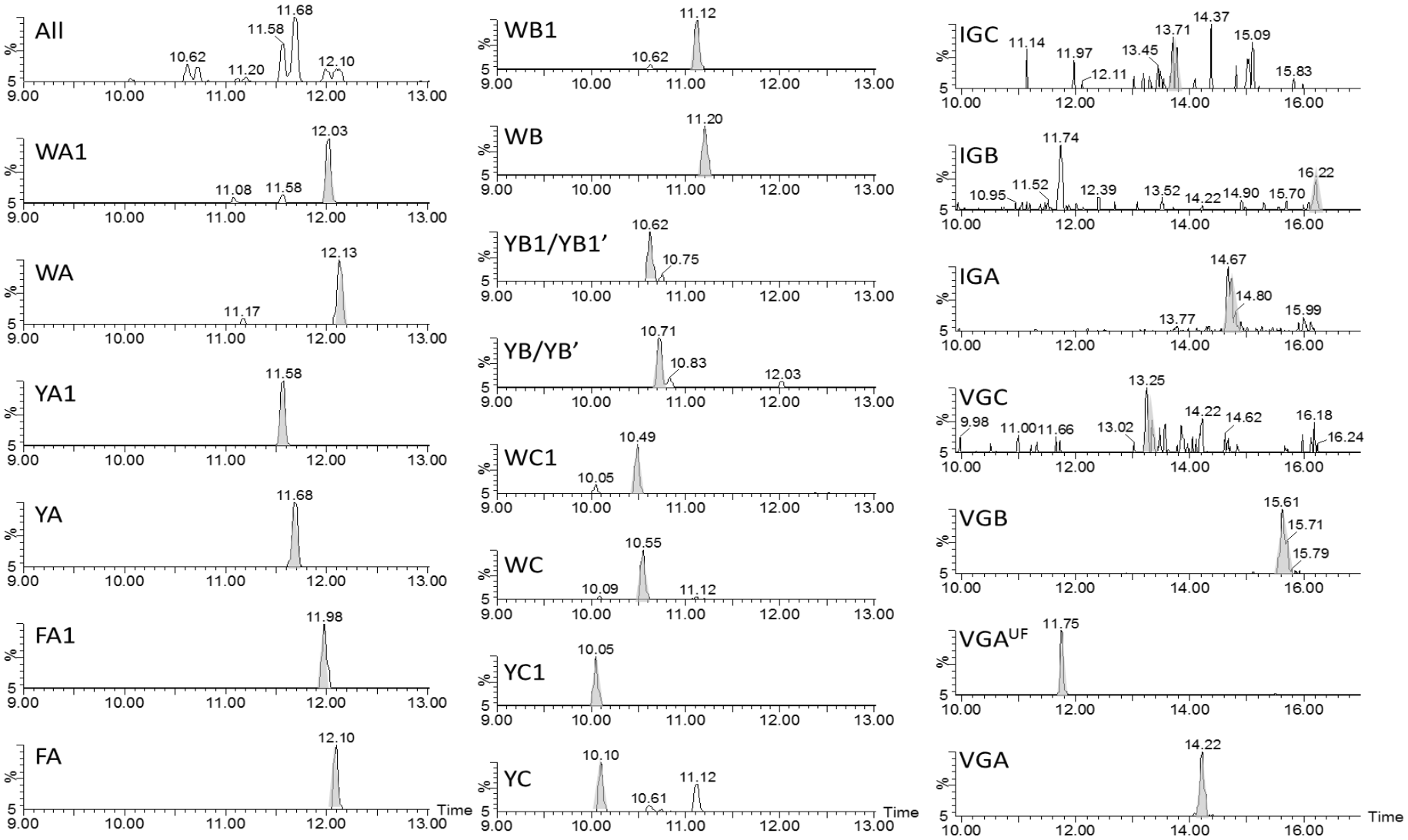

Figure S2.3 Example of extracted chromatograms of doubly charged peptide ions in tyrothricin complex (20 ppm error) for production 3 unsupplemented used to determine peptide identities (ID) with comparison to standard tyrocidine mixture (refer to Fig. S2.4).

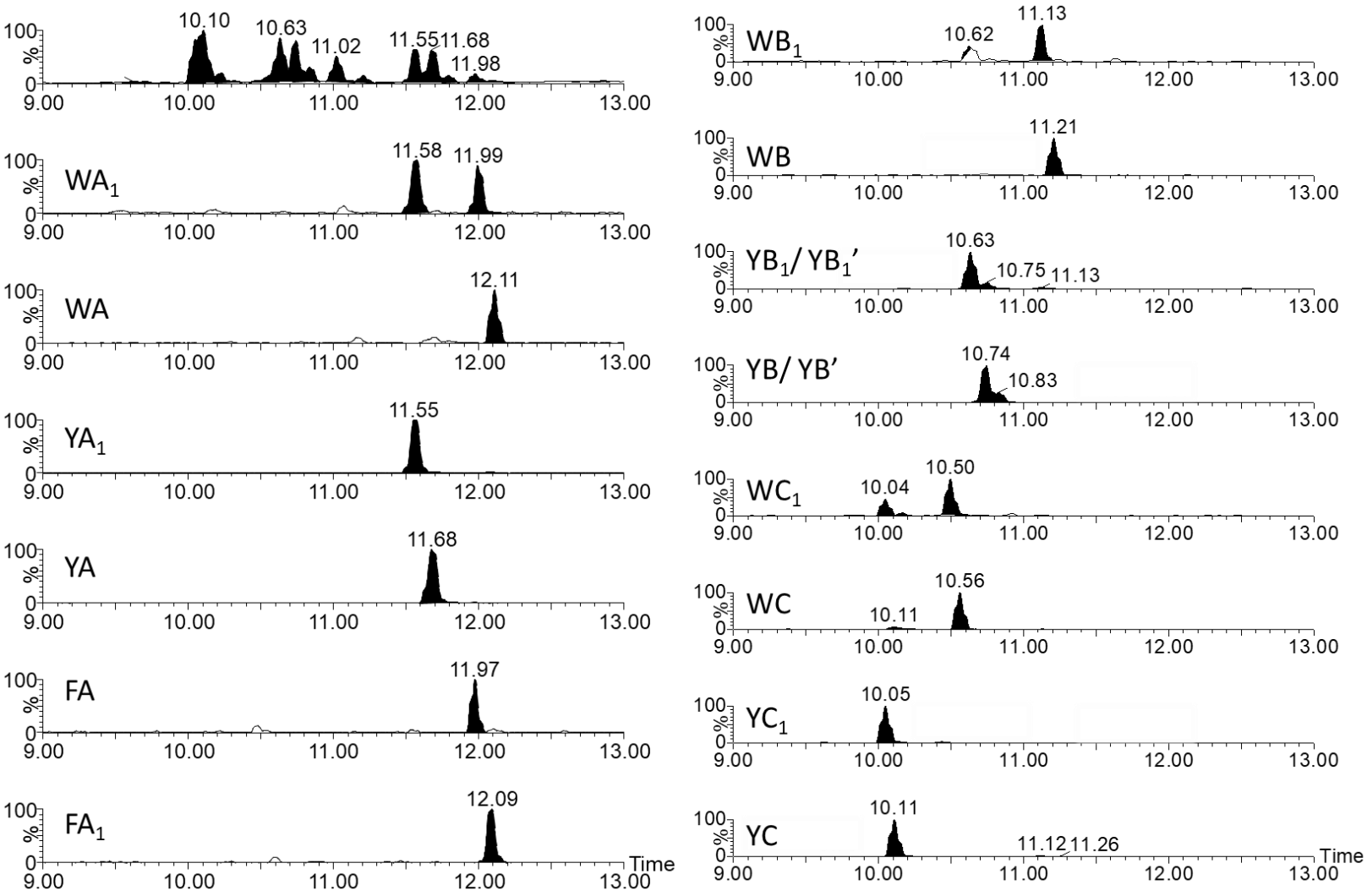

Figure S2.4 Example of extracted chromatograms of doubly charged peptide ions in tyrothricin complex (20 ppm error) for standard tyrocidine mixture used to determine peptide identities (ID).

Table S2.1 Heatmap summary of absolute signal intensities of the peptide contributing to the crude production extracts Peptide identity (ID) was derived from correlating the doubly charged monomer ions $[M+2H]^{2+}$ in tyrothricin complex (<20 ppm error) in extracted chromatograms with that of the peptide ions in standard commercial tyrocidine mixture. The absolute peptide signal of the doubly changed ion is depicted as a heat map with blue the lowest contribution and pink the highest contribution in each extract. These absolute peptide signals were used to calculate the % signal contribution of each peptide in each extract (see Table 2.6).

Peptide ID	Rt (min)	Trc mix	P1U	P2U-1	P2U-2	P3U	P2F-1	P2F-2	P3F-1	P3F-2	P1W	P2W-1	P2W-2	P3W
WA_1	12.04	7268	3596	3864	3273	18105	12028	9082	7297	26253	961	1472	470	1148
WA	12.12	9890	16298	20749	19079	27355	59786	39891	15963	51078	2809	9582	1403	3890
YA_1	11.59	95066	15644	17909	13645	58217	112459	74268	22625	88748	575	729	102	535
YA	11.69	96196	63515	97820	79877	102646	405969	351356	54856	139072	1909	3946	760	3297
FA_1	11.98	1419	524	566	287	7401	37812	29050	904	4048	84	99	13	143
FA	12.09	1999	3170	3696	2888	17891	198706	160947	2658	10842	204	198	62	526
WB_1+ unk	11.12	13253	9145	15048	12327	9843	1455	1115	8636	35484	9196	48416	3470	24309
WB	11.20	41663	65213	97725	91709	21703	14367	10439	27457	106944	71524	292653	28209	142051
YB_1	10.62	147103	39403	56037	54877	33597	7902	5286	32731	114743	2461	3658	990	1621
YB	10.71	136359	98684	162148	153554	36222	41972	29199	40340	134344	11789	34002	4805	8001
WC_1	10.49	27975	36221	54389	45726	4020	2564	1954	11915	50865	147408	813860	97046	461650
WC	10.55	44562	109963	168558	151905	4704	7415	5192	16973	62669	358734	1360129	222757	603460
YC_1	10.05	119028	50793	85048	63939	4334	1041	621	10696	43075	26130	111992	10508	14754
YC	10.10	252193	219223	372702	321415	12492	12880	9552	22500	91235	127904	422362	59083	76505
IGC	14.37	1304	2143	1322	851	205	170	172	144	265	651	617	206	91
IGB	11.74	2118	23129	9755	1745	542	1179	597	425	447	6152	3580	667	441
IGA	14.67	4850	13479	10042	8935	3307	4175	2500	2986	6320	11586	52583	13580	7953
VGC	13.25	6634	4569	5248	4190	784	1042	653	347	1328	800	873	228	178
VGB	15.31	1199	2869	1744	1642	2507	2804	2249	743	2704	758	343	87	427
VGA^{UF}	11.75	3018	42552	15710	2972	1151	1314	1428	1002	1006	10355	6410	1790	1199
VGA	14.22	19269	58877	56257	47926	11439	17894	9228	9120	25834	43934	272630	62699	30452
Total Signal		1032366	879010	1256337	1082762	378465	944934	744779	290318	997304	835924	3440134	508935	1382631

Chapter 3
Mass spectrometry studies on the interaction of the tyrocidines and analogues with metal salts

3.1 Introduction

The propensity of tyrocidines to adhere to a variety of surfaces makes these naturally produced antimicrobial peptides promising agents for the fabrication of robust antimicrobial nanomaterials. Previous studies indicate that the structured self-assembly of the tyrocidines into dimers, tetramers, and other higher oligomers in aqueous solutions assists their association and surface adhesion [1,2]. The ordered oligomerisation of the tyrocidines is of interest due to the influence disordered aggregation and formation of stable nanostructures have on the antimicrobial activity of the tyrocidines. It is hypothesised that the smaller oligomers, particularly dimers, serve as both the building blocks for peptide self-assembly and membrane-active moieties. The activity of the tyrocidines is therefore based on a 'critical point' of oligomerisation, forming dimers and oligomeric structures from which amphipathic dimers can be released [1–6]. Excessive stable oligomerisation and unwanted aggregation could lead to the trapping of these active moieties and diminished activity of the otherwise potent tyrocidines [5,7]. The arrangement and/or rearrangement of formulations to favour amphipathic dimers and small oligomers in solution, or release of such moieties from surfaces, could therefore greatly enhance the biological activity whilst maintaining the robustness of the tyrocidines.

Metals and their electrostatic interactions with biomolecules play a crucial role in important biological processes essential for all forms of life. Metals are often found in both eukaryotes and prokaryotes as constituents of proteins [8–11]. A systematic bioinformatic survey showed that of known enzymes an estimate of 40% are metal-dependent and require metal co-factors to function [8]. Moreover, proteins often incorporate metal ions to stabilize their biologically active higher order structure [12–14]. Understanding peptide:metal interactions offers deeper insight on the structure-function relationship and how specific peptide structures can be manipulated with the addition of certain metal ions. Metals have been classified into three major groups based on their biological function and influences: (1) non-essential metals, (2) toxic metals and metalloids and (3) essential metals. The nonessential metals with no known biological effects are Rb, Cs, Sr, and T. The toxic metals are Ag, Cd, Sn, Au, Hg, Ti, Pb, Al and metalloids are Ge, As, Sb and Se. The essential metals have

known biological functions and are required by most living organisms to survive. These metals include Na, K, Mg, Ca, V, Mn, Fe, Co, Ni, Cu, Zn, Mo, and W [15]. Sodium and potassium are crucial constituents for sodium–potassium ATPase function and the active osmoregulation of cells [10,16]. Magnesium and calcium have a vital structural role in nucleotide complexes and calcium acts as a secondary messenger in cells [17–21]. Iron is often used for electron transfer in redox reactions and zinc partakes in enzyme catalysis [8]. Although these essential metals are crucial to maintain cellular processes, organisms require a state of metal homeostasis to ensure proper biological function. The presence of certain heavy metals or excessive intra-cellular concentrations of essential metals are toxic. Non-essential metals , such as gold and silver, have no known biological function yet show great biological effects and toxicity. Since metals cannot be synthesised nor degraded, organisms require sensitive mechanisms capable of sensing fluctuations in metals. In bacteria, these mechanisms often use peptides and metalloproteins to capture, transport, store, leak, sequester and reduce metal ions to ensure metal availability while avoiding the risk of intoxication or starvation [15,22–24].

Pilot studies successfully fabricated metal nanoparticles using tyrocidines as a reducing agent [V. Kumar, unpublished data]. This work suggested the presence of peptide:metal interactions capable of dictating tyrocidine oligomerisation and nano-assembly. The influence of metals and their concentration on the oligomerisation of the tyrocidines was therefore investigated. The metals utilised in this study include alkali earth metals (Mg^{2+} and Ca^{2+}), transition metals (Fe^{2+}, Cu^{2+}, Ag^{+} and Au^{3+}) and the post-transitional metal zinc (Zn^{2+}). The selection of metals for this study was based on a multitude of factors including, bioavailability, ion size, oxidation state, electronegativity, and reduction potential as well as their role in biochemical processes, toxicity, and bacterial survival. The influence of these different metal salts on the oligomerisation, conformation, and nanostructure formation of tyrocidines can be assessed using a range of biophysical methods, such as fluorescence, UV-visible spectrophotometry, circular dichroism (CD), including magnetic CD, nuclear magnetic resonance spectrometry, X-ray crystallography, various electron microscopy techniques and various mass spectrometry techniques. In this study, travelling wave ion mobility (TWIM) linked to high-resolution electrospray mass spectrometry was used to monitor the oligomeric profile of the tyrocidine-metal salt formulations (Fig. 3.1).

Ion mobility Mass Spectrometry (IM-MS) is a technique which separates and characterises analyte ions based on their gas-phase movement through an electric field offering valuable

data unattainable via conventional mass spectrometry methods. IM-MS is a sensitive technique capable of separating and characterising analyte species with equivalent mass or *m/z* based on differences in shape, conformation, collision cross-sections (CCS) and charged states. Ions are separated by the opposing forces of the electric field applied and collisions (CCS) with a neutral buffer gas (drift gas) in a Drift tube (drift-gas filled chamber). The time taken by each ion to travel through the drift tube is recorded as its drift time. Using the ion drift time, the travel velocity can be calculated if the electric field strength is known, and the ions' mobility can be determined. Moreover, the collision cross section (CCS) of an ion can be determined to calibrate the chamber and ensure accurate IM-MS analysis [26–29].

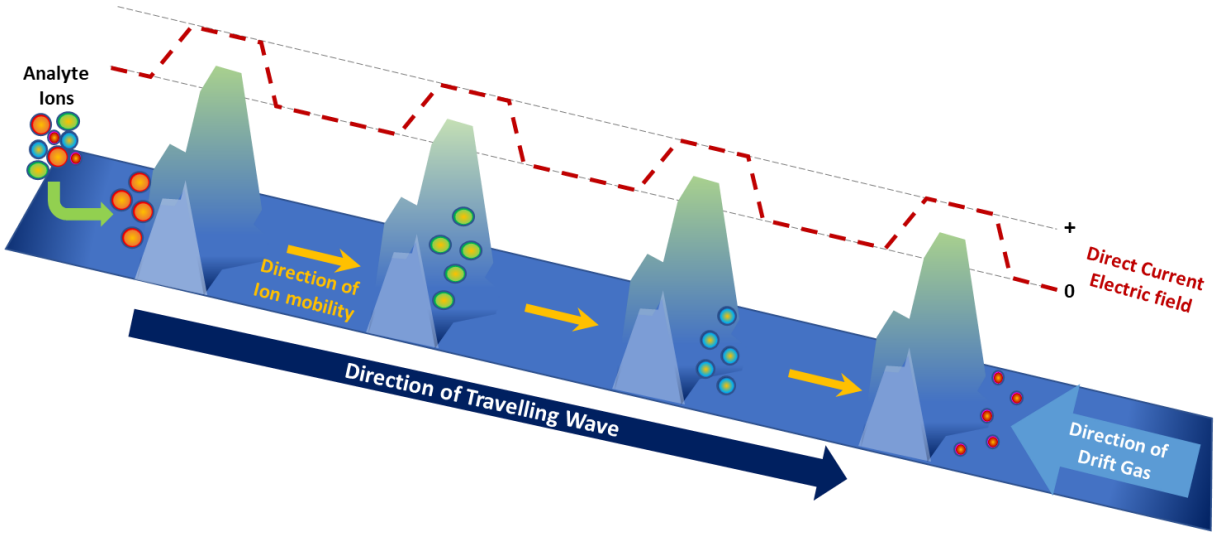

Figure 3.1 Travelling wave principle of Travelling-wave (TWIM-MS) ion mobility mass spectrometry. A direct current creates an electric field (red dashed line) which alternates between positive (+) and zero (0) creating a travelling wave potential (dark blue arrow) which drives the analyte ions through the drift tube. The direction of ion mobility (yellow arrow) is parallel to the travelling wave and opposed by the direction of the drift gas (light blue arrow). Compact ions with high mobility ride the travelling wave and experience less collisions with the opposing drift gas allowing shorter drift times. Figure adapted from Giles *et al.* [25].

Drift-tube (DTIM-MS) and travelling-wave (TWIM-MS) ion mobility mass spectrometers are two types of commercially available IM-MS analysers. The DTIM-MS approach utilises an axial field of constant intensity to push ions through the gas-filled drift tube whereas the TW-IMS approach uses an alternating electric field. The TWIM-MS system has stacked-ring-of electrodes which carries a pulsating direct current (DC) voltages and alternating radio frequency (RF) to the drift tube. The electrodynamic TWIM-MS field alternates between two sections (positive and zero) parallel to the direction of travel of the ions in the drift tube (Fig. 3.1). In the zero-field section ions remain stationary and in the positive-field section ions with

travel at their ion-specific velocities. This fluctuating electric field creates the travelling wave potential (as shown in Fig. 3.1) which drives the analyte ions through the drift tube. Ions with higher charge states experience a higher electric force and therefore a higher ion mobility. In turn, ions with higher mobility experience higher travel velocity and remain within the positive section of the wave for longer permitting shorter drift times. Ions with lower mobility are surpassed by the travelling wave potentials and experience longer drift times. Moreover, compact molecules travel with higher velocity than larger molecules which experience more collisions with the opposing drift gas [27,29,30]. This multifactorial separation has made IM-MS a popular tool for rapidly analysing the structures and conformations of molecules, compounds and complex samples [31–37].

Since DTIM-MS uses uniform voltage gradient, the ion drift times are directly related to CCS via the Mason–Schamp relationship [27,38]. However, TWIM-MS uses a dynamic pulsed voltage creating a travelling wave potential which varies with drift time and tube length. The CCS values for TWIM-MS are therefore determined using known CCS values and the measured drift times of the analyte ions via an empirical calibration relationship [39–41]. Besides the intricacy of CCS determination, TWIM-MS has lower voltage requirements, increased sensitivity, improved resolution, and reduced ion loss compared to DTIM-MS and was therefore used in this study. Since TWIMS does not necessitate high voltages for separation, it can be easily extended to longer optical path lengths, which radically improves resolution. In contrast, increasing the DTIMS path length demands high operational voltages, even at high data acquisition rates [27]. It is important to note that both gas phase mass spectrometric techniques remove organic solvent and water molecules, in turn, eliminating hydrophobic and polar interactions. In addition, only stable non-covalent complexes and oligomers are capable of withstanding the exposure to high collision forces, energy potentials and temperatures within the instrumentation during IM-MS analysis Therefore ensuring that all complexes detected are that of stable electrostatic non-covalent interactions such as H-bonds and ionic interactions [27,32,42–44]. In this chapter we report the TWIM-MS investigation the cyclodecapeptides' self-assembling behaviour to form different oligomers or complexes in the presence of different metals. The capability to direct peptide self-assembly and nanostructure formation, via the formulation of tyrocidines with selected metals, holds the potential for the development of novel antimicrobial nanodrugs against stubborn pathogens and biofilms. Such metal-containing composite can have effective antimicrobial applications in food packaging, biomedical devices, and coatings as self-sterilising materials.

3.2 Materials

Trc mix and pure Tpc C (>90% purity) were extracted and purified as described in Chapter 2. Analytical grade ethanol (EtOH) was supplied by Merck (Darmstadt, Germany). Analytical grade water (MilliQ water) was prepared by filtering water via a reverse osmosis plant using a Millipore-Q® water purification system (Milford, USA). 300 mesh carbon coated grids were purchased from Agar Scientific Ltd. Silver nitrate ($AgNO_3$), sodium chloride (NaCl), magnesium chloride ($MgCl_2$) and copper chloride ($CuCl_2$) were supplied by Merck (Darmstadt, Germany). Calcium chloride ($CaCl_2$) and magnesium nitrate ($Mg(NO_3)_2$) were supplied by Saarchem (Midrand, South Africa). Sodium nitrate ($NaNO_3$), potassium chloride (KCl), zinc chloride ($ZnCl_2$) and gold (III) chloride ($HAuCl_4$) , leucine enkephalin acetate salt hydrate (>95%) and poly-DL-alanine (Poly-Ala) were supplied by Sigma-Aldrich (St. Louis, USA). Iron (II) chloride ($FeCl_2$) were supplied by Fluka Chemicals (Buchs, Switzerland).

3.3 Methods

3.3.1 Peptide:metal formulation and nanoparticle fabrication

The peptides selected for the formulations include Trc mixture (Trc mix) containing predominantly TrcA, TrcB and TrcC and their Lys-analogues. Trc mix was formulated with a selection of metal salts in an array of peptide:metal molar ratios (4:1, 2:1, 1:1, 1:2 and 1:4). All peptide:metal formulations had a final solvent composition of 15 % EtOH-water (*v/v*) and maintained a fixed peptide concentration of 50 µM. The metal salts used for the formulations include chloride salts (NaCl, KCl, $FeCl_2$, $MgCl_2$, $CuCl_2$, $CaCl_2$, $ZnCl_2$ and $HAuCl_4$) and nitrate salts ($AgNO_3$, $Mg(NO_3)_2$, $NaNO_3$). The selected peptides were dissolved in 60 % EtOH-water (*v/v*) (organic shock), sonicated and then double diluted with to 30 % EtOH-water (*v/v*) binary formulation before being added to selected metal salts. All metal salts were dissolved in analytical quality water (Milli-Q water) to the different concentrations required for formulations of different molar ratios. To limit the influence of residual contaminants such as detergents on the formulations, only pyrolysed glassware and ultra-high purity solvents were utilised in the preparation of the formulations.

3.3.2 Electrospray Ionisation and UPLC linked Mass Spectrometry

Samples were analysed at the Central Analytical Facility (CAF), Stellenbosch University, with the assistance of Prof. Marietjie Stander. The electrospray ionisation mass spectrometry (ESI-MS) system comprised of a Waters Synapt G2 quadrupole time-of-flight

(Q-TOF) mass spectrometer, a Z-spray electrospray ionisation source and a photodiode array detector. The ESI-MS solvent used consisted of 0.1 % formic acid in 60 % ACN in water (*v/v/v*). Sample volumes of 2 µL were injected via a Waters Acquity® UPLC into the ESI-MS system allowing direct infusion with a flow rate of 0.3 mL/min at a source temperature of 120 °C, cone voltage of 15 V, extraction cone voltage at 4V, desolvation temperature at 275 C and Nitrogen desolvation gas flow set at 650 L/h. The ESI-MS data was collected in positive continuum mode scanning from 300-2000 (*m/z*) at a rate of 0.2 scans per second. UPLC linked MS (UPLC-MS) was used to identify the identity and contribution of peptides crude production extracts and commercial Trc mix extracts. The samples were resuspended in 50% ACN: water (*v/v*) and subsequently centrifuged at 10 621×*g* for 10 minutes to remove any particulate material. Crude production extracts were prepared to a concentration of 500 µg/mL and HPLC purified fractions to a concentration of 250 µg/mL. Both ESI-MS and UPLC-MS analysis was performed and maintained under the same conditions as described in Chapter 2.

3.3.3 Ion Mobility Linked Electrospray Ionisation Mass Spectrometry

The ion mobility spectrometry-linked ESMS (IM-MS) analysis was done on the instrument described above with the same settings and solvents. IM-MS was achieved by enabling the travelling-wave ion mobility cell in the ESI-MS system. High resolution mass calibration of the instrument was performed using sodium formate and in-analysis calibration was performed using leucine enkephalin single point lock spray (m/z = 556.2771). Poly-Alanine (Poly-Ala) was used as the calibration standard to calibrate the travelling wave ion mobility cell's drift time. The IM-MS data was collected in positive mode scanning from 200-2100 (*m/z*) at a rate of 0.2 scans per second. The travelling wave ion mobility experimental instrument parameters were set as follows: extraction cone at 4 V, helium cell gas flow at 180 mL/min and ion mobility buffer (N2) gas at 90 mL/min. A mobility trap and extract height at 15 and 0 V, respectively, and a trapping release period of 200 µs. A wave height ramp (100 %) from 8 to 20 V and wave height linear velocity ramp (20 %) from 1000 to 650 m/s at 200 m/s. A trap collision energy at 15 V, a transfer collision cell energy of 0 eV and a desolvation temperature of 275 °C. The trap collision energy for the lock spray calibration was 4 V.

3.3.4 Data analysis

The Mass Spectrometry data was collected and analysed using Waters MassLynx V4.1 software (Milford, USA) and Driftscope v2.9 software. The linear poly-Ala calibration curve (FIG) used to determine the collisional cross-section (CCS) calculations was constructed as described by Michaelevski *et al*.[45] and Rautenbach *et al.* [32]. The percentage contribution for each major peptide in Trc mix was determined as described by Ruotolo *et al.*[46] (refer to supplementary data). Peptide oligomers were identified from the IM-MS spectra and the percentage contribution of each species to the total signal was calculated as follows:

$$\text{Contribution } (\%) = \frac{\text{Signal Intensity of Peak}}{\sum \text{ Peak Signal Intensities}} \times 100 \qquad \textbf{Equation 3.1}$$

MaxEnt 3 analysis confirmed the identity of the charged peptide oligomeric species. The theoretical masses used to identify the species are summarised in Table S3.1, Table S3.5, and Table S3.6. The theoretical masses of the tyrocidines and analogues and their amino acid sequences are also summarised in Table 2.1 (Chapter 2).

3.4 Results and Discussion

3.4.1 Tracking peptide self-assembly and oligomerisation with ESI-MS

The self-assembling nature of the tyrocidines into higher-order structures has been well established in older tyrocidine literature [47–49] and more recently by the BIOPEP Peptide Group [1,2,7,50]. Higher order oligomeric species have consistently been observed when analysing the tyrocidines regardless of the purity, concentration, or organic solvent. Previously investigators observed the oligomerisation of tyrocidines from dimers up to octamers using ESI-MS [1,2,7]. Moreover, the prevalence to form dimeric species increases with increasing peptide purity [7,50] as illustrated in the ESI-MS mass spectra of Figs. 3.2 and 3.3. Since the amphipathic peptide dimers are believed to be both the building blocks of higher-order structures and the active moieties against microbes [7,50], the ability to influence peptide oligomerisation through formulation can have drastic influences on peptide structure and activity with promising future applications. Oligomeric species detected by direct injection ESI-MS for TrcC and TpcC in purified peptide and peptide mixtures (Trc mix) are annotated in Fig. 3.2. It is important to note that the ESI-MS spectra are expressed in percentage signal intensity (y-axis) and protonated mass (x-axis). Therefore, the peak heights (% signal) of similar species (i.e., the monomeric peptides) within the same spectra

remain relative and can therefore be compared to one another. However, direct comparisons between peak heights of non-similar species (i.e., between monomers, dimers, and trimers) and between samples (i.e., between Trc mix and pure TrcC) cannot be made. However, one can use the species ratios (% contribution) to compare both non-similar species and samples (i.e., comparing species contribution within or between Trc mix and purified TrcC). The same applies to the IM-MS ion profiles that will be discussed later in this study.

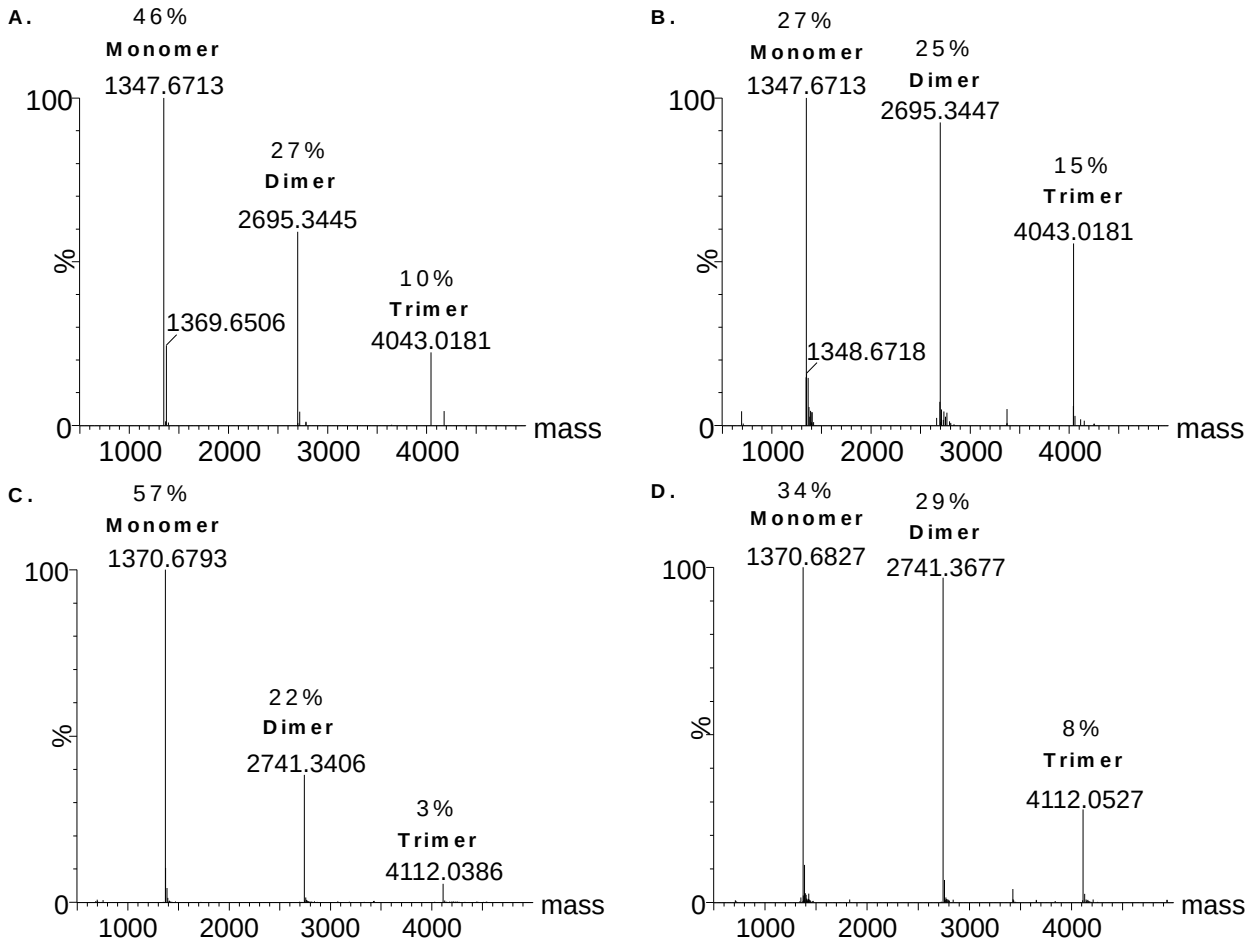

Figure 3.2 MaxEnt 3 analysed UPLC-MS mass spectra illustrating the oligomerisation of peptide analogues in peptide mixtures and purified peptides (>90% purity). The percentage signal intensity (%) is plotted on the y-axis and mass (Da) on the x-axis. The oligomerisation of TrcC is shown for Trc mix (**A**) and purified TrcC (**B**). The oligomerisation of TpcC is shown for Trp supplemented crude extract (**C**) and purified TpcC (**D**). The percentage contribution, calculated as per Equation 3.1, is indicated above each oligomer identity in bold. Oligomeric species up to octamers are found and were accounted for in the percentage contribution calculations. For ease of viewing, select peptide oligomeric species (monomers, dimers, and trimers) are represented and denoted in bold above the respective theoretical species masses (Da) as determined via MaxEnt 3 analysis. See Chapter 2 for production and purification of crude extracts and pure peptides.

Fig. 3.2 illustrates that peptide oligomerisation into higher order homo-oligomers increases with increasing peptide purity. Even though oligomeric species up to octamers are found and were accounted for in the percentage contribution calculations, only select peptide species (monomers, dimers, and trimers) are shown for ease of viewing. Both the peptide mixtures (Fig. 3.2. A and C) and the purified peptides (Fig. 3.2 B and D) show a prevalence of monomers > dimers > trimers (in order of percentage contribution). However, the purified peptides have a lower percentage contribution towards monomers and a higher percentage contribution towards larger homo-oligomers relative to their peptide-mixture counterparts. The Trc mix (Fig. 3.2A) exhibits a higher ratio of monomeric (46%) and dimeric (27%) TrcC species and a lower ratio of trimeric (10%) TrcC species than the purified TrcC (Fig. 3.2B) with 27% monomeric, 25% dimeric and 15% trimeric TrcC species. The Trp supplemented crude extract (Fig. 3.2C) exhibits a higher ratio of monomeric TpcC species (57%) and a lower ratio of dimeric (22%) and trimeric (3%) TpcC species than the purified TpcC with 34% monomeric, 29% dimeric and 8% trimeric TpcC species. Only homo-oligomeric species were considered while investigating the oligomerisation of TrcC and TpcC represented in Fig. 3.2. Although the increase in homo-oligomeric species in purified peptide can be attributed to the absence of hetero-oligomers and is therefore expected, the loss in monomeric species between peptide-mixture and purified sample is still of interest. This loss in monomer contribution associated with the increased contribution of larger oligomers (specifically dimers) in purified peptide indicates the potential uptake of monomers to form larger oligomers as suggested by Rautenbach *et al.* [7]. On the other hand, the competition to form stable hetero-dimers, and hetero-tetramers that are separated via UPLC-MS is not accounted for in the UPLC-MS analysis of single peptides in mixtures (Fig. 3.2). Although the peptide is concentrated in the UPLC peak, in the mixture, it will have a lower effective concentration lowering the mass drive for oligomerisation. The complexity of UPLC-MS of a matured 24 hour old sample of Trc mix is shown in Fig. 3.3 illustrating the loss of some dimers, mostly heterodimers and tetramers from each peptide peak, as they are retained on the column longer. However, even in the major peptide peaks there is homodimers/tetramers and heterodimers/tetramers, with the easily identifiable heterodimers/tetramers indicated in the spectra in green (Fig. 3.3 A-F). The oligomerisation behaviour and increased prevalence of dimers and larger oligomers observed for the purified tyrocidines agree with what has been observed in a number of previous studies [1,4,7,47,48]. Moreover, the loss of monomers at higher purity and concentration, supports the suspected role dimers and larger oligomers play in peptide aggregation and the loss of

antimicrobial activity observed for purer peptide analogues explored in Chapter 4. Although this oligomerisation behaviour of purified tyrocidines has promising applications for nanoformulations, the IM-MS analysis in this study was not performed using pure peptides due to their limited availability. For this study, Trc mix was used to determine the influence metals have on peptide oligomerisation and the further analysis of pure peptide nanoformulations and application in antimicrobial formulations are presented in Chapter 4.

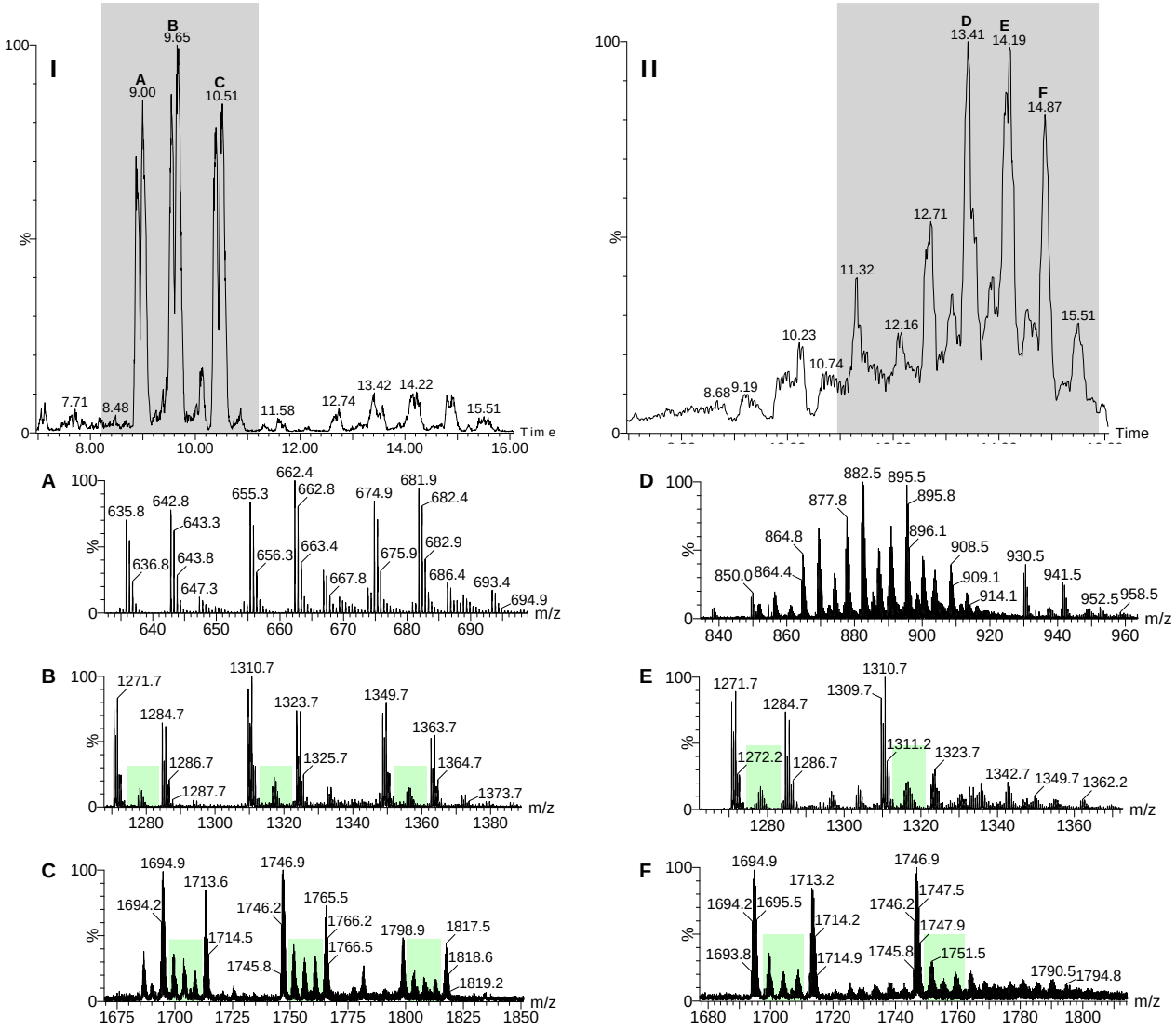

Figure 3.3 UPLC-MS analysis of 24 hour matured 1.0 mg/mL Trc mix in 50% acetonitrile with chromatogram (**I**) showing base peak intensity chromatogram and chromatogram (**II**) showing the profile of the triply charged dimers (shown in **D**). The doubly charged monomeric species $[M+2H]^{2+}$ (**A**), singly charged monomeric species $[M+H]^{+}$ and doubly charged dimeric species $[2M+2H]^{2+}$ (**B**), triply charged tetrameric species $[4M+3H]^{3+}$(**C**) correlate with the large peaks in I. The triply charged dimers $[2M+3H]^{3+}$ (**D**), doubly charged dimeric species $[2M+2H]^{2+}$ (**E**), triply charged tetrameric species $[4M+3H]^{3+}$(**C**) correlate with the peaks in II. Also refer to Table 3.1 and Table S3.1 (supplementary data).

3.4.2 IM-MS analysis of peptide oligomerisation

Analysis of peptide oligomerisation with UPLC-MS is possible yet complex and time consuming with long run times. As the oligomerisation of the peptides is not only solvent, concentration, identity, and purity sensitive, but also time sensitive. In this study, IM-MS was used as a tool for rapid detection and simplified monitoring of peptide oligomerisation in Trc mix formulations with metals [35,40,51]. However, as the tyrocidines self-assemble to form higher-order oligomers: the accurate identification of the peptides becomes increasingly intricate. The larger the oligomer: the greater the scale of potential peptide analogue combinations, and subsequently the number of overlapping masses, *m/z* values (as seen in Fig. 3.6) and IM-MS drift times. To illustrate this complexity, Table 3.1 summarises the overlap within the dimeric species where 11 out of the 21 combinations (highlighted in green) have similar masses and are therefore indistinguishable from one another based on mass alone. Moreover, seven doubly charged dimeric species' $[2M+2H]^{2+}$ masses (highlighted in blue) match singly charged monomeric masses $[M+H]^{+}$ (refer to Table 2.1 in Chapter 2 for singly charged monomeric peptide masses).

Table 3.1 Summary of the mass-to-charge ratio (*m/z*) and theoretical mass (Da) values for the doubly charged dimeric species $[2M + 2H]^{2+}$ of the six major tyrocidines present in the Trc mix. Matching dimeric masses are highlighted in green and masses matching monomeric species masses highlighted in blue.

Theoretical Dimer [2M] Mass (Da)						
Peptide Identity	YA	YA_1	YB	YB_1	YC	YC_1
YA	2539.3092					
YA_1	2553.3249	2567.3405				
YB	2578.3201	2592.3358	2617.3310			
YB_1	2592.3358	2606.3514	2631.3467	2645.3623		
YC	2617.3310	2631.3467	2656.3419	2670.3576	2695.3528	
YC_1	2631.3467	2645.3623	2670.3576	2684.3732	2709.3685	2723.3841
Doubly Charged Dimer $[2M+2H]^{2+}$ Mass-to-Charge Ratio (*m/z*)						
Peptide Identity	YA	YA_1	YB	YB_1	YC	YC_1
YA	**1270.6624**					
YA_1	1277.6703	**1284.6781**				
YB	1290.1679	1297.1757	**1309.6733**			
YB_1	1297.1757	1304.1835	1316.6812	**1323.6890**		
YC	1309.6733	1316.6812	1329.1788	1336.1866	**1348.6842**	
YC_1	1316.6812	1323.6890	1336.1866	1343.1944	1355.6921	**1362.6999**

Although IM-MS allows for the differentiation of oligomeric species which would (with more conventional mass spectrophotometry) be indistinguishable from one another due to their similar or identical masses and *m/z* values, certain species also exhibit similar drift times and are therefore only distinguishable with IM-MS analysis when their mass, *m/z* value and cross collisional section (CCS) are both considered. The CCS values are highly dependent on the structure and conformation of the peptide and their oligomers. The average CCS areas ($Å^2$) for the ionic species of interest namely, monomers $[M+H]^+$, doubly charged monomers $[M+2H]^{2+}$ and dimers $[2M+2H]^{2+}$ is summarised in Table S3.2 (supplementary data). These CCS areas calculated correlated well with those previously reported [7,32,52] and confirmed the reliability of IM-MS profiling of oligomer formation.

3.4.3 IM-MS tracking of complexation of peptides in Trc mix with metal ions

Pilot studies on the fabrication of metal nanoparticles using the tyrocidines as a reducing agent suggested the presence of peptide:metal interactions capable of dictating peptide oligomerisation [unpublished data]. These studies are discussed further in Chapter 4. In this study, the influence of different metals on the oligomerisation of the peptides in Trc mix was observed by formulating 50 µM Trc mix with increasing concentrations of metal salts. Trc mix was formulated with an array of metal salts (refer to Table S3.4 in supplementary data). The selection of metals was based on a multitude of factors including bio-availability, ion size, oxidation state, electronegativity, and reduction potential as well as their role in bacterial growth, antimicrobial peptide production and regulation as discussed in the introduction. The metals utilised in this study include alkali earth metals (Mg^{2+} and Ca^{2+}), a transition metal (Fe^{2+}), group 11 transition metals (Cu^{2+}, Ag^+ and Au^{3+}) and the post-transitional metal (Zn^{2+}). The influence of the selected metals and their concentration on the oligomerisation of the tyrocidines was investigated by tracking the percentage signal contribution (Equation 3.1) of the different ionic species at the different peptide:metal ratios (4:1,2:1, 1:1, 1:2 and 1:4). IM-MS profiles and three-dimensional renderings of such profiles (Driftscope) were used to visualise the peptide oligomerisation behaviour of the Trc mix formulations. The Driftscope in Fig. 3.4 illustrates the oligomerisation pattern of a fresh and 4 hour matured 50 µM Trc Mix sample in the absence of metal. The IM-MS analysis of the unformulated Trc Mix detected doubly charged monomeric species $[M+2H]^{2+}$ (b), doubly charged dimeric species $[2M+2H]^{2+}$ (c), singly charged monomeric species $[M+H]^+$ (d), and triply charged tetramers $[4M+3H]^{3+}$(e). The maturation of the Trc mix sample resulted in well-defined IM-MS peaks as shown in Fig. 3.4 (II, A and C). This suggests the oligomerisation

and self-assembly of the peptide into its respective oligomers over time. The tendency of the tyrocidines to self-assemble, aggregate and oligomerise is well recorded in previous studies and was therefore expected with the maturation of the sample [2,4,6,7,47,53]. The maturation of peptide:metal formulations and the peptides oligomerisation behaviour are investigated later in this chapter.

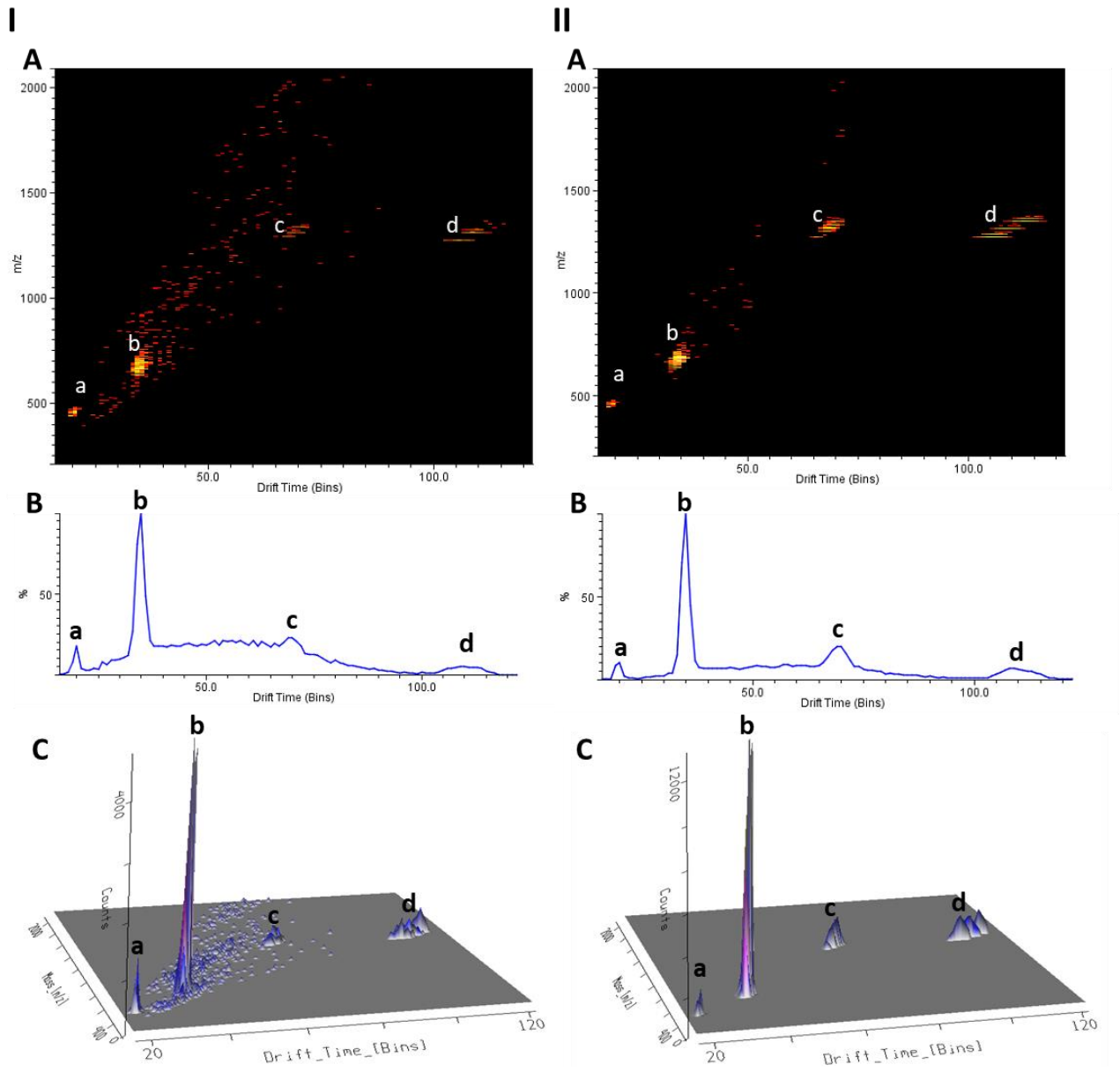

Figure 3.4 IM-MS profiles of species detected for a fresh (**I**) and 4 hour matured (**II**) 50 µM Trc mix sample in 15% EtOH-water. The 2D (**A**) and 3D (**C**) DriftScope profiles of the IM-MS (**B**) are annotated as follows: unidentified triply charged ions (**a**), doubly charged monomers $[M+2H]^{2+}$ (**b**), doubly charged dimeric species $[2M+2H]^{2+}$ (**c**), and singly charged monomers $[M+H]^{1+}$ (**d**).

The presence of the triply charged species at a drift time of 2.09 (a) was of particular interest since the masses detected in the mass spectra did not match that of a triply charged peptide oligomers for any of the samples. However, the percentage contribution of this triply charged species increased with the introduction and increasing concentration of metals. Although the triply charged masses detected are that of fragmented peptide in the 50µM Trc mix control, further investigation revealed that certain formulations with metals displayed masses corresponding to that of the respective peptide:metal complexes. The theoretical monoisotopic masses for the different peptide:metal complexes were calculated for the tyrocidine analogues in Trc mix and potential combinations of peptide monomers and metal ions were investigated as shown with the example of iron in Table S3.5 and Table S3.6 (supplementary data) where the oxidation states and isotopes of the different metals were considered. Since the *m/z* range for triply charged peptide:metal complexes will vary between metals, the signal over an *m/z* range of 436.801 to 468.741 was analysed for the 2.09 peak and used in the percentage contribution calculations for consistency across formulations. Although this *m/z* range may exclude certain peptide:metal complexes, it also excludes the noise from smaller contaminants such as plasticisers. The triply charged peptide:metal complexes were detected and identified using the ion spectra (*m/z*) and MaxEnt 3 spectra (protonated monoisotopic mass) where applicable. Only masses and *m/z* values with a calculated ppm error below 20 were considered and referred to as peptide:metal complexes. Due to the complexity of the peptide mixture and its oligomers, the total signal for each molecular ion from a selection of oligomers (singly charged monomers, doubly charged dimers, and triply charged peptide:metal complexes) in the ion mobility profile were used to compare their contribution ratio (% signal contribution) relative to one another (sum of selected species) in peptide preparations and formulations for the remainder of this study.

3.4.4 Interaction and complex formation of Trc mix with transition metal Fe^{2+}

An example of peptide:metal complex formation is clearly illustrated in the Trc mix formulations with $FeCl_2$. The experimental complexes matched the predicted *m/z* values and isotope pattern modelled by MassLynx 4.03 as shown in Fig. 3.5. The isotope model of iron (A) follows an isotope pattern of: ^{54}Fe, ^{56}Fe then ^{57}Fe with ^{56}Fe (55.9349 Da) being the most abundant isotope at 92% signal contribution. Both the experimental (B and D) and modelled (C) *m/z* spectra followed the expected isotope pattern (A) with ^{56}Fe contributing to the major peaks. The experimental *m/z* values for the peptide:metal complexes (D) matched that of

peptide complexed with Fe^{2+} ions. The isotope model for the peptide:metal complex between Fe^{2+} and TrcC showed *m/z* values matching that of the experimental results and an error of >5 ppm from the calculated *m/z* values when both iron and peptide isotopes were considered. Fig. 3.6 shows an example of the IM-MS profile for 50 µM Trc mix formulated with 200 µM $FeCl_2$ (1:4 ratio) and the oligomeric species detected.

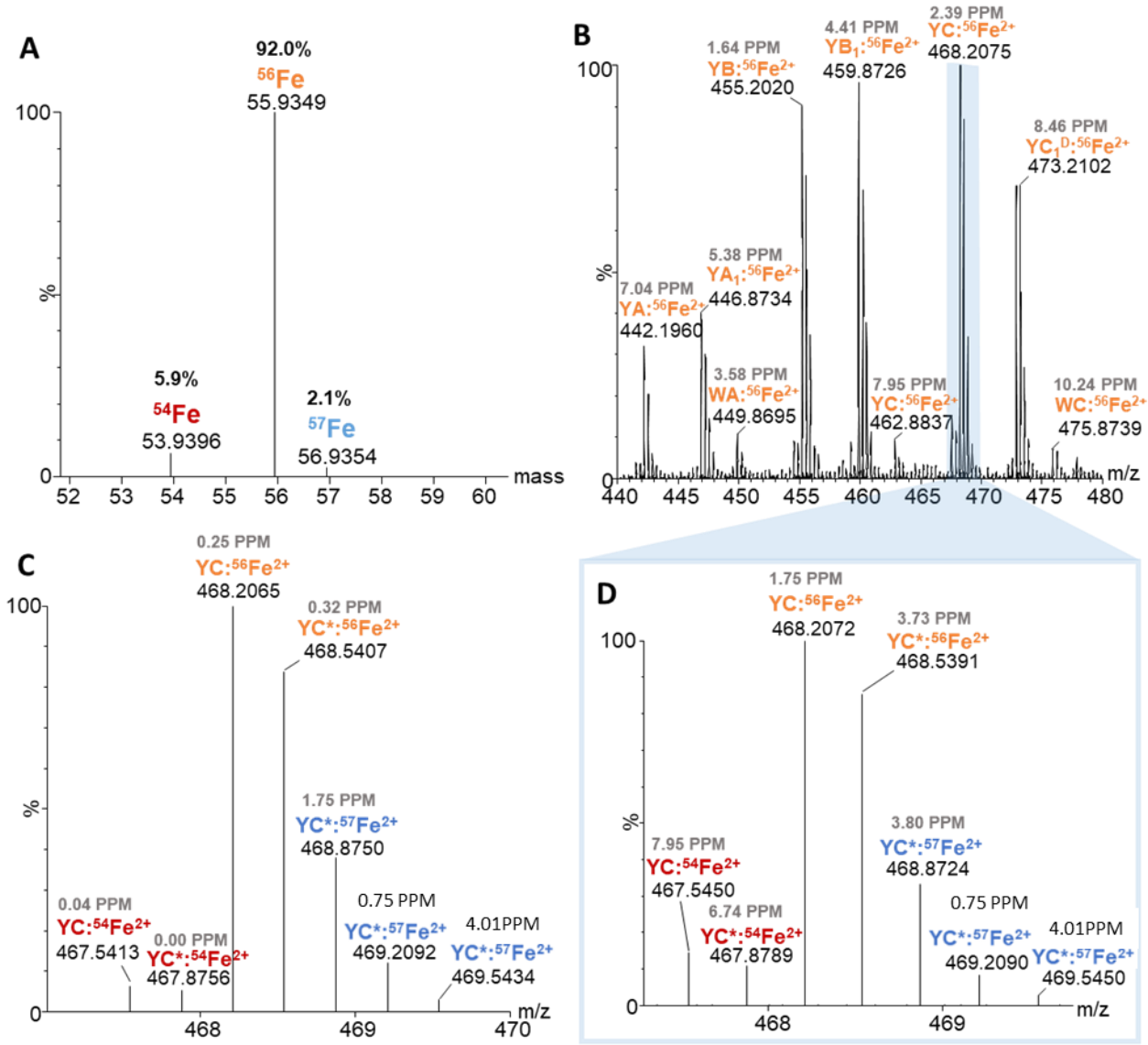

Figure 3.5 Isotope models and experimental *m/z* spectra of peptide:metal complexes. MassLynx derived isotope models illustrate the predicted isotope pattern of iron (**A**) and YC:Fe^{2+} complexes(**C**). Experimental m/z spectra illustrate the of triply charged peptide:metal complexes detected at a drift time of 2.09 for 50 µM Trc mix formulated with 200 µM $FeCl_2$ (**B**) and the and isotope patterns followed as shown for the YC:Fe^{2+} complexes (**D**).The putative iron isotopes ^{54}Fe (red), ^{56}Fe (orange) and ^{57}Fe (blue) and the respective complexes are highlighted in colour and annotated above each relative peak. The ppm error of each *m/z* value is annotated above the complex identity in light grey and the peptide isotopes with ^{13}C are indicated with an Asterix (YC*).

Fig. 3.6A shows the IM-MS ion profile with the percentage signal intensity (y-axis) and drift time (x-axis) of each species. The ESI-MS mass spectra of each respective drift peak (B-D) is indicated with an arrow (a-d) and annotated with the relevant peptide identities detected. Oligomeric species detected for 1:4 Trc mix formulations with iron include: triply charged peptide:metal complexes at drift time of 2.09 (a), doubly charged monomers $[M+2H]^{2+}$ and peptide:metal complexes $[M+Fe\pm H]^{2+}$ at drift time of 3.74 (b), doubly charged dimers $[2M+2H]^{2+}$ at drift time of 7.48 (c) and singly charged monomers $[M+H]^{+}$ at drift time of 11.99 (d).

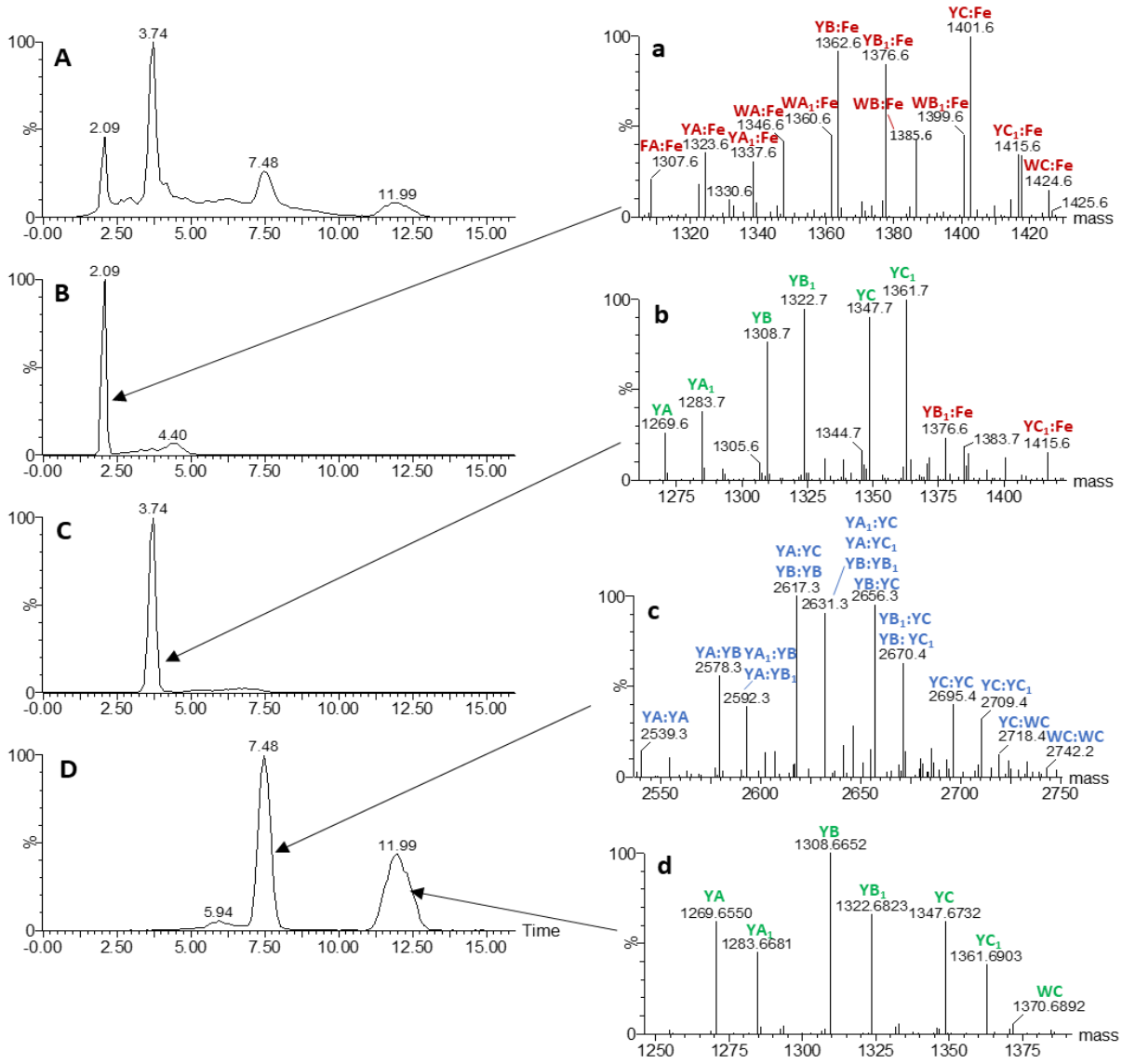

Figure 3.6. IM-MS profile of species detected for 1:4 Trc mix:Fe^{2+} formulation in 15% EtOH-water with extracted mass profiles: (**A**), triply charged peptide:metal complexes $[M+Metal\pm nH]^{3+}$ (**B**) doubly charged monomers $[M+2H]^{2+}$ and peptide:metal complexes $[M+Fe\pm H]^{2+}$ (**C**) doubly charged dimers $[2M+H]^{2+}$ and singly charged monomers $[M+H]^{+}$(**D**). Corresponding MaxEnt3 ESI-MS spectra of each species are shown with annotated species masses and identity.

As shown in Figs. 3.5 and 3.6 iron formed complexes with the tyrocidine and tryptocidine A, B and C analogues present in Trc mix. Such complexes were detected in formulations across each iron concentration. Although the formation of complexes remained consistent across increasing metal concentration, the percentage contribution of these triply charged species increased. An example of the influence metal concentration has on peptide:metal complex formation and peptide oligomerisation behaviour are depicted in the three-dimensional Driftscope (Fig. 3.7) of fresh samples of 50 µM Trc mix formulated with 25 µM (Fig.3.7, I) and 200 µM (Fig 3.7, II) iron. Although direct comparisons based on peak height cannot be made between the two IM-MS ion profiles of the different samples, shifts in peptide oligomerisation can be compared.

The highest peak in both Fig. 3.7 (I and II) is that of the doubly charged species (b) which includes both doubly charge monomers $[M+2H]^{2+}$ and peptide:metal complexes $[M+Metal\pm nH]^{2+}$. Even though doubly charged peptide:metal complexes were detected, they had low prevalence and the poor separation between doubly charged peptide masses and doubly charged complexes in the IM-MS analysis (as shown in Fig. 3.6b). Although notable changes in the doubly charged species contribution are not to be ignored, these were not considered for the purpose of this study due to the complexity of the IM-MS analysis. Similarly, larger oligomers were observed but also not studied in detail for reasons mentioned in sections 3.4.2 and 3.4.3. However, the triply charged species predominantly included peptide:metal complexes and was therefore considered. Both formulations with iron (Fig. 3.7, I and II) show a shift towards triply charged species (a) compared to Trc mix alone (refer to Fig. 3.4), with the 1:4 formulation (II) showing a higher prevalence (>2000 counts) of triply charged species than the 1:2 formulation. This increase in triply charged species is associated with shifts in both higher order (e and f) and smaller (c and d) peptide oligomers. Formulations with 200 µM iron showed incidence of larger oligomers tetramers (e) and hexamers (f), alluding that increasing iron concentration may promote the self-assembly of peptides into larger oligomers (Fig. 3.7). However, like Trc mix alone (refer to Fig. 3.4), the maturation of both 1:2 (A and C) and 1:4 (B and D) formulations also resulted in continued peptide oligomerisation and assembly into larger peptide oligomers as shown in Fig. S3.2 (supplementary data). This observation suggests that the formation of peptide:metal complexes influence or are influenced by the formation and/or dissociation of peptide oligomeric species. Similar changes in peptide oligomerisation behaviour within formulations were observed with other metals and metal concentrations as well. The relationships

between peptide-metal complex formation, peptide oligomerisation and metal concentration were therefore investigated further by tracking changes in the percentage contribution of monomer, dimers and peptide:metal complexes as discussed below.

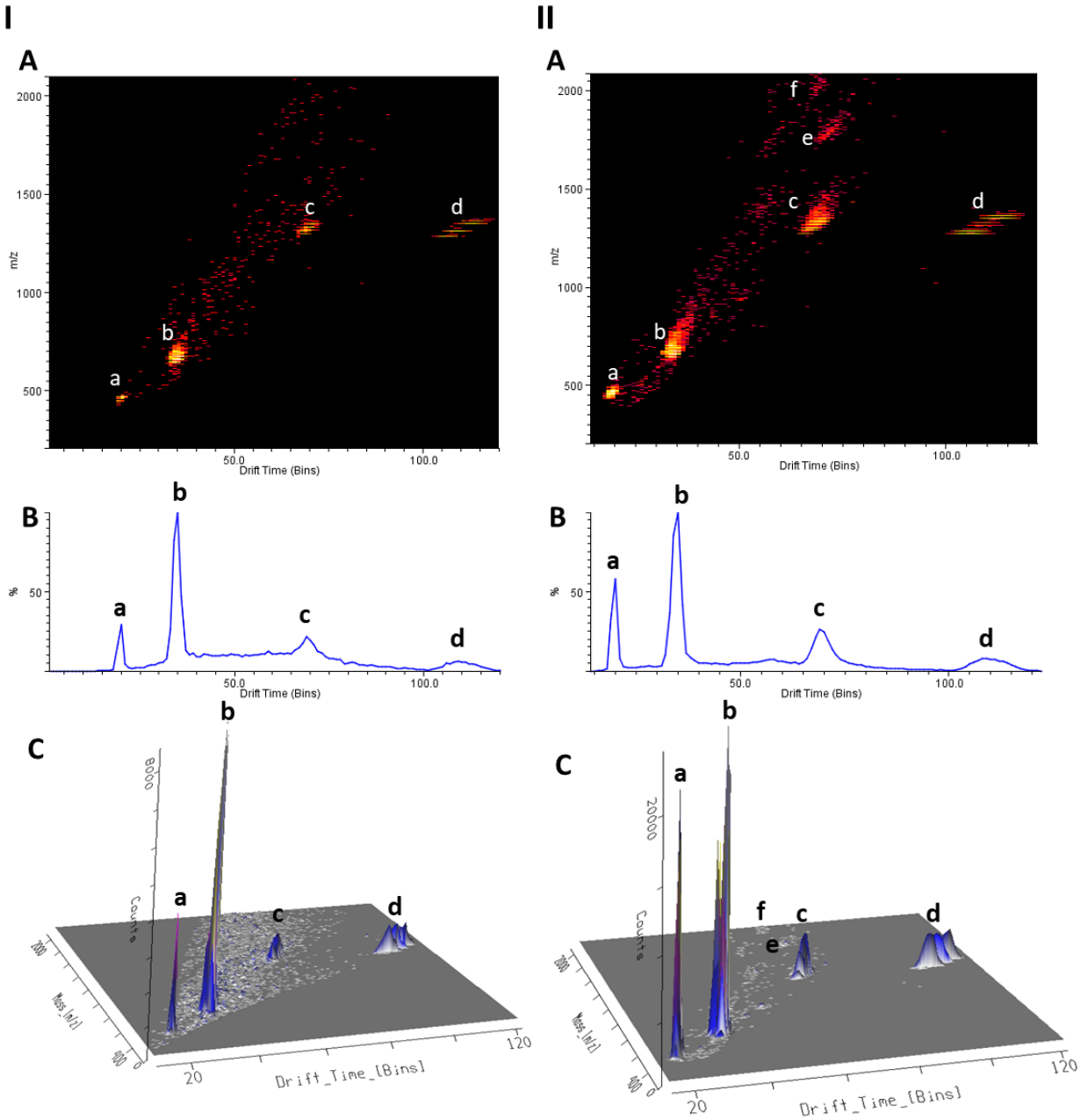

Figure 3.7 IM-MS profile of species detected for fresh 2:1 Trc mix-Fe^{2+} (**I**) and 1:4 Trc mix-Fe^{2+} (**II**) formulations in 15% EtOH-water . The 2D (**A**) and 3D (**C**) DriftScope profiles of the IM-MS (**B**) are annotated as follows: triply charged complexes $[M+Metal\pm nH]^{3+}$(**a**), doubly charged monomeric species $[M+2H]^{2+}$and peptide:metal complexes $[M+Metal\pm nH]^{2+}$ (**b**), doubly charged dimeric species $[2M+2H]^{2+}$ (**c**), singly charged monomeric species $[M+H]^{1+}$ (**d**) triply charged tetramers $[4M+3H]^{3+}$(**e**) and quadruply charged hexamers $[6M+4H]^{4+}$(**f**).

3.4.5 Contribution trends of monomers, dimers, and peptide:metal complexes across metal salt concentrations

Trends between the ion signal contributions of singly charged monomeric $[M+H]^+$, doubly charged monomeric species $[M+2H]^{2+}$, doubly charged dimeric species $[2M+2H]^{2+}$ and triply charged peptide:metal complexes $[M+Metal\pm H]^{3+}$ were investigated to determine the influence of metal salts on peptide oligomerisation. Although larger oligomers were detected, only the contribution of the predominant drift peaks were considered in the contribution analysis described below. The signal contribution (%) of each species detected across an m/z range of 436-1390 was calculated using Equation 3.1. The doubly charged monomers had the largest drift peak and was included in the *m/z* range used to calculate the signal contributions of the different ionic species. However, due to the very high signal contribution and potential contamination of the doubly charged monomers with peptide:metal complexes, they were not illustrated in the signal contribution figures depicted below. Another major factor considered in the signal contribution comparisons of peptide formulations with different metal concentrations was the suppression of the IM-MS ion signal by the negatively charged counter-ions (Cl_2^- and NO_3^-) present in metal salts. As the concentration of the metal in formulation increases two-fold, so does the concentration of negative counter-ions and thereby the ion suppression [54,55]. Although overall decreases in the ion signal of formulations with higher metal salt concentrations can be expected, due to the counter ion influence. The IM-MS ion signal suppression was assumed to be consistent between species within the same metal salt concentration in formulations.

Changes between the ionic species for fresh and matured peptide:metal formulations with the doubly charged metals Mg^{2+} (A), Ca^{2+} (B), Fe^{2+} (C) and Zn^{2+} (D) are summarised in Fig. 3.8. For all four formulations, a decrease in monomers $[M+H]^+$ and dimers $[2M+2H]^{2+}$ is mirrored by an increase in peptide:metal complexes $[M+Metal\pm H]^{3+}$ and vice versa. Interestingly, the monomer and dimer curve for the magnesium formulation intercepts the peptide:metal complex curve at and below a metal salt concentration of 25 µM. Whereas for the calcium formulation, only the dimer curve intercepts the peptide:metal complex curve below 25 µM $CaCl_2$. For iron the peptide signal shows an initial drop in monomer and dimers is mirrored by a spike in Trc:Fe^{2+} at 25 µM metal salt. However, the triply charged peptide:metal complex signal only intercepts the singly charged monomer signal at the highest metal salt concentration (200 µM $FeCl_2$). In contrast, zinc formulations showed an initial spike in monomer and dimer signal mirrored by a drop in Trc mix:Zn^{2+} at 25 µM metal

salt followed by an intercept of all three species at 50 µM metal salt. The changes in oligomerisation behaviour around 25 µM for all four formulations suggests that the peptide:metal ratio of 2:1 could be acting as a “critical point” for complex formation and that peptide monomers and/or dimers have a role in peptide-metal interactions.

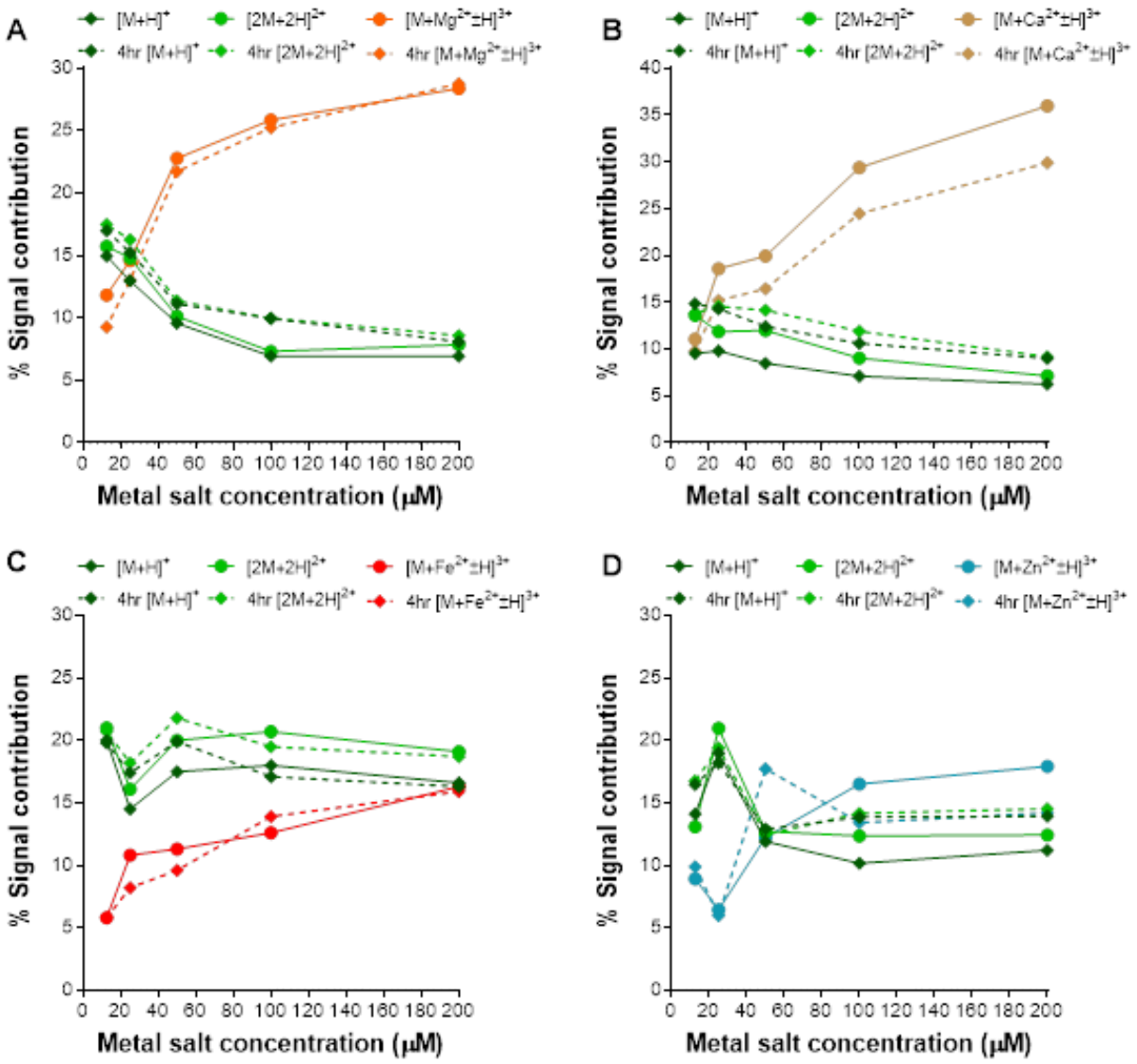

Figure 3.8 Percentage of IM-MS signal contributions (%) for Trc mix formulated with increasing molar concentrations (µM) of metal (II) chloride salts. Singly charged monomeric Trc Mix $[M+H]^+$ (dark green), doubly charged dimers $[2M+2H]^{2+}$ (bright green) and triply charged peptide:metal complexes for formulations with (**A**) magnesium $[M+Mg^{2+}±H]^{3+}$ (orange), (**B**) calcium $[M+Ca^{2+}±H]^{3+}$ (beige), (**C**) iron $[M+Fe^{2+}±H]^{3+}$(red) and (**D**) zinc $[M+Zn^{2+}±H]^{3+}$ (teal). The solid lines show the trend of fresh samples, while the dotted lines show the trends of 4 hour matured samples.

Despite all four formulations in Fig. 3.8 having 2+ charged metal ions, the complex formation and oligomerisation behaviour of iron and zinc differs greatly to that of the group two metal ions magnesium and iron. Overall, Iron and zinc had a higher signal contribution for monomers and dimers and lower contribution for the peptide:metal complexes than magnesium and calcium. Magnesium and calcium have a near inverse relationship between the triply charged complexes and the monomer and dimers with peptide:metal complexes rising to a signal contribution above 25% and the monomer and dimer signal dropping below 10%. The inverse relationships between peptide monomers, dimers, and peptide:metal complexes were maintained even after a four-hour maturation of the formulations as shown by the dotted lines in Fig. 3.8. Interestingly, calcium and magnesium showed a slight loss in contribution of triply charged peptide:metal complexes associated with an increased contribution of monomer and dimer signal indicating the potential release of smaller peptide species from larger oligomers or peptide:metal assemblies in these formulations. As aforementioned, many factors likely contribute to the formation and maintenance of these peptide:metal complexes and the nature of complex formation cannot be confirmed via IM-MS analysis. However, basic chemistry principles still provide valuable insight on how these metal ions could be interacting with the peptide to form peptide:metal complexes and why certain metal ions demonstrate different complex formation behaviours.

Since all four of the metals in Fig. 3.8 have a 2+ charge ion and a negative standard reduction potential (see Table S3.3 in supplementary data), these charged metal ions are unlikely to reduce to form neutral metals. This, in turn, allows for the interaction of the peptide with the 2+ charged metal ions to form the triply charged complexes, as shown in Figs. 3.5 and 3.6. Iron has the least negative reduction potential (-0.44 V) of the four metal and is therefore more likely to reduce and form doubly charged peptide:metal complexes with neutral metal $[M+Fe+H]^{2+}$ as detected via IM-MS and shown in Fig. 3.6b. Fe^{2+} is closely followed by Zn^{2+} (-0.76 V), then Mg^{2+}(-2.37) and finally Ca^{2+}(-2.87). Moreover, magnesium and calcium are both group two alkaline earth metals with an electronegativity of 1.31 and 1.0 , respectively. Whereas iron is a transitional metal and zinc a post-transitional metal with electronegativities of 1.83 and 1.65, respectively (see Table S3.4 in supplementary). Magnesium and calcium, with the lower electronegativity, are therefore more likely to share electrons, maintaining the peptide:metal complex and allowing the coordinate bonding of these metals [56,57] Since the electronegativity and ion size maintain an inverse relationship, increasing electronegativity with decreasing atomic/ion radii due to higher electron density, the role of electronegativity and atomic/ion radii is treated as one. These

basic principles of metal electronegativities and reduction potentials driving complex formation, although unconfirmed, is explored further with the group 11 metals discussed below and agrees with the principles applied and observed in the fabrication of peptide-metal nanoparticles (Chapter 4).

3.4.5.1 Exploring the interaction or Trc mix peptides with group 11 metals: Cu^{2+}, Ag^{+} and Au^{3+}

Formulations with the group 11 metals copper (Fig. 3.9A), silver (Fig. 3.9B) and gold (Fig. 3.9C) demonstrated changes in peptide monomer and dimer signals yet all three formulations lacked triply charged peptide:metal complexes. Interestingly, all three group 11 metals have higher electronegativities than zinc, iron, calcium, and magnesium. The large electronegativities suggest that these group 11 metal ions would rather 'steal' electrons to form neutral atoms than maintain peptide-metal complexes. The lack of complexes can therefore be expected. However, the changes in the dimeric and monomeric signal in the absence of peptide:metal complexes with increasing metal concentration implies that these metal ions still influence peptide oligomerisation in a different manner than the doubly charged metal ions discussed above. The group 11 metal ions used in this study each differ by one charge Ag^{+}, Cu^{2+} and Au^{3+}. It is important to reiterate that peptide:metal complex formation and complex stability as well as accurate identification of such complexes is highly dependent on the oxidation state and stability of the metal ion. As discussed in section 3.4.4 it was assumed that the charge of the peptide:metal complex $[M+Metal\pm H]^{3+}$ is carried either by the peptide, the metal or both. For the doubly charged peptides (Mg^{2+}, Ca^{2+}, Fe^{2+} and Zn^{2+}) above, the formation of triply charged $[M+Metal^{2+}+H]^{3+}$ complexes with 2+ metal ions were confirmed via IM-MS analysis as shown for the example of iron in Figs. 3.5 and 3.6.

Since each of the group 11 ions investigated had different charges, different potential triply charged peptide:metal complexes were expected for each. For example, silver could form a triply charged complex with a neutral silver atom $[M+Ag+3H]^{3+}$ or charged ion $[M+Ag^{+}+2H]^{3+}$. Meanwhile, gold (III) was expected form complexes similar to iron which has two major oxidation states (+2 or +3), while copper was expected to form complexes like Mg^{2+}, Ca^{2+}, and Zn^{2+}. Only triply charged peptide:metal complexes were considered for this study and were not detected for the group 11 metals. Nonetheless, the oxidation state of the metal ion still provides valuable insight on how these metal ions may interact with the peptide without forming peptide:metal complexes. The chemical properties and electronegativities of the metal salts are summarised in Table S3.3 and Table S3.4 in supplementary data. Copper

and silver have minor difference between their electronegativities, 1.90 and 1.93, respectively and exhibited similar signal contribution trends with an initial decrease in monomers $[M+H]^+$ and dimers $[2M+2H]^{2+}$ followed by increase and then a gradual decrease again. However, much like iron and zinc, the overall signal contribution of either formulation differed greatly. Copper demonstrated an overall gain in monomer and dimer signal (Fig. 3.9A) whereas silver demonstrated an overall loss (Fig. 3.9B). This is further illustrated with the IM-MS profile comparison of the 1:2 formulations of copper (Fig. 3.9D) and silver (Fig. 3.9E) against the 50 µM Trc mix control (green) where copper (blue) had a higher ion signal than peptide alone for both matured and fresh samples while silver (grey) has a maintained a lower ion signal. Like calcium and magnesium, gold led to an inverse relationship between the oligomers. However, in the case of gold (Fig. 3.9C), the decrease in monomer signal contribution is not mirrored by an increase in peptide:metal complexes but rather peptide dimeric species in the fresh formulation (solid line). Gold has the largest electronegativity (2.54) throughout the selection of metals used in this study (Table S3.4) and showed the lowest contribution of monomeric peptide (<5%) mirrored by an increase in dimeric peptide (18.2%) for fresh formulations at a 1:2 peptide:metal ratio. However, the matured sample sustained a trend resembling that of fresh silver formulations (Fig. 3.9B), with the loss of monomer and dimer contribution as the concentration of gold increases. A reminder that the percentage contributions of each peptide species is relative to the sum of signal intensities for the selected peptide oligomers analysed. Even though Fig. 3.9F shows an overall higher ion signal for dimers (drift time at 7.84) in the 1:2 matured gold sample, the contribution of dimers to the sum of species investigated within the sample is less (14.4%) than the fresh sample (18.2%). It can therefore be noted that the maturation of samples increases the overall prevalence of monomers and dimers, yet the contribution of dimers within the sample may still be less than the fresh. The same principle applies to all comparisons between matured and fresh samples.

The IM-MS ion profile of silver (Fig. 3.9E) and gold (Fig. 3.9F) showed a loss in signal of the singly charged monomeric (11.88 drift time) and doubly charged dimeric (7.48 drift time) drift peaks associated with a slight shift in peptide fragments at 5.94 drift time for formulations with 100 µM metal. Both silver and gold have an overall signal contribution below that of the 50 µM Trc mix control with gold having a near complete loss of signal for monomeric species in the fresh formulation. The maturation (dotted line) of silver and gold formulations led to overall an increase in monomer dimer signal. However, both matured samples still showed a lower ion signal compared to the matured peptide alone. Matured silver formulations

showed an overall gain in monomer and dimer contributions compared to fresh samples. However, gold showed a gain in monomer and a loss in dimer contributions at higher metal concentrations compared to the fresh samples. It should be noted that solutions of gold (III) chloride are known be relatively unstable and readily reduced to metallic gold [58,59]. The instability of gold in solution could potentially disrupt peptide oligomers and structure integrity, resulting in a higher prevalence of peptide fragments as suggested by the broadened peak at 5.94 drift time for the fresh samples and more defined peptide fragment peak in the matured samples. The same applies to silver which also readily reduces. Unfortunately, such peptide fragments could have overlapping species masses and drift times with the peptide dimers and monomers. The increased prevalence of peptide fragments could therefore be masked by or contribute to the peptide monomer and dimer signal. Careful consideration was therefore taken in selecting, analysing and calculating contributions using peptide species mass ranges to minimise this shortcoming. Nonetheless, the broadening of peaks does make the accurate differentiation challenging. The larger dimer signal contributions for gold and silver could, although minimal, still be attributed to the increased prevalence of peptide fragments. However, the overall loss of monomers and dimers in the absence of triply charged peptide:metal complex formation still suggests that the formulations with these metals either promotes peptide self-assembly into higher order structures and/or the disruption or modification of these smaller peptide oligomers. Moreover, the readiness of these metals to reduce is promising for the fabrication of metal nanoparticles.

Au^{3+} has the largest positive reduction potential (+1.50 V) amongst all the metals selected for this study (see Table S3.3). Gold is therefore a strong oxidising agent that would readily gain electrons to form a neutral metal atom. The same applies for silver with a standard reduction potential of (+0.96 V). The readiness of gold and silver to reduce, and subsequently nucleate, allows for the formation of metal nanoparticles in the presence of a reducing agent. The overall loss of monomer and dimer signal for gold and silver suggests that the peptide is acting as a reducing agent allowing the reduction of the charged metal ions. The absence of peptide:metal complexes can therefore be attributed to the nucleation of neutral metal atoms and the formation of metal nanoparticles. Pilot studies confirmed that gold and silver nanoparticles were formed in formulation with Trc mix (data not shown). Moreover, previous studies have successfully fabricated of metal nanoparticles using peptides as reducing agents [60–64]. Like silver and gold, copper has a positive reduction potential. However, copper's reduction potential to form a neutral metal ion (+0.34 V) is

higher than that of silver and gold. Copper is therefore less likely to interact and be reduced by the peptide. The IM-MS ion profile of copper (Fig. 3.9D) showed that the signal contribution of peptide monomers and dimers for the 1:2 formulation with copper is higher than that of the Trc mix control for fresh and mature samples This could be due to the release of monomeric and dimeric species via the disruption of larger oligomers as theorised and illustrated for metal +2 ion formulations in section 3.4.5.

Fig. 3.10 tracks the changes in prevalence of the peptide analogues within the monomeric drift peak (11.88 ms) for Trc mix (A), copper (B), silver (C) and gold (D). By tracking these changes, insight can be gained on how and which peptide analogues are interacting with the metal ions. Only the mass spectra of the matured samples are shown as they had well defined ion mobility peaks. In Fig. 3.10 the Trc mix control and copper formulation follow similar trends with YB analogues having the highest signal contribution. Although silver and gold both showed an overall loss in signal contribution for the monomeric species compared to the Trc mix control (Fig. 3.9), the loss of certain peptide analogues was greater than others for each metal. Silver (Fig. 3.10C) showed a lower contribution for A, B_1 and C analogues, and gold (Fig. 3.10D) for B and C analogues. These findings propose that each metal had distinct preferences for certain peptide analogues. The loss of C and A analogues with the silver formulations was of particular interest due to the differences in the aromatic dipeptide structure between the three analogues. The A analogues, Cyclo-(fPFfNQYVOL), have phenylalanine residues at position 3 and 4 whereas the C analogues, Cyclo-(fPWwNQYVOL), have bulkier tryptophan residues. Meanwhile, TrcB has a phenylalanine at position 3 and tryptophan at position 4. The TrcB analogues, YB and YB_1 differ from one another by only a lysine/ornithine at position 7.

Interestingly, TrcA and TrcC have shown to self-assemble and form large ion-conducting pores capable of passing large organic molecules through the phospholipid bilayer of bacterial cells. It has also been proposed that the stable amphipathic dimer structures of these tyrocidines may act as seeding active structures allowing the peptide to interact with target membranes [5,50,65]. The loss in monomer and dimer signal for silver could therefore be due to the self-assembly of TrcC and TrcA into these higher order structures capable of interacting and transporting silver ions. Chapter 4 explores the biophysical and antimicrobial characterisation of silver formulations with the tryptophan rich C analogues TrcC and TpcC.

.

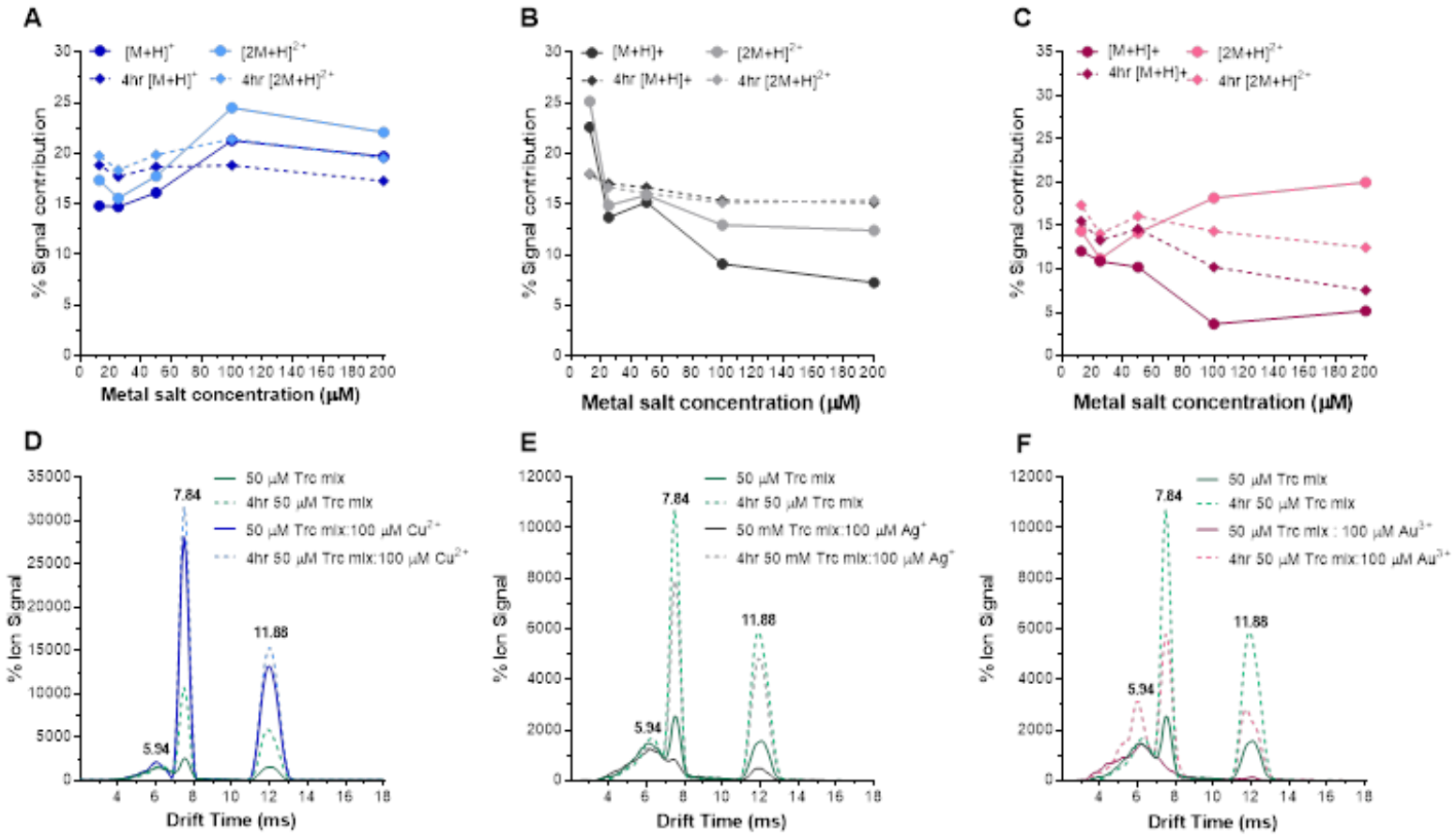

Figure 3.9 Percentage of IM-MS signal contributions of singly charged monomers and doubly charged dimers for fresh (solid line) and matured (dotted line) Trc mix formulations with increasing molar concentrations of metal salts including: $CuCl_2$ (**A**), $AgNO_3$ (**B**) and $HAuCl_4$ (**C**). IM-MS profile showing signal (y-axis) and drift time (x-axis) of monomers (11.88) and dimers (7.48) for 50µM Trc mix (green) and formulations with 200 µM (1:2 peptide:metal ratio) of $CuCl_2$ (**D**) in blue, $AgNO_3$ (**E**) in grey and $HAuCl_4$ in pink (**F**). The solid lines show the trend of fresh samples, while the dotted lines show the trends of 24 hour matured samples.

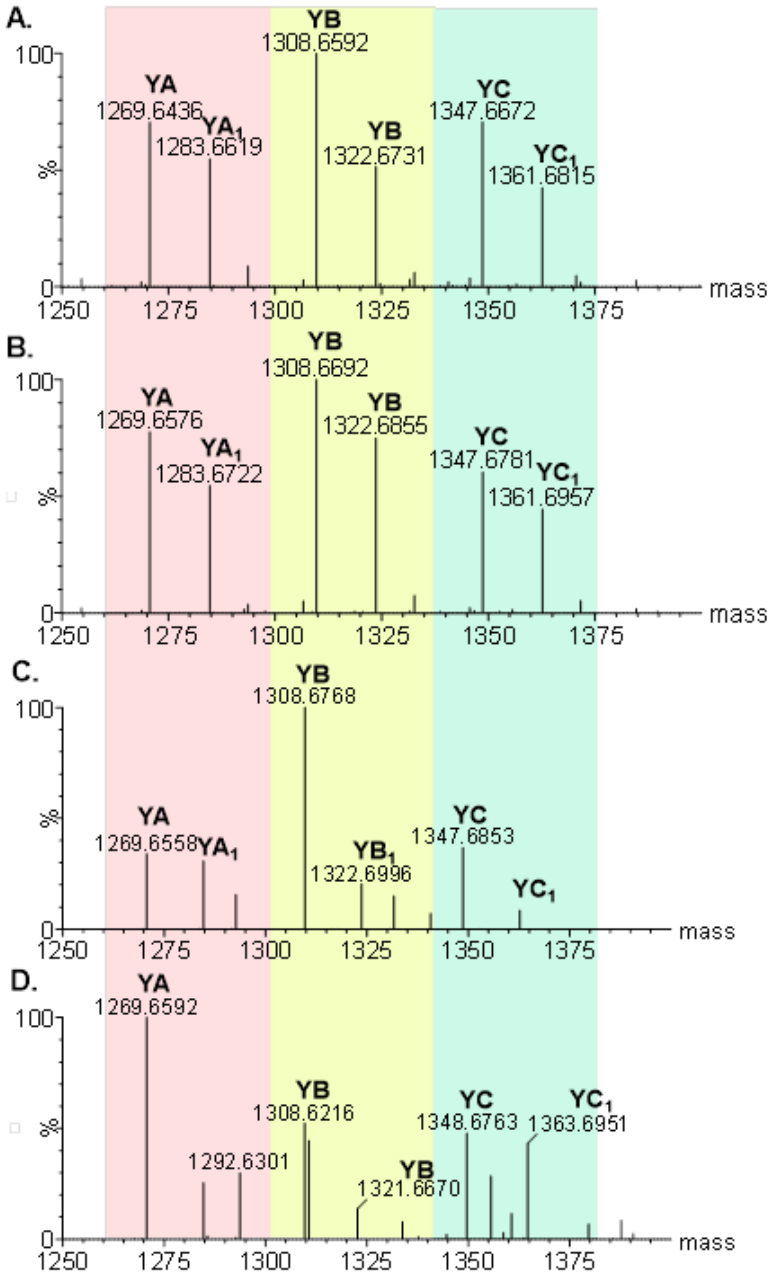

Figure 3.10 ESI-MS showing the monoisotopic monomer mass (x-axis) for the singly charged monomers (drift time 11.88) highlighting the change in percentage signal (y-axis) of the A (blue), B (green) and C (red) analogues for 50 µM Trc mix (**A**) and formulations with 100 µM of the group 11 metals copper (**B**), silver (**C**) and gold (**D**).

Formulations with gold showed the introduction of unidentified peptide masses, likely that of damaged peptides or peptide adducts. This agrees with the broadened and increased prevalence of the IM-MS peak (drift time of 5.94) in both fresh and matured samples (Fig. 3.9F). Although gold is a noteworthy candidate for nanoparticle fabrications, it is a highly reactive and expensive metal and was therefore not used for the studies in Chapter 4.

3.5 Conclusions

The IM-MS analysis of peptide:metal formulations in this study revealed that the formulation of tyrocidines with select metals alters the peptides' self-assembling behaviour to favour different oligomers in the presence of different metals. The influence of the selected metals and their concentration on the oligomerisation of the tyrocidines was investigated by tracking the percentage signal contribution of the different ionic species at the different peptide:metal ratios (4:1,2:1, 1:1, 1:2 and 1:4). Formulation of Trc mix with doubly charged metal ions (Mg^{2+}, Ca^{2+}, Fe^{2+} and Zn^{2+}) allowed the formation of triply charged peptide:metal $[M+Metal^{2+}\pm H]^{3+}$ complexes at 2.09 drift time. The formation of stable peptide:metal complexes is multifaceted and the conditions under which peptide:metal complexes form cannot be confirmed via the IM-MS analysis in this study. However, the detection and accurate identification of such complexes is supported by isotope models. Complexes were also detected via IM-MS after four-hour maturation of the formulations, indicating that the peptide:metal complex structures are stable and maintained over time. Moreover, increasing concentrations of metal led to an increase in the respective peptide:metal complex signal contribution. This observation indicates that the formation of peptide:metal complexes influence or is influenced by the formation and/or breakdown of peptide oligomeric species. Larger peptide oligomers could be disrupted to release smaller oligomers to be incorporated in the peptide:metal complexes or smaller peptide oligomers could be incorporated to form larger oligomers with peptide:metal complexes incorporated into the higher order structures. However, the loss in monomers and dimers and peptide:metal complexes suggests that the monomeric and dimeric species participate in the formation of peptide metal complexes. The experimental *m/z* values observed for the triply charged complexes in the ESI-MS spectra matched the theoretical values for peptide monomer and metal ion combinations $[M+Metal^{2+}+H]^{3+}$ confirming the uptake of peptide monomers to form peptide:metal complexes. The assembly of metals with peptide dimers could perhaps lead to larger higher order structures. Again, the complexity of these larger oligomers makes it difficult to differentiate and identify complexes even with IM-MS and was therefore not considered in this study.

Interestingly group 11 metals did not form peptide:metal complexes that could be detected with IM-MS, even after maturation of the samples. However, these formulations did show changes in the monomer and dimer signal in the absence of complexes. Formulations of gold showed a higher prevalence of peptide fragments indicating a disruption in peptide

oligomers and structure integrity likely due to the high reactivity of gold in solution [58,59]. Gold and silver both have positive reduction potentials and likely reduce to form a neutral metal atom in the presence of the tyrocidines. Pilot studies confirmed that the tyrocidines can act as reducing agents for the formation of gold and silver nanoparticles (data not shown). Moreover, these findings agreed with that of previous studies that have confirmed the formation of metal nanoparticles using tryptophan and tryptophan-rich peptides [60–64]. The overall loss of monomer and dimer signal for gold and silver can therefore be attributed to the oxidation of peptide and the absence of peptide:metal complexes can be attributed to the nucleation of neutral metal atoms and the formation of metal nanoparticles. Monomeric species losses showed preferences for certain peptide analogues (Fig. 3.10), namely TrcA and TrcC. These preferences indicate that certain peptide analogues may play a greater role in the reduction and fabrication of gold and silver nanoparticles, as well as the changes in peptide oligomer profiles for these group 11 formulations. The IM-MS analysis of peptide:metal formulations therefore gave valuable insights on the interactions between peptide and metal, and how such interactions may dictate peptide oligomerisation and therefore activity. The potential to fabricate metal nanoparticles using the tyrocidines is promising for future applications in bio-nanomaterials. The biophysical and antimicrobial properties of the peptide formulations with the group 11 metals were therefore investigated further in Chapter 4.

3.6 References

[1] W. van Rensburg, M. Rautenbach, Creating robust antimicrobial materials with sticky tyrocidines, Antibiotics. 11 (2022). https://doi.org/10.3390/antibiotics11020174.

[2] W. van Rensburg, The tyrocidines in the creation of antimicrobial cellulose and sterilising materials, Stellenbosch University, Stellenbosch, South Africa, 2020. http://hdl.handle.net/10019.1/108461.

[3] Y. Masoudi, W. van Rensburg, B. Barnard-Jenkins, M. Rautenbach, The influence of cellulose-type formulants on anti-*Candida* activity of the tyrocidines, Antibiotics. 10 (2021). https://doi.org/10.3390/antibiotics10050597.

[4] H.H. Paradies, H. Reichelt, Formation and structures of tyrocidine B in solution in the presence of water, AIP Adv. 10 (2020) 75007. https://doi.org/10.1063/1.5144852.

[5] P.J. Loll, EC. Upton, V. Nahoum, N.J. Economou, S. Cocklin, The high resolution structure of tyrocidine A reveals an amphipathic dimer, Biochim Biophys Acta. 1838 (2014) 1199–1207. https://doi.org/10.1016/jBbamem.2014.01.033.

[6] V. Kumar, W. van Rensburg, J.L. Snoep, H.H. Paradies, C. Borrageiro, C. de Villiers, R. Singh, KB. Joshi, M. Rautenbach, Antimicrobial nano-assemblies of tryptocidine C, a tryptophan-rich cyclic decapeptide, from ethanolic solutions, Biochimie. (2022). https://doi.org/10.1016/jBiochi.2022.08.017.

[7] M. Rautenbach, V. Kumar, JA. Vosloo, Y. Masoudi, R.J. van Wyk, MA. Stander, Oligomerisation of tryptocidine C, a Trp-rich cyclodecapeptide from the antimicrobial tyrothricin complex, Biochimie. (2021). https://doi.org/10.1016/jBiochi.2020.12.006.

[8] C. Andreini, I. Bertini, G. Cavallaro, G.L. Holliday, J.M. Thornton, Metal ions in biological catalysis: From enzyme databases to general principles, J. Biol. Inorg. Chem. 13 (2008) 1205–1218. https://doi.org/10.1007/s00775-008-0404-5.

[9] E.G. Dedyukhina, V.K. Eroshin, Essential metal ions in the control of microbial metabolism, Process Biochem. 26 (1991) 31–37. https://doi.org/10.1016/0032-9592(91)80005-A.

[10] J.S. Klein, O. Lewinson, Bacterial ATP-driven transporters of transition metals: Physiological roles, mechanisms of action, and roles in bacterial virulence, Metallomics. 3 (2011) 1098–1108. https://doi.org/10.1039/c1mt00073j.

[11] K.J. Waldron, JC. Rutherford, D. Ford, N.J. Robinson, Metalloproteins and metal sensing, Nature. 460 (2009) 823–830. https://doi.org/10.1038/nature08300.

[12] JE. Page, MA. Skiba, T. Do, AC. Kruse, S. Walker, Metal cofactor stabilization by a partner protein is a widespread strategy employed for amidase activation, Proc. Natl. Acad. Sci. U. S. A. 119 (2022). https://doi.org/10.1073/PNAS.2201141119/-/DCSUPPLEMENTAL.

[13] Y. Takagi, N. Uchida, Y. Anraku, T. Muraoka, Stabilization of bicelles using metal-binding peptide for extended blood circulation, Chem. Commun. 5164 (2022) 5164. https://doi.org/10.1039/d2cc01058e.

[14] M. Rautenbach, P. Swart, M.J. Van Der Merwe, The interaction of analogues of the antimicrobial lipopeptide, iturin A2, with alkali metal ions, Bioorganic Med. Chem. 8 (2000) 2539–2548. https://doi.org/10.1016/S0968-0896(00)00186-3.

[15] PB. Tchounwou, C.G. Yedjou, A.K. Patlolla, D.J. Sutton, Heavy metals toxicity and the environment, In: Luch, A. (eds) Molecular, Clinical and Environmental Toxicology. Experientia Supplementum, vol 101. Springer, Basel. https://doi.org/10.1007/978-3-7643-8340-4_6.

[16] N. White, H. Sadeeshkumar, A. Sun, N. Sudarsan, R.R. Breaker, Na+ riboswitches regulate genes for diverse physiological processes in bacteria, Nat. Chem. Biol. 18 (2022) 878–885. https://doi.org/10.1038/s41589-022-01086-4.

[17] V. Arige, D.I. Yule, Spatial and temporal crosstalk between the cAMP and Ca2+ signaling systems, Biochim. Biophys. Acta - Mol. Cell Res. 1869 (2022) 119293. https://doi.org/10.1016/jBbamcr.2022.119293.

[18] C. Sissi, M. Palumbo, Effects of magnesium and related divalent metal ions in topoisomerase structure and function, Nucleic Acids Res. 37 (2009) 702–711. https://doi.org/10.1093/nar/gkp024.

[19] JA. Cowan, Structural and catalytic chemistry of magnesium-dependent enzymes, 2002. https://doi.org/10.1023/A:1016022730880.

[20] O. Weisss, J. Holdeni, C. Rulka, RA. Kahn7, Nucleotide binding and cofactor activities of purified bovine brain and bacterially expressed ADP-ribosylation factor, J. Biol. Chem. 264 (1989) 21066–21072.

[21] CF. Chang, H. Shuman, A.P. Somlyo, Electron probe analysis, X-ray mapping, and electron energy-loss spectroscopy of calcium, magnesium, and monovalent ions in log-phase and in dividing Escherichia coli B cells, J. Bacteriol. 167 (1986) 935–939. https://doi.org/10.1128/jb.167.3.935-939.1986.

[22] G. Weiss, P.L. Carver, Role of divalent metals in infectious disease susceptibility and outcome, Clin Microbiol Infect. 24 (2018) 16–23. https://doi.org/10.1016/jCmi.2017.01.018.

[23] S. Curiel-Alegre, B. Velasco-Arroyo, C. Rumbo, A.HA. Khan, JA. Tamayo-Ramos, C. Rad, J.L.R. Gallego, R. Barros, Evaluation of biostimulation, bioaugmentation, and organic amendments application on the bioremediation of recalcitrant hydrocarbons of soil, Chemosphere. 307 (2022) 1–12. https://doi.org/10.1016/jChemosphere.2022.135638.

[24] R.M. Sterritt, J.N. Lester, Interactions of heavy metals with bacteria, Sci. Total Environ. 14 (1980) 5–17. https://doi.org/10.1016/0048-9697(80)90122-9.

[25] K. Giles, SD. Pringle, K.R. Worthington, D. Little, J.L. Wildgoose, R.H. Bateman, Applications of a travelling wave-based radio-frequency-only stacked ring ion guide, Rapid Commun. Mass Spectrom. 18 (2004) 2401–2414. https://doi.org/10.1002/rcm.1641.

[26] AB. Kanu, P. Dwivedi, M. Tam, L. Matz, H.H. Hill, Ion mobility-mass spectrometry, J. Mass Spectrom. J. Mass Spectrom. 43 (2008) 1–22. https://doi.org/10.1002/jms.1383.

[27] CB. Morris, JC. Poland, JC. May, JA. McLean, fundamentals of ion mobility-mass spectrometry for the analysis of biomolecules, Methods Mol. Biol. 2084 (2020) 1–31. https://doi.org/10.1007/978-1-0716-0030-6_1.

[28] C. Horvath, W. Melander, Liquid Chromatography with Hydrocarbonaceous Bonded Phases; Theory and Practice of Reversed Phase Chromatography*, J. Chromatogr. Sci. 15 (1977) 393–404. http://dxDoi.org/10.1093/chromsci/15.9.393.

[29] AA. Shvartsburg, RD. Smith, Fundamentals of traveling wave ion mobility spectrometry, Anal. Chem. 80 (2008) 9689–9699. https://doi.org/10.1021/ac8016295.

[30] J.N. Dodds, E.S. Baker, ion mobility spectrometry: fundamental concepts, instrumentation, applications, and the road ahead, J. Am. Soc. Mass Spectrom. 30 (2019) 2185–2195. https://doi.org/10.1007/s13361-019-02288-2.

[31] B.T. Ruotolo, CC. Tate, D.H. Russell, Ion mobility-mass spectrometry applied to cyclic peptide analysis: Conformational preferences of gramicidin S and linear analogs in the gas phase, J. Am. Soc. Mass Spectrom. 15 (2004) 870–878. https://doi.org/10.1016/j.jasms.2004.02.006.

[32] M. Rautenbach, N.M. Vlok, HA. Eyéghé-Bickong, M.J. van der Merwe, MA. Stander, An Electrospray ionization mass spectrometry study on the "*in vacuo*" hetero-oligomers formed by the antimicrobial peptides, surfactin and gramicidin S, J. Am. Soc. Mass Spectrom. 28 (2017) 1623–1637. https://doi.org/10.1007/s13361-017-1685-0.

[33] D.J. Weston, R. Bateman, ID. Wilson, T.R. Wood, C.S. Creaser, Direct analysis of pharmaceutical drug formulations using ion mobility spectrometry/quadrupole-time-of-flight mass spectrometry combined with desorption electrospray ionization, Anal. Chem. 77 (2005) 7572–7580. https://doi.org/10.1021/ac051277q.

[34] EC.Y. Chan, S.N. Lee, W.Y. Chun, T.G. Lin, Pharmaceutical metabolite profiling using quadrupole/ion mobility spectrometry/time-of-flight mass spectrometry, Rapid Commun. Mass Spectrom. 23 (2009) 384–394. https://doi.org/10.1002/rcm.3887.

[35] S. Trimpin, DE. Clemmer, Ion mobility spectrometry/mass spectrometry snapshots for assessing the molecular compositions of complex polymeric systems, Anal. Chem. 80 (2008) 9073–9083. https://doi.org/10.1021/ac801573n.

[36] P. Dwivedi, B. Bendiak, B.H. Clowers, H.H. Hill, Rapid resolution of carbohydrate isomers by electrospray ionization ambient pressure ion mobility spectrometry-time-of-flight mass spectrometry (ESI-APIMS-TOFMS), J. Am. Soc. Mass Spectrom. 18 (2007) 1163–1175. https://doi.org/10.1016/j.jasms.2007.04.007.

[37] C. Uetrecht, R.J. Rose, E. van Duijn, K. Lorenzen, A.J.R. Heck, Ion mobility mass spectrometry of proteins and protein assemblies, Chem. Soc. Rev. 39 (2010) 1633–1655. https://doi.org/10.1039/b914002f.

[38] EA. Mason, H.W. Schamp, Mobility of gaseous Ions in weak electric fields, Ann. Phys. (N. Y). 4 (1958) 233–270. https://doi.org/10.1016/0003-4916(58)90049-6.

[39] M.L. Feuerstein, M. Hernández-Mesa, Y. Valadbeigi, B. Le Bizec, S. Hann, G. Dervilly, T. Causon, Critical evaluation of the role of external calibration strategies for IM-MS, Anal. Bioanal. Chem. (2022). https://doi.org/10.1007/s00216-022-04263-5.

[40] LC. Nye, J.P. Williams, NC. Munjoma, M.P.M. Letertre, M. Coen, R. Bouwmeester, L. Martens, J.R. Swann, J.K. Nicholson, R.S. Plumb, M. McCullagh, LA. Gethings, S. Lai, J.I. Langridge, J.PC. Vissers, ID. Wilson, A comparison of collision cross section values obtained via travelling wave ion mobility-mass spectrometry and ultra high performance liquid chromatography-ion mobility-mass spectrometry: Application to the characterisation of metabolites in rat urine, J. Chromatogr. A. 1602 (2019) 386–396. https://doi.org/10.1016/jChroma.2019.06.056.

[41] J.N. Dodds, JC. May, JA. McLean, Correlating Resolving Power, Resolution, and Collision Cross Section: Unifying Cross-Platform Assessment of Separation Efficiency in Ion Mobility Spectrometry, Anal. Chem. 89 (2017) 12176–12184. https://doi.org/10.1021/acsAnalchem.7b02827.

[42] C. Bich, S. Baer, MC. Jecklin, R. Zenobi, Probing the Hydrophobic Effect of Noncovalent Complexes by Mass Spectrometry, J. Am. Soc. Mass Spectrom. 21 (2010) 286–289. https://doi.org/10.1016/j.jasms.2009.10.012.

[43] S. Zhang, C.K. Van Pelt, DB. Wilson, Quantitative determination of noncovalent binding interactions using automated nanoelectrospray mass spectrometry, Anal. Chem. 75 (2003) 3010–3018. https://doi.org/10.1021/ac034089d.

[44] M. Rautenbach, P. Swart, M.J. Van Der Merwe, Sequence specific stabilization of a linear analog of the antifungal lipopeptide iturin A_2 by sodium during low energy electrospray ionization mass spectrometry conditions, J. Am. Soc. Mass Spectrom. 12 (2001) 505–516. https://doi.org/10.1016/S1044-0305(01)00232-X.

[45] I. Michaelevski, N. Kirshenbaum, M. Sharon, T-wave ion mobility-mass spectrometry: Basic experimental procedures for protein complex analysis, J. Vis. Exp. (2010) 1985. https://doi.org/10.3791/1985.

[46] K. Richardson, D. Langridge, S.M. Dixit, B.T. Ruotolo, an improved calibration approach for traveling wave ion mobility spectrometry: robust, high-precision collision cross sections, Anal. Chem. 93 (2021) 3542–3550. https://doi.org/10.1021/acsAnalchem.0c04948

[47] M. Thies, H.H. Paradies, Self-assembly of tyrocidines in nanotubular structures, MRS Online Proc. Libr. 489 (1998) 145–151. https://doi.org/10.1557/proc-489-145.

[48] H. Henrich Paradies, H.H. Paradies, Structure of tyrocidine micelles in isotropic aqueous solution, J. Pharm. Sci. 78 (1989) 230–234. https://doi.org/10.1002/jps.2600780312.

[49] MA. Ruttenberg, T.P. King, LC. Craig, The Use of the tyrocidines for the study of conformation and aggregation behavior, J. Am. Chem. Soc. 87 (1965) 4196–4198. https://doi.org/10.1021/ja01096a040.

[50] G. Munyuki, GE. Jackson, GA. Venter, KE. Kövér, L. Szilágyi, M. Rautenbach, B.M. Spathelf, B. Bhattacharya, D. Van Der Spoel, β-sheet structures and dimer models of the two major tyrocidines, antimicrobial peptides from Bacillus aneurinolyticus, Biochemistry. 52 (2013) 7798–7806. https://doi.org/10.1021/bi401363m.

[51] J.N. Hoskins, S. Trimpin, S.M. Grayson, Architectural differentiation of linear and cyclic polymeric isomers by ion mobility spectrometry-mass spectrometry, 44 (2011) 6915–6918. https://doi.org/10.1021/ma2012046.

[52] R.J. Van Wyk, Development of cyclodecapeptides from the tyrothricin complex as anticancer peptides, Stellenbosch University, Stellenbosch, South Africa, 2019. http://hdl.handle.net/10019.1/105712.

[53] H.H. Paradies, Aggregation of tyrocidine in aqueous solutions, Biochem. Biophys. Res. Commun. 88 (1979) 810–817. https://doi.org/10.1016/0006-291X(79)91480-3.

[54] T.M. Annesley, Ion suppression in mass spectrometry, Clin. Chem. 49 (2003) 1041–1044. https://doi.org/10.1373/49.7.1041.

[55] R. King, R. Bonfiglio, C. Fernandez-Metzler, C. Miller-Stein, T. Olah, Mechanistic investigation of ionization suppression in electrospray ionization, J. Am. Soc. Mass Spectrom. 11 (2000) 942–950. https://doi.org/10.1016/S1044-0305(00)00163-X.

[56] D.P. Malenov, SD. Zarić, Stacking interactions of aromatic ligands in transition metal complexes, Coord. Chem. Rev. 419 (2020) 213338. https://doi.org/10.1016/jCcr.2020.213338.

[57] DD. Carlton, KA. Schug, A review on the interrogation of peptide–metal interactions using electrospray ionization-mass spectrometry, Anal. Chim. Acta. 686 (2011) 19–39. https://doi.org/10.1016/JACA.2010.11.050.

[58] K. Soo Nam, B. Hi Jung, J. Woong An, T. Jun Ha, T. Tran, M. Jun Kim, Use of chloride-hypochlorite leachants to recover gold from tailing, (2008). https://doi.org/10.1016/j.minpro.2007.12.003.

[59] X. Sun, S. Dong, E. Wang, One-step preparation of highly concentrated well-stable gold colloids by direct mix of polyelectrolyte and HAuCl4 aqueous solutions at room temperature, J. Colloid Interface Sci. 288 (2005) 301–303. https://doi.org/10.1016/j.jcis.2005.02.079.

[60] S. Si, T.K. Mandal, Tryptophan-based peptides to synthesize gold and silver nanoparticles: A mechanistic and kinetic study, Chem. - A Eur. J. 13 (2007) 3160–3168. https://doi.org/10.1002/chem.200601492.

[61] M. Iosin, P. Baldeck, S. Astilean, Study of tryptophan assisted synthesis of gold nanoparticles by combining UV-Vis, fluorescence, and SERS spectroscopy, J. Nanoparticle Res. 12 (2010) 2843–2849. https://doi.org/10.1007/s11051-010-9869-6.

[62] V. Kumar, N.K. Mishra, S. Gupta, KB. Joshi, Short peptide amphiphile cage facilitate engineering of gold nanoparticles under the laser field, ChemistrySelect. (2017). https://doi.org/10.1002/slct.201601548.

[63] S. Roy, T.K. Das, Study of Interaction between tryptophan, tyrosine, and phenylalanine separately with silver nanoparticles by fluorescence quenching method, J. Appl. Spectrosc. 82 (2015) 598–606. https://doi.org/10.1007/s10812-015-0151-7.

[64] S. Gupta, M. Kashyap, V. Kumar, P. Jain, V. Vinayak, KB. Joshi, Peptide mediated facile fabrication of silver nanoparticles over living diatom surface and its application, J. Mol. Liq. (2018). https://doi.org/10.1016/j.molliq.2017.11.086.

[65] M. Wenzel, M. Rautenbach, JA. Vosloo, T. Siersma, C.H.M. Aisenbrey, E. Zaitseva, WE. Laubscher, W. van Rensburg, JC. Behrends, B. Bechinger, L.W. Hamoen, The multifaceted antibacterial mechanisms of the pioneering peptide antibiotics tyrocidine and gramicidin S, MBio. 9 (2018). https://doi.org/10.1128/mBio.00802-18.

[66] R. Chang, Chemistry, 7th ed., 2002, McGraw-Hill Science/Engineering/Math, New York.

3.7 Supplementary data

Table S3.1 Summary of the theoretical *masses (Da)* for monomeric species of the six major tyrocidines present in Trc mix.

Monomeric Species Masses (Da)				
Peptide Identity	**Theoretical *Mr* M**	**Singly Charged $[M+H]^{+}$**	**Doubly Charged $[M+2H]^{2+}$**	**Triply Charged $[M+3H]^{3+}$**
YA	1269.6546	1270.6624	635.8351	424.2260
YA_1	1283.6703	1284.6781	642.8430	428.8979
YB	1308.6655	1309.6733	655.3406	437.2297
YB_1	1322.6812	1323.6890	662.3484	441.9015
YC	1347.6764	1348.6842	674.8460	450.2333
YC_1	1361.6921	1362.6999	681.8539	454.9052

3.7.1 CCS calibration curves and calculations

$$t'_D = t_0 - \frac{c\sqrt{m/z}}{1000}$$ **Equation S3.1**

$$\Omega' = \frac{\Omega}{z \times \sqrt{1/\mu}}$$ **Equation S3.2**

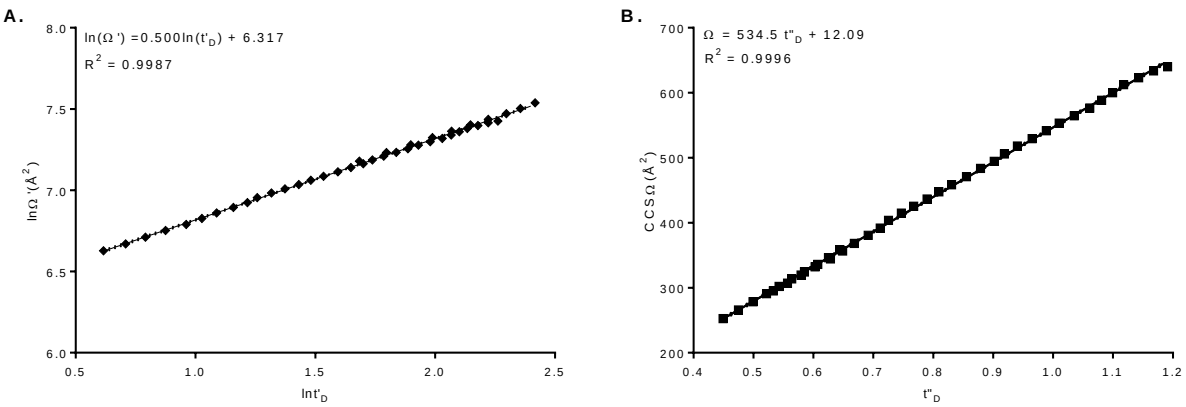

Figure S3.1 Linear CCS calibration curves constructed according to Ruotolo *et al.* [31]. **A.** The charge corrected CCS (ln Ω′) plotted against the corrected drift time (ln t′D) for polyAla species with the equation of the linear fit ($\ln(\Omega') = X\ln t'_D + A$) and correlation coefficient (R^2) denoted in the upper left corner. **B.** The CCS areas (Ω) of poly-Ala species obtained from literature [REF WR 68] plotted against the doubly corrected drift time (t''_D) values of the observed poly-Ala species with the equation of the linear fit ($\Omega = X(t''_D) + A$) and correlation coefficient (R^2) denoted in the upper left corner.

Table S3.2 The average CCS areas of the ionic species for the major peptides in Trc mix as determined from their drift times using the poly-Ala calibration curve. The CCS areas were determined from two repeats and the standard deviation (SD) is given. The ionic species summarised include monomers $[M+H]^+$, doubly charged monomers $[M+2H]^{2+}$ and dimers $[2M+2H]^{2+}$.

Peptide Identity	AbbrA	Variable amino acid residues[b]	CCS Ω (Å2) ± SD		
			$[M+H]^+$	$[M+2H]^{2+}$	$[2M+2H]^{2+}$
TrcA	YA	F^3-f^4-Y^7	359 ± 2	389 ± 0	553 ± N/A*
TrcB	YB	W^3-f^4-Y^7	362 ± 0	395 ± 0	559 ± 3
TrcC	YC	W^3-w^4-Y^7	369 ± 1	394 ± 0	576 ± 3

[a]The first letter in the abbreviations refers to the amino acid residues phenylalanine (Phc/F), tyrosine (Trc/Y) and tryptophan (Tpc/W) at position seven of the Trcs.
[b]Conventional one-letter abbreviations for variable residues with lower- and upper-case letters representing D-amino and L-amino acids, respectively. Residue position indicated in superscript.
* SD not applicable due to absence of dimers species $[2M+2H]^{2+}$ in repeat.

3.7.2 Metal properties and peptide:metal complexes

Table S3.3 Standard reduction potential (E°V) at 25°C for select metals adapted from Chang [66]

Increasing strength as oxidising agent ↑

Half-Reaction	**E°(V)**
$Au^{3+}(aq) + 3e^- \rightarrow Au(s)$	+1.50
$Cl_2(g) + 2e^- \rightarrow 2Cl^-(aq)$	+1.36
$NO_3^-(aq) + 4H^+(aq) + 3e^- \rightarrow NO(g) + 2H_2O$	+0.96
$Ag^+(aq) + e^- \rightarrow Ag(s)$	+0.80
$Fe^{3+}(aq) + e^- \rightarrow Fe^{2+}(aq)$	+0.77
$Cu^+ + 2e^- \rightarrow Cu$	+0.52
$Cu^{2+}(aq) + 2e^- \rightarrow Cu(s)$	+0.34
$AgCl(s) + e^- \rightarrow Ag(s) + Cl^-(aq)$	+0.22
$Cu^{2+}(aq) + 2e^- \rightarrow Cu^+(aq)$	+0.15
$2H^{2+}(aq) + 2e^- \rightarrow H_2(g)$	0.00
$Fe^{2+}(aq) + 2e^- \rightarrow Fe(s)$	-0.44
$Zn^{2+}(aq) + 2e^- \rightarrow Zn(s)$	-0.76
$Mg^{2+}(aq) + 2e^- \rightarrow Mg(s)$	-2.37
$Ca^{2+} + 2e^- \rightarrow Ca$	-2.87

These are the standard state values for all half-reactions at a concentration of 1M for dissolved species and a pressure of 1 atm for gases.

Increasing strength as reducing agent →

Table S3.4 Summary of characteristics of metal salts selected for formulations with peptide (adapted from Chang [66]).

Metal	Oxidation States[a]	Atomic Mass (u)	Electronegativity (Pauling's Scale)	Atomic Radius (Å)	Ionic Radius (Å)	First ionisation energy (kcal/g.mol)	Chloride Salt	Nitrate Salt
Mg	**+2**	23.9850	1.31	1.6	0.7	176.0	$MgCl_2$	$Mg(NO_3)_2$
Ca	**+2**	39.9626	1.00	2.0	1.0	141.0	$CaCl_2$	$Ca(NO_3)_2$
Fe	+2,**+3**	53.9396	1.83	1.3	0.8	182.0	$FeCl_2$	-
Cu	**+2**,+3	62.9296	1.93	1.3	0.7	178.0	CuCl2	-
Ag	**+1**	106.9051	1.90	1.4	1.3	175.0	-	$AgNO_3$
Au	+1,**+3**	196.9666	2.54	1.5	1.4	213.0	$HAuCl_4$	-
Zn	**+2**	63.9291	1.65	1.4	0.7	216.0	$ZnCl_2$	-

Table S3.5 Summary of theoretical monoisotopic peptide:iron and ion complex masses for tyrocidine analogues in Trc mix

Theoretical Monomeric Petide:Metal Complexes													
Complex Identity	FA	YA	YA_1	YB	YB_1	YC	YC_1	WA	WA_1	WB	WB_1	WC	WC_1
[M+Metal] (mass)													
^{54}Fe	1307.6	1323.6	1337.6	1362.6	1376.6	1401.6	1415.6	1346.6	1360.6	1385.6	1399.6	1424.6	1438.6
Doubly Charged [M+Metal ± nH]$^{2+}$ (*m/z*)													
^{54}Fe	654.8	662.8	669.8	682.3	689.3	701.8	708.8	674.3	681.3	693.8	700.8	713.3	720.3
$^{54}Fe^{2+}$	653.8	661.8	668.8	681.3	688.3	700.8	707.8	673.3	680.3	692.8	699.8	712.3	719.3
Triply Charged [M+Metal ± nH]$^{3+}$ (*m/z*)													
^{54}Fe	436.9	442.2	446.9	455.2	459.9	468.2	472.9	449.9	454.5	462.9	467.6	475.9	480.6
$^{54}Fe^{2+}$	436.2	441.5	446.2	454.5	459.2	467.5	472.2	449.2	453.9	462.2	466.9	475.2	479.9

Table S3.6 Summary of the theoretical and experimental triply charged peptide:iron and chloride complex masses (*m/z* values) for tyrocidine analogues found in Trc mix.

Peptide:Iron Complex [M+Metal] Mass (Da)				
Complex Identity	^{54}Fe	^{56}Fe	^{57}Fe	^{58}Fe
	53.9	55.9	56.9	57.9
FA	1307.6	1309.6	1310.6	1311.6
YA	1323.6	1325.6	1326.6	1327.6
YA_1	1337.6	1339.6	1340.6	1341.6
YB	1362.6	1364.6	1365.6	1366.6
YB_1	1376.6	1378.6	1379.6	1380.6
YC	1401.6	1403.6	1404.6	1405.6
YC_1	1415.6	1417.6	1418.6	1419.6
WA	1346.6	1348.6	1349.6	1350.6
WA_1	1360.6	1362.6	1363.6	1364.6
WB	1385.6	1387.6	1388.6	1389.6
WB_1	1399.6	1401.6	1402.6	1403.6
WC	1424.6	1426.6	1427.6	1428.6
WC_1	1438.6	1440.6	1441.6	1442.6

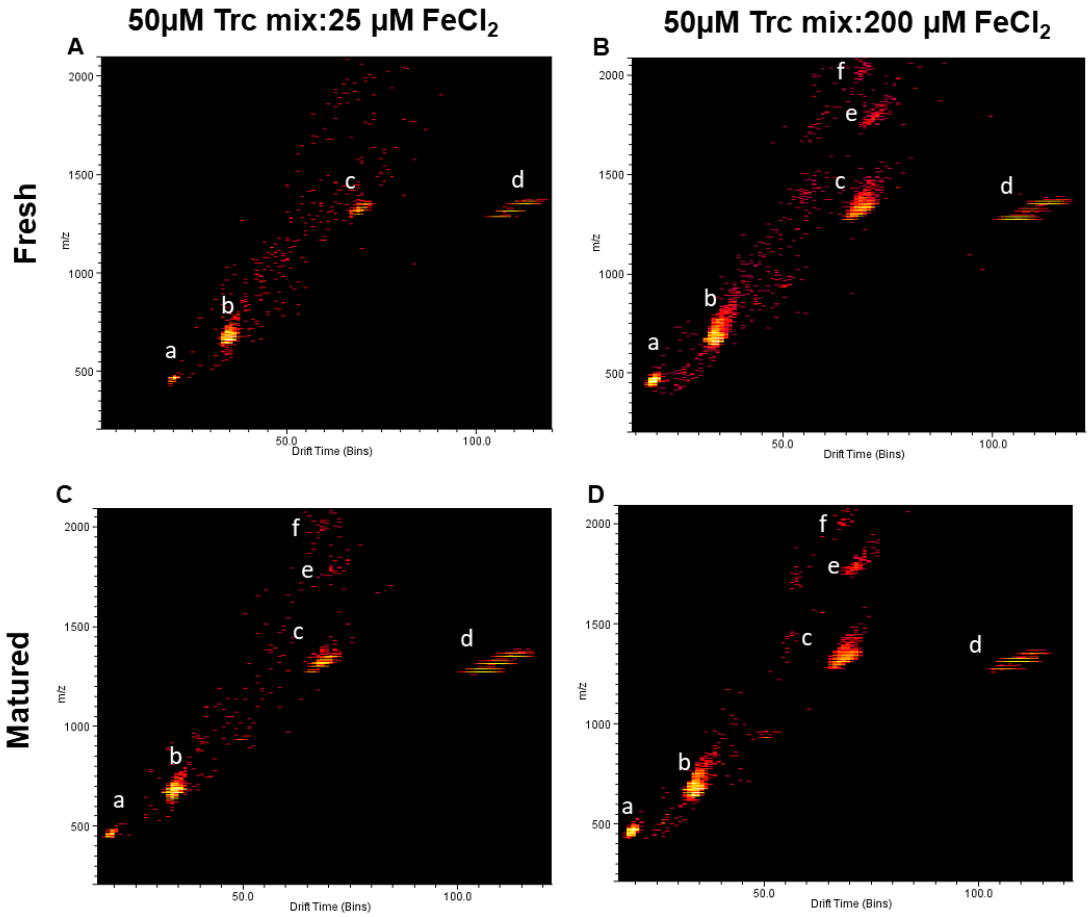

Figure S3.2 Comparison of IM-MS DriftScope profiles of fresh (**A** and **B**) and 4hr matured (**C** and **D**) Trc mix formulations at the peptide:metal ratio (2:1) with 25 µM $FeCl_2$ and highest peptide:metal ratio (1:4) with (**A** and **B**) and 200 µM (**B** and **D**).

Chapter 4

Biophysical and bioactive properties of tyrocidine nanoformulations with group 11 metals

4.1 Introduction

The stagnated discovery of novel drug classes and the ever-growing dilemma of antimicrobial resistance has prompted researchers to reconsidered, modify, and improve currently available antimicrobials to develop novel drugs or drug applications with activity against drug resistant pathogens and/or a low risk of resistance development in future [1,2]. Moreover, the application new and improved development tools, such as nanotechnology, shows promise for the fabrication of novel drugs and drug therapies even with older antimicrobials. In general, antimicrobial peptides have shown great promise as alternative drug treatments due to their multiple modes of action and unlikelihood to have resistance developed against them. Additionally, advances in nanotechnology have highlighted the potential of metal nanoparticles (MNPs) for the fabrication and development of novel nano-drugs and delivery systems [3]. The rapid synthesis of metal nanoparticles via chemical reduction and photoinduced electron transfer (PET) has been extensively studied, particularly for the incorporation of MNPs in nano-polymers and other nanomaterials for improved biological and/or antimicrobial applications [4–6]. Recently, combinational therapies of AMPs and MNPs have gained interested as the hybridisation these two agents holds the potential for the development of novel nano-drugs and the revitalisation and/or improvement of currently available drugs and drug therapies [3,7]. Moreover, the green synthesis of MNPs via the reduction by AMPs, and the subsequent formation of antimicrobial peptide-metal nanoparticle (AMP-MNP) hybrids has recently gained interest due to their combined physiochemical, optical, and antimicrobial properties.

Gram-positive *Staphylococcus aureus* (*S. aureus*) and Gram-negative *Escherichia coli* (*E. coli*) are two often harmless, but ever-present bacterium commonly found in humans the surfaces or environments they interact with [8,9]. Unfortunately, like many opportunistic pathogens, the imbalance, pathogenesis, and contamination of these organisms may lead to lethal infections. Moreover, the contamination of foods and food contact surfaces could lead to crop spoilage and disease spread. A growing concern with both *S. aureus* and *E. coli* as pathogens is the prevalence of drug-resistant strains and the role of these pathogens in the development of biofilms which challenge the effective treatment of these pathogens . Moreover, the steady decreased sensitivity of *S. aureus* and *E. coli* towards commonly used

β-lactams class of antibiotics over the years is great cause for concern and demands the development of a novel antibacterial drug therapy against these common pathogens.

In this study the antimicrobial drug Tyrothricin is revisited. Particularly the group of antimicrobial cyclic decapeptides (CDPs) naturally produced by the tyrothricin complex, the tyrocidines and tyrocidine analogues. Although these cyclic-peptides have shown to be potent antimicrobials against a broad range of microorganisms including drug resistant pathogens, previous investigations have reported poor activity of tyrocidine peptide mixtures and single analogues against Gram-negative *E. coli* [10–13]. Conversely, some of the group 11 metals, namely copper [14–17], silver [16,18–20], and gold [20,21] have shown antimicrobial activity against both *S. aureus* and *E. coli*. Many studies have successfully synthesised metal nanoparticles using antimicrobial peptides and amino acid residues often assisted by PET via sample irradiation. Such studies have indicated that tryptophan and tryptophan-containing peptides assist the reduction of free metal ions and stabilisation of subsequent metal nanoparticles [6,22,23]. Moreover, the interactions between and encapsulation of metal nanoparticles during the peptide self-assembly has shown promising alterations in drug delivery systems [24,25]. In this study the potential of the tryptophan-rich tyrocidines (TrcC and TpcC) and tyrocidine mixtures (Trc mix) to act as a reducing and stabilising agent for the fabrication of metal nanoparticles, particularly those of the with the group 11, metals were investigated to improve the antimicrobial activity of the peptides towards Gram-negative *E. coli.* Formulations of each peptide with the group 11 metals were optimised to induced nanoparticle fabrication and the successful fabrication of cyclodecapeptide-metal nanoparticle (CDP-MNP) nanoformulations was characterised and confirmed using an array of biophysical analysis including UV-Vis spectrophotometry, fluorometry and electron microscopy. The antimicrobial activity of CDP-MNP nanoformulations against both *S. aureus* and *E. coli* were tested via solid surface assays to determine the viability of CDP-MNP nanoformulations for future antimicrobial surface applications.

4.2 Materials

Gramicidin S, tyrothricin and gentamicin was supplied by Sigma (St. Louis, MO, USA). Trc mix, pure TpcC (>95% purity) and pure TrcC as determined by ultra-performance liquid chromatography linked to mass spectrometry as described in Chapter 2. Analytical grade ethanol (EtOH) was supplied by Merck (Darmstadt, Germany). Analytical grade water (MilliQ water) was prepared by filtering water via a reverse osmosis plant using a Millipore-Q®

water purification system (Milford, USA). 300 mesh carbon coated grids were purchased from Agar Scientific Ltd. (Stansted, UK). Gold (III) chloride ($HAuCl_4$) of 99.9% purity was supplied by Sigma-Aldrich (St. Louis, USA). Copper chloride ($CuCl_2$) and silver nitrate ($AgNO_3$) of 99.9% purity were supplied by Merck (Darmstadt, Germany). Agar, yeast extract, tryptone, Na_2HPO_4, and KH_2PO_4 were also supplied by Merck (Darmstadt, Germany).Sigma-Aldrich (St. Louis, MA, USA) supplied resazurin sodium salt. Black 96-well polystyrene plates and sodium chloride was supplied by Merck (Wadeville, South Africa). Greiner 96 Well UV-Star® Microplates and petri dishes were obtained from Lasec (Cape Town, South Africa). Clear 96-well microplates were supplied by Thermo-Fisher Scientific (Waltham, MA, USA) and sterile Falcon® tubes by Becton Dickson Labware (Lincoln Park, USA). Laboratory strains of *Staphylococcus aureus* RN4220 and *Escherichia coli ATCC 13076* were obtained from the BIOPEP culture collection (department of Biochemistry, Stellenbosch University).

4.2.1 *Peptide-metal formulation and nanoparticle fabrication*

The peptides selected for the formulations include Trc mixture (Trc mix) containing predominantly TrcA, TrcB and TrcC and their Lys-analogues and pure (>90% purity) TpcC and TrcC purified in Chapter 2. All peptide was formulated with a silver nitrate ($AgNO_3$) in an array of peptide:metal molar ratios (4:1, 2:1, 1:1, 1:2,1:3 and 1:4). All peptide:metal formulations had a final solvent composition of 15 % (*v/v*) EtOH-water (*v/v*). The selected peptides were dissolved to 200µM in 60 % EtOH-water (*v/v*) (organic shock) and sonicated before being added to metal salt solution. All metal salts were dissolved in analytical quality water (Milli-Q water) to the different concentrations required for formulations of different molar ratios. The peptide:metal formulation at a solvent composition of 30 % EtOH-water (*v/v*) was either irradiated (IR) or not irradiated (NonIR) before being double diluted down to the final peptide:metal concentrations and solvent composition of 15 % EtOH-water (*v/v*). All samples were kept in covered or amber vials to minimise light exposure outside of irradiation with green laser. To limit the influence of residual contaminants such as detergents on the formulations, only pyrolysed glassware and ultra-high purity solvents were utilised in the preparation of the formulations. Selected peptide:metal formulations were irradiated between 10 to 30 minutes or until a visual colour change was observed using a green laser at 532 nm to allow photoinduced nanoparticle formation.

4.2.2 *UV-Visible and Fluorescence spectroscopy*

Peptide-metal nanoformulations were prepared as described above (see 4.2.1). To confirm the presence or absence of a surface plasmonic resonance (SPR) bands in formulations was confirmed via UV–visible (UV-Vis) spectrophotometry. A doubling dilution series of the peptide, metal and nanoformulation solutions were prepared in duplicate in 96 well microtiter plates (with a minimum working volume of 200 µL) and analysed via UV–vis spectrophotometry using a Tecan Spark 10M Multi-mode Microplate Reader controlled by the Spark Control™ software (Tecan Group Ltd, Mennedorf, Switzerland) at ambient temperatures across 200 nm to 800 nm with a bandwidth of 3.5 nm. Fluorescence was performed on a Varioskan 3.01.15 instrument, controlled by SkanIT Software 2.4.3 (Thermo-Fischer Scientific, Waltham, MA USA). The excitation wavelength was 280 nm and emission were collected from 295 nm to 450 at 100 ms intervals with wavelength step size of 1 nm and bandwidth of 5 nm. Data collected was analysed with GraphPad Prism® V 6.0.

4.2.3 *Electron Microscopy*

For both scanning transmission electron microscopy (STEM) and transmission electron microscopy (TEM), 2 µL of freshly prepared sample was placed on a 300-mesh carbon coated copper grid and dried under vacuum in a desiccator. All STEM images were recorded under high vacuum mode using high resolution scanning transmission electron microscope dual beam system (Zeiss MERLIN FEG SEM, Zeiss, Oberkochen, Germany) operating at WD of 3.8-3.9 mm and EHT of 20 kV with a 200pA probe and 5 diode STEM detector. STEM microscopy was performed at Electron Microscopy Unit of the Central Analytical Facility (Stellenbosch University, South Africa).

4.2.4 *Culturing of target organisms*

A freezer stock of *S. aureus* RN 4220 and *E. coli* ATCC 13076 were streaked out onto LB agar plates (0.5% *m/v* yeast extract, 1% *m/v* NaCl, 1% m/v tryptone and 1.5% *m/v* agar in water) and incubated at 37°C for minimum 24 h until defined colonies formed. Starter cultures were made by inoculating 3 mL of LB growth medium with 3-5 colonies of the target organism and incubated at 37°C shaking (150 RPM) at an angle overnight. Subcultures (1%) were made from the starter culture into 6 mL of fresh LB media and incubated at 37 °C by shaking at 150 RPM at an angle until the mid- exponential growth phase was reached for each organism. The cell concentration for each organism at the mid-exponential growth phase was determined using classical plate counts. The optical density (OD) was

determined at 600 nm with a path length of 1.0 cm. *S. aureus* (OD = 0.30; ± 1.4 × 10^8 cells/mL and *E. coli* (OD = 0.40; 4 × 10^7 cells/mL).

4.2.5 *Solid surface antimicrobial and synergism assays*

The resazurin solid surface antimicrobial assay was adapted and performed according to van Rensburg *et al.*[26] All peptide-metal nanoformulations were prepared as described above (see 4.2.1). Formulated peptide:metal preparations in a final solvent concentration of 15% EtOH-water in water were transferred directly into 96-well plates followed by an overnight drying step under vacuum. A 10 µL aliquot of subculture for each respective target organism was transferred to each well of the 96-well plates and incubated for an hour at 37°C. Media served as a sterility control while gramicidin S and gentamycin served as a positive inhibition controls against *S. aureus* and *E. coli*, respectively. After incubation 90 µL PBS (phosphate buffer saline) followed by 10 µL resazurin dye (0.30 mg/mL in PBS) was added to each well and incubated covered for 90 min at 37°C. Fluorescence readings were recorded via Tecan Spark 10M Multi-mode Microplate Reader controlled by the Spark Control™ software, (Tecan Group Ltd, Mennedorf, Switzerland) with excitation set at 530 nm and emission at 590 nm. The percentage metabolic inhibition, based on resorufin fluorescence (FS), was calculated as shown in Equation 4.1. Readings were taken at time points selected for optimal resazurin conversion for each target organism as described in van Rensburg *et al*. [26]. All data collected was analysed using GraphPad Prism® V 6.0.

$$\text{Growth Inhibition of Target Organism (\%)} = \frac{\text{FS of sample} - \text{FS of avg blank}}{\text{FS of growth control} - \text{FS aveg blank}} \times 100 \qquad \textbf{Equation 4.1}$$

The combinatorial effect between peptide and silver was assessed via the comparison of IC_{50} values of peptide and silver alone and in combination. The fractional inhibitory concentration index (FICI) was calculated using the Equation 4.2 where C_A and C_B are the IC_{50}s of the peptide and silver alone and C_{AB} and C_{BA} are the IC_{50}'s of the combination of the two agents in the peptide:Ag^+ formulation. A FIC index of ≤ 0.9 was defined as synergism, >0.9 to 1.1 as additive, and > 1.1 as antagonistic [27] Also refer to discussion below for more details.

$$\text{FIC index} = \frac{C_{AB}}{C_A} + \frac{C_{BA}}{C_B} \qquad \textbf{Equation 4.2}$$

4.3 Results and Discussion

In Chapter 3 the interactions between tyrocidines and different metals were reported for an ion mobility mass spectrometry (IM-MS) investigation. Results from the IM-MS analysis indicated that formulations of Trc mix with copper, silver and gold altered the oligomerisation behaviour of the tyrocidines without forming peptide-metal complexes. A loss of monomers and dimers suggested that these species interact with the group 11 metals in a different manner, likely reducing metal ions to form metal nanoparticles. The potential of tyrocidines to aid nanoparticle formation is promising for the synthesis of AMP-MNP nanoformulations and the development of potent antimicrobial agents. In this study the fabrication of nanoparticles using Trc mix and tryptophan-rich C analogues (TpcC and TrcC) with the group 11 metals was optimised and characterised to determine the potential for such formulations as novel antimicrobial agents.

4.3.1 *Bioactivity of Trc mix formulations with selected group 11 metals*

Formulations of Trc mix, TrcC and TpcC with the group 11 metals of different peptide and metal concentrations were tested against *S. aureus* to screen for peptide:metal formulations with promising antimicrobial characteristics. Since irradiation of metal salts in the presence of reducing agents have shown to allow the photo-induced (via PET) and accelerated fabrication of metal nanoparticles, irradiated and non-irradiated formulations were investigated [4,24]. Formulations at different peptide:metal ratios (1:1, 1:2 and 1:4) of 12.5 µM Trc mix (green) with silver (grey), copper (blue) and gold (pink) are shown in Fig. 4.1A. Trc mix alone showed 100% inhibition of *S. aureus* metabolism at 12.5 µM. All peptide-metal formulations, except that of gold, showed 100% inhibition of *S. aureus* irrespective of sample irradiation (Fig. 4.1A). Both irradiated (IR) and nonirradiated formulations with gold (Trc mix:Au^{3+}) exhibited significant losses in activity at a 1:4 peptide:metal ratio compared to copper and silver as indicated on Fig. 4.1A. Considering the increased prevalence of peptide fragments at higher concentrations of gold observed in Chapter 3, the loss of activity at the 1:4 ratio could be due to the disruption of peptide integrity due to the high reactivity of gold [28,29]. Irradiation of gold formulations may accelerate gold neutralisation, nucleation, and subsequent fabrication of gold nanoparticles. Therefore, reducing peptide disruption and maintaining better activity as seen for the irradiated samples of gold, Trc mix:Au^{3+} (IR). Controls of the group 11 metals alone showed poorer activity against *S. aureus* than the peptide:metal formulations, as can be expected due to the high potency of Trc mix against *S. aureus*.

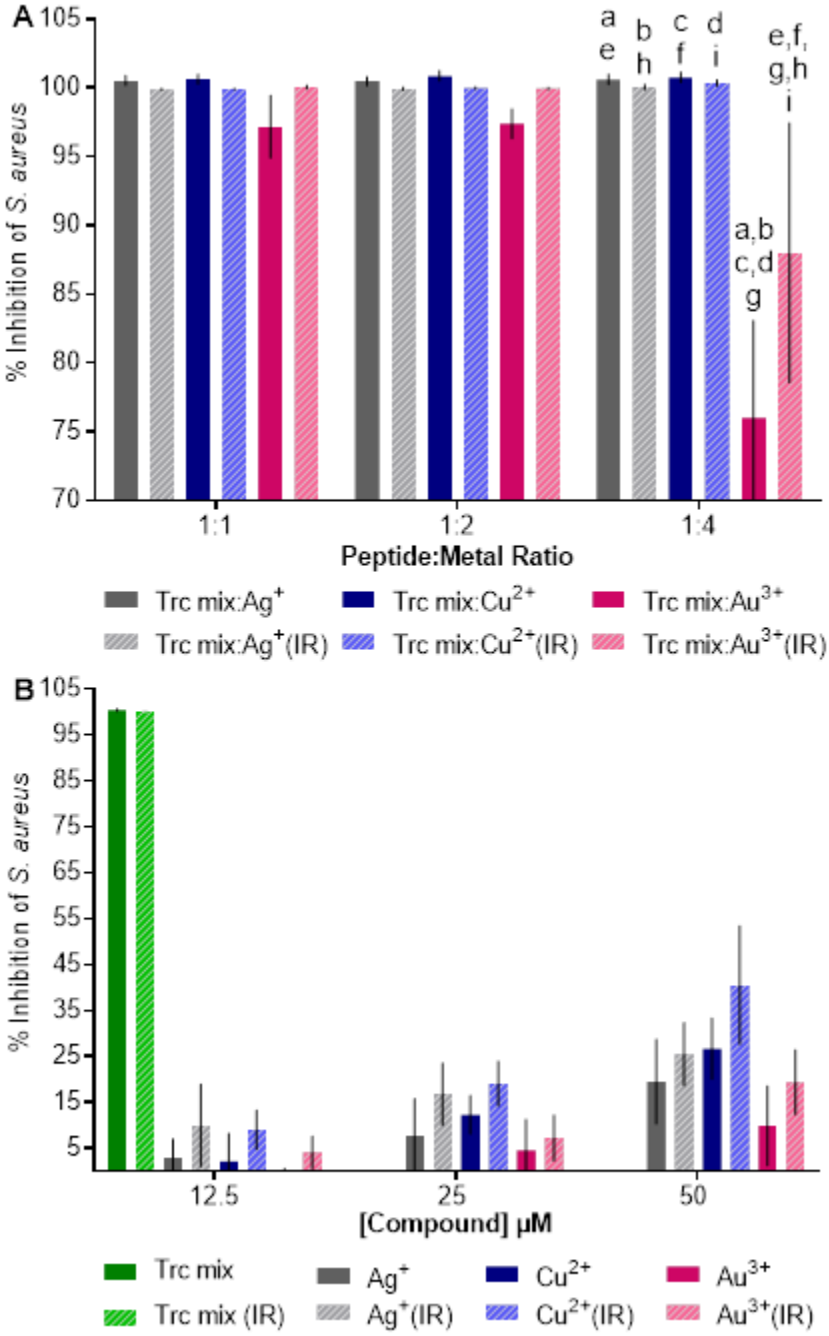

Figure 4.1 Inhibition of *S. aureus* by irradiated (IR) and non-irradiated formulations. In (**A**) the inhibition of formulations of 12.5 µM Trc mix with silver (grey), gold (pink) and copper (blue) salts are shown at different Trc mix: metal ratios of 1:1, 1:2 and 1:4. In (**B**) the inhibition of metal salts at different concentrations and peptide at 12.5 µM are shown. Each bar represents the mean with standard error of the mean (SEM) shown in (**A**) [n=6-8] and (**B**) [n=6-8]. Comparison of mean inhibition for the different peptide:metal formulations was performed via Two-way Anova Bonferroni multiple comparison test and indicated where $P<0.001$ (a, b, c and d), $P<0.01$ (e, f and g) and $P<0.5$ (h and i).

However, the inhibition of *S. aureus* by group 11 metals did show a dose response where increasing metal concentrations resulted in increased *S. aureus* growth inhibition. Copper

[14–17], silver [16,18–20], and gold [20,21] ions and nanoparticles have shown to inhibit *S. aureus* growth. The increased inhibition with increasing metal concentrations can therefore be expected. Although the irradiated metal controls showed seemingly higher activity against *S. aureus* than their non-irradiated counterparts, no significant differences ($P<0.05$) were observed between irradiated and non-irradiated metals or between group 11 metals. This indicated that irradiation of formulations between 10-15 minutes does not adversely influence bioactivity. Although AuNPs have previously shown to be effective against *S. aureus* [20,21], formulations with Trc mix and gold were not considered for further investigations due to loss in bioactivity against *S. aureus* in this study. Copper nanoparticles have also previously reported activity against *S. aureus* [14,17]. Formulations with copper showed promising antimicrobial activity against *S. aureus* as. However, the formation of CuNPs using the Trc mix as a reducing agent was not confirmed in this study (data not shown). To form CuNPs, the divalent copper ions (Cu^{2+}) in the copper chloride solution must be reduced to form metallic Cu. Unfortunately, copper has a low reduction potential and is therefore highly susceptible to oxidation [17,30]. The formation of stable CuNPs with metallic Cu therefore requires both a reduction and capping agent [30]. The oxidative nature of copper, and the stability of CuNPs with peptide as a capping agent, are factors to consider for future nanoparticle formulation with copper and tyrocidines. However, irradiation of Trc mix:Ag^{+} formulations induced nanoparticle formation (see discussion below). Only peptide formulations with silver were therefore investigated for the remainder of this study.

4.3.2 *Optimisation of peptide:Ag^{+} nanoformulations*

To prepare peptide:metal nanoformulations the formation of metal nanoparticles needed to first be confirmed. Optical colour changes of metal salt solutions are useful qualitative indicators of the formation and morphology of metal nanoparticles [31]. The formation of nanoparticles could therefore be confirmed with visible colour changes in the peptide:metal formulations. However, factors influencing the formation and morphology of MNPs, and therefore solution colour, are multi-fold. Such factors include and are likely not limited to the: die-electric environment [24,32], metal salt concentration [31–34], temperature [31,35], irradiation methodology [33,36] and precursors, capping/reducing agents used in MNP synthesis [35,37–39]. To successfully fabricate nanoparticles such factors must therefore be considered when developing peptide:metal nanoformulations. It has been well reported that the extent of MNP formation is highly reliant on and limited to the availability of the metal precursor, the stabilising/capping agent, and the reducing agent. MNP agglomeration will cease once available metal precursor is depleted. Excess metal salt will therefore promote

agglomeration and growth of MNPs. Larger MNPs are insoluble and tend to precipitate out of solution [32,40]. The optimisation of peptide:metal nanoformulations is therefore essential to ensure the solubility, stability, and integrity of the formulant.

The use of tyrosine and tryptophan, as well as peptides rich in these amino acids, have illustrated that these moieties can act both as a reducing and stabilising/capping agent [6,22,23,41]. The hybridisation of peptides and metals also have promising applications in drug delivery systems [24,25]. A study by Gupta *et al.* [24] reported the successful encapsulation of the photoinduced AgNPs by a biotinylated di-tryptophan peptide during the peptide self-assembly process. Moreover, this work highlighted the importance of solvent polarity for controlling the AgNP morphology and synthesis of such peptide-AgNP hybrids. It was reported that an increase in solvent polarity slowed the rate of AgNP synthesis and altered the AgNP morphology. In this study, the tryptophan-containing tyrocidines were investigated as a potential reducing and stabilising agent for the green synthesis of AgNPs in ethanolic solutions. To achieve this, peptide:metal ratios and solvent conditions needed to be optimised. To optimise the nanoparticle fabrication methodology peptide:metal formulations were prepared in a variety of % (*v/v*) EtOH-water environments before being exposed to different irradiation methods (green laser or sunlight) as depicted in Fig. 4.2. For this study, peptide:metal nanoformulations were prepared in a final solvent concentration of 15% (*v/v*) EtOH-water, the solvent condition commonly used for broth-type bioassays [10,13,42–45]. However, the NP synthesis was tested in varying solvent polarity environments including: 15 %, 30 % and 60 % (*v/v*) EtOH-water (Fig. 4.2A). To circumvent the influence of thermo-plasmonic heating on NP synthesis, samples were not irradiated longer than 15 min [35]. Irradiation of Trc mix:Ag^+ (1:4) formulations in both 15% and 30 % EtOH-water resulted in a visible colour change of the sample solution. Contrasting to findings by Gupta *et al.* [24], formulations in 60 % EtOH-water (lower polarity) did not indicate AgNP synthesis (no visible colour change was observed). Irradiation of 50 µM Trc mix:Ag^+(1:4) formulations in 15% EtOH-water via green laser (532 nm) resulted in a pale-yellow/orange colour while irradiation via sunlight yielded a red/brown colour, indicative of likely larger polycrystalline and/or polydispersed AgNPs [32,40]. The yellow colour observed in 30 % formulations is characteristic of silver nanoparticles, particularly smaller nanospheres [31,46,47]. The shape, size and uniformity of MNPs has been closely correlated to their bioactivity, with spherical MNPs showing promising antimicrobial properties [3,48]. The Irradiation via a green laser (532 nm) of formulations in 30% EtOH-water was therefore selected for further investigation (Fig. 4.2B).

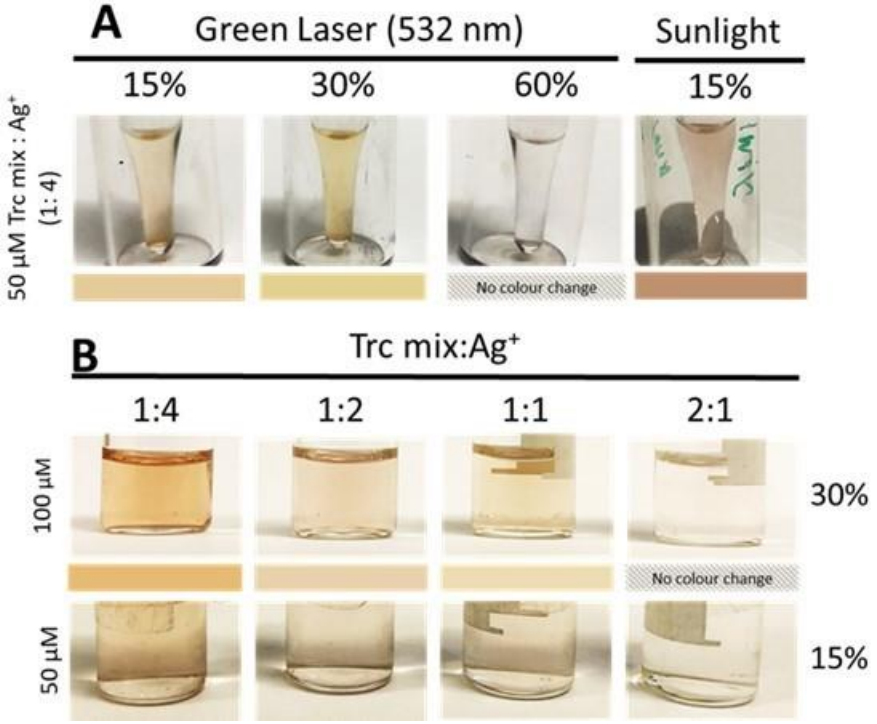

Figure 4.2 Optimisation of Trc mix:Ag^+ nanoformulations in different ethanolic solutions and peptide:metal ratios.(**A**) Visual colour changes in different % ethanol in water (*v/v*) solvent environments (15%, 30%, 60%) after irradiation (15 min) with green laser (532 nm) or sunlight. (**B**) Green laser irradiated Trc mix:Ag+ formulations at different peptide:metal ratios (1:4, 1:2, 1:1 and 2:1) in 15% EtOH-water with 50 µM Trc mix.

Fig. 4.2B shows the formulations that were irradiated at 532 nm. Formulations with different concentrations of silver were tested in formulation with 100 µM Trc mix in peptide:metal ratios equivalent to those analysed via IM-MS in Chapter 3. Irradiation of 1:4 formulations at 30% EtOH-water resulted in a bright orange colour. Irradiation at 1:2 resulted in a pale-yellow/orange colour while irradiation at 1:1 resulted in a pale-yellow colour. Formulations at 2:1 showed no visible colour change. Formulations in 30 % EtOH-water were double diluted down with water to a final solvent concentration of 15 % EtOH-water. Dilution of formulations from 30% to 15% EtOH-water showed no drastic colour changes, with colour profiles of the different ratios of Trc mix:Ag^+ formulations maintained after the dilution. The difference in formulation colour between 1:4 Trc mix:Ag^+ formulations in Fig. 4.2A and B indicate that the starting peptide concentration influences the nanoparticle formation. The orange colour indicates a spectral shift to longer wavelengths (red shift). A study by Thomas *et al.* [49] reported that tyrosine capped AgNPs (Tyr-AgNPs) change the solution colour from yellow to deep orange due to the aggregation of Tyr-AgNPs. Trc mix is rich in the tyrocidines, TrcA, TrcB and TrcC, as reported in Chapter 2. The orange colour seen for the 50 µM Trc mix formulations with silver could therefore indicate the aggregation of silver nanoparticles due to the availability of tyrosine residues. However, as aforementioned, the agglomeration

of AgNPs is limited to both the availability of the precursors and the effectiveness of the stabilising agent. The shift towards brighter orange colour in the formulations with higher $AgNO_3$ concentration (1:4 and 1:2) is therefore more likely due to the increased concentration of the silver precursor resulting in the formation of larger AgNPs [31]. Differences in colour between the 1:4 in 30% in Fig. 4.2A and 1:4 in the 30% in Fig. 4.2B could therefore be due to the extent and speed of AgNP formation due to the starting peptide concentration. Formulations for the remainder of this study were prepared a per Fig. 4.2B as this gave the most reliable formation of AgNPs.

4.3.3 *Spectrophotometric characterisation of peptide:Ag^+ nanoformulations*

The optimised peptide:metal nanoformulations were further characterised using UV-Vis spectrophotometry. The visible light spectra for irradiated 50 µM Trc mix:Ag^+ (Fig .4.3A) and 50 µM TpcC:Ag^+ (Fig. 4.3D) showed a decreased absorbance between 260-295 nm across peptide:metal ratios compared to silver and peptide alone. This absorbance range includes the excitation wavelengths of tryptophan (≈280 nm), tyrosine (≈270 nm) and phenylalanine (≈260 nm) [23,50]. Both Trc mix and TpcC preparations contain tryptophan, phenylalanine and tyrosine. However, TpcC is richer in tryptophan and Trc mix richer in tyrosine. The higher absorbance between 260-295 nm observed for the TpcC formulations can therefore be expected. The second derivative of UV-Vis spectral data provides useful information on the behaviour of organic compounds in mixtures. Resolution of bands where overlap between chromophores may be observed can be improved by plotting the second derivative of the UV–visible spectrum curve [51–53]. The second derivative spectra plotted in Fig. 4.3 (B and E) indicate six absorbance maxima (λ_{max}) namely that of tyrosine (λ_{max} = 268 nm, 270 nm and 273 nm) and tryptophan (λ_{max} = 281 nm, 289 nm and 291 nm) in different environments [51–53] and possibly participating in hydrogen bonds (H-bonds). The presence of tyrosine in the TpcC sample is likely due to contamination with analogous TrcC (<5%) during production and purification (see Chapter 2).

As seen in the UV spectra (Fig. 4.3A), the second derivative spectra also indicate a loss in absorbance of both tryptophan and tyrosine (Fig. 4.3B). This loss is probably due to the change tryptophan's and tyrosine's environments because of a change in conformation and movement into a more polar environment that is created by the interaction with water or metal ions. Alternatively, this decrease in absorption may be the consequence of a loss or aromatic character because oxidation of tryptophan and/or tyrosine residues (chemical modification). The red shift observed in Fig. 4.3B for tyrosine and tryptophan residues indicates that these moieties are likely participating in H-bonds. Interestingly, formulations

with Trc mix did not show a dose dependent changes in absorbance indicating that silver likely interacts with a single tryptophan residue, with saturation at the lowest concentration tested. However, formulations with TpcC showed a dose response indicating the interaction of more than one of the three Trps with silver, with each having different binding/reaction kinetics indicated by the dependence on the silver concentration. Although kinetic studies of the different peptide analogues and silver would provide valuable insight for the optimisation of peptide:metal nanoformulations, such advanced analysis was not conducted in this study. The role of tryptophan in the peptide-silver interactions therefore remains speculative and worthy of future investigation.

Due to the significant impact of the physicochemical properties on the antimicrobial properties of AgNPs, the nanoparticles in nanoformulations needed to be characterised. Although visible colour changes served as a valuable indicator of successful AgNP formation in the Trc mix:Ag^+ formulations, changes in AgNP formation and morphology cannot be reliably detected nor confirmed by colour changes visible to the naked eye. The use of UV-Vis spectroscopy is therefore a useful tool, not only for the characterisation of peptide in formulation, but the confirmation and structural characterisation of metal nanoparticles as well. Changes in metal shape and size influence the surface geometry of the particle and therefore the surface plasmon resonance (SPR). Shifts in the position or shape of plasmon absorption band therefore indicates changes in nanoparticle size and shape. A SPR shift to longer wavelengths (red-shift) is often associated with larger particle size, while fewer SPR peaks with greater nanoparticle uniformity [46,47,54–56]. Peptide:metal formulations were therefore characterised using UV-Vis spectroscopy as shown in Fig. 4.3.

The visible light spectra (Fig. 4.3C) show the formation of an SPR band ($\lambda_{max} \approx 480$) for Trc mix:$Ag^+$ for formulations at ratios 1:1; 1:2 and 1:4 confirming the successful fabrication of AgNPs as suggested by the colour changes observed in Fig. 4.2B. Formulations at 2:1 did not show a defined SPR band in agreement with the lack of colour change observed in Fig. 4.2B. However, formulations of 2:1 did show an increased absorbance between 340-600 nm compared to both peptide and metal alone, this suggests the presence of peptide-metal interactions capable of forming AgNPs. Although the peptide:metal ratio of 2:1 may be below the AgNP formation threshold, it is expected that this formulation with less silver would form less and therefore likely smaller AgNPs.

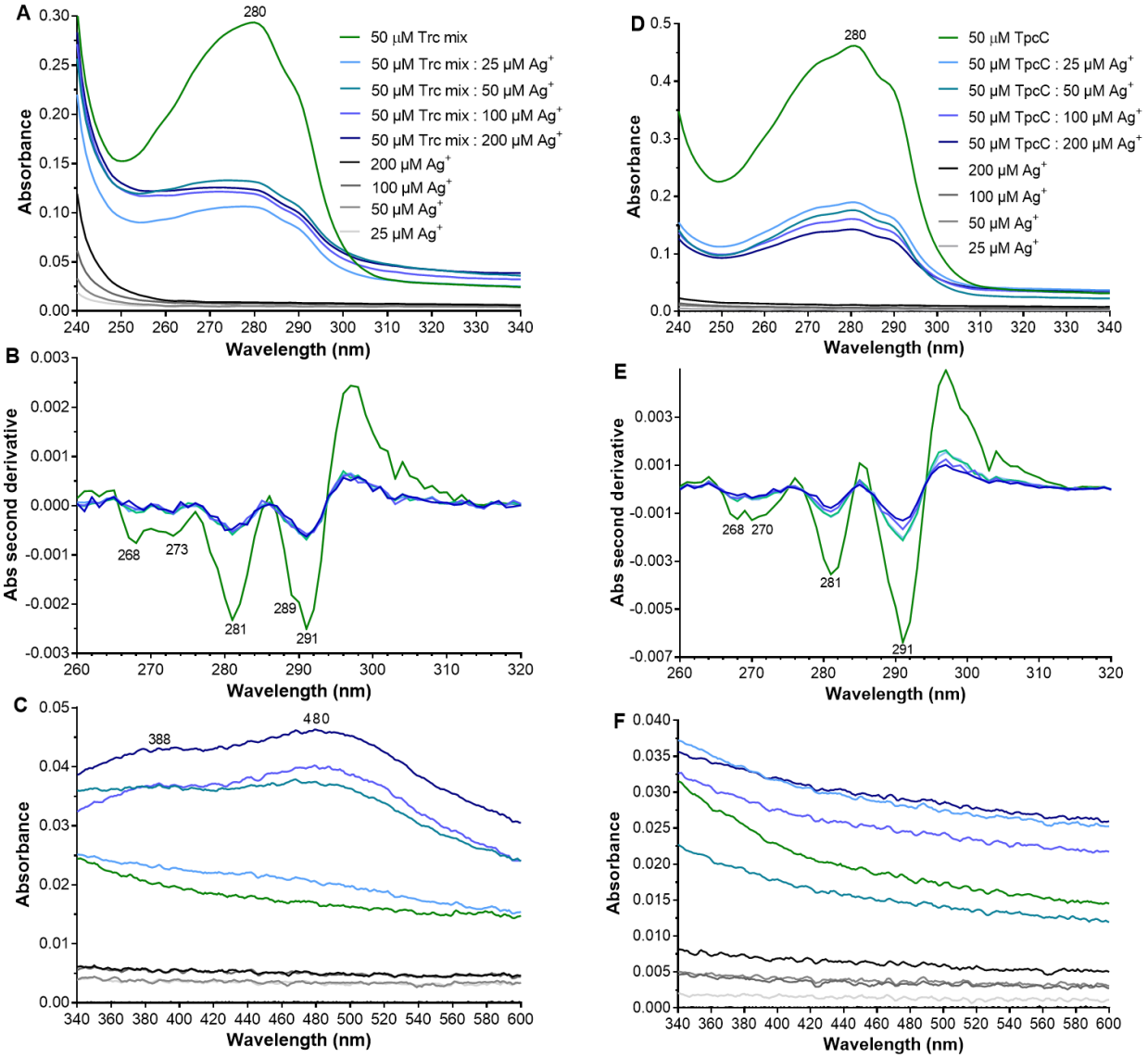

Figure 4.3 Spectrophotometric analyses of irradiated 50 µM peptide formulated with Ag^+ at different peptide:Ag^+ ratios (2:1, 1:1, 1:2 and 1:4). **A** and **D** show the UV spectra for Trc mix and TpcC formulations with silver, respectively. **B** and **E** show the second derivative spectra of A and D to determine the λ_{max} of the peptide separations. **C** and **F** shows the visible spectra of Trc mix and TpcC formulations with silver, respectively, to determine the formation of SPR bands. The spectra in A, B and C represent the average of 4 determinations and those in D, E and F of two determinations.

The lack of a defined SPR band but the slight increase in absorption could therefore be due to some silver nanoparticles that were formed, but too low a AgNP concentration for good detection. Formulations at ratios of 1:4, 1:2 and 1:1 showed the most prominent SPR bands Fig. 4.3C and the clearest colour changes (Fig. 4.2B). However, these formulations also showed the formation of two absorbance maxima (λ_{max} ≈ 388 nm and 480 nm). The presence of two SPR peaks indicated the formation of AgNPs with poly-morphology. This is supported by the range of orange/yellow colours observed in Fig. 4.2B. The increased

absorbance for increasing silver concentrations indicates a higher abundance of AgNPs, while the peak at 480 nm indicates the formation of larger AgNPs as expected. The formation of SPR band in Trc mix:Ag^+ formulations therefore confirmed that Trc mix successfully acted as a reducing agent for the fabrication of silver nanoparticles. Conversely, no defined SPR peaks were detected for TpcC:Ag^+ formulations. However, an increase in absorption between 340-600 nm (Fig. 4.3F) was observed for most peptide:metal nanoformulations alike to 2:1 formulations with Trc mix. The increased absorbance of peptide:metal nanoformulations is therefore still indicative of TpcC-Ag^+ interactions capable of forming AgNPs. However, the lack of defined peaks may signify that the rate of such interactions is slower in formulations with TpcC than those with Trc mix nanoformulations. This result was unexpected as previous studies have reported that tryptophan residues and tryptophan-containing peptides readily form photo-induced nanoparticles [22–25,41,49,57–59]. The dose dependent loss in absorbance between 260-295 nm (Fig. 4.3D) is greater than that of Trc mix formulations, indicating that tryptophan plays an important role in peptide:metal formulations irrespective of the formation of a clear SPR band. This is confirmed by the second derivative spectra of TpcC formulations (Fig. 4.3E) which indicated the dose dependent loss is that of tryptophan absorbance. Further investigations were therefore required to confirm the formation of AgNPs in TpcC formulations.

4.3.4 *Spectrofluorometric characterisation of peptide:Ag^+ nanoformulations*

Spectrofluorometric characterisation provides valuable insight on the peptide-metal interactions favourable for AgNP formation and the fabrication of peptide:metal nanoformulations. Alterations in tryptophan availability were observed by tracking shifts in the intrinsic fluorescence of the aromatic amino acid rich TpcC and Trc mix. Fig. 4.4 illustrates the fluorescence emission of formulations with Trc mix (A) and TpcC (B). Samples were excited at 295 nm to minimise residual fluorescence of aromatic amino acids other than tryptophan. Formulations with both Trc mix (Fig. 4.4 A) and TpcC (Fig. 4.4 B) showed quenching of the peptide fluorescence signal and minor shifts in emission maxima (λ_{em}) with the introduction of metals to the peptide formulation. The emission maxima of 50 µM Trc mix (Fig. 4.4 A) and 50 µM TpcC (Fig. 4.4 B) in 15% EtOH-water was found to be around 338 nm, while formulations with silver showed a λ_{em} around 340 nm for both peptides.

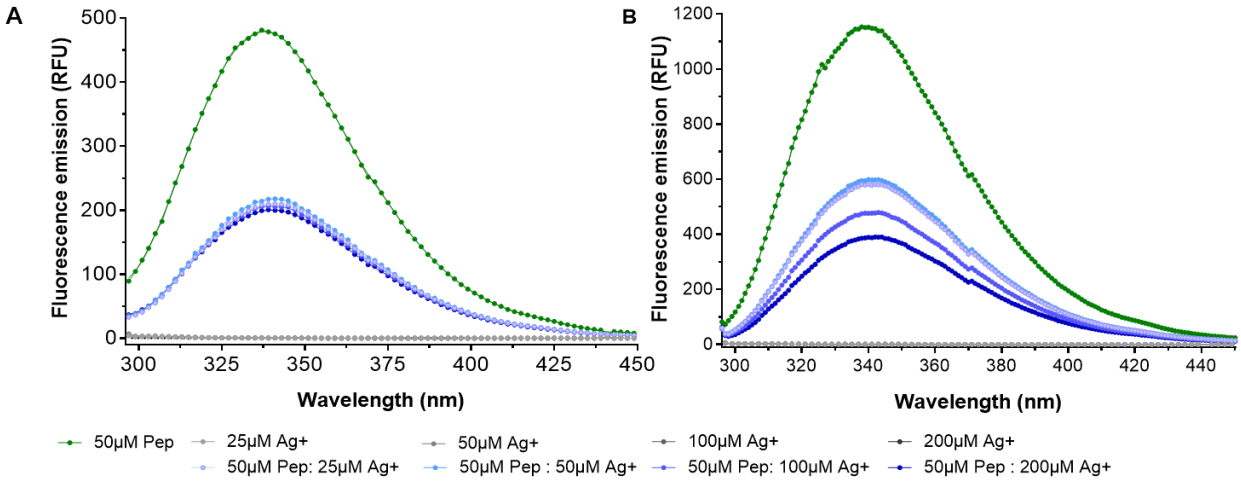

Figure 4.4 Fluorescence emission spectra (excitation at 295 nm) of irradiated 50 µM peptide (Pep) formulated in 15% EtOH-water with Ag^+ at different peptide:Ag^+ ratios (2:1, 1:1, 1:2 and 1:4) with **A** showing the spectra of Trc mix and **B** those of TpcC. Spectra data are the average of four determinations.

The fluorescence of tryptophan is closely linked to its solvent environment and local environment [23,50,60]. Trc mix formulations (Fig. 4.4 A) with silver at 2:1, 1:1, 1:2 and 1:4 resulted in a λ_{em} at 341, 341, 339 and 339 nm, respectively. The blue shift in λ_{em} of formulations with higher silver concentrations (1:2 and 1:4) compared to formulations at lower silver concentrations (2:1 and 1:1) indicates a shift of tryptophan residues towards a more hydrophobic environment [23,50,60]. TpcC formulations (Fig. 4.4 B) with silver at 2:1, 1:1, 1:2 and 1:4 resulted in a λ_{em} at 340.0, 340, 343 and 344 nm, respectively. This indicated that at the lower sliver ratios the environment of the Trp residues is not greatly influenced. However, in contrast to formulations with Trc mix, the red shift at the higher silver ratio indicated the presence of polar interactions with the Trp residue likely due to the exposure of the tryptophan-containing peptides to polar moieties such as water, metal ions and counter-ions. The Trp residues may therefore shift towards a hydrophilic environment to interact with the more polar silver ions [23,50,60]. The red and blue shifts for formulation with Trc mix and TpcC at higher silver concentrations suggests that the behaviour of the peptide is dictated by the peptide:metal ratio and that the formation of AgNPs may exhibit a threshold ratio, likely that above 1:1 (if spectrophotometric analysis is also considered).

Even though slight shifts were observed between formulations of different ratios, an overall red-shift was observed across peptide:metal formulations compared to peptide alone. This indicates the presence of polar interactions with both tryptophan-containing peptides. It important to note that the presence of water has been shown to promote the assembly of non-amphipathic and hydrophobic structures towards the hydrophobic core of the peptide

oligomers [61,62]. Moreover, such self-assembly of the Trcs report quenching of fluorescence intensity when compared to peptide in more nonpolar solvent systems [61]. The increased polarity could therefore promote the self-assembly of the peptides. However, both peptide and peptide:Ag^+ nanoformulations were all dissolved in 15% EtOH-water. Therefore, the influence of water on peptide assembly need not be accounted for when comparing the quenching of unformulated peptide to the peptide formulated and irradiated in silver salt solution. Nonetheless, the increased polarity due to free metal salt ions could potentially promote peptide-assembly leading to fluorescence quenching.

The loss of fluorescence observed could therefore be attributed to the self-assembly of peptide due to the interactions of peptide with the more polar metal salt environment and not the metal ion itself. However, the formation of SPR bands for Trc mix:Ag^+ and increased absorbance between 340-600 nm for TpcC:Ag^+ formulations suggest that interactions between peptide and metal are indeed present. Interestingly, TpcC formulations with silver showed a clear dose dependent quenching of fluorescence intensity, with a further decrease in fluorescence for formulations above a 1:1 ratio. This quenching correlates with the dose dependent shifts in λ_{em}, as well as the dose dependent loss in aromatic amino acid (tryptophan) absorbance at 280-290 nm (refer to Fig. 4.3 D and E). Again, suggesting that a 1:1 ratio may be a critical peptide:metal ratio for AgNP formation. Although Trc mix seemingly showed a similar trend, all four formulations had nearly similar fluorescence intensities, indicating that the introduction of silver to the formulation had a greater influence on the peptide than the specific concentration of silver itself. This could explain the increased readiness of Trc mix:Ag^+ formulations to form nanoparticles when compared to TpcC:Ag^+ as shown in Fig. 4.3. It should however be noted that the potentially slower rate of AgNP formation in TpcC:Ag^+ formulations could be due to a multitude of factors and is not necessarily an indication of poorer AgNP synthesis. Further characterisation of TpcC:Ag^+ nanoformulations are discussed in more detail later in this chapter.

The fluorescence quenching and shifts in λ_{em} observed in the spectrofluorometric analysis of both peptide:metal formulations indicated the association and/or incorporation of the peptides with/in AgNP structures. Particularly due to interactions between tryptophan residues and silver. Moreover, the overall fluorescence quenching for both peptides in formulation with silver is prominent and further supported by the loss in aromatic amino acid absorbance at 280 nm as shown in the UV spectra in Fig. 4.3 (A and D) where tryptophan is responsible for the greatest absorbance. The loss in absorbance at 280 nm, presence of SPR bands (340-600 nm) and fluorescence quenching (300-450 nm) therefore agrees with

the proposed critical role of the aromatic amino acids, particularly tryptophan, in these peptides for the reduction of silver ions to form AgNPs.

4.3.5 Electron microscopy of peptide:Ag^+ nanoformulations

Due to the multifactorial influences on AgNP formation, irradiated samples were only considered peptide:AgNP nanoformulations once the presence of a surface plasmonic resonance (SPR) band via UV–visible spectrophotometry is confirmed, or silver nanoparticles were detected via electron microscopy. Unlike Trc mix formulations, formulations with TpcC did not report well-defined SPR bands. However, as aforementioned, spectrophotometric and spectrofluorimetric analysis in TpcC formulations with metal were still observed. Irradiated TpcC:Ag^+ formulations were therefore analysed using STEM to detect and record AgNP formation. STEM analysis of 50 µM TpcC unformulated and formulated with silver in 15% EtOH-water not only confirmed the formation of spherical nanoparticles after 15 minutes of irradiation at 532 nm but also highlighted changes in peptide morphology (Fig. 4.5).

Recent findings by Kumar *et al.* [61] reported that TpcC self-assembles to form defined peptide nano-assemblies similar the peptide structures observed in this study (Fig. 4.5A). STEM sample preparations of peptide-silver formulations where not stained for organic materials, the darkened spheres seen in Fig. 4.5 (B and C) are therefore that of inorganic material, in this case spherical AgNPs. Interestingly, in 50 µM TpcC:Ag^+ nanoformulations seemingly encapsulate spherical AgNP as suggested by the aforementioned spectrophotometric and spectrofluorometric analysis (Figs.4.3 and 4.4). The TpcC-AgNP structures observed via STEM indicates that the peptide may associate with, and subsequently oligomerise around smaller (<100 nm) AgNPs (Fig. 4.5B). In this they form a peptide-AgNP seeding structure, which with continued peptide self-assembly, form larger peptide structures with AgNPs incorporated in them (Fig. 4.5C). The encapsulation of AgNPs by TpcC is promising for antimicrobial application where the peptide can act as a carrier and/or controlled release of AgNPs. Unfortunately, due time limitations on the electron microscope, only formulations with 50 µM TpcC in 15% EtOH-water were imaged.

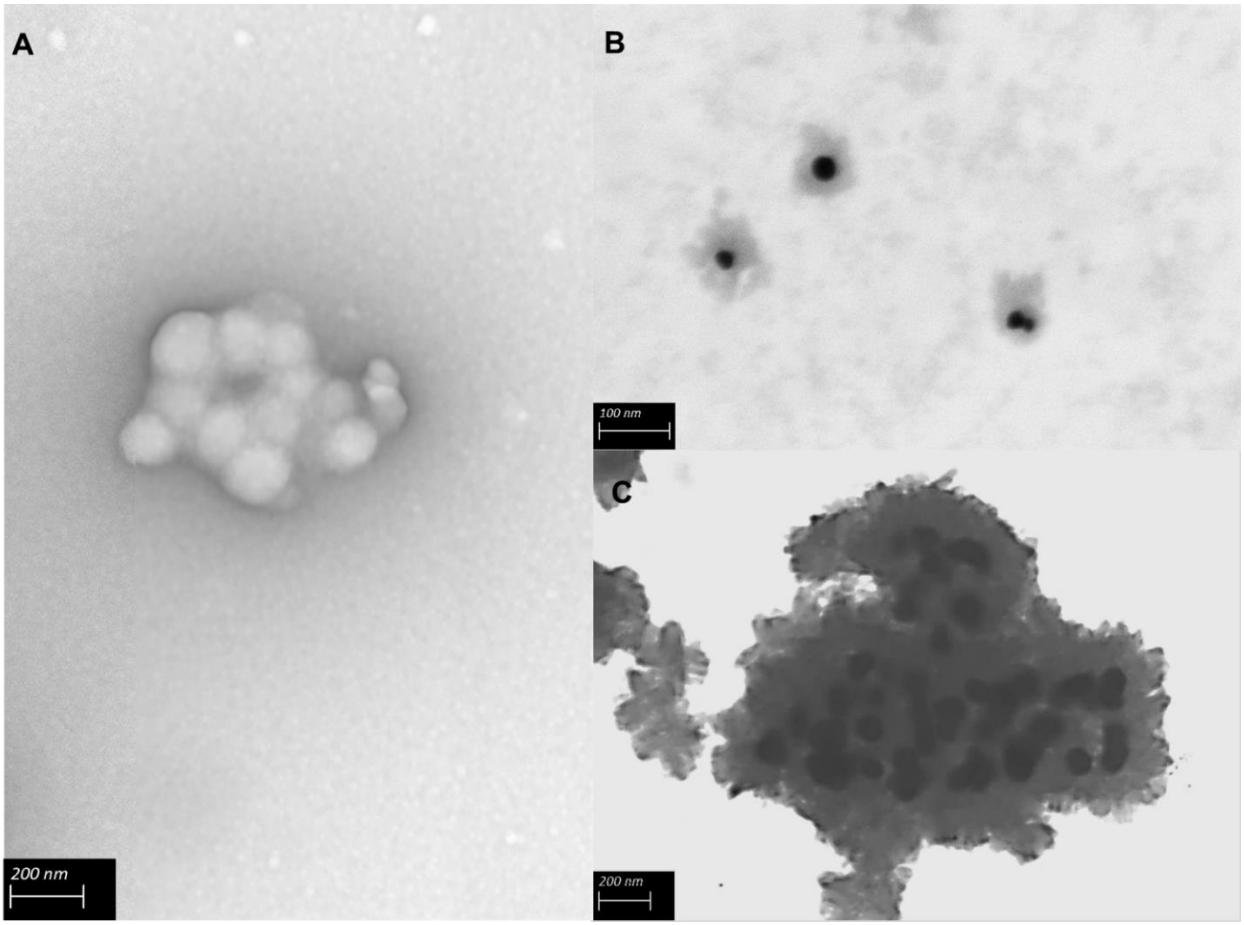

Figure 4.5 STEM images of 50 µM TpcC unformulated (**A**) and formulated (1:3) with silver (**B** and **C**) 15% EtOH-water Images were recorded using Zeiss MERLIN SEM operated at 20.00kV, image contrast was adjusted to show darker metal nanoparticles.

The tyrocidines and tyrocidine analogues have shown activity against a variety of pathogens [43,45,63–65] including Gram-positive and Gram-negative bacteria [10–13,42]. Although tyrocidine mixtures have shown to have higher potency against microbial pathogens compared to its single tyrocidine analogues [10,11,42,45,64], both pure analogues and tyrocidine mix have, to our knowledge, no MIC's reported below 100 µM against *E. coli* [10–13]. A study by Marques *et al.* [13] reported that TrcA (M_r = 1269.65) analogues are active against drug resistant *S. aureus strains* (ATCC 33592 and ATCC 29213) at an MIC of 32 µg/mL (≈25 µM) for the most active analogues and >128 µg/mL (>100 µM) against *E.coli* (ATCC 29212) for the rest of the analogues. While, another study by Spathelf *et al.* [10] reported no more than 50% inhibition of *E. coli* growth by <200 µg/mL of both Trc mix and pure tyrocidine analogues, while the more polar B/B_1 and C/C_1 analogues had higher activity against the Gram positive bacterium *Micrococcus luteus* than the more hydrophobic A/A_1 analogues. Both these studies, however, indicated that the tyrocidine analogues, although effective against Gram-positive *S. aureus*, have poor activity against Gram-negative *E. coli*.

Marques *et al.* [13] indicated that modifications and/or substitution of amino-acid residues and the position of such residues in the ring structure of TrcA strongly influences the peptides antimicrobial activity. Interestingly, a study by Wenzel *et al*. [12] further confirmed that the tyrocidine C analogue TrcC (cyclo-[fPWwNQYVOL]) was more active against another Gram positive bacterium *S. aureus* than the A analogue (cyclo-[fPFfNQYVOL]) TrcA. It was proposed that the presence of the bulky tryptophan residues at the variable aromatic dipeptide unit could be associated with the higher pore-forming capacity and therefore bioactivity of TrcC [12]. Studies by Rautenbach *et al.* [62] reported that the intrinsic self-assembly of tryptophan-rich TpcC displayed oligomerisation behaviour similar to that found for TrcC found by Munyuki *et al.* [66], while Kumar *et al.* [61] noted that such structures drive the peptide oligomerisation behaviour into peptide larger nano-assemblies. However, the antimicrobial activity observed by Kumar *et al.* [61] for TpcC against *S. aureus* was shown to be likely related to the release of active dimer moieties from larger TpcC nano-assemblies. Silver is well known for its antimicrobial properties. Ag^+ and AgNPs have shown antimicrobial activity against variety of organisms including both *S. aureus* and *E. coli* [18–20].

The formation of the AgNP encapsulated TpcC nano-assemblies observed in Fig. 4.5 therefore suggests that such structures could not only release smaller active moieties of TpcC but also AgNPs. Thereby improving the antimicrobial potency of the tyrocidines against *E. coli.* To characterise their antimicrobial activity, peptide:metal nanoformulations were tested against both Gram-positive *S. aureus* and Gram-negative *E. coli*. Solid surface assays showed activity against *S. aureus* (Fig. 4.6) and *E. coli* (Fig. 4.7) for peptide:Ag^+ formulations with TpcC (A and B), TrcC. (C and D) and Trc mix (E and F). Each peptide was formulated with silver at peptide:metal ratios of 1:1,1:2, 1:3 and 1:4. All formulations, except the 1:1 ratio, showed a maintenance or a slight improvement in bioactivity against *S. aureus* compared to peptide and silver alone. A general increase in bioactivity against *E. coli* for peptide:Ag^+ nanoformulations with TpcC, TrcC and Trc mix was also observed. All three peptide preparations therefore showed either a maintained or increased potency against both *S. aureus* and *E. coli* when formulated with silver. The poorer bioactivity observed for formulations at a 1:1 ratio indicates that a critical peptide:metal ratio (>1:1) is responsible for the shift bioactivity of the nanoformulation. This is further supported by the spectrophotometric and spectrofluorometric analysis discussed earlier, where changes in absorbance and fluorescence of formulations occurred above the 1:1 ratio, indicating that this is a critical peptide:metal ratio for AgNP formation. Interestingly, TpcC alone demonstrated inhibition against *E. coli*, while TrcC and the Trc mix both remained relatively

ineffective against *E. coli*. This indicates that the introduction of a tryptophan at position 9 could be responsible for the shift in bioactivity of the tyrocidine.

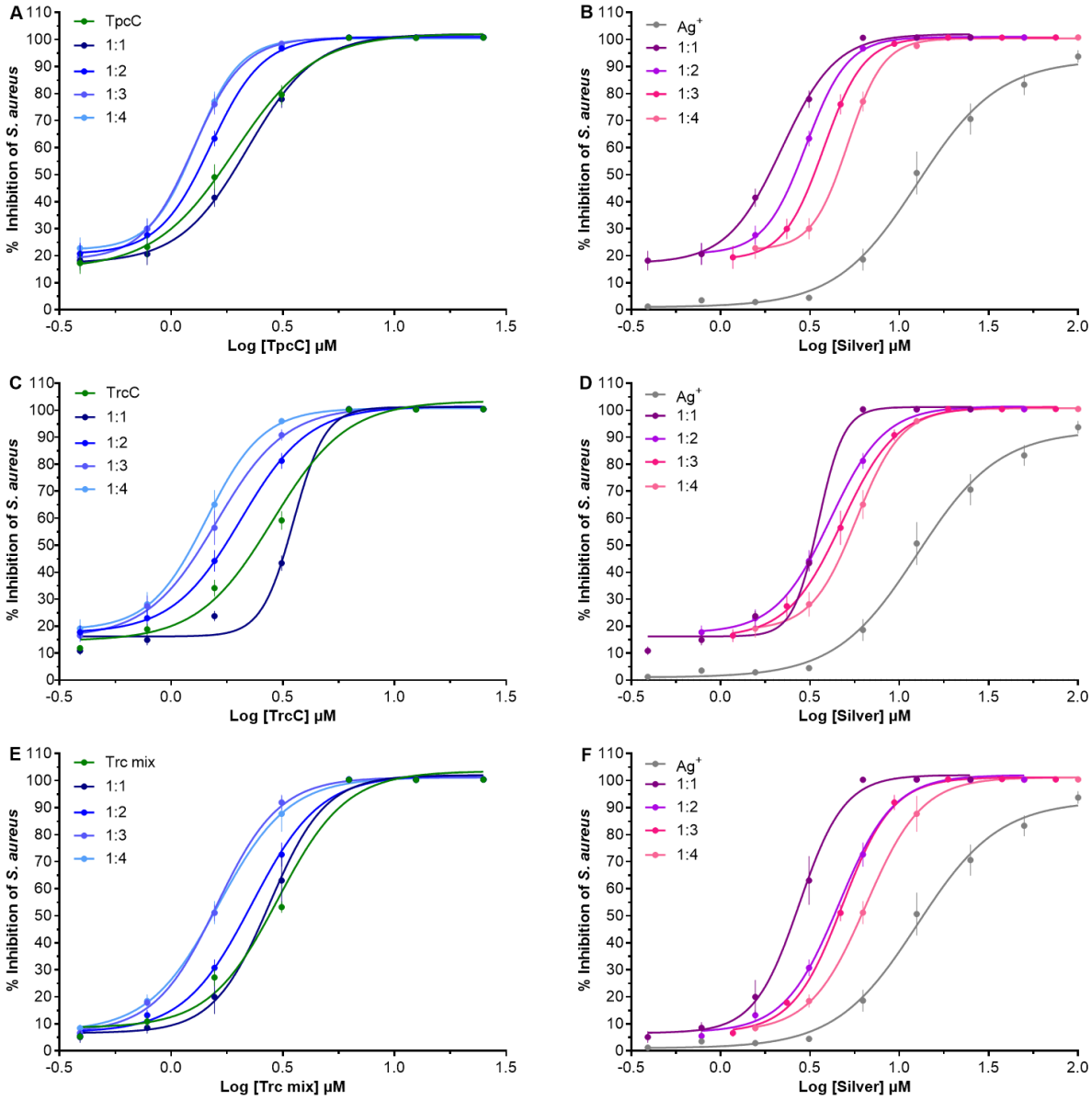

Figure 4.6 Representative dose responses against *S. aureus* for irradiated peptide:metal nanoformulations (1:1, 1:2, 1:3 and 1:4) for TpcC (**A** and **B**), TrcC (**C** and **D**) and Trc mix (**E** and **F**) with silver. Percentage *S. aureus* growth Inhibition (%) of formulations are plotted against the contributions of peptide concentration (A,C and E) and silver concentration (B,D and F) in each formulation. Each data point represents the average of duplicate results for two biological repeats with two technical repeats (8 determinations) with SEM indicated by error bars.

These results agree with the suggested role of tryptophan in pore formation and antimicrobial activity in findings by Marques *et al.*[13] and Wenzel *et al.*[12]. Although TpcC displayed activity against *E. coli*, it only showed about 85% inhibition at 25 µM indicating a minimum inhibitory concentration about this concentration. All three peptide preparation

therefore did not show 100% inhibition of Gram-negative *E. coli* and the minimum inhibitory concentrations of Trc mix, TpcC and TrcC must therefore be above 25 µM as found by other studies [10–13].

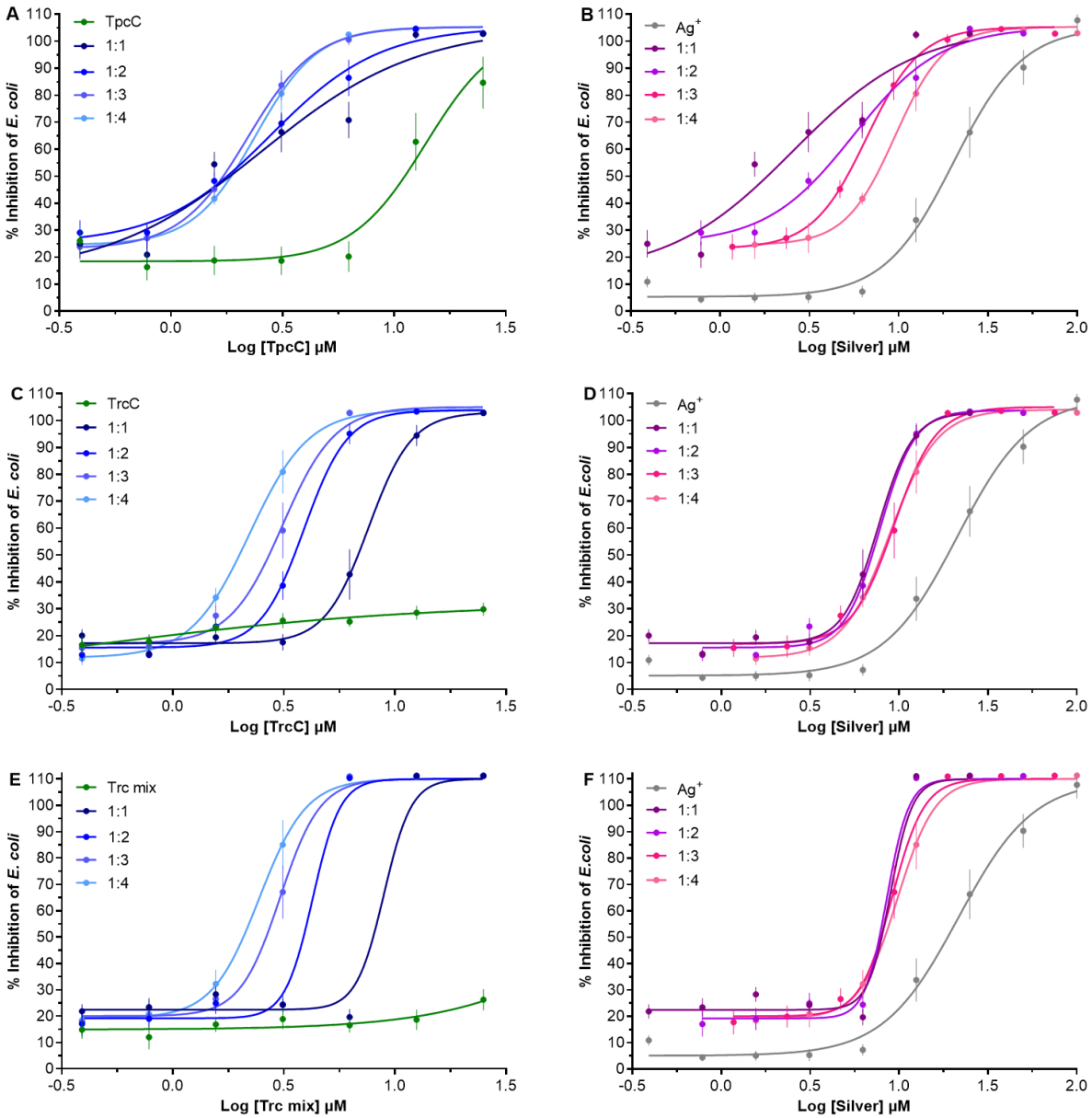

Figure 4.7 Representative dose responses against *E. coli* for irradiated peptide:metal nanoformulations (1:1, 1:2, 1:3 and 1:4) for TpcC (**A** and **B**), TrcC (**C** and **D**) and Trc mix (**E** and **F**) with silver. Percentage Inhibition of formulations are plotted against contributions of peptide concentration (**A**,**C** and **E**) and silver concentration (**B**, **D** and **F**). Each data point represents the average of duplicate results for two biological repeats with two technical repeats (8 determinations) with SEM indicated by error bars.

A summary of IC_{50}'s for the above assays (Figs 4.6 and 4.7) are recorded in Table 4.1. Formulations with TpcC showed the lowest IC_{50}'s against both target organisms. Against *S. aureus* IC_{50}'s below that of peptide alone (1.94 µM) was recorded for the TpcC:Ag^+

nanoformulations at ratio of 1:2 (IC_{50}=1.50 µM), 1:3 (IC_{50}=1.27 µM) and 1:4 (IC_{50}=1.29 µM). Nanoformulations with TrcC also recorded an IC_{50} below that of peptide alone (2.82 µM) at ratios of 1:2 (IC_{50}=2.04 µM), 1:3 (IC_{50}=1.57 µM) and 1:4 (IC_{50}=1.42 µM). While all formulations with Trc mix showed a lower IC_{50} than of Trc mix alone (IC_{50}=3.01 µM). It can be noted that the purified analogues showed lower IC_{50}'s than Trc mix, and that TpcC was had a lower IC_{50} than TrcC. The increased activity against *S. aureus* of peptides alone is therefore TpcC>TrcC>Trc mix. This is contrary to previous studies which have shown Trc mix to be more effective than single peptide analogues against another Gram-positive bacterium, *Listeria monocytogenes* [10,42]. Spathelf *et al.* [10] showed that Trc mix peptide mixture is more active against *L. monocytogenes* than its isolated TrcA, TrcB and TrcC analogues. While Leussa *et al.* [42] indicated that the three predominant analogues in Trc mix (TrcA, TrcB and TrcC) are more effective against *L. monocytogenes* than TpcC. Both studies, however, indicated that the differences in activity of the peptide mixture and single analogues is likely due to differences in the hydrophobicity and oligomeric structure of the peptides and therefore its ability to interact with the cell wall structure of the target organism [12]. The difference in activities against *S. aureus* could therefore be attributed to the polar solvent environment (15% EtOH-water) and/or peptide concentration range (0.40 µM–25 µM) and the influence of such factors on peptide oligomerisation and therefore activity [11,61,62,67–69]. The spectrophotometric analysis in this study also showed that Trc mix successfully acted as a reducing agent for the formation of AgNPs, the interaction of tyrocidines in Trc mix peptide mixture with silver would likely have resulted in the modification of some of the Trp containing peptides including TrcA, TrcC and TrcB. Some loss of activity that is not remediated by the presence of AgNPs can therefore be expected.

Only TpcC displayed activity against *E. coli* (IC_{50} = 13.57 µM). IC_{50}'s recorded by BIOPEP peptide group [unpublished data] and other studies [10–13] were used to determine putative combinational shifts. An IC_{50} below that of peptide (100 µM) for silver alone (19.43 µM) was recorded for the peptide:silver nanoformulations with all three peptides at all four ratios suggesting a significant combinational effect. TpcC overall showed the lowest IC_{50}'s compared to TrcC and Trc mix at all four ratios whilst TrcC and Trc mix displayed similar IC_{50}'s. This reinforces that the introduction of a tryptophan at position 9 could be responsible for the shift bioactivity of the tyrocidines. It is worth noting that the IC_{50} for silver is that of Ag^+ and not AgNPs. This is because Ag^+ requires a reducing agent to form nanoparticles. Future work could consider isolated AgNPs to determine the inhibitory effects of AgNPs alone.

Table 4.1 Summary of combinational shifts in IC_{50}'s, given in µM, against *S. aureus* and *E. coli* for irradiated peptide:silver formulations (1:1, 1:2, 1:3 and 1:4) of TpcC, TrcC and Trc mix. Putative IC_{50}'s selected for peptides against *E. coli* are indicated with an Asterix (*). Data is the average of duplicate results for two biological repeats with two technical repeats (8 determinations) with SE indicated in brackets below.

		S. aureus			*E. coli*		
Parameter	**Ratio**	**Trc mix**	**TrcC**	**TpcC**	**Trc mix**	**TrcC**	**TpcC**
IC_{50} (µM)	Ag^+:	14.27	14.27	14.27	19.43	19.43	19.43
	Peptide	3.01	2.82	1.94	*100	*100	13.57
IC_{50} (µM) [peptide]	1:1	2.83 (0.4)	3.53 (0.1)	2.20 (0.2)	8.86 (0.3)	8.07 (1.2)	3.59 (1.7)
	1:2	2.35 (0.2)	2.04 (0.2)	1.50 (0.1)	4.26 (0.1)	3.92 (0.3)	3.19 (1.0)
	1:3	1.62 (0.1)	1.57 (0.3)	1.27 (0.1)	2.97 (0.4)	3.09 (0.5)	2.32 (0.4)
	1:4	1.82 (0.3)	1.42 (0.2)	1.29 (0.1)	2.46 (0.3)	2.35 (0.4)	2.52 (0.4)
IC_{50} (µM) [silver]	1:1	2.83 (0.4)	3.53 (0.1)	2.20 (0.2)	13.29 (0.4)	8.07 (1.2)	3.64 (1.7)
	1:2	4.70 (0.4)	4.10 (0.3)	3.00 (0.1)	12.77 (0.2)	7.83 (0.6)	6.47 (1.9)
	1:3	4.85 (0.2)	4.69 (0.7)	3.79 (0.3)	11.87 (1.4)	9.26 (1.4)	7.03 (1.1)
	1:4	7.26 (1.2)	5.68 (0.6)	5.14 (0.3)	14.73 (1.4)	9.37 (1.3)	10.17 (1.6)

To investigate the combinational effects of peptide in formulation with silver the fractional inhibitory concentration indexes (FIC indexes) were calculated as per Equation 4.2 for the different peptide:Ag^+ nanoformulations are summarised in Table 4.2. Formulations mostly showed an additive or weak antagonistic effect against *S. aureus*. Antagonism (FICI>1) was observed for TrcC at a 1:1 ratio (FICI = 1.51), while additivity (≤1) was observed for formulation at a 1:3 ratio for all three peptides; Trc mix (FICI = 0.88) TrcC (FICI = 0.89) and TpcC (FICI = 0.93). The strong synergism observed for Trc mix and TrcC against *E. coli* can be expected due to the high putative IC_{50}'s. Interestingly, 1:1 TpcC:Ag^+ ratio had the lowest FIC index (0.39) followed by 1:3 (0.55) displaying synergism between peptide and silver. Although synergism was maintained for all four ratios of TpcC:Ag^+ nanoformulations, increasing silver concentrations lead to higher FICI's therefore a loss in synergy. This behaviour although similar, differs slightly to that Trc mix and TrcC. Formulations at 1:3 and 1:2 showed the strongest synergy for Trc mix and TrcC, respectively. Thereafter

formulations with a higher concentrations of silver showed a loss in activity for both peptides. This indicates that each peptide has may have a different pivotal peptide:metal ratio of synergy.

Table 4.2 FICs and FIC indexes of irradiated peptide:metal formulations (1:1, 1:2, 1:3 and 1:4) of TpcC, TrcC and Trc mix with silver against *S. aureus* and *E. coli*. Antagonism, additivity, and synergism is indicated as per key below.

		S. aureus			*E. coli*		
Parameter	**Peptide:metal**	**Trc mix**	**TrcC**	**TpcC**	**Trc mix**	**TrcC**	**TpcC**
FIC [peptide]	1:1	0.92	1.24	1.14	0.09	0.08	0.19
	1:2	0.77	0.72	0.78	0.04	0.04	0.20
	1:3	0.53	0.56	0.65	0.03	0.03	0.16
	1:4	0.54	0.51	0.67	0.02	0.02	0.18
FIC [silver]	1:1	0.21	0.26	0.16	0.75	0.64	0.21
	1:2	0.35	0.31	0.23	0.72	0.66	0.45
	1:3	0.36	0.36	0.28	0.77	0.79	0.54
	1:4	0.48	0.43	0.39	0.83	0.75	0.78
FIC index	1:1	1.15	1.51	1.30	0.78	0.51	0.46
	1:2	1.12	1.02	1.00	0.71	0.45	0.58
	1:3	0.88	0.89	0.93	0.65	0.52	0.55
	1:4	1.12	0.91	1.04	0.79	0.52	0.72

Key

Antagonism	Weak antagonism	Additive	Weak synergism	Synergism	Strong synergism

The respective isobolograms are illustrated in Fig. 4.8. Here the synergy between peptide and silver concentration is clearly illustrated with anything on the dotted blue line as additivity and within the grey window as weak additivity, anything above as antagonism and anything below as synergism. Nanoformulations of all three peptides with silver showed synergy against *E. coli* and mostly additivity against *S. aureus*. With different peptide:metal ratios showing different combinational effects. Overall formulations of peptide with AgNPs at a peptide:Ag^{+} ratio above 1:3 showed improved activity against *S. aureus* and introduced novel potent antimicrobial activity against *E. coli*. The poor activity of the tyrocidines against *E. coli* was therefore successfully improved with the introduction of antimicrobial AgNPs.

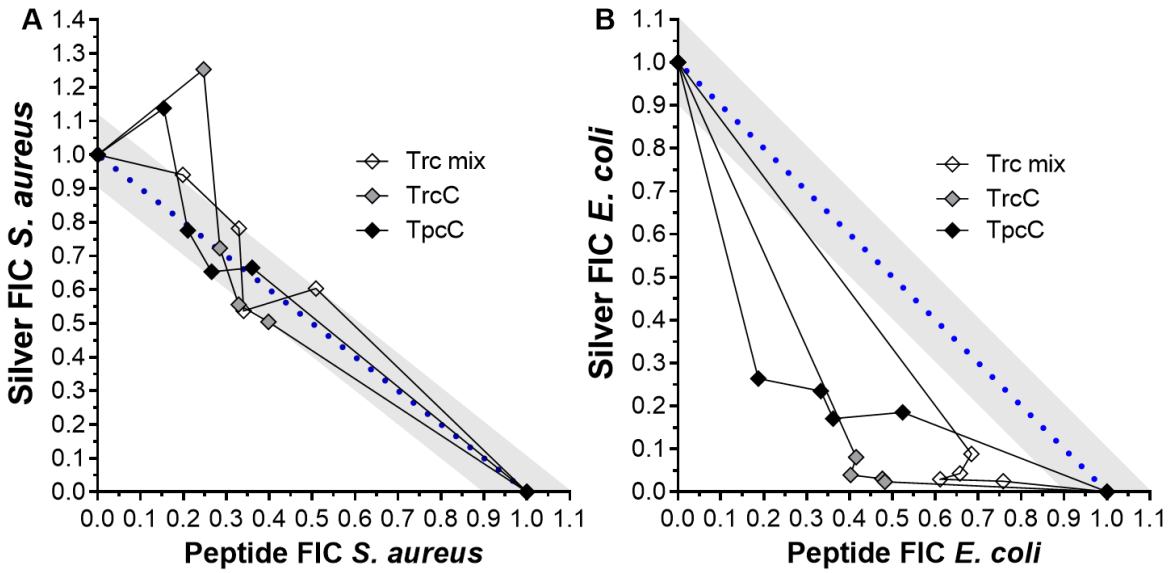

Figure 4.8 Isobolograms showing the comparison of FICs of peptide versus silver for irradiated peptide:metal formulations (1:1, 1:2, 1:3 and 1:4) against *S aureus* (A) and *E. coli* (B). The FICs (for peptide (Trc mix, TrcC and TpcC) and silver were calculated as per Equation 4.2. The diagonal dotted line represents the cut-of FIC index value of additivity with the grey shaded area in each graph showing the additive limits of the FIC index =1±0.1. Data points above this area indicates antagonism and below synergism.

4.4 Conclusion

This study aimed to successfully fabricate CDP-MNP hybrids with heightened antimicrobial activity. Formulations of single tyrocidines analogues (TrcC and TpcC) and a peptide mixture (Trc mix) with copper, silver and gold were screened against *S. aureus* for promising antimicrobial properties. Although copper and gold nanoparticles are known for their antimicrobial action [14–21], formulations with silver showed the greatest promise for the formation of potent CDP-MNP hybrids. Optimisation of peptide:metal nanoformulations indicated a strong influence of silver precursor concentration, peptide concentration and solvent environment on the formation of AgNPs as indicated by colour changes in the formulation solution. This is likely due the peptide oligomerisation behaviour [26,61,67] and nature of AgNP formation [24,31,32,47,54]. The influence of silver concentration on AgNP formation was further confirmed by spectrophotometric and spectrofluorometric analysis of 50 µM Trc mix and TpcC in peptide:Ag^+ formulations with a solvent environment of 15% EtOH-water. Alterations in the interactions of both Trc mix and TpcC with the formulation environment were observed, with TpcC indicating a dose dependent change. It was therefore concluded that the formation of AgNPs is highly influenced by the peptide:metal ratios as expected [6,22,25,54]. Moreover, changes in tryptophan absorbance (260-295 nm)

and fluorescence (340-600 nm) indicated an affinity of silver for tryptophan containing peptides in agreement with previous studies [6,22,41]. This indicates the Trp-rich peptides may act as both a reducing agent and stabilising agent for AgNP formation. The formation of silver nanoparticles due to peptide-metal interactions was confirmed by the presence of an SPR band in UV-Vis spectrophotometry and inorganic nanoparticles in electron microscopy. Formulations of Trc mix, TpcC and TrcC were shown to successfully induced the green synthesis and encapsulation of spherical silver nanoparticles.

The combinational effect of the robust tyrocidines with the antimicrobial silver nanoparticles as CDP-MNP hybrids showed great promise for antimicrobial applications. Although the antimicrobial activity of the tyrocidines has been extensively investigated against a plethora of microbes including drug resistant pathogens [10,11,42,45,64]. Previously investigated tyrocidines and analogues have shown poor activity against Gram-negative *E. coli* [10–13]. Solid surface antimicrobial assays against two target organisms, Gram-positive *S. aureus* and Gram-negative *E. coli*, were performed to test the viability of the CDP-MNP hybrids fabricated in this study as formulations for applications in antimicrobial surfaces. All three peptides alone showed potent activity (IC_{50} ≤ 3.01 µM) against *S. aureus*. However, only TpcC showed activity against *E. coli*. To our current knowledge, no studies have successfully reported the antimicrobial activity of the tryptophan rich TpcC analogue against *S. aureus* and *E. coli*. This study is therefore the first to report that TpcC is effective against both *S. aureus* and *E. coli* with a 50% inhibitory concentration of 1.94 µM and 13.57 µM, respectively. Previous studies have indicated that the addition/substitution and/or position of a tryptophan residue may improve the antimicrobial activity of the tyrocidines and analogues [12,13,62,66,68], and that the presence or absence of tryptophan residues influence the affinity of silver ions to the peptide [41,70]. The improved antimicrobial activity observed for both TpcC alone and in formation, is therefore in agreement with the claims of these studies. Nonetheless, formulations of all three peptides with silver showed improved activity against both *S. aureus* and *E. coli* , particularly at a peptide:Ag^+ ratio of 1:3. Novel antimicrobial activity against *E. coli* for the tyrocidines in formulation with silver was therefore confirmed without sacrificing the potent antimicrobial activity of the tyrocidines against *S. aureus*. Although multiple factors were shown to influence CDP-MNP formation. The variability in physiochemical, optical, and antimicrobial properties of AgNPs and tyrocidines under different CDP-MNP fabrication conditions is favourable for the alteration and optimisation of drug delivery systems. The use of the CDP-MNP formulations for surface applications therefore has great promise with further formulations optimisation.

4.5 References

[1] K. Lewis, The science of antibiotic discovery, Cell. 181 (2020) 29–45. https://doi.org/10.1016/JCELL.2020.02.056.

[2] WHO Geneva, Global action plan on antimicrobial resistance, Microbe Mag. 10 (2015) 354–355. https://doi.org/10.1128/microbe.10.354.1.

[3] S. Ruden, K. Hilpert, M. Berditsch, P. Wadhwani, A.S. Ulrich, Synergistic interaction between silver nanoparticles and membrane-permeabilizing antimicrobial peptides, Antimicrob. Agents Chemother. 53 (2009) 3538–3540. https://doi.org/10.1128/AAC.01106-08.

[4] S. Dadashi-Silab, S. Doran, Y. Yagci, Photoinduced electron transfer reactions for macromolecular syntheses, Chem. Rev. 116 (2016) 10212–10275. https://doi.org/10.1021/acsChemrev.5b00586.

[5] Y.N. Tan, J.Y. Lee, D.IC. Wang, Uncovering the Design rules for peptide synthesis of metal nanoparticles, J. Am. Chem. Soc. 132 (2010) 5677–5686. https://doi.org/10.1021/ja907454f.

[6] M. Iosin, P. Baldeck, S. Astilean, Study of tryptophan assisted synthesis of gold nanoparticles by combining UV–Vis, fluorescence, and SERS spectroscopy, J. Nanoparticle Res. 12 (2010) 2843–2849. https://doi.org/10.1007/s11051-010-9869-6.

[7] A. León-Buitimea, C.R. Garza-Cárdenas, JA. Garza-Cervantes, JA. Lerma-Escalera, J.R. Morones-Ramírez, The demand for new antibiotics: antimicrobial peptides, nanoparticles, and combinatorial therapies as future strategies in antibacterial agent design, Front. Microbiol. 11 (2020). https://doi.org/10.3389/fmicb.2020.01669.

[8] I.F. Jaja, C.-J.I. Jaja, N.V. Chigor, M.U. Anyanwu, E.K. Maduabuchi, J.W. Oguttu, E. Green, Antimicrobial resistance phenotype of *Staphylococcus aureus* and *Escherichia coli* isolates obtained from meat in the formal and informal sectors in South Africa, Biomed Res. Int. 2020 (2020) 1–11. https://doi.org/10.1155/2020/3979482.

[9] D. Gutiérrez, S. Delgado, D. Vázquez-Sánchez, B. Martínez, M.L. Cabo, A. Rodríguez, J.J. Herrera, P. García, Incidence of *Staphylococcus aureus* and analysis of associated bacterial communities on food industry surfaces, Appl. Environ. Microbiol. 78 (2012) 8547–8554. https://doi.org/10.1128/AEM.02045-12.

[10] B.M. Spathelf, M. Rautenbach, Anti-listerial activity and structure-activity relationships of the six major tyrocidines, cyclic decapeptides from *Bacillus aneurinolyticus*, Bioorganic Med. Chem. 17 (2009) 5541–5548. https://doi.org/10.1016/jBmc.2009.06.029.

[11] W. van Rensburg, M. Rautenbach, Creating robust antimicrobial materials with sticky tyrocidines, antibiotics. 11 (2022) 174. https://doi.org/10.3390/antibiotics11020174.

[12] M. Wenzel, M. Rautenbach, JA. Vosloo, T. Siersma, C.H.M. Aisenbrey, E. Zaitseva, W.E. Laubscher, W. van Rensburg, JC. Behrends, B. Bechinger, L.W. Hamoen, The multifaceted antibacterial mechanisms of the pioneering peptide antibiotics tyrocidine and gramicidin S, MBio. 9 (2018). https://doi.org/10.1128/mBio.00802-18.

[13] MA. Marques, D.M. Citron, CC. Wang, Development oftyrocidine A analogues with improved antibacterial activity, Bioorganic Med. Chem. 15 (2007) 6667–6677. https://doi.org/10.1016/jBmc.2007.08.007.

[14] A. Reyes-Jara, N. Cordero, J. Aguirre, M. Troncoso, G. Figueroa, Antibacterial effect of copper on microorganisms isolated from bovine mastitis, Front. Microbiol. 7 (2016). https://doi.org/10.3389/fmicb.2016.00626.

[15] J. Baker, S. Sitthisak, M. Sengupta, M. Johnson, R.K. Jayaswal, JA. Morrissey, Copper stress induces a global stress response in *Staphylococcus aureus* and represses sae and agr expression and biofilm formations, Appl. Environ. Microbiol. 76 (2010) 150–160. https://doi.org/10.1128/AEM.02268-09.

[16] H.T. Michels, J.O. Noyce, C.W. Keevil, Effects of temperature and humidity on the efficacy of methicillin- resistant *Staphylococcus aureus* challenged antimicrobial materials containing silver and copper, Lett. Appl. Microbiol. 49 (2009) 191–195. https://doi.org/10.1111/j.1472-765X.2009.02637.x.

[17] S. Jadhav, S. Gaikwad, M. Nimse, A. Rajbhoj, Copper oxide nanoparticles: Synthesis, characterization and their antibacterial activity, J. Clust. Sci. 22 (2011) 121–129. https://doi.org/10.1007/s10876-011-0349-7.

[18] D. Chudobova, S. Dostalova, B. Ruttkay-Nedecky, R. Guran, MA.M. Rodrigo, K. Tmejova, S. Krizkova, O. Zitka, V. Adam, R. Kizek, The effect of metal ions on *Staphylococcus aureus* revealed by biochemical and mass spectrometric analyses, Microbiol. Res. 170 (2015) 147–156. https://doi.org/10.1016/j.micres.2014.08.003.

[19] H. Wang, M. Wang, X. Xu, P. Gao, Z. Xu, Q. Zhang, H. Li, A. Yan, R.Y.T. Kao, H. Sun, Multi-target mode of action of silver against *Staphylococcus aureus* endows it with capability to combat antibiotic resistance, Nat. Commun. 12 (2021). https://doi.org/10.1038/s41467-021-23659-y.

[20] A. Elbehiry, M. Al-Dubaib, E. Marzouk, I. Moussa, Antibacterial effects and resistance induction of silver and gold nanoparticles against *Staphylococcus aureus* -induced mastitis and the potential toxicity in rats, Microbiologyopen. 8 (2019) e00698. https://doi.org/10.1002/mbo3.698.

[21] Z.E. Nazari, M. Banoee, AA. Sepahi, F. Rafii, A.R. Shahverdi, The combination effects of trivalent gold ions and gold nanoparticles with different antibiotics against resistant *Pseudomonas aeruginosa*, Gold Bull. 45 (2012) 53–59. https://doi.org/10.1007/s13404-012-0048-7.

[22] S. Si, T.K. Mandal, Tryptophan-based peptides to synthesize gold and silver nanoparticles: a mechanistic and kinetic study, Chem. - A Eur. J. 13 (2007) 3160–3168. https://doi.org/10.1002/chem.200601492.

[23] S. Roy, T.K. Das, Study of Interaction Between tryptophan, tyrosine, and phenylalanine separately with silver nanoparticles by fluorescence quenching Method, J. Appl. Spectrosc. 82 (2015) 598–606. https://doi.org/10.1007/s10812-015-0151-7.

[24] S. Gupta, V. Kumar, KB. Joshi, Solvent mediated photo-induced morphological transformation of AgNPs-peptide hybrids in water-EtOH binary solvent mixture, J. Mol. Liq. 236 (2017) 266–277. https://doi.org/10.1016/j.molliq.2017.03.114.

[25] G. Pandit, K. Roy, U. Agarwal, S. Chatterjee, Self-Assembly mechanism of a peptide-based drug delivery vehicle, ACS Omega. 3 (2018) 3143–3155. https://doi.org/10.1021/acsomega.7b01871.

[26] W. van Rensburg, W.E. Laubscher, M. Rautenbach, High throughput method to determine the surface activity of antimicrobial polymeric materials, MethodsX. 8 (2021) 101593. https://doi.org/10.1016/j.mex.2021.101593.

[27] S.H. Haji, FA. Ali, S.T.H. Aka, Synergistic antibacterial activity of silver nanoparticles biosynthesized by carbapenem-resistant Gram-negative *bacilli*, Sci. Rep. 12 (2022). https://doi.org/10.1038/s41598-022-19698-0.

[28] K.S. Nam, B.H. Jung, J.W. An, T.J. Ha, T. Tran, M.J. Kim, Use of chloride–hypochlorite leachants to recover gold from tailing, Int. J. Miner. Process. 86 (2008) 131–140. https://doi.org/10.1016/j.minpro.2007.12.003.

[29] X. Sun, S. Dong, E. Wang, One-step preparation of highly concentrated well-stable gold colloids by direct mix of polyelectrolyte and $HAuC_{l4}$ aqueous solutions at room temperature, J. Colloid Interface Sci. 288 (2005) 301–303. https://doi.org/10.1016/j.jcis.2005.02.079.

[30] A. Khan, A. Rashid, R. Younas, R. Chong, A chemical reduction approach to the synthesis of copper nanoparticles, Int. Nano Lett. 6 (2016) 21–26. https://doi.org/10.1007/s40089-015-0163-6.

[31] A.L. González, C. Noguez, J. Beránek, A.S. Barnard, size, shape, stability, and color of plasmonic silver nanoparticles, J. Phys. Chem. C. 118 (2014) 9128–9136. https://doi.org/10.1021/jp5018168.

[32] E. Saion, E. Gharibshahi, K. Naghavi, Size-controlled and optical properties of monodispersed silver nanoparticles synthesized by the radiolytic reduction method, Int. J. Mol. Sci. 14 (2013) 7880–7896. https://doi.org/10.3390/ijms14047880.

[33] H. Liu, X. Gu, C. Wei, H. Fu, P.J.J. Alvarez, Q. Li, S. Zheng, X. Qu, D. Zhu, Threshold concentrations of silver ions exist for the sunlight-induced formation of silver nanoparticles in the presence of natural organic matter, Environ. Sci. Technol. 52 (2018) 4040–4050. https://doi.org/10.1021/acs.est.7b05645.

[34] A. Chhatre, P. Solasa, S. Sakle, R. Thaokar, A. Mehra, Color and surface plasmon effects in nanoparticle systems: Case of silver nanoparticles prepared by microemulsion route, Colloids Surfaces A Physicochem. Eng. Asp. 404 (2012) 83–92. https://doi.org/10.1016/jColsurfa.2012.04.016.

[35] N.K. Mishra, V. Kumar, KB. Joshi, Thermoplasmonic effect of silver nanoparticles modulates peptide amphiphile fiber into nanowreath-like assembly, Nanoscale. 7 (2015) 20238–20248. https://doi.org/10.1039/c5nr06577a.

[36] N.K. Mishra, V. Kumar, KB. Joshi, Fabrication of gold nanoparticles on biotin-di-tryptophan scaffold for plausible biomedical applications, RSC Adv. 5 (2015) 64387–64394. https://doi.org/10.1039/C5RA11121H.

[37] S. Kéki, J. Török, G. Deák, L. Daróczi, M. Zsuga, Silver nanoparticles by PAMAM-assisted photochemical reduction of Ag+, J. Colloid Interface Sci. 229 (2000) 550–553. https://doi.org/10.1006/jcis.2000.7011.

[38] S. Gupta, M. Kashyap, V. Kumar, P. Jain, V. Vinayak, KB. Joshi, Peptide mediated facile fabrication of silver nanoparticles over living diatom surface and its application, J. Mol. Liq. 249 (2018) 600–608. https://doi.org/10.1016/j.molliq.2017.11.086.

[39] Y. Wang, X. Yang, T. Liu, Z. Li, D. Leskauskas, G. Liu, JB. Matson, Molecular-level control over plasmonic properties in silver nanoparticle/self-assembling peptide hybrids, J. Am. Chem. Soc. 142 (2020) 9158–9162. https://doi.org/10.1021/jacs.0c03672.

[40] S. Agnihotri, S. Mukherji, S. Mukherji, Size-controlled silver nanoparticles synthesized over the range 5–100 nm using the same protocol and their antibacterial efficacy, RSC Adv. 4 (2014) 3974–3983. https://doi.org/10.1039/C3RA44507K.

[41] T. Shoeib, K.W.M. Siu, AC. Hopkinson, Silver ion binding energies of amino acids: Use of theory to assess the validity of experimental silver ion basicities obtained from the kinetic method, J. Phys. Chem. A. 106 (2002) 6121–6128. https://doi.org/10.1021/jp013662z.

[42] A.N. yang. N. Leussa, M. Rautenbach, Detailed SAR and PCA of the tyrocidines and analogues towards leucocin A-sensitive and leucocin A-resistant *Listeria monocytogenes*, Chem. Biol. Drug Des. 84 (2014) 543–557. https://doi.org/10.1111/cbdd.12344.

[43] A.M. Troskie, A. de Beer, JA. Vosloo, K. Jacobs, M. Rautenbach, Inhibition of agronomically relevant fungal phytopathogens by tyrocidines, cyclic antimicrobial peptides isolated from *Bacillus aneurinolyticus*, Microbiology. 160 (2014) 2089–2101. https://doi.org/10.1099/mic.0.078840-0.

[44] M. Rautenbach, A.M. Troskie, JA. Vosloo, M.E. Dathe, Antifungal membranolytic activity of the tyrocidines against filamentous plant fungi, Biochimie. 130 (2016) 122–131. https://doi.org/10.1016/jBiochi.2016.06.008.

[45] Y. Masoudi, W. van Rensburg, B. Barnard-Jenkins, M. Rautenbach, The influence of cellulose-type formulants on anti-*Candida* activity of the tyrocidines, Antibiotics. 10 (2021) 597. https://doi.org/10.3390/antibiotics10050597.

[46] K. Kolwas, A. Derkachova, M. Shopa, Size characteristics of surface plasmons and their manifestation in scattering properties of metal particles, J. Quant. Spectrosc. Radiat. Transf. 110 (2009) 1490–1501. https://doi.org/10.1016/j.jqsrt.2009.03.020.

[47] K.L. Kelly, E. Coronado, L.L. Zhao, GC. Schatz, The optical properties of metal nanoparticles: The influence of size, shape, and dielectric environment, J. Phys. Chem. B. 107 (2003) 668–677. https://doi.org/10.1021/jp026731y.

[48] K. Shameli, MB. Ahmad, SD. Jazayeri, P. Shabanzadeh, P. Sangpour, H. Jahangirian, Y. Gharayebi, Investigation of antibacterial properties silver nanoparticles prepared via green method, Chem. Cent. J. 6 (2012) 1–10. https://doi.org/10.1186/1752-153X-6-73.

[49] A. Thomas, U. Sivasankaran, K.G. Kumar, Biothiols induced colour change of silver nanoparticles: A colorimetric sensing strategy, Spectrochim. Acta Part A Mol. Biomol. Spectrosc. 188 (2018) 113–119. https://doi.org/10.1016/j.saa.2017.06.040.

[50] AB.T. Ghisaidoobe, S.J. Chung, Intrinsic Tryptophan fluorescence in the detection and analysis of proteins: A focus on Förster resonance energy transfer techniques, Int. J. Mol. Sci. 15 (2014) 22518–22538. https://doi.org/10.3390/ijms151222518.

[51] L.H. Lucas, BA. Ersoy, LA. Kueltzo, SB. Joshi, D.T. Brandau, N. Thyagarajapuram, L.J. Peek, C.R. Middaugh, Probing protein structure and dynamics by second-derivative ultraviolet absorption analysis of cation-π interactions, Protein Sci. 15 (2006) 2228–2243. https://doi.org/10.1110/ps.062133706.

[52] V. Rodenas, M. García, C. Sánchez-Pedreñ, M. Albero, Simultaneous determination of propacetamol and paracetamol by derivative spectrophotometry, Talanta. 52 (2000) 517–523. www.elsevierCom/locate/talanta (accessed January 2, 2023).

[53] W. Xu, H. Yu, F. Yang, F. Yang, D. Liu, K. Lu, H. Gao, Y. Song, Second derivative UV–visible spectroscopy characterizing structural components of dissolved and particulate organic matter in an

urbanized river, Environ. Sci. Eur. 34 (2022) 29. https://doi.org/10.1186/s12302-022-00609-z.

[54] A. Amirjani, F. Firouzi, D.F. Haghshenas, Predicting the size of silver nanoparticles from their optical properties, Plasmonics. 15 (2020) 1077–1082. https://doi.org/10.1007/s11468-020-01121-x.

[55] Y. Bao, B. Zhao, D. Hou, J. Liu, F. Wang, X. Wang, T. Cui, The redshift of surface plasmon resonance of colloidal gold nanoparticles induced by pressure with diamond anvil cell, J. Appl. Phys. 115 (2014) 223503. https://doi.org/10.1063/1.4882187.

[56] S. Raza, W. Yan, N. Stenger, M. Wubs, NA. Mortensen, Blueshift of the surface plasmon resonance in silver nanoparticles: substrate effects, Opt. Express. 21 (2013) 27344. https://doi.org/10.1364/OE.21.027344.

[57] A. Rai, S. Pinto, T.R. Velho, A.F. Ferreira, C. Moita, U. Trivedi, M. Evangelista, M. Comune, K.P. Rumbaugh, P.N. Simões, L. Moita, L. Ferreira, One-step synthesis of high-density peptide-conjugated gold nanoparticles with antimicrobial efficacy in a systemic infection model, Biomaterials. 85 (2016) 99–110. https://doi.org/10.1016/jBiomaterials.2016.01.051.

[58] L. Polavarapu, Q.-H. Xu, A single-step synthesis of gold nanochains using an amino acid as a capping agent and characterization of their optical properties, Nanotechnol. 19 (2008) 075601. https://doi.org/10.1088/0957-4484/19/7/075601.

[59] I. Pal, V.P. Brahmkhatri, S. Bera, D. Bhattacharyya, Y. Quirishi, A. Bhunia, H.S. Atreya, Enhanced stability and activity of an antimicrobial peptide in conjugation with silver nanoparticle, J. Colloid Interface Sci. 483 (2016) 385–393. https://doi.org/10.1016/j.jcis.2016.08.043.

[60] F.W.J. Teale, G. Weber, Ultraviolet fluorescence of the aromatic amino acids, Biochem. J. 65 (1957) 476–482. https://doi.org/10.1042/bj0650476.

[61] V. Kumar, W. van Rensburg, J.L. Snoep, H.H. Paradies, C. Borrageiro, C. de Villiers, R. Singh, KB. Joshi, M. Rautenbach, Antimicrobial nano-assemblies of tryptocidine C, a tryptophan-rich cyclic decapeptide, from ethanolic solutions, Biochimie. 204 (2023) 22–32. https://doi.org/10.1016/jBiochi.2022.08.017.

[62] M. Rautenbach, V. Kumar, JA. Vosloo, Y. Masoudi, R.J. van Wyk, MA. Stander, Oligomerisation of tryptocidine C, a Trp-rich cyclodecapeptide from the antimicrobial tyrothricin complex, Biochimie. 181 (2021) 123–133. https://doi.org/10.1016/jBiochi.2020.12.006.

[63] M. Rautenbach, A.M. Troskie, JA. Vosloo, Antifungal peptides: To be or not to be membrane active, Biochimie. 130 (2016) 132–145. https://doi.org/10.1016/jBiochi.2016.05.013.

[64] A.M. Troskie, M. Rautenbach, N. Delattin, JA. Vosloo, M. Dathe, B.PA. Cammue, K. Thevissen, Synergistic activity of the tyrocidines, antimicrobial cyclodecapeptides from *Bacillus aneurinolyticus*, with amphotericin B and caspofungin against *Candida albicans* biofilms, Antimicrob. Agents Chemother. 58 (2014) 3697–3707. https://doi.org/10.1128/AAC.02381-14.

[65] M. Rautenbach, N.M. Vlok, M. Stander, HC. Hoppe, Inhibition of malaria parasite blood stages by tyrocidines, membrane-active cyclic peptide antibiotics from *Bacillus* brevis, Biochim Biophys Acta. 1768 (2007) 1488–1497. https://doi.org/10.1016/jBbamem.2007.01.015.

[66] G. Munyuki, G.E. Jackson, GA. Venter, K.E. Kövér, L. Szilágyi, M. Rautenbach, B.M. Spathelf, B. Bhattacharya, D. Van Der Spoel, β-sheet structures and dimer models of the two major tyrocidines, antimicrobial peptides from *Bacillus aneurinolyticus*, Biochemistry. 52 (2013) 7798–7806. https://doi.org/10.1021/bi401363m.

[67] H.H. Paradies, Aggregation of tyrocidine in aqueous solutions, Biochem. Biophys. Res. Commun. 88 (1979) 810–817. https://doi.org/10.1016/0006-291X(79)91480-3.

[68] MA. Ruttenberg, T.P. King, LC. Craig, J. SvU, R. Breslow, D. Chipman, The use of the tyrocidines for the study of conformation and aggregation behavior, J. Am. Chem. Soc. 87 (1965) 4196–4198. https://doi.org/10.1021/ja01096a040.

[69] H.H. Paradies, H. Reichelt, Formation and structures of tyrocidine B oligomers in solution in the presence of water, AIP Adv. 10 (2020) 075007 1-10. https://doi.org/10.1063/1.5144852.

[70] D.M. Close, P. Wardman, Calculation of standard reduction potentials of amino acid radicals and the effects of water and incorporation into peptides, J. Phys. Chem. A. 122 (2018) 439–445. https://doi.org/10.1021/acs.jpca.7b10766.

Chapter 5
Conclusions and Future Studies

5.1 Introduction

The primary aim of this study was to successfully fabricate cyclodecapeptide-metal nanoparticle hybrids (CDP-MNP) with improved antimicrobial action against model target organisms namely, *Escherichia coli* (*E. coli*) and *Staphylococcus aureus* (*S. aureus*). To achieve this, aromatic residue rich and tryptophan-rich cyclodecapeptides (CDPs) were required for the fabrication of metal nanoparticles (MNPs) due to the proposed role of aromatic residues, especially tryptophan in peptide-assisted synthesis of metal nanoparticles [1–4]. Aromatic residue rich cyclodecapeptide mixtures and tryptophan-rich peptide analogues were therefore produced and purified to be applied in formulations with select alkali earth, transition, and post-transitional metals. To identify and track potentially favourable and/or unfavourable changes in peptide composition and behaviour, shifts in peptide oligomerisation within formulations was characterised via mass spectrophotometric analysis.

Promising formulations of the peptide preparations with group 11 metals were screened against *S. aureus* to detect changes in antimicrobial activity and aid the selection of formulations for further testing. From these studies, formulations with silver were identified as the most promising combination for the fabrication of antimicrobial nanoformulations. The peptide-assisted fabrication of silver nanoparticles (AgNPs) with selected peptide:Ag^{+} formulations was subsequently optimised by exposing formulations to different solvent environments and concentration ratios. The peptide-assisted formation of AgNPs was confirmed by characteristic changes in solution colour and the formation of surface plasmonic resonance (SPR) bands as observed by UV-Visible light (UV-Vis) spectrophotometry [5,6]. Changes in peptide structure and conformation due to AgNP synthesis was reported using spectrophotometric and spectrofluorometric techniques. While the presence, shape, and structure of CDP-MNP hybrids was confirmed via scanning-transmission electron microscopy (STEM). Finally, to confirm improved antimicrobial activity, peptides, metals, and peptide:metal nanoformulations were tested against Gram-negative bacterium *E. coli* and Gram-positive bacterium *S. aureus* in solid surface assays. The combinational interactions between the two antimicrobial agents (antimicrobial cyclodecapeptides and silver nanoparticles) were determined using fractional inhibitory

concentrations and isobolograms, to illustrate the peptide:metal ratio-dependent synergism and additive effect of nanoformulations against both target organisms.

5.2 Experimental Conclusions and Future Studies

5.2.1 Production and purification of tryptophan-containing antimicrobial peptides and their analogues

To decipher the biophysical and antimicrobial characteristics of the different tyrocidines and analogues in formulation with metals, adequate amounts of tyrocidine mixture (Trc mix) and purified peptide analogues (TrcC and TpcC) was required. The production of tryptophan-containing Trcs was successfully achieved by shifting the peptide production profiles of *Brevibacillus parabrevis* (*Br. parabrevis*) producer cultures to favour tryptophan-rich tyrocidines utilising culture manipulation methodologies developed by BIOPEP peptide group at Stellenbosch University [7]. The subsequent purification of Trcs was achieved through a series of steps including the removal of linear gramicidins and organic extraction of the tyrocidines and analogues from the bacterial culture, followed by the purification of single peptide analogues using reverse-phase high-performance liquid chromatography (RP-HPLC). The purification of tryptophan-rich Trcs was of particular interest for this study due to the role of tryptophan in the fabrication of metal nanoparticles [1–4]. For commercial Trc mix (aromatic residue rich tyrocidine standard), the organic extraction step was sufficient for the removal of linear gramicidins and to obtain a pure peptide mixture (>96% purity). However, for the crude peptide extracts reverse phase high resolution liquid chromatography (RP-HPLC) purification was necessary for the isolation of single peptide analogues. The RP-HPLC purification of Trcs proved challenging due to the intrinsic oligomerisation and aggregation behaviour of the peptides [8,9].

To aid the purification process *Br. parabrevis* cultures were supplemented with different concentrations (10 mM or 20 mM) of either tryptophan (Trp) or phenylalanine (Phe). A total of three *Br. parabrevis* peptide productions were carried out. Production one (P1) and two (P2) used *Br. Parabrevis* ATCC1068 strains whilst production three (P3) used *Br. Parabrevis* ATCC8185 strains. Each production had a supplemented (Trp/Phe) and unsupplemented bacterial culture to track the changes in peptide production profiles. Changes in peptide production profiles were tracked, peptide identity was confirmed, and peptide purity was determined using electrospray ionisation mass spectrometry (ESI-MS) and ultra-performance liquid chromatography linked mass spectrometry (UPLC-MS).

Notably, supplementation of cultures with 20 mM tryptophan resulted in the production of a modified gramicidin (VGA^{uf}). Although the results from this study cannot ascertain the potential role that amino acid supplementation concentration may play in aberrated production, future work could investigate this relationship for applications in optimised or modified peptide production and purification. Nonetheless, the amino acid supplementation of *Br. parabrevis* cultures with tryptophan still promoted the production of tryptophan-rich Trcs (C analogues) which, in turn, eased the purification process and allowed for sufficient yields (≥1mg) of tryptophan-rich tryptocidine C (WC/WC_1) and tyrocidine C (YC/YC_1). RP-HPLC purification of tryptophan supplemented production two (P2W) yielded HPLC fractions of 6.36 mg high purity tryptocidine C/C_1 (>99%) and 1.94 mg high purity tyrocidine C (>94%). An overall total of four RP-HPLC fractions from productions one and two successfully yielded sufficient amount (≥ 1mg) of tryptocidine (WC/C_1) and tyrocidine (YC/C_1) analogues of high purity (>90%). These pure fractions C analogues were used for the formulation of peptide with metals in this study.

5.2.2 Mass spectrometry studies on the interaction of the tyrocidines and analogues with metal salts

The self-assembling nature and oligomerisation behaviour of the tyrocidines allows for the formation of stable higher order structures and thereby robust antimicrobial nanomaterials [9–11]. Meanwhile, studies have indicated that insufficient or excessive oligomerisation and aggregation of peptide may adversely influence its bioactivity [9,11–14]. Ion mobility mass spectrometry (IM-MS) studies revealed that the formulation of tyrocidines with select metals alters the peptides' self-assembling behaviour to favour different oligomers in the presence of different metals. The prospect of using metal salts as a tool to direct peptide self-assembly and dictate nanostructure formation therefore holds great potential for the development of novel antimicrobial nanodrugs against stubborn pathogens and biofilms. Formulation of Trc mix with magnesium ($MgCl_2$), calcium ($CaCl_2$), iron ($FeCl_2$) and zinc ($ZnCl_2$) metal salts resulted in the formation of stable triply charged peptide-metal $[M+Metal^{2+}+H]^{3+}$ complexes of tyrocidines with the respective metal ions (Mg^{2+}, Ca^{2+}, Fe^{2+} and Zn^{2+}). Due to the nature of IM-MS analysis, only stable non-covalent complexes and oligomers can withstand the exposure to the high collision forces, energy potentials and temperatures within the instrumentation. The peptide-metal complexes were therefore considered to be likely that of strong coordination bonds between peptide and metal ions [15,16]. Experimental *m/z* values of the triply charged complexes matched (<10 ppm) the theoretical values calculated for

peptide monomer and metal ion combinations $[M+Metal^{2+}+H]^{3+}$. This confirmed the formation of peptide:metal complexes between peptide monomers and the doubly charged metal ions and was further supported by isotope models of peptide with Fe^{2+} ions. Stable peptide-metal complexes were also detected after the maturation of the formulations, indicating stability over time as well. Increases in the metal salt concentration of the formulations resulted in an increased prevalence of peptide-metal complexes. Furthermore, a higher incidence of larger peptide oligomers (tetramers and hexamers) was observed for formulations at higher metal concentrations. These observations indicated that the formation of peptide-metal complexes either influences or is influenced by the formation and/or breakdown of peptide oligomeric species. Whether the introduction of metals prevents the formation of, or promotes the breakdown of, larger oligomers could not be confirmed in this study. However, an inverse relationship between peptide-metal complex and monomer/dimer contributions was observed. A decrease in monomer and dimer signal contributions was associated with an increased contribution of peptide-metal complexes indicating that monomeric and dimeric species participate in the complex formation process. The observed loss in monomers could be due to complex-forming interactions between peptide and metal. Peptide dimers may interact with metals to form higher order structures and oligomers, which due to their complexity were not considered in this study. Nonetheless, the formation of peptide-metal complexes with different metals, and subsequent shifts in peptide oligomerisation behaviour, gives valuable insight on the interactions of the tyrocidines with metal ions. Future studies could further explore peptide-metal reaction kinetics, complex structures, and binding energies to better understand these interactions and their structural conformation.

Contrastingly, peptide-metal complexes were not detected via IM-MS in peptide formulations with group 11 metals, even with the maturation of the samples. Nonetheless, formulations with copper (Cu^{2+}), silver (Ag^{+}) and gold (Au^{3+}) showed changes in peptide oligomerisation behaviour in the absence of complexes. This indicated that these metals interact with peptide structures in a different manner. A major factor to consider when investigating peptide-metal interactions is the role of different metals in bacterial systems. Magnesium, calcium, iron and zinc are all considered essential metals and play a crucial role in bacterial growth and cell maintenance [17–21], While, the group 11 metals are known for their antimicrobial properties [22–26]. Nonetheless, imbalances in both essential and non-essential metals is considered a stress factor for many bacteria and can be lethal [17,22,27]. The capture, transport, storage, leakage, sequestering and reduction of metal ions is

therefore vital to ensure metal availability while avoiding the risk of intoxication or starvation [22,27,28]. The tendency of the tyrocidines to form interact and form complexes with metals could therefore be beneficial for the survival the producer organism *Br. parabrevis*. Binding to these metals, if not to be used by *Br. parabrevis* itself, would deprive competing microbes of these essential metals. The supplementation of *Br. parabrevis* cultures with different transition metals and tracking of metal uptake, metal preferences and production profile changes could also be an interesting avenue of further investigation for the screening of promising peptide-metal interactions, perhaps even for future applications in bio-mineralisation [29,30].

Pilot studies confirmed that the tyrocidines, like other aromatic-amino acid rich peptides [1,2], allowed the formation of gold and silver nanoparticles. The ability of Trc mix to form nanoparticles is also confirmed by the investigations in Chapter 3. The loss of monomer and dimer contributions in silver and gold therefore suggests that these peptide species interact with metal ions, by acting as a reducing agent, to neutralise metal ions and subsequently induce the formation of metal nanoparticles [31–33]. Moreover, the preference of TrcA and TrcC analogues in monomeric species losses indicate that certain peptide analogues may play a greater role in the peptide-Ag^{+} and peptide-Au^{3+} interactions. It is worth noting that TrcA and TrcC analogues oligomerise to form ion-conducting pores in the phospholipid bilayer of bacterial cells and that the dimers of these analogues act as the seeding structures for target membrane interactions [9,14,34,35]. The loss of TrcA and TrcC monomers, for silver and gold could therefore be due to the self-assembly of TrcC and TrcA into higher order structures capable of interacting with or transporting gold and silver ions [36,37]. Future studies could therefore also investigate the interactions between metals and different peptide analogues to screen for promising peptide-metal interactions for applications as antimicrobial agents. Exploring the preferences of certain peptide analogues within each metal formulation would provide more information on the role of certain peptide analogues and metals in peptide oligomerisation and nano-assemblies. Moreover, the role of monomers and dimers in the formation of peptide metal complexes should be an avenue of further investigation. Formulations of pure peptide analogues can be analysed using IM-MS to determine changes in oligomerisation behaviour and better understand the role of different peptide analogues and oligomeric species. Additional metal formulation concentrations should also be investigated to determine how or whether the decreasing monomer/dimer trend is maintained across increasing metal concentrations. Plateaus in

signal contribution for monomers, dimers or complexes would provide valuable information on the threshold of peptide-metal interaction and is of notable importance for future studies.

5.2.3 Biophysical and bioactive properties of tyrocidine nanoformulations with group 11 metals

The peptide-assisted fabrication of metal nanoparticles and subsequent formation of antimicrobial CDP-MNP hybrids was investigated in Chapter 4. Previous studies have indicated that tryptophan-residues and tryptophan-rich peptides act as both a reducing and stabilising agent for the formation of MNPs [1–4]. The mass spectrometry studies on the interaction of the tyrocidines and analogues with metal salts in Chapter 3 showed promising interactions between the tyrocidines and the group 11 metals (copper, silver, and gold). The commercial tyrocidine peptide mixture (Trc mix) and single tryptophan-rich C analogues (TpcC and TrcC) purified in Chapter 2, were therefore formulated with the selected group 11 metals to assist the fabrication of copper, silver, and gold nanoparticles. Screening of Irradiated and non-irradiated peptide-metal formulations against *S. aureus* via solid surface assays identified formulations with silver to be the most promising for the fabrication of potent CDP-MNP hybrids. The peptide-assisted fabrication of AgNPs was optimised yielding a range of pale yellow to bright orange colloid colours under different formulation conditions. Formulations of peptide in 15% ethanol-water (%*v/v*), the solvent condition commonly used for broth-type bioassays [11,38], was selected for further investigations. However, formulations in 30% ethanol-water (%*v/v*) environments also showed the formation of AgNPs and are worth investigating further in future solid surface antimicrobial assays. Meanwhile, formulations at 60% showed no AgNP formation. This could be attributed to the amphipathic nature of the tyrocidines and their oligomerisation behaviour in more non-polar environments [9,11]. Future studies could investigate the peptide oligomerisation dependent formation of AgNPs by investigating peptide:metal formulations in a wider range of solvent environments.

Spectrophotometric and spectrofluorometric analysis of peptide:Ag^{+} formulations of 50 µM Trc mix and TpcC in 15% ethanol-water (%*v/v*) confirmed interactions between metal ions and tryptophan-containing peptides. Although the kinetics of the peptide-silver binding relationship was not investigated further in this study, future work could explore the role of the tryptophan residues in the formation of CDP-MNPs conjugates by tyrocidines and tryptocidines with silver. Changes in the UV-Vis spectra, of both Trc mix and TpcC in the presence of silver, indicated that their aromatic amino acid residues play a role in the

reaction and/or binding with Ag^+. The presence of surface plasmon resonance (SPR) bands in the visible light spectrum confirmed the formation of AgNPs. Scanning transmission microscopy (STEM) confirmed these AgNPs to be spherical in shape. STEM further revealed that the peptides encapsulated AgNPs in an oligomeric peptide nano-assembly structures.

Antimicrobial solid surface assays confirmed that the encapsulation of AgNPs by Trc mix, TrcC and TpcC maintains the antimicrobial action of the peptides towards *S. aureus* and significantly improves the activity against *E. coli* at certain peptide:metal ratios, notably, when the concentration of metal is three times that of peptide (1:3). Synergy between peptide and silver was observed with *E. coli* as a target, while an additive effect was recorded for most formulations against *S. aureus*. Antimicrobial assays also revealed intrinsic activity of TpcC against both *S. aureus* and *E. coli*. To our current knowledge, this is the first study to successfully report activity of this tryptophan-rich C analogue against these Gram-positive and Gram-negative pathogens. The potent antimicrobial action of TpcC agrees with previous studies which propose that the aromatic amino acid tryptophan dictates peptide self-assembly behaviour and the structural conformation of the peptides aromatic dipeptide moiety [9,11]. The enhanced activity of TpcC is therefore likely due to its interactions with the cell wall of the target organism [14]. Nonetheless, the native activity of TpcC was improved when in formulated with silver. The self-assembly of peptides has been shown to aid peptide-assisted nanoparticle synthesis and nanoparticle encapsulation [36,37]. The improved activity of TpcC compared to Trc mix and TrcC in formulation, could be associated to the peptides strong tendency to oligomerise and encapsulate AgNPs, resulting in stable peptide-metal conjugates [39,40]. Overall, the formulation of all three peptide preparations with silver showed promising activity for future applications as potent antimicrobial nano-drugs for topical or surface treatment applications. Due to the well-recorded systemic toxicity [41–44] of the tyrocidines and silver, topical applications rather than systemic applications would be considered in future studies. However, the variability in CDP-MNP fabrication conditions shows promise for the modification and optimisation of this nano-drug for different drug delivery systems, therapies and applications. Future studies could investigate the haemolytic properties and *in vitro* viability of these nano-formulations. Moreover, the surface stability of matured nanoformulations is worth future investigation to determine the robustness of this novel nano-drug [10].

5.3 Last Word

This study successfully fabricated photo-induced peptide-assisted AgNPs by formulating aromatic amino acid-rich cyclodipeptide mixture (Trc mix) and tryptophan-rich single C analogues (TpcC and TrcC) with silver and irradiating the formulation with a constant wave green laser (532 nm) to initiate photo-induced electron transfer. The predicted role of tryptophan-residues in the reduction and stabilisation of AgNP formation was supported by mass spectrometry, spectrophotometric, spectrofluorometric characterisation of the peptide:metal nanoformulations in this study. Moreover, mass spectrometry characterisation of peptide:metal formulations confirmed the formation of peptide-metal complexes with cationic ions of the group two metals, magnesium and calcium, transition metal, iron, and post-transitional metal ,zinc. These complexes were maintained after maturation and exposure to the harsh mass spectrometry analysis conditions and are likely that of strong coordination bonds between peptide amides, aromatic residues and metals [15,45–51]. The detection and identification of these stable peptide-metal complexes therefore highlight the affinity of the tyrocidines and tyrocidine analogues for these essential metals and queries the multifactorial role that the tyrocidines play in survival mechanisms of *Br. parabrevis*. During sporulation a subset of the *Br. parabrevis* cells produces and releases the antimicrobial peptide complex tyrothricin (which contains the tyrocidines and analogues) via a self-sacrifice mechanism to eradicate competing organisms and ensure *Br. parabrevis* spore survival [52]. The interactions of the cyclodecapeptides with the charged metal ions investigated in this study elude that these peptides play a role in metal ion transport. The tyrocidines have been shown to oligomerise, creating large pores in the cell membranes of target organisms, thereby promoting an influx of large molecules (which may include charged metal ions) into the host organism [14,34,35]. The formation of peptide-metal conjugates and incorporation of MNPs into peptide oligomeric structures [11,36,37] could also play a role in the capture, transport, storage, neutralisation and sequestering of metal ions to minimise the risk of intoxication or starvation [22,27]. The absence of peptide-metal complexes with group 11 metals, formation of AgNPs and encapsulation of AgNPs (as confirmed in Chapter 3) supports the latter where heavy metals are neutralised and sequestered to prevent intoxication. Although this may be an indicator of already existing resistance of *Br. parabrevis* against heavy metal treatment [53,54]. The resulting conjugated CDP-MNP hybrids has great potential for the development of a novel antimicrobial nanodrugs against other target organisms. Moreover, the combined modes of action of the

antimicrobial peptides and metal nanoparticles reduce the risk of resistance development against the nanoformulation by target organisms [55]. To better understand the role of peptide and metals in metal complex formation and peptide-metal interactions, the binding affinities and kinetics of these interactions would need to be analysed and the nature of the subsequent complexes characterised. Methodologies to further characterise peptide-metal complexes may include: UV-Visible light [56], fluorescence [57], circular dichroism [9], Fourier-transform infrared spectrometry [58] and nuclear magnetic resonance spectroscopy [40,59], as well as, theoretical computational and molecular modelling methodologies [60–62]. Nonetheless, the formation and encapsulation of AgNPs by Trc mix, TpcC and TrcC was confirmed in this study via spectrophotometric, spectrofluorimetric and STEM analysis. Antimicrobial solid surface assays showed great promise for the application of these AgNP encapsulated peptide-metal hybrids in antimicrobial surface treatments [10,63,64] against two pathogens commonly associated with contact surface contamination [65,66], *S. aureus* and *E. coli*. Interestingly, unprecedented activity for peptide analogue tryptocidine C (TpcC) against *S. aureus* and *E. coli* was reported in this study. However, all peptide:metal nanoformulations showed enhanced activity against *S. aureus* and *E. coli*. Although the formation of conjugates varied in different formulation conditions, this variability may be favourable for the manipulation and development of alternate nanoformulations with different biological functions and physiochemical properties. The capability to tweak these nanoformulations therefore allows versatility for future drug structures and delivery systems. Leaving room for the development of novel nanodrugs, from the same formulation, for alternate applications. The tryptophan-rich tyrocidines and analogues therefore hold great promise for the development and fabrication of peptide-metal nanodrugs and perhaps even nanomaterials.

5.4 References

[1] M. Iosin, P. Baldeck, S. Astilean, Study of tryptophan assisted synthesis of gold nanoparticles by combining UV–Vis, fluorescence, and SERS spectroscopy, J. Nanoparticle Res. 12 (2010) 2843–2849. https://doi.org/10.1007/s11051-010-9869-6.

[2] S. Si, T.K. Mandal, Tryptophan-based peptides to synthesize gold and silver nanoparticles: A mechanistic and kinetic study, Chem. A. Eur. J. 13 (2007) 3160–3168. https://doi.org/10.1002/chem.200601492.

[3] T. Shoeib, K.W.M. Siu, A.C. Hopkinson, Silver ion binding energies of amino acids: Use of theory to assess the validity of experimental silver ion basicities obtained from the kinetic method, J. Phys. Chem. A. 106 (2002) 6121–6128. https://doi.org/10.1021/jp013662z.

[4] S. Roy, T.K. Das, Study of Interaction Between tryptophan, tyrosine, and phenylalanine separately with silver nanoparticles by fluorescence quenching method, J. Appl. Spectrosc. 82 (2015) 598–606. https://doi.org/10.1007/s10812-015-0151-7.

[5] A. Amirjani, F. Firouzi, D.F. Haghshenas, Predicting the size of silver nanoparticles from their optical properties, Plasmonics. 15 (2020) 1077–1082. https://doi.org/10.1007/s11468-020-01121-x.

[6] A.L. González, C. Noguez, J. Beránek, A.S. Barnard, Size, shape, stability, and color of plasmonic silver nanoparticles, J. Phys. Chem. C. 118 (2014) 9128–9136. https://doi.org/10.1021/jp5018168.

[7] J.A. Vosloo, M.A. Stander, A.N.N. Leussa, B.M. Spathelf, M. Rautenbach, Manipulation of the tyrothricin production profile of *Bacillus aneurinolyticus*, Microbiology. 159 (2013) 2200–2211. https://doi.org/10.1099/mic.0.068734-0.

[8] R.C. Williams, D.A. Yphantis, L.C. Craig, Noncovalent association of tyrocidine B, Biochemistry. 11 (1972) 70–77. https://doi.org/10.1021/bi00751a013.

[9] M. Rautenbach, V. Kumar, J.A. Vosloo, Y. Masoudi, R.J. van Wyk, M.A. Stander, Oligomerisation of tryptocidine C, a Trp-rich cyclodecapeptide from the antimicrobial tyrothricin complex, Biochimie. 181 (2021) 123–133. https://doi.org/10.1016/j.biochi.2020.12.006.

[10] W. van Rensburg, M. Rautenbach, Creating robust antimicrobial materials with sticky tyrocidines, Antibiotics. 11 (2022) 174. https://doi.org/10.3390/antibiotics11020174.

[11] V. Kumar, W. van Rensburg, J.L. Snoep, H.H. Paradies, C. Borrageiro, C. de Villiers, R. Singh, K.B. Joshi, M. Rautenbach, Antimicrobial nano-assemblies of tryptocidine C, a tryptophan-rich cyclic decapeptide, from ethanolic solutions, Biochimie. 204 (2023) 22–32. https://doi.org/10.1016/j.biochi.2022.08.017.

[12] C. Duy, J. Fitter, How Aggregation and conformational scrambling of unfolded states govern fluorescence emission spectra, Biophys. J. 90 (2006) 3704–3711. https://doi.org/10.1529/biophysj.105.078980.

[13] M.A. Ruttenberg, T.P. King, L.C. Craig, J. SvU, R. Breslow, D. Chipman, The Use of the Tyrocidines for the Study of Conformation and Aggregation Behavior, J. Am. Chem. Soc. 87 (1965) 4196–4198. https://doi.org/10.1021/ja01096a040.

[14] M. Wenzel, M. Rautenbach, J.A. Vosloo, T. Siersma, C.H.M. Aisenbrey, E. Zaitseva, W.E. Laubscher, W. van Rensburg, J.C. Behrends, B. Bechinger, L.W. Hamoen, The multifaceted antibacterial mechanisms of the pioneering peptide antibiotics tyrocidine and gramicidin S, MBio. 9 (2018). https://doi.org/10.1128/mBio.00802-18.

[15] D.D. Carlton, K.A. Schug, A review on the interrogation of peptide–metal interactions using electrospray ionization-mass spectrometry, Anal. Chim. Acta. 686 (2011) 19–39. https://doi.org/10.1016/J.ACA.2010.11.050.

[16] B.T. Ruotolo, C.C. Tate, D.H. Russell, Ion mobility-mass spectrometry applied to cyclic peptide analysis: Conformational preferences of gramicidin S and linear analogs in the gas phase, J. Am. Soc. Mass Spectrom. 15 (2004) 870–878. https://doi.org/10.1016/j.jasms.2004.02.006.

[17] P.B. Tchounwou, C.G. Yedjou, A.K. Patlolla, D.J. Sutton, Heavy metal toxicity and the environment, in: Luch, A. (eds) Molecular, Clinical and Environmental Toxicology. Experientia Supplementum, 2012, vol 101. Springer, Basel, pp. 133–164. https://doi.org/10.1007/978-3-7643-8340-4_6.

[18] J.S. Klein, O. Lewinson, Bacterial ATP-driven transporters of transition metals: Physiological roles, mechanisms of action, and roles in bacterial virulence, Metallomics. 3 (2011) 1098–1108. https://doi.org/10.1039/c1mt00073j.

[19] N. White, H. Sadeeshkumar, A. Sun, N. Sudarsan, R.R. Breaker, Na^+ riboswitches regulate genes for diverse physiological processes in bacteria, Nat. Chem. Biol. 18 (2022) 878–885. https://doi.org/10.1038/s41589-022-01086-4.

[20] V. Arige, D.I. Yule, Spatial and temporal crosstalk between the cAMP and Ca2+ signaling systems, Biochim. Biophys. Acta - Mol. Cell Res. 1869 (2022) 119293. https://doi.org/10.1016/j.bbamcr.2022.119293.

[21] C. Sissi, M. Palumbo, Effects of magnesium and related divalent metal ions in topoisomerase structure and function, Nucleic Acids Res. 37 (2009) 702–711. https://doi.org/10.1093/nar/gkp024.

[22] R.M. Sterritt, J.N. Lester, Interactions of heavy metals with bacteria, Sci. Total Environ. 14 (1980) 5–

17. https://doi.org/10.1016/0048-9697(80)90122-9.

[23] J.R. Sheldon, E.P. Skaar, Metals as phagocyte antimicrobial effectors, Curr. Opin. Immunol. 60 (2019) 1–9. https://doi.org/10.1016/j.coi.2019.04.002.

[24] A. Reyes-Jara, N. Cordero, J. Aguirre, M. Troncoso, G. Figueroa, Antibacterial effect of copper on microorganisms isolated from bovine mastitis, Front. Microbiol. 7 (2016). https://doi.org/10.3389/fmicb.2016.00626.

[25] A.S. Joshi, P. Singh, I. Mijakovic, Interactions of gold and silver nanoparticles with bacterial biofilms: Molecular interactions behind inhibition and resistance, Int. J. Mol. Sci. 21 (2020) 1–24. https://doi.org/10.3390/ijms21207658.

[26] D. Chudobova, S. Dostalova, B. Ruttkay-Nedecky, R. Guran, M.A.M. Rodrigo, K. Tmejova, S. Krizkova, O. Zitka, V. Adam, R. Kizek, The effect of metal ions on *Staphylococcus aureus* revealed by biochemical and mass spectrometric analyses, Microbiol. Res. 170 (2015) 147–156. https://doi.org/10.1016/j.micres.2014.08.003.

[27] G. Weiss, P.L. Carver, Role of divalent metals in infectious disease susceptibility and outcome, Clin. Microbiol. Infect. 24 (2018) 16–23. https://doi.org/10.1016/j.cmi.2017.01.018.

[28] S. Curiel-Alegre, B. Velasco-Arroyo, C. Rumbo, A.H.A. Khan, J.A. Tamayo-Ramos, C. Rad, J.L.R. Gallego, R. Barros, Evaluation of biostimulation, bioaugmentation, and organic amendments application on the bioremediation of recalcitrant hydrocarbons of soil, Chemosphere. 307 (2022) 1–12. https://doi.org/10.1016/j.chemosphere.2022.135638.

[29] T. Sakaguchi, J.I.B. Janairo, M. Lussier-Price, J. Wada, J.G. Omichinski, K. Sakaguchi, Oligomerization enhances the binding affinity of a silver biomineralization peptide and catalyzes nanostructure formation, Sci. Rep. 7 (2017) 1400. https://doi.org/10.1038/s41598-017-01442-8.

[30] F. Reith, B. Etschmann, C. Grosse, H. Moors, M.A. Benotmane, P. Monsieurs, G. Grass, C. Doonan, S. Vogt, B. Lai, G. Martinez-Criado, G.N. George, D.H. Nies, M. Mergeay, A. Pring, G. Southam, J. Brugger, Mechanisms of gold biomineralization in the bacterium Cupriavidus metallidurans, Proc. Natl. Acad. Sci. 106 (2009) 17757–17762. https://doi.org/10.1073/pnas.0904583106.

[31] A. Shenava, Synthesis of silver nanoparticles by chemical reduction method and their antifungal activity, Int. Res. J. Pharm. 4 (2013) 111–113. https://doi.org/10.7897/2230-8407.041024.

[32] N.R. Jana, L. Gearheart, C.J. Murphy, Evidence for seed-mediated nucleation in the chemical reduction of gold salts to gold nanoparticles, Chem. Mater. 13 (2001) 2313–2322. https://doi.org/10.1021/cm000662n.

[33] N.T.K. Thanh, N. Maclean, S. Mahiddine, Mechanisms of nucleation and growth of nanoparticles in solution, Chem. Rev. 114 (2014) 7610–7630. https://doi.org/10.1021/cr400544s.

[34] G. Munyuki, G.E. Jackson, G.A. Venter, K.E. Kövér, L. Szilágyi, M. Rautenbach, B.M. Spathelf, B. Bhattacharya, D. Van Der Spoel, β-sheet structures and dimer models of the two major tyrocidines, antimicrobial peptides from *Bacillus aneurinolyticus*, Biochemistry. 52 (2013) 7798–7806. https://doi.org/10.1021/bi401363m.

[35] P.J. Loll, E.C. Upton, V. Nahoum, N.J. Economou, S. Cocklin, The high resolution structure of tyrocidine A reveals an amphipathic dimer, Biochim. Biophys. Acta - Biomembr. 1838 (2014) 1199–1207. https://doi.org/10.1016/j.bbamem.2014.01.033.

[36] S. Gupta, V. Kumar, K.B. Joshi, Solvent mediated photo-induced morphological transformation of AgNPs-peptide hybrids in water-EtOH binary solvent mixture, J. Mol. Liq. 236 (2017) 266–277. https://doi.org/10.1016/j.molliq.2017.03.114.

[37] G. Pandit, K. Roy, U. Agarwal, S. Chatterjee, Self-assembly mechanism of a peptide-based drug delivery vehicle, ACS Omega. 3 (2018) 3143–3155. https://doi.org/10.1021/acsomega.7b01871.

[38] B.M. Spathelf, M. Rautenbach, Anti-listerial activity and structure-activity relationships of the six major tyrocidines, cyclic decapeptides from *Bacillus aneurinolyticus*, Bioorganic Med. Chem. 17 (2009) 5541–5548. https://doi.org/10.1016/j.bmc.2009.06.029.

[39] Y.N. Tan, J.Y. Lee, D.I.C. Wang, Uncovering the design rules for peptide synthesis of metal

nanoparticles, J. Am. Chem. Soc. 132 (2010) 5677–5686. https://doi.org/10.1021/ja907454f.

[40] I. Pal, V.P. Brahmkhatri, S. Bera, D. Bhattacharyya, Y. Quirishi, A. Bhunia, H.S. Atreya, Enhanced stability and activity of an antimicrobial peptide in conjugation with silver nanoparticle, J. Colloid Interface Sci. 483 (2016) 385–393. https://doi.org/10.1016/j.jcis.2016.08.043.

[41] M. Rautenbach, N.M. Vlok, M. Stander, H.C. Hoppe, Inhibition of malaria parasite blood stages by tyrocidines, membrane-active cyclic peptide antibiotics from *Bacillus brevis*, Biochim Biophys Acta. 1768 (2007) 1488–1497. https://doi.org/10.1016/j.bbamem.2007.01.015.

[42] A.M. Troskie, A. de Beer, J.A. Vosloo, K. Jacobs, M. Rautenbach, Inhibition of agronomically relevant fungal phytopathogens by tyrocidines, cyclic antimicrobial peptides isolated from *Bacillus aneurinolyticus*, Microbiology. 160 (2014) 2089–2101. https://doi.org/10.1099/mic.0.078840-0.

[43] C. Qin, X. Zhong, X. Bu, N. Lee, J. Ng, Z. Guo, Dissociation of antibacterial and hemolytic activities of an amphipathic peptide antibiotic, (2003). https://doi.org/10.1021/jm0341352.

[44] M. Stauss-Grabo, S. Atiye, T. Le, M. Kretschmar, N. Manuela Stauss-Grabo, Decade-long use of the antimicrobial peptide combination tyrothricin does not pose a major risk of acquired resistance with Gram-positive bacteria and *Candida* spp, Pharmazie. 69 (2014) 838–841. https://doi.org/10.1691/ph.2014.4686.

[45] M. Rautenbach, N.M. Vlok, H.A. Eyéghé-Bickong, M.J. van der Merwe, M.A. Stander, An Electrospray ionization mass spectrometry study on the "*in vacuo*" hetero-oligomers formed by the antimicrobial peptides, surfactin and gramicidin S, J. Am. Soc. Mass Spectrom. 28 (2017) 1623–1637. https://doi.org/10.1007/s13361-017-1685-0.

[46] C. Bich, S. Baer, M.C. Jecklin, R. Zenobi, Probing the hydrophobic effect of noncovalent complexes by mass spectrometry, J. Am. Soc. Mass Spectrom. 21 (2010) 286–289. https://doi.org/10.1016/j.jasms.2009.10.012.

[47] C.B. Morris, J.C. Poland, J.C. May, J.A. McLean, Fundamentals of ion mobility-mass spectrometry for the analysis of biomolecules, Methods Mol. Biol. 2084 (2020) 1–31. https://doi.org/10.1007/978-1-0716-0030-6_1.

[48] M. Rautenbach, G.D. Gerstner, N.M. Vlok, J. Kulenkampff, H. V. Westerhoff, Analyses of dose-response curves to compare the antimicrobial activity of model cationic α-helical peptides highlights the necessity for a minimum of two activity parameters, Anal. Biochem. 350 (2006) 81–90. https://doi.org/10.1016/j.ab.2005.11.027.

[49] D.P. Malenov, S.D. Zarić, Stacking interactions of aromatic ligands in transition metal complexes, Coord. Chem. Rev. 419 (2020) 213338. https://doi.org/10.1016/j.ccr.2020.213338.

[50] D. Łoboda, H. Kozłowski, M. Rowińska-Żyrek, Antimicrobial peptide–metal ion interactions – A potential way of activity enhancement, New J. Chem. 42 (2018) 7560–7568. https://doi.org/10.1039/C7NJ04709F.

[51] N.T.T. Nga, H.V. Tran, C.H. Dang, An investigation on the synthesis, structure and specific properties of Zn(II) and Cu(II) complexes with tryptophan, Biointerface Res. Appl. Chem. 13 (2022) 2. https://doi.org/10.33263/BRIAC131.002.

[52] R.J. Dubos, R.D. Hotchkiss, The production of bactericidal substances by aerobic sporulating bacilli, J. Exp. Med. 73 (1941) 629–640. https://doi.org/10.1084/jem.73.5.629.

[53] A. Rizvi, B. Ahmed, A. Zaidi, M.S. Khan, Biosorption of heavy metals by dry biomass of metal tolerant bacterial biosorbents: an efficient metal clean-up strategy, Environ. Monit. Assess. 192 (2020) 801. https://doi.org/10.1007/s10661-020-08758-5.

[54] P.S. Kidd, V. Álvarez-López, C. Becerra-Castro, M. Cabello-Conejo, Á. Prieto-Fernández, Potential role of plant-associated bacteria in plant metal uptake and implications in phytotechnologies, in: Adv. Bot. Res., London :, 2017: pp. 87–126. https://doi.org/10.1016/bs.abr.2016.12.004.

[55] A. León-Buitimea, C.R. Garza-Cárdenas, J.A. Garza-Cervantes, J.A. Lerma-Escalera, J.R. Morones-Ramírez, The demand for new antibiotics: Antimicrobial peptides, nanoparticles, and combinatorial therapies as future strategies in antibacterial agent design, Front. Microbiol. 11 (2020). https://doi.org/10.3389/fmicb.2020.01669.

[56] W. Xu, H. Yu, F. Yang, F. Yang, D. Liu, K. Lu, H. Gao, Y. Song, Second derivative UV–visible spectroscopy characterizing structural components of dissolved and particulate organic matter in an urbanized river, Environ. Sci. Eur. 34 (2022) 29. https://doi.org/10.1186/s12302-022-00609-z.

[57] A.B.T. Ghisaidoobe, S.J. Chung, Intrinsic tryptophan fluorescence in the detection and analysis of proteins: A focus on Förster resonance energy transfer techniques, Int. J. Mol. Sci. 15 (2014) 22518–22538. https://doi.org/10.3390/ijms151222518.

[58] L. D'Souza, P. Devi, M.P. Divya Shridhar, C.G. Naik, Use of Fourier Transform Infrared (FTIR) spectroscopy to study cadmium-induced changes in *Padina tetrastromatica* (Hauck), Anal. Chem. Insights. 2008 (2008) 135–143. https://doi.org/10.4137/117739010800300001.

[59] D.W. Juhl, W. van Rensburg, X. Bossis, J.A. Vosloo, M. Rautenbach, B. Bechinger, Tyrocidine A interactions with saccharides investigated by CD and NMR spectroscopies, J. Pept. Sci. 25 (2019) 3163. https://doi.org/10.1002/psc.3163.

[60] M.M. Hasan, I. Shahriar, M.A. Ali, M.A. Halim, M.Q. Ehsan, Experimental and computational studies on transition metals interaction with Leucine and Isoleucine, J. Mol. Struct. 1270 (2022) 133862. https://doi.org/10.1016/j.molstruc.2022.133862.

[61] D.M. Close, P. Wardman, Calculation of standard reduction potentials of amino acid radicals and the effects of water and incorporation into peptides, J. Phys. Chem. A. 122 (2018) 439–445. https://doi.org/10.1021/acs.jpca.7b10766.

[62] S. Franco-Ulloa, D. Guarnieri, L. Riccardi, P.P. Pompa, M. De Vivo, Association mechanism of peptide-coated metal nanoparticles with model membranes: A coarse-grained study, J. Chem. Theory Comput. 17 (2021) 4512–4523. https://doi.org/10.1021/acs.jctc.1c00127.

[63] S. Ruden, A. Rieder, I. Chis Ster, T. Schwartz, R. Mikut, K. Hilpert, Synergy pattern of short cationic antimicrobial peptides against multidrug-resistant *Pseudomonas aeruginosa*, Front. Microbiol. 10 (2019). https://doi.org/10.3389/fmicb.2019.02740.

[64] S. Ruden, K. Hilpert, M. Berditsch, P. Wadhwani, A.S. Ulrich, Synergistic interaction between silver nanoparticles and membrane-permeabilizing antimicrobial peptides, Antimicrob. Agents Chemother. 53 (2009) 3538–3540. https://doi.org/10.1128/AAC.01106-08.

[65] I.F. Jaja, C.-J.I. Jaja, N.V. Chigor, M.U. Anyanwu, E.K. Maduabuchi, J.W. Oguttu, E. Green, Antimicrobial resistance phenotype of *Staphylococcus aureus* and *Escherichia coli* isolates obtained from meat in the formal and informal sectors in South Africa, Biomed Res. Int. 2020 (2020) 1–11. https://doi.org/10.1155/2020/3979482.

[66] D. Gutiérrez, S. Delgado, D. Vázquez-Sánchez, B. Martínez, M.L. Cabo, A. Rodríguez, J.J. Herrera, P. García, Incidence of *Staphylococcus aureus* and analysis of associated bacterial communities on food industry surfaces, Appl. Environ. Microbiol. 78 (2012) 8547–8554. https://doi.org/10.1128/AEM.02045-12.